UNIVERSITY OF SOUTHAMPTON

FACULTY OF ENGINEERING AND APPLIED SCIENCE

DEPARTMENT OF CIVIL ENGINEERING

# BEHAVIOUR OF SLEEVED BOLT CONNECTIONS IN PRECAST CONCRETE BUILDING FRAMES

by

Sherif Ali Mohtady Mohamed

(B.Sc.,M.Sc.)

A thesis submitted for the degree of
Doctor of Philosophy
in Structural Engineering

February 1992

UNIVERSITY OF SOUTHAMPTON

ABSTRACT

FACULTY OF ENGINEERING AND APPLIED SCIENCE

DEPARTMENT OF CIVIL ENGINEERING

Doctor of Philosophy

# BEHAVIOUR OF SLEEVED BOLT CONNECTIONS IN PRECAST CONCRETE BUILDING FRAMES

by Sherif Ali Mohtady Mohamed

This thesis describes an experimental investigation and an associated finite element study of the behaviour of sleeved bolt beam-to-column connections. Despite the popularity of such connections in precast concrete building frames, little experimental data has been available regarding their behaviour under static vertical loading. For this reason, two series of tests were performed on full scale joints.

The main focus of the first series was to examine the effect of bolts density per joint on its strength, stiffness and failure mode. In the second series, the influence of concrete confinement upon the joint ultimate strength was studied. Failure of joints was mostly governed by shear yielding of the bolts. However, concrete failure was reported when much weaker concrete with minimum confinement was employed. Deformation data obtained from all tests was used to interpret the joint behaviour. Test results have also shown that increasing the number of bolts per joint not only increases its ultimate strength but improves its load-deflection and moment-rotation characteristics as well.

The parameters affecting the behaviour of such connections have been used to develop three-dimensional finite element models of both the single and double-bolted joints. This was achieved by using the software package (ANSYS). Material properties, geometrical dimensions, boundary conditions and loading were carefully given as input data to represent, as realistically as possible, those of the tested joints. Material nonlinearity was considered for both steel and concrete. The opening and closing of initial geometric gap at the interface between the bolt and the sleeve were also accounted for. The developed models were then used to determine the stress and deformation distributions within the joint components. The models reached their ultimate loads successfully. They predicted with a very good accuracy the joints response under loading. Also they provided useful information which could not be obtained from the experimental part of the investigation, e.g. degradation of the surrounding concrete material and development of tensile stresses in the column steel links. The numerical results were verified against the corresponding experimental values whenever possible.

Finally, the main conclusions based on both parts of the work and recommendations for further work have been given.

## ACKNOWLEDGEMENTS

I would like to take this opportunity to express my sincere gratitude to my supervisor Dr. C.K. Jolly for his knowledgeable and skillful guidance throughout this research programme. His ready advice and constructive comments greatly contributed to the steady progress of the project.

Special thanks are owed to Dr. A.C. Lock for his kind assistance in computer and modelling related problems.

Comments made by Dr. J.M. Lovegrove regarding the work are much appreciated.

I am particularly grateful for the assistance given by the staff of the Civil Engineering Heavy Structures Laboratory. Their close co-operation contributed not only to the motivation of the experimental part of this research but to making the task of its preparation a pleasant one.

Thanks are extended to all past and present colleagues within the department for their useful advice and fruitful discussions.

Finally, but not least, I gratefully acknowledge the ever-present encouragement and generosity of my parents. Their affection, sacrifice and unlimited financial and moral support have made the successful completion of this work possible.

## DEDICATION

To My Parents

Who Gave Too Much And Received Too Little.

## CONTENTS

# CHAPTER ONE

# INTRODUCTION

## 1.1 General

The employment of precast concrete members by the construction industry has increased rapidly throughout the world over the past two decades. Advantages such as speed of erection, better quality, dimensional precision and above all reduction of costs have made precast concrete superior to its cast-in-situ counterpart. A precast structure consists of a number of prefabricated members which, when connected together on site, form a finished structure. Typical structural members are beams, columns, slabs and wall panels. It has been found that satisfactory performance of the structure as a whole and its economy depend to a great extent on the proper selection and design of the connection. As a result, engineers have been continually working to develop more efficient and more economical connections.

## 1.2 Structural Connections

A structural connection can be simply defined as an assembly of components which are arranged in a way to transmit forces from one member to another. In view of the importance of connections, and to ensure that the strength of a partially completed or completed structure must not be governed by the strength of the connections, the connection must not be the weak link in the structure. Since the introduction of precast concrete, many types and varied forms of connections have been developed for use. Details of each depend greatly on the magnitude and the type of the forces to be transmitted.

In skeletal frame construction, beam-to-column connections are the most critical part of the structural concept because they must be capable of transmitting axial forces, shear forces and bending moments safely and without excess deformation. In this type of connection, the most common problem which usually arises is the concentration of the force, as there is a small junction region and a large force to be transmitted through this region. This force concentration reduces the connection's rigidity.

## 1.3 Concepts of Connection Design

It is a common practice to design most of the precast concrete frames as pin-jointed under all conditions of loadings. Designers usually pay more attention to the design of the connections rather than members. This is perhaps due to the non-availability of design codes which cover the practical design of connections. Only little reference, dealing with the connections design, could be cited in the literature [1-3]. However, it is essential to consider connection problems and their ramifications at all stages of work, from conceptual studies through to construction.

A connection must be designed to resist the loads it will be required to carry during the lifetime of the structure. In most connections, load will be transferred through several elements of the connection by various mechanisms, e.g. shear and/or flexural strength, compression, bearing, bond, anchorage and friction. Each of these mechanisms establishes the forces to be used in designing the connection.

Load transfer through connections may be accomplished by: welding projecting reinforcing bars and encasing them with cast-in-situ concrete; by use of mechanical devices such as bolts, brackets or embedded structural steel sections; by employing composite construction techniques, or by applying a prestressing force across the connecting surfaces. A combination of any of the above methods is also widely acceptable. Any other method provided that

it satisfies both the principles of statics and the stress requirements of codes for the materials involved can be introduced. However, it is of vital importance to test an innovative connection, before approving it, to determine its behaviour at both working and ultimate loads.

The requirements of an ideal structural connection have been listed in References [1,4-6] and these can be summarised as follows:

a) Structural Adequacy

As has been mentioned above, a connection must have the strength to resist the forces to which it will be subjected during its lifetime. Some of these forces are apparent, caused by dead and live loads, wind and earthquakes loads. Others are not so obvious such as those caused by shrinkage, creep and temperature changes. The joint should have the ability to accommodate relatively large deformations without failure. Sufficient rigidity, in all directions, is also required to achieve stability of the connected parts during construction.

b) Economy

Maximum economy of precast concrete construction is achieved when connection details are kept as simple as possible, consistent with adequate performance and ease of erection. Simplicity of the connection details may have a greater influence on the total economy of the structure than would a reduction in weight of the main members. To minimise the erection time, it is advisable to have standard shapes and dimensions of connections for a particular structure whenever possible.

c) Tolerance

Tolerance is the measure of deviations which must be accommodated

in the connection. It is important to specify tolerances on dimensional accuracy which can be achieved in manufacture and on site. Tolerances must be within the limits permitted for each type of connection [7,8].

d) Durability

Evidence of poor durability is usually exhibited by corrosion of exposed steel elements, or by cracking and spalling of concrete. Cover should protect all bars and steel inserts against both corrosion and fire.

e) Appearance

After erection, it is desirable to have an invisible connection giving the structure the appearance of monolithic concrete. It is also important for it to have a neat and clean finish without any unwanted shadow lines or cracks.

## 1.4 Beam-to-Column Connections

Most common types of beam-to-column connections in precast concrete can be divided, according to the structural members involved in their formation, into three main groups as follows:

### 1.4.1 Reinforced Concrete Corbels

Corbels are widely used in industrial buildings construction. They usually project from the faces of columns at certain levels to work as horizontal seats for beams to be connected as shown in Figure (1.1a). They are designed to be capable of transmitting vertical and horizontal loads from beams to columns. Such loads are always transmitted by direct bearing, through bearing plates, on corbels. Behaviour of corbels under loading has been the subject of many research works in the past 25 years. Many design formulae and charts have been proposed to predict its ultimate

strength [9-17]. Today, the methods of designing corbels adopted by current Codes of Practice [18,19] are mainly based on one of the following two concepts of design:

1. The "truss analogy concept" which considers the corbel as a simple strut-and-tie system acted upon by an external force as illustrated in Figure (1.1b). The applied external force is assumed to be in equilibrium, at failure, with the corbel internal forces. These forces are a tensile force in the main top steel and an inclined compressive force in the concrete. Such assumption implies that the corbel mode of failure is a flexural one. As a result, an additional step must be taken in the design process to eliminate the possibility of shear failure at the plane of maximum shear, i.e. the column-corbel interface.

2. The "shear friction theory" which assumes that when a corbel is overloaded, a crack would form along its interface with the column. As the load tends to produce slippage along the cracked plane, and due to the roughness of the crack, a separation is assumed to take place. This separation develops a tensile stress in the reinforcement crossing the interface. Assuming a full anchorage of the reinforcement, the tension would provide a clamping force on the concrete creating a compressive stress across the interface to maintain equilibrium [5]. Developed forces and stresses at the interface are shown in Figure (1.1c). Shear friction theory was originally introduced by Mast [20], and was later modified by Hermansen and Cowan [11] to be more applicable for the design of corbels.

Although the above two design concepts are different in their predictions of the mode of failure, they deal with the corbel ultimate strength as a function of its geometrical and material properties. A review and details of cited design proposals, together with a critical comparison between them have been

published by the author elsewhere [21].

It is worth mentioning that all corbel design methods place a great emphasis on the detailing of a corbel such as geometrical proportions, reinforcement anchorage, bearing stress and stirrups details. This is essential as improper detailing proved to have a great effect on a corbel's behaviour and substantially alter its ultimate strength [9]. In practice, improper detailing may arise during design, fabrication or erection. Adequate recommendations concerning the corbel detailing are given in the design sources [1,18,19].

In recent studies [22,23], different types of steel fibres were used in an attempt to replace the stirrups in reinforced concrete corbels. The introduction of the fibres showed a considerable increase in the corbel's shear strength. The adoption and development of such technique may lead to the elimination of the need for the complex reinforcement detailing which has to be met to comply with the above design recommendations.

### 1.4.2 Steel Inserts

In this type of connection, steel inserts can be incorporated into the column, into the beam or into both of them. Steel bolts are usually needed for bolting the inserts together during the erection process. Inserts may be also jointed together by bearing on each other. Compared with the reinforced concrete corbels, steel inserts produce simple detailed connections with much higher ductility. Besides, they have the advantage of keeping the connection within the depth of the beam, i.e. a uniform construction depth can be obtained. On the other hand, they require special consideration regarding the minimisation of voids formation under the embedded members during casting. Special care must also be given to the projecting parts during handling and lifting to avoid their distortion.

Different types and shapes of steel inserts have been in use [1,6]. However, the cast-in-billet, shown in Figure (1.2a), is the most popular one of this group. The billet can be in the form of steel plate, I-section or hollow structural steel member. It is enclosed by the column reinforcement cage and projects outward a distance sufficient to provide the proper bearing as it will act as a steel corbel. The end of the beam incorporates a steel lining to the entire bearing area to provide a uniform contact surface.

Under loading, a high compressive stress develops in the concrete immediately beneath the embedded section at the loaded end. Another zone of compressive stress appears at the top of the far end, see Figure (1.2b). Based on conservative simple assumptions, design equations have been developed for connections with various steel sections [3]. These design equations were later criticised for assuming a 'constant' depth of the compression zone below the embedded steel section, i.e. independent of the eccentricity of the applied load. As a result, experimental studies were conducted on certain steel shapes to investigate the effect of the steel section shape, its geometrical proportions, length of the embedded part, column reinforcement and load eccentricity on the joint's load-carrying capacity [24,25]. Experimental results were then used to improve the above design equations.

Current design recommendations pay high attention to the bearing area as in most cases beam shear is transferred through direct bearing between the steel inserts. Confinement of concrete embedding the inserts has also to be ensured as in most reported cases [26,27], failure was due to the tensile splitting of concrete in the plane of the embedded plate. Lengths of both the embedded and protruding parts of the steel insert are crucial to avoid any premature failure of the joint. Other Limits concerning the design and construction processes can be found in References [1,3,6].

### 1.4.3 Metal Connectors

A wide variety of connectors such as threaded bolts, anchor bolts and headed studs are found in many kinds of precast concrete connections. This is most pronounced in the prestressed and precast concrete industry. Types of bolts and threaded connectors are well documented [28]. Selection of a connector, to be involved in forming a connection, is highly governed by its properties such as dimensions and design strength. Standard lists covering the available ranges of such properties are usually provided by the manufacturer. Connectors can be subjected to tension, shear or their combination.

Anchor bolts design is mainly dependent on whether the bolt is fully or partially embedded in concrete. The design strength is taken as the lesser of the strengths based on steel failure or concrete failure (with pull-out cone or wedge cone). Nominal tensile and shear capacity of short anchor bolts are reviewed and presented in References [29,30]. In this review, the authors focused on isolated single bolt anchorages. They found that several commonly used design procedures were significantly unconservative. Moreover, they reported that using some of these equations led to different predictions from the test results.

Ueda et al. [31] investigated the shear resistance of single- and double-bolt anchorages embedded in plain concrete. They found that the maximum shear capacity of double-bolt anchorages with large spacings could be 40-60% more than that of a single-bolt anchorage with the same edge distance. Recently, a review of the current design procedures of anchor bolts was presented by Lynch et al. [32]. In this review, a special emphasis was given to the tensile and shear capacity of multiple-anchorages with overlapping stress cones.

Numerical models for single-bolt anchorages under tensile loads were developed to study the most relevant influences on

anchorages [33,34]. The two-dimensional non-linear finite models showed a good agreement with test results. Crack propagation in the anchoring zones was also obtained successfully. However, some of these models failed prematurely. It is believed that if the models were expanded to three-dimensional analysis, more realistic ultimate loads could have been obtained.

In Figure (1.3a), headed studs are used to carry the shear load from a precast concrete beam. Being generally made of steel, welding to bracket plates or similar devices allows for shear transfer as shown in the figure. Then shear is transmitted from the welded studs to the concrete through bearing. In addition to the shear carried by the joint, the joint can be subjected to a tensile force, as shown in Figure (1.3b). The ultimate strength of a headed stud joint depends highly on the diameter, spacing, embedment length and design strengths of the studs.

As with the case of the anchor bolts, nominal tensile and shear capacity of headed studs are reviewed and presented in References [29,30]. Based mainly on this review, Shaikh and Yi [35] reported a comprehensive design procedure for the welded headed studs. In their design equations, they allowed for different edge conditions, stud groups and combined shear and tensile loadings.

A primary disadvantage of the use of studs is that close tolerances are always associated with their placement in concrete. Dependence on the strength of welds is another disadvantage of this connection.

The classification of beam-to-column connections into three main groups (corbels, steel inserts and metal connectors) was given as representative, but countless variations and combinations of two or more of these groups may be developed. Several alternative means for interconnecting beams and columns are suggested in References [1-3,6,28].

Nowadays, structural research and development in precast beam-to-column connections follows one of the following four co-ordinated programmes:

1. A research programme to develop and evaluate new connections in terms of design concepts, materials and technologies. This is done with the purpose to produce more efficient connection and to reduce erection time and costs. The connection designed and tested by El-ghazaly et al. [36] is a good example of this research approach.

2. The purpose of this programme is to develop recommendations for the seismic design of precast concrete building frames based on sound analytical and experimental research. As a result of the increasing demand for introducing such recommendations, a number of studies were carried out in North America over the past few years [37-39].

3. The research is carried out on well established connections to provide more comprehensive data on their behaviour. Then, using this data to either improve the existing design equations or study the effect of connections on the overall performance of the connected members under loading. Current research undertaken at the University of Nottingham to investigate the moment-rotation effects on the stability of columns in skeletal frames is a typical example of this trend of research [40].

4. A research programme performed on widely used connections, with the aim of providing basic research data that is not currently available. The obtained data usually gives the designer a better understanding of the connection's behaviour and contributes to the development of relevant design recommendations. In this study reported herein, the research carried out on sleeved bolt connections exemplifies this approach.

## 1.5 Sleeved Bolts Connection

Today, bolted connections stand as one of the most extensively used connections in the construction field. Its popularity stems from the following facts:

1. Compared with other types of connections, it does not require a lot of supervision so it is suitable for site conditions.

2. It can be fastened quickly so if rapid construction is to be achieved, the connection will support load as soon as the bolts are tightened.

3. The rigidity of the connection is relatively high due to the use of high tensile bolts.

4. In its finished form, there is no visible protrusion below the beam lower soffit. This is usually in accordance with the architectural and functional requirements.

A sleeved bolt connection shown in Figure (1.4), which had been in use for a long time, is a typical example of such connections. It provides an efficient structural connection. Its formation can be briefly described as follows:

A group of high tensile, grade 8.8 steel bolts, threaded both ends, are passed through mild steel sleeves embedded through the breadth of a reinforced concrete column. The bolts are also passed through matching holes drilled in two stiffened steel brackets as shown in Figure (1.4). Then, the pair of brackets on opposite sides of the column are held in position by tightening a hexagonal nut on each bolt's end. At this stage, each bracket can serve as a seat angle for the incoming beam end. Having usually a recessed end, the beam confines the bracket within its cross section.

## 1.6 Potential Failures

Figure (1.5) shows a typical sleeved bolt connection supporting a recessed reinforced concrete beam. Potential failure locations, shown in this figure, can be grouped in the following three groups:

### 1.6.1 Potential Failures in The Beam:

a) Flexural failure due to the yield of the longitudinal tension reinforcement in the bottom of the beam. This is usually accompanied with the formation of flexural cracks in the beam's bending span.

b) Shear failure of the concrete near the beam end. This is characterised by the extending of inclined cracks, initiated at the maximum shear plane, towards the top face of the beam.

c) Concrete crushing at the top face of the beam where maximum compressive stress is found.

d) Yield of the longitudinal reinforcement provided immediately above the cast-in bearing plate at the beam end.

e) Yield of shear reinforcement provided in the form of either steel links or bent-up bars.

f) Failure due to improper anchorage of tensile reinforcing bars and the steel links close to the beam end.

g) Bearing failure due to the high local stresses at the beam end which acts as an inverted corbel. Local cracks are most likely to occur at the inner edge of the bearing plate.

The above listed failure modes were reported and predicted in previous experimental and numerical investigations [41-43]. It

was found that the ultimate load and consequently the failure mode were highly sensitive towards the details of the beam end. The amount and arrangement of reinforcement, distance of reaction from the full depth section of the beam and the presence of horizontal loading affected the behaviour of the beam end.

It was also found that secondary modes of failure can be excluded by adopting effective beam detailing and meeting the requirements of bond, anchorage and bearing stresses of Codes of Practice [18,19]. Adequate recommendations on detailing and design of recessed beam ends are given in References [1,3,44].

The serviceability behaviour of the recessed beams (half joints) has been the subject of a recent research [45]. In this research, Clark et al. reported an extensive test data supported by finite element analyses. They concluded that the service load behaviour was improved significantly by providing inclined reinforcement in a half joint. They also revealed that bearing type had an obvious effect on the service load strains, crack patterns and failure load.

1.6.2 Potential Failures in Steel Members:

a) Yield bearing of the bracket's loaded plate may occur if the bearing strength of the bracket's material is exceeded.

b) Bending failure of the loaded plate is also possible if it is not well stiffened.

c) Fracture of the fillet welds used in connecting the different parts of at the steel bracket.

d) Bearing of the bolts against the top of the bracket's matching holes. This may lead to a failure if there is insufficient end distance allowing the bolt to split out through the plate.

e) Shear failure of the bolt takes place when the applied load exceeds the bolt's shear capacity. A critical shear plane is more likely to pass through the bolt's threaded area where the cross section area is reduced.

These failure modes can be excluded by making the bracket's loaded plate sufficiently thick and stiff. Also by designing the fillet welds to be capable of transferring the loads safely between the connected parts. The above mentioned failure modes have been reported and discussed in detail [46,47]. Extensive studies have been carried out in the field of bolted connections in structural steel frames. In these studies, details of the connection, welding effects, type and arrangement of bolts were examined. The reader is referred to References [48,49] for excellent lists of published works on steel frames with bolted connections. However, in this study, failure modes of steel components are not of particular interest as they have more accurately predictable performance.

1.6.3 Potential Failures in The Column:

a) Yielding of the sleeve at its loaded end due to the bearing of the bolt. This is always accompanied with progressive concrete crushing in the cover region directly beneath the sleeve's loaded end.

b) The horizontal component of the force normal to the curved external sleeve surface causes cracks formation in the column below the bolt level. These cracks may develop downwards reducing the capability of the connection to support the applied load.

c) As the concrete looses its tensile strength below the bolt level, axial tensile stresses start to develop in the steel links found in this region causing them to yield at higher loads.

d) Spalling of the column face immediately below the bolts level may occur. This occurs as a result of the high developed bearing stress in this area.

e) In the case of applying unsymmetrical loading at both ends of the connection, a bending moment may develop causing the formation of side cracks in the column.

Despite the many publications which addressed the previous two types of failures, i.e. failures in the recessed beam and in the steel members, little published data exists regarding the potential failures in the column [21]. Moreover, no design or detailing recommendations could be found covering the sleeved bolt connections. Since the behaviour of such connections is a topic not covered by current design sources [1-3,18,19] it warranted further study.

## 1.7 Work Scope

This study is concerned with the investigation of sleeved bolt connections under the application of symmetrical vertical loading only. To achieve this, four full scale tests were carried out, varying the number of bolts per joint as an experimental parameter. This series of tests was used to examine the effect of bolt density on the overall joint behaviour, e.g. failure mode, strength and stiffness. To assess the effect of concrete strength and its confinement on the load-carrying capacity of a single-bolted joint, another series of tests were subsequently carried out with lower concrete strength. In this test series, different degrees of concrete confinement were provided to the joints.

It is well known that instrumentation used in measuring details of stress concentrations in concrete have a great effect on the accuracy of the results. Due to this apparent problem, numerical models using the finite element method have been developed to

show the development and distribution of these stresses. It was also intended that the finite element modelling method would be calibrated against the test data for subsequent use to simulate the behaviour of tested joints at both working and ultimate loads.

## 1.8 Thesis Layout

In this thesis, the details are given in Chapter two of the tests carried out on joints involving one, two, three and four sleeved bolts. This is followed in Chapter three by a discussion of the experimental results. Chapter four presents the numerical part of the investigation concerning the finite element model development and its geometry, together with a description of the finite element package used (ANSYS). Chapter five sets out the basic properties used for the numerical modelling of concrete material. The numerical results and their comparison with those obtained experimentally are covered in Chapter six. The effect of concrete strength and its confinement on a single-bolted joint is examined both numerically and experimentally in Chapter seven. Finally, Chapter eight summarises the general conclusions and formulates recommendations for future work.

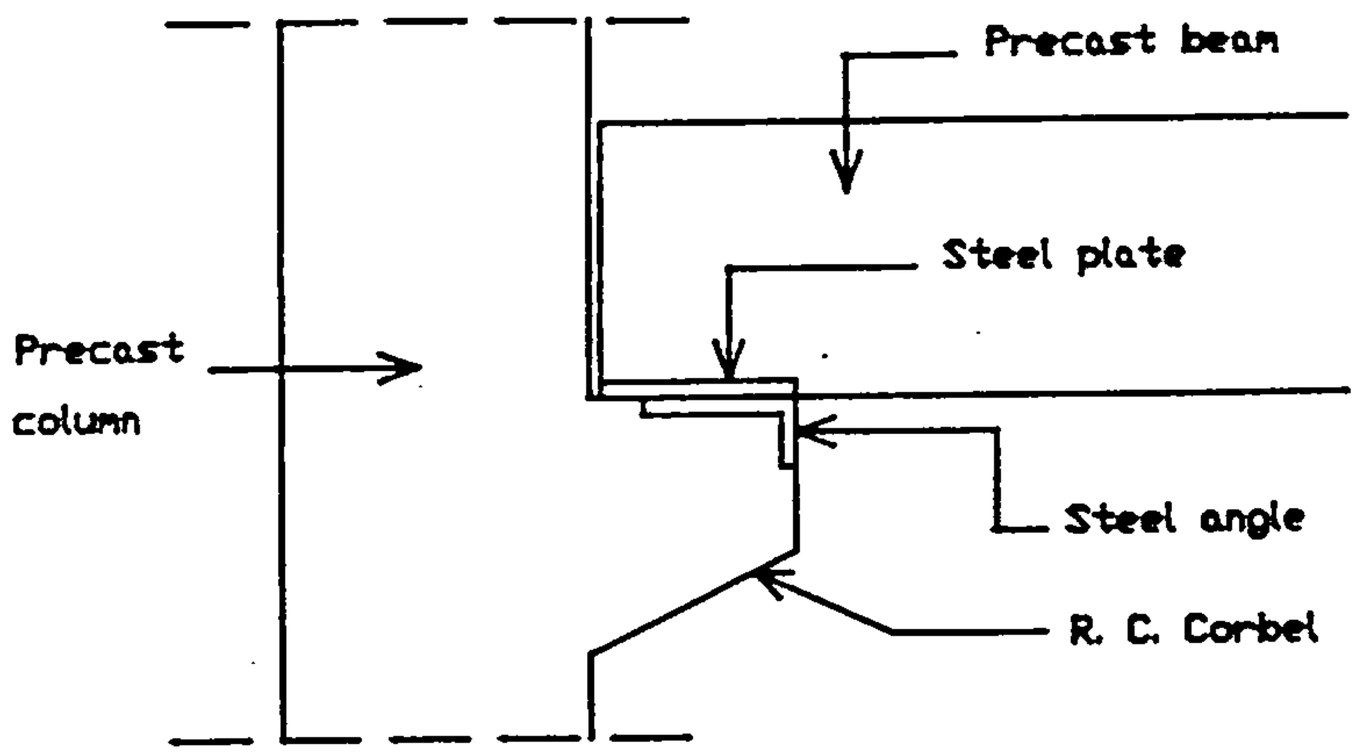


FIGURE (1.1a) : A BEAM-TO-COLUMN CONNECTION WITH A REINFORCED CONCRETE CORBEL.

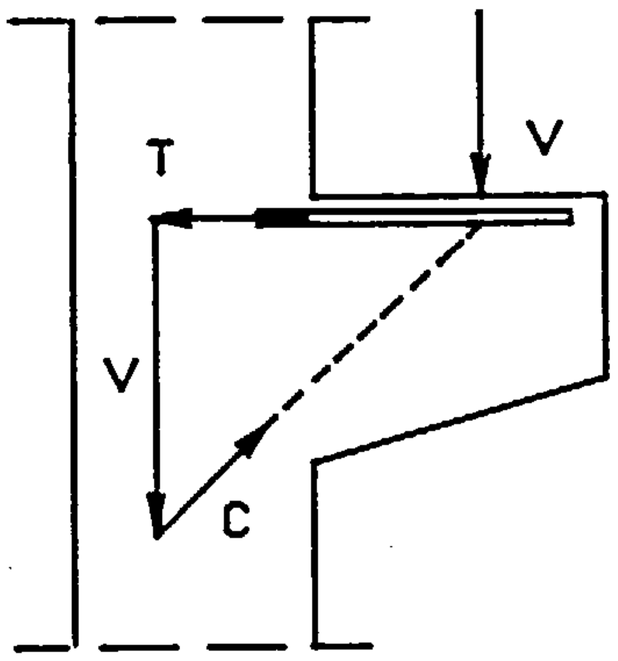


V Applied load

T Tensile force

C Compressive force

FIGURE (1.1b) : SIMPLE TRUSS ANALOGY FOR DESIGNING CORBELS.

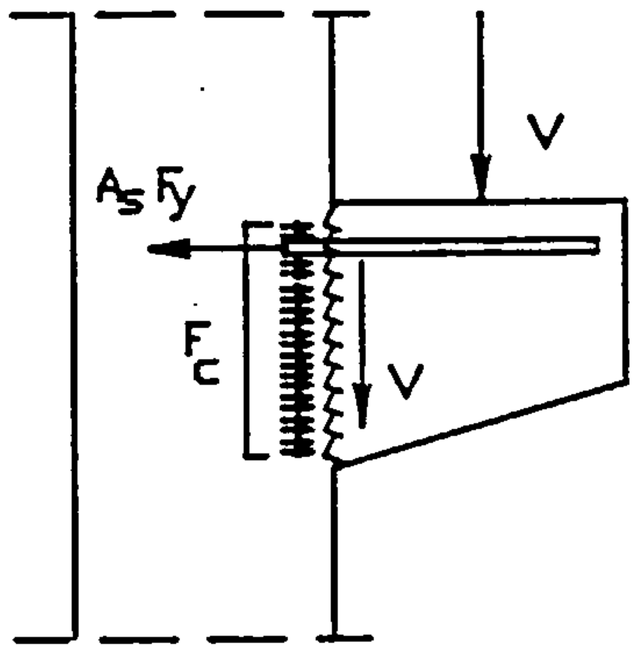


V Applied load

$F_y$ Yield stress

$A_S$ Steel area

$F_C$ Compressive force

FIGURE (1.1c) : FORCES AND STRESSES AT A COLUMN-CORBEL INTERFACE.

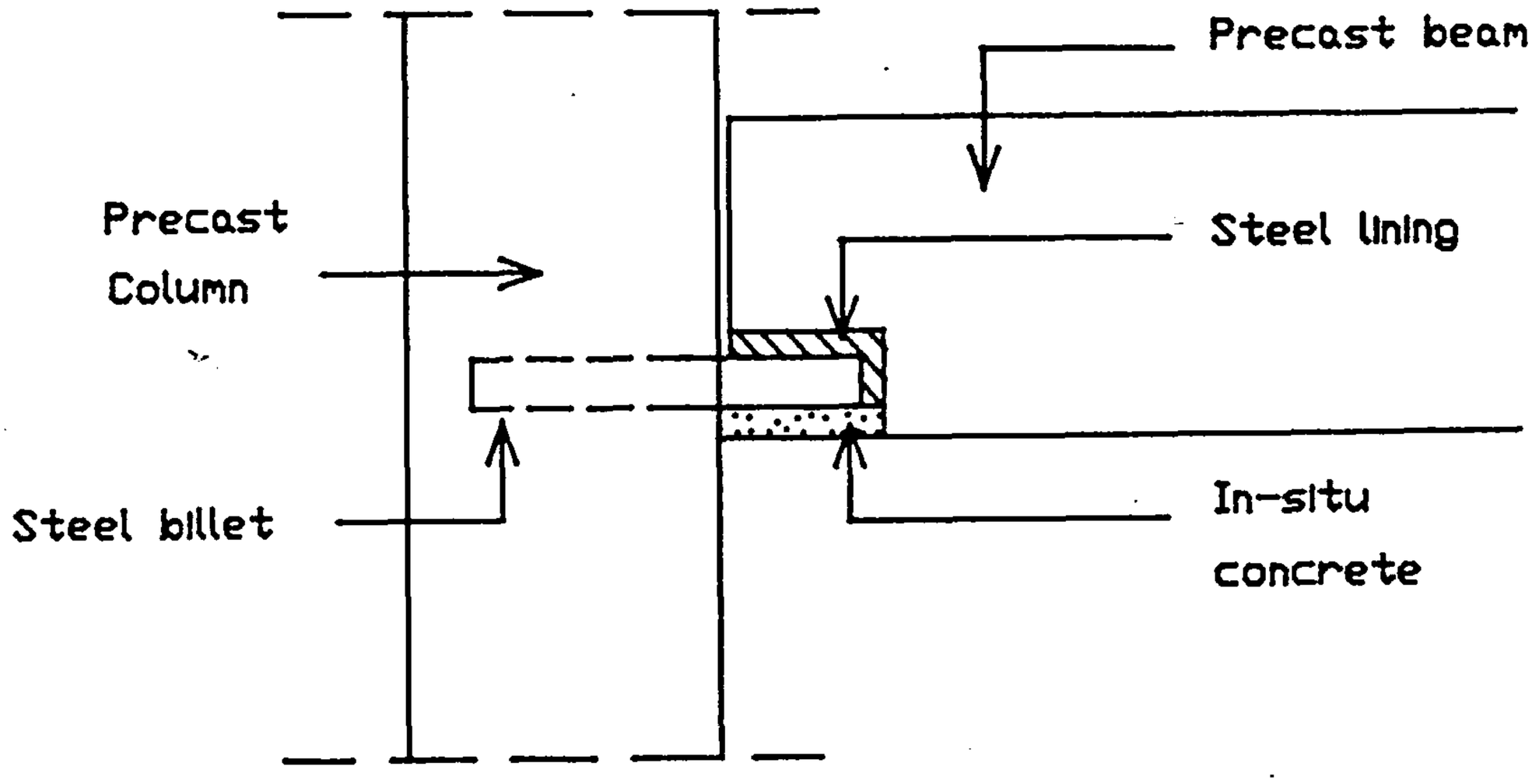


FIGURE (1.2a) : A BEAM-TO-COLUMN CONNECTION USING A STEEL BILLET.

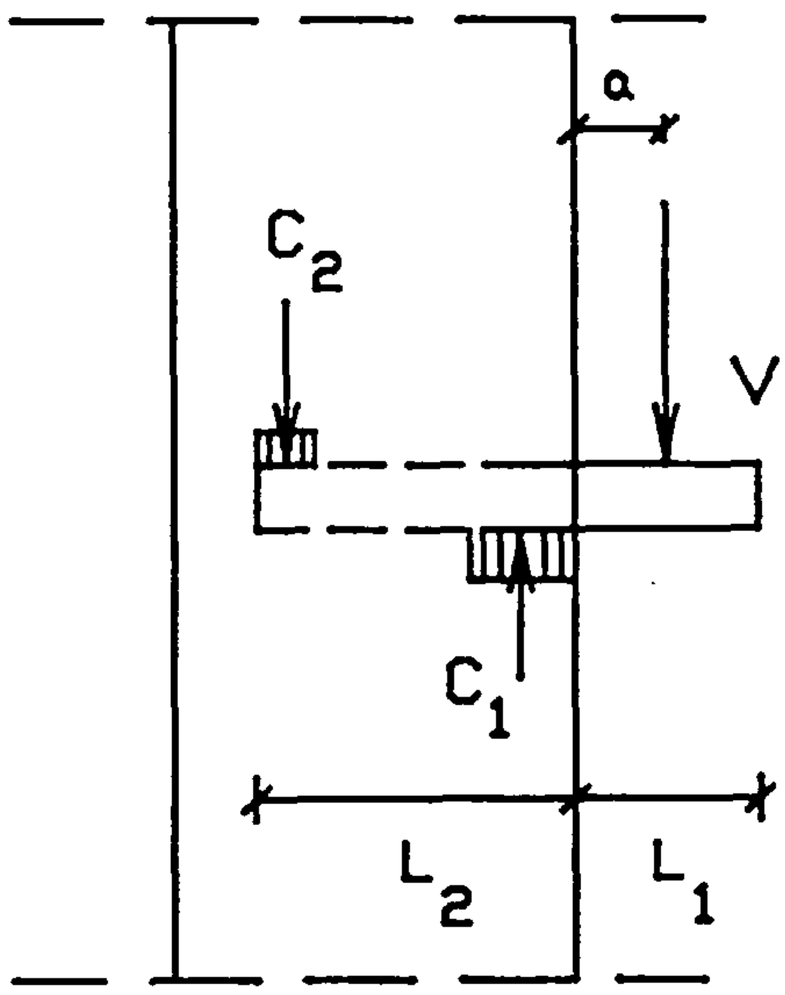


| | |
|---|---|
| V | Applied load |
| $C_1$ & $C_2$ | Compressive forces |
| a | Load eccentricity |
| $L_1$ | Projecting length |
| $L_2$ | Embedment length |

FIGURE (1.2b) : FORCE SYSTEM FOR A STEEL BILLET LOADED IN SHEAR.

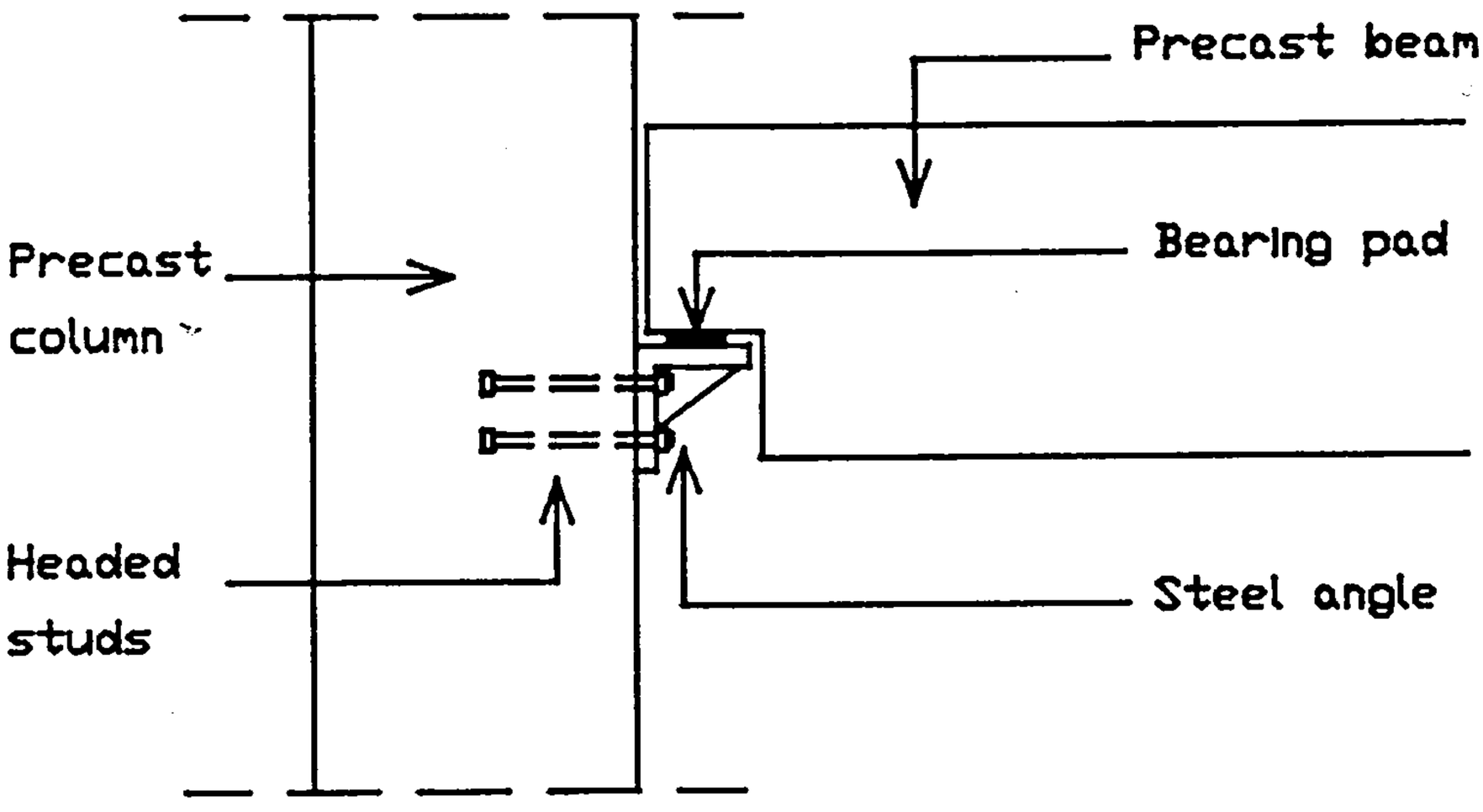


FIGURE (1.3a) : A BEAM-TO-COLUMN CONNECTION USING HEADED STUDS.

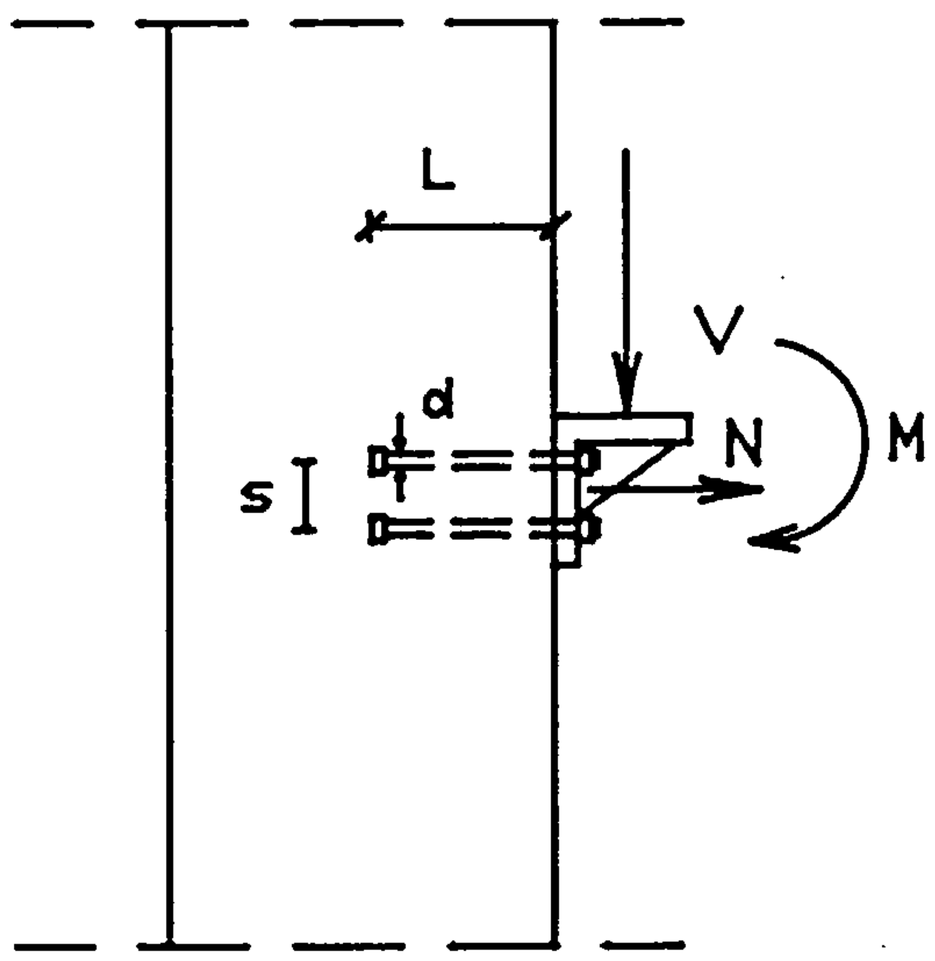


| | |
|---|---|
| V, N | Applied forces |
| M | Applied moment |
| L | Embedment length |
| d | Stud diameter |
| s | Stud spacing |

FIGURE (1.3b) : TYPICAL DESIGN ELEMENTS FOR A HEADED STUDS JOINT.

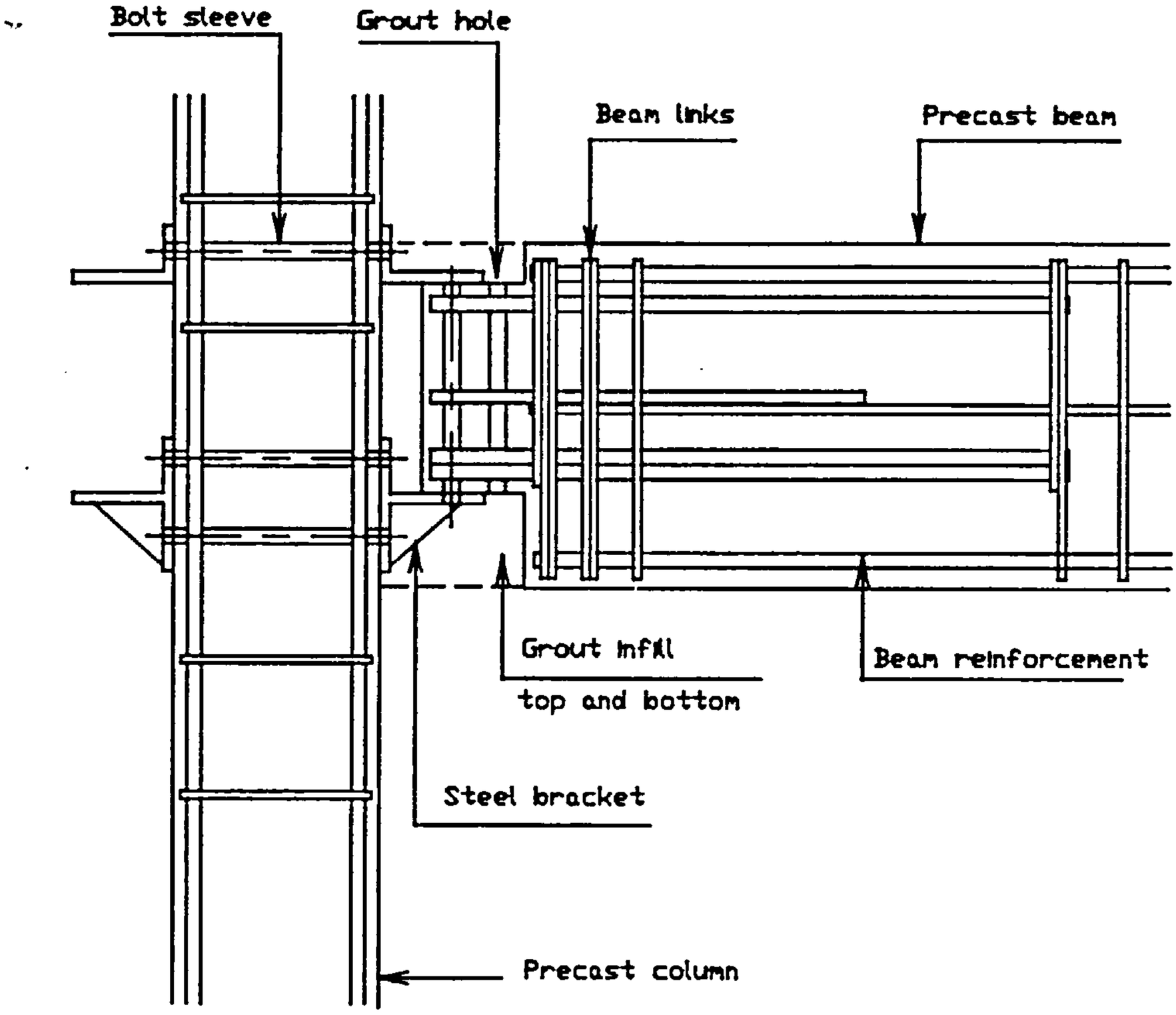


FIGURE (1.4) : STANDARD DETAILS OF A SLEEVED BOLTS CONNECTION.

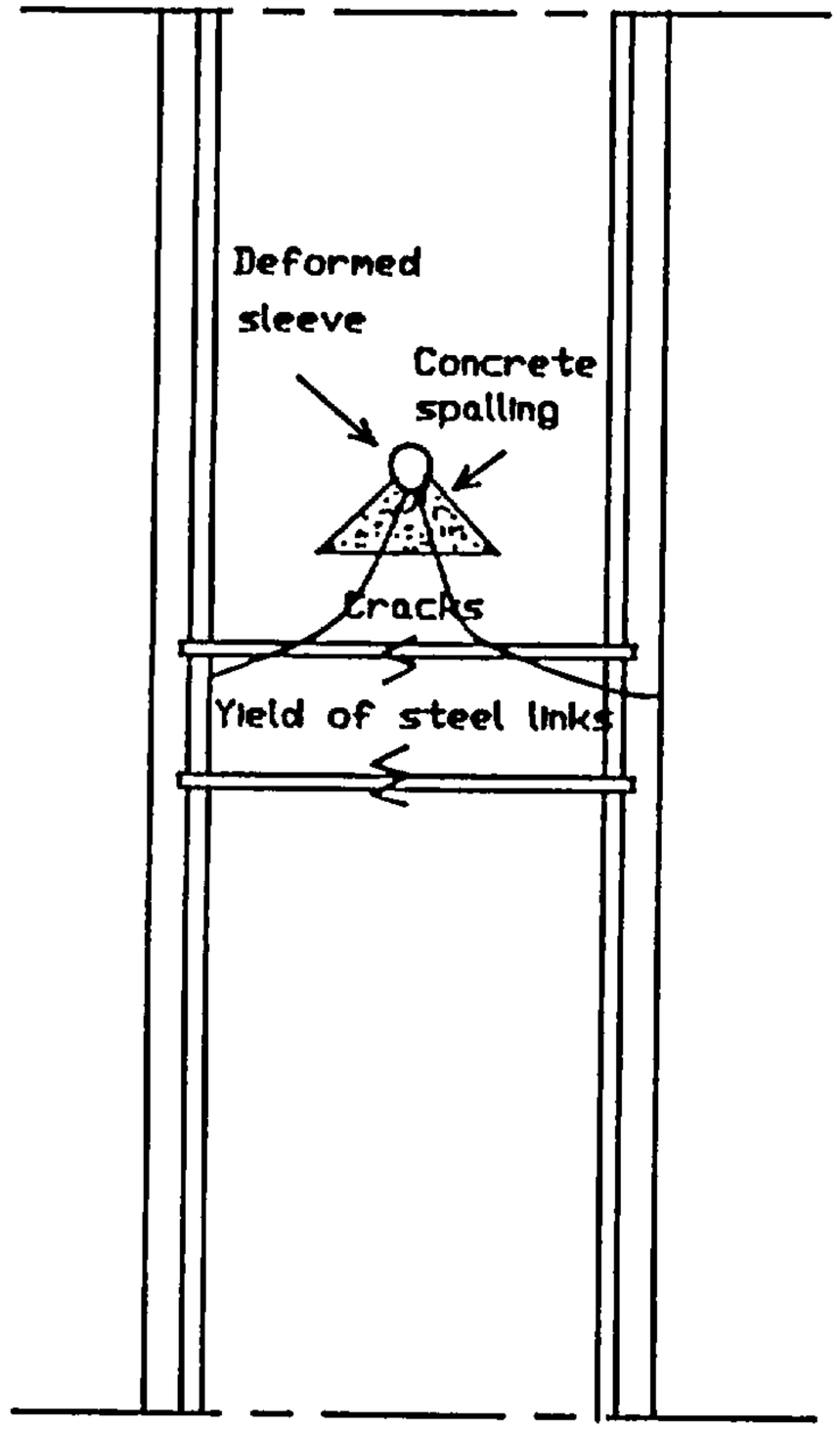


Column face after
bracket's removal

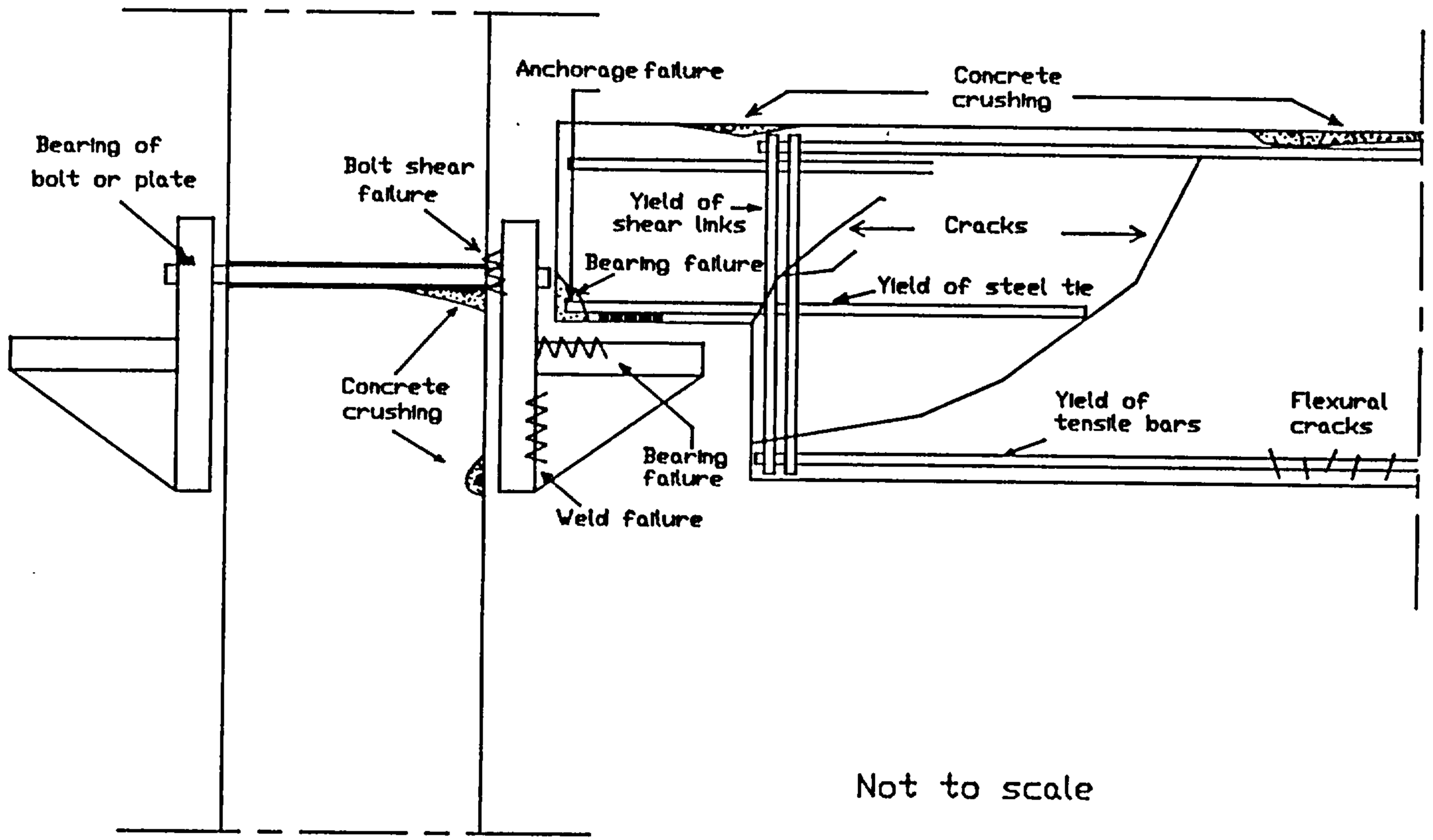


Side view of the connection

Not to scale

FIGURE (1.5) : POTENTIAL FAILURE LOCATIONS IN A SLEEVED BOLTS CONNECTION.

# CHAPTER TWO

# EXPERIMENTAL PROGRAMME

## 2.1 Introduction

A well known approach for proposing recommendations regarding the design of a structural connection is to determine the performance under both working and ultimate loads. This is usually achieved by having a statistically large number of properly devised and performed tests. Such a technique is always associated with high costs and time consumption, but nevertheless it leads to better understanding of the connection behaviour. The lack of published test information on the behaviour of sleeved bolt connections raised the need for their testing. In view of the high local and bearing stresses developed, and the susceptibility of the concrete faces to spalling, testing was considered to be the most effective way of determining the load carrying capability of the less ductile concrete component. The intent of the series of tests described in this chapter, is to assess the effect of the number of bolts per joint on its general behaviour.

The experimental work for this investigation was carried out in the Heavy Structural Laboratory at the University of Southampton. In this chapter, the details of test specimen, instrumentation and other experimental considerations used during the course of the testing programme are described.

## 2.2 Test Programme

As can be seen from the description of the connection, given earlier in Chapter 1, its formation comprises different materials. For this reason it is not surprising to expect that

its performance can be greatly affected by the characteristics of these materials.

Variables which may have an effect on the connection's ultimate capacity can be summarised as follows:

1. Number, size, spacing and arrangement of bolts per joint.

2. Presence, size and spacing of steel links surrounding the joint.

3. Yield strengths of steel members, i.e. bolt, sleeve, links, and brackets.

4. Concrete properties, i.e. compressive and tensile strengths.

5. Geometrical properties of steel brackets, such as plate thickness, diameter of the mounting holes and the clear edge distance between the holes and the nearest edge of the plate.

6. Size of fillet welds which are used in forming the steel brackets.

When the connection is under pure shear loading, the load is transferred from the bracket to the column through the bolts. Bearing of the bolts on the sleeves then transmits the load to the concrete. Thus two principal modes of failure of the connection are susceptible to occur at ultimate load. They are,

a) The bolt may fail by being sheared off completely, most likely at the threaded portion where the shear plane passes. This will happen if the concrete is strong enough.

b) The concrete may crush beneath the sleeve sufficiently for the sleeve to move vertically downward through it causing a lateral force to develop. This force is equivalent to the

horizontal component of the force normal to the curved external sleeve surface as shown in Figure (2.1). Such force causes a tensile stress in this region. If the stress has a value higher than the concrete tensile strength, a vertical crack would appear. This is followed by development of tensile forces in the links beneath the sleeve causing them to yield at higher loads. After link yielding, the already cracked concrete would support no further loading and failure would be inevitable.

In either mode of failure, the concrete beneath the sleeve near the loaded end becomes crushed locally due to the high bearing pressure induced by the bolt shank.

In this test programme the number of bolts per joint was the principal experimental parameter. To achieve this, the test programme was divided into four tests. Each of these involved a joint with a different number of bolts ranging from one to four in steps of one. One test specimen was designed to accommodate all four joints. The arrangement of the joints is described in detail in the following section. At the end of each test, the specimen had to be removed from the testing machine and cut off below the level of influence of the last test.

## 2.3 Design of Test Specimen

The test specimen was a reinforced concrete column of 300mm square cross section and a total height of 2740mm. Details of the column are shown in Figure (2.2). The column had a rectangular base 900 × 300mm. This wide breadth was chosen for the following reasons:

1. To increase the stability of the column during its assembly process.

2. During testing, the column would be held in the vertical

position. Therefore, it was required to have a larger load distribution area between the column base and the testing machine base.

3. This breadth was the maximum allowable within the restriction of the available curing tank size.

4. The 900mm breadth made it possible to have an inclination of 45 degrees on two opposite sides of the column. This angle was a convenient one from the construction point of view.

To account for the four different joints, a total of 10 mild steel sleeves of 300mm length each, were cast in and arranged in four groups. The number and spacing of them are shown in Figure (2.2). This arrangement was adopted to allow for the required tests to be carried out as mentioned earlier. Each sleeve had an internal diameter of 27.0mm with a 3.0mm uniform wall thickness. This value of internal diameter was chosen as the bolts to be used in the tests had a 24.0mm nominal diameter.

A minimum vertical spacing of 500mm was adopted for the distance between any two successive top rows in any group. This value was chosen so that any concrete cracks which occurred during testing one group of sleeves would neither reach nor affect the next group.

The column was reinforced with four 25mm longitudinal deformed steel bars. 8mm steel links, at 50mm centres, were used along the column height . This value of links spacing had to be slightly changed if interference with sleeves would occur. Each main bar had a 50mm protruding length from the column's squared end which passed through the shutter to ensure accurate location during the casting. Cutting these protruding lengths flush with the concrete surface resulted in having uniform bars cross sections with smooth surfaces. This allowed holes to be drilled in these bars afterwards to facilitate fixing part of the test setup as will be

explained in Section 2.5.

A horizontal spacing of 65mm between vertical centrelines of any two adjacent sleeves was kept constant throughout the column.

## 2.4 Concrete Casting and Curing

The concrete mix was white Portland cement, 5mm down fine aggregate, 10mm and 20mm coarse aggregate in the ratio 1 : 1.48 : 0.85 : 1.7, with a water/cement ratio of 0.375. The mix was designed, using the DoE mix design procedure [50], to give a 28 days target mean strength of 52.0 $N/mm^2$. White cement concrete was used as it tends to be better than Portland cement concrete in crack detection. Four batches were required in order to cast the column. Three 100mm cubes, one 100x200mm cylinder and one 500x100x100mm prism were cast as control specimens for each batch. These specimens were used to measure the ultimate compression strength, the tensile splitting strength and the flexural strength for the concrete.

The batching was done by weight and the mixing was done in a $0.1m^3$ capacity rotary mixer in the Concrete Laboratory. Both the aggregate and the cement were placed in the mixer first and then the right amount of water was added as the mixing continued. The ingredients for each batch were mixed for three minutes. The fresh concrete was immediately transferred from the mixer to the formwork. Slump tests were carried out for two batches to check the workability of the fresh concrete. The concrete had a moderately high workability as the slump values were 65mm and 75mm.

The concrete was cast in a wooden mould placed on a baseboard laid horizontally on the floor. Care was taken to insert the sleeves in their exact locations. These locations were carefully marked on the baseboard and a set of solid cylindrical timber dowels were nailed to the centres of these markings. Each piece

had a diameter slightly less than the sleeve internal diameter and a height of 30mm.

The reinforcement was placed as a cage, then the sleeves were slotted over the nailed timber dowels which held one end of each sleeve in position. Another set of similar timber dowels, nailed to cross members connected to the mould, was provided at the top of sleeves to ensure the sleeves were firmly fixed in position during casting and vibrating. These dowels also helped in preventing concrete grout from passing into the sleeves.

Before casting, the baseboard was cleaned and the mould was treated with oil to ensure a good surface finish on the concrete. A set of spacers was used to ensure a consistent 40mm concrete cover along the column edges. These edges were chamfered by using plastic chamfer edge profiles. The control specimens moulds were cleaned and coated with mould oil. As they were filled with fresh concrete they were vibrated on a vibrating table.

The concrete once placed in the mould was vibrated, and at the end of casting the concrete top surface was levelled and smoothed. The formwork and moulds were then moist cured with damp hessian and plastic sheets. The column was then stripped from the mould the following day, lifted out by an overhead electrical crane and laid horizontally in the curing tank. The column was left in the tank for 15 days at 20 degrees when it was removed for setting up the tests.

## 2.5 Test Hardware

### 2.5.1 Steel Bolts

Each steel bolt used throughout the test programme had a nominal diameter of 24mm and a total length of 390mm. This length, which includes a threaded part of 35mm on each end, was chosen to avoid having the threads in direct contact with the sleeves' inner

surface during testing. Another reason was to allow for the tightening of a nut, on each side, after passing the bolt through the thickness of the bracket's back plate. When assembling there was no trace of dirt or rust on the bolts' surfaces.

### 2.5.2 Steel Brackets

The brackets were made from grade 43 steel plates. Figure (2.3) shows the details of their dimensions and patterns used in the tests. Each bracket consisted of three parts:

a) A vertical back plate of 20mm thickness with a specified number of 27mm holes drilled in it. Number of holes and dimensions of the plate were chosen according to the number and arrangement of tested bolts in the joint. Care was taken during drilling the holes to minimise misalignment errors.

b) A horizontal plate of 15 or 20mm thickness was attached to the vertical one by a full penetration arc weld. This plate worked as a seat plate to allow for the load to be directly applied on the joint.

c) Webs, which were designed to carry safely the applied shear force, were welded to both the vertical and the horizontal plates. Apart from the first single-hole pair of brackets, each bracket had two webs. Web thickness was either 15 or 20mm depending on the predicted shear force to be carried.

All welds used in connecting these parts together were fillet welds. They were designed in accordance with BS 5950 [51], to be capable of transferring the loads safely between the connected parts.

### 2.5.3 Loading Plates

The loads applied to the joints were transferred from the testing

machine by means of two mild steel plates 300mm high by 250mm wide by 40mm thick as shown in Figure (2.4). This thickness was chosen to avoid buckling of the plates under the application of maximum load. Both top and bottom surfaces of the plates were machined to provide uniform regular surfaces in contact with the machine platten and the brackets respectively. In all tests, the top surfaces of the plates were not less than 50mm higher than the column top to avoid applying any direct load on the column.

### 2.5.4 Testing Machine

The hydraulic machine used in applying the load in all tests had a maximum capacity of 1500 KN. It had two flat plattens, the bottom one could be moved in and out of the rig by means of rollers while the top one could only be moved vertically and fixed at set intervals. To apply a load on a specimen the bottom platten is moved vertically, thus pressing the tested specimen against the fixed top platten. At any stage of loading, the value of the applied load was indicated by the machine's calibrated dial.

### 2.5.5 Mounting Frame

Having common measurable quantities to monitor in all tests, as will be seen in Section 2.7, raised the need of having a single frame surrounding the joint. This frame could be used in all four tests for holding the measuring equipments in the required positions. This was achieved by using two U-shaped steel plates, 6mm thick, fixed to the top of the column. It should be noted that top of the column was an unloaded area of concrete during testing. Therefore, the top of the column provided an origin for the measured quantities, i.e. it eliminated potential movements of the column with respect to the testing machine. Each of the U-plates had two slots so that it could be connected independently to the column by two 12mm bolts. The slots provided flexibility in horizontal adjustment as each bolt was bolted into

a 12mm threaded hole drilled and tapped in the main column bars. The holes were drilled after having the initially protruding part (approx. 50mm in length) of each bar cut to have the bar ends flush with the column top. Subsequent tests also had the bar ends flush with the top face after previously tested sections of column had been cut away. Figure (2.5) and Plate (2.1) show details of the mounting frame.

An 8mm hole was drilled and tapped in each protruding edge of the U-plates. Four steel rods of 12mm diameter and 500mm length were connected to these edges by means of 8mm bolts, see Figure (2.5). This was simply done by having a female thread in each rod's end to meet the bolts. In the meantime, the bottom threads were used for connecting the rods to a closed steel frame. This closed frame which was in the form of four 6mm steel plates, bolted together at the corners, was provided to increase both rigidity and stability of the whole mounting frame.

## 2.6 Test Setup

The bottom platten of the machine was pulled out from the rig and the position of the column base was carefully marked on by reference lines. This was done as it was important to have the column centralized in the rig so that the applied load would be divided equally between the brackets.

The vertical steel rods, connected to the bottom closed frame, were lowered over the top of the column. After the column was held vertically in this position, the U-plates were connected to the column top as has been described in the previous section. Effort was taken to ensure levelling of each plate individually. Then the lower part of the frame was lifted to have the top of the rods connected to the protruding edges of the U-plates. This was followed by adjusting the frame in position around the joint and ensuring that the whole mounting frame is rigid enough to hold the transducers.

At this stage, the brackets could be offered up to the column faces and the bolts were passed through the brackets' matching sleeved holes. Two nuts were used per bolt to hold it in position. Care was taken to have the brackets horizontally levelled after finger tightening the nuts. After mounting all the transducers, the two thick steel loading plates were put in position with the help of an electrical crane. The loading plates were resting vertically on the horizontal plates of the brackets creating a 60mm load eccentricity from the column face as shown in Figure (2.4). A 500mm long threaded rod was provided across the top of the plates (passing clear over the column top) to be used as a safety restraint during testing. This was also to stop the plates from falling after failure of joints. The general arrangement for the test setup is shown diagramatically in Figure (2.4) and photographically in Plates (2.2) and (2.3).

Having the column on the bottom platten, the latter was then pushed back to its original position in the test rig. The top platten was lowered until it reached the nearest possible distance to the thick plates where it could be fixed in position. The bottom platten began to be moved upwards until the top of both thick plates came at the same time into contact with the top platten. At this stage the test was ready to be started.

## 2.7 Instrumentation

### 2.7.1 Transducers

The load-deflection characteristic is the fundamental information required for any bolted connection. One major problem faced in preparing the test is that the data needed for such deflections is often from locations inaccessible to instrumentation. To overcome this problem, some measurements had to be taken as representative for other actual ones. This is demonstrated in measuring a bolt's vertical deflection as will be described in the following section.

The instrumentation for each test was almost identical. However, some slight changes had to be made to account for the increase in number of tested bolts per joint. For each bracket, a number of linear displacement transducers were positioned on the mounting frame in such a way that the following quantities could either be measured directly, or be determined from other readings, at successive increments of loadings:

1. The downward vertical deflection of both the top and bottom edges of the bracket's back plate. The former was measured at the centreline of each bolt while the latter was measured at the plate mid-span.

2. The variation of the concrete sideway deflection along both sides of the brackets.

3. The longitudinal deflection of the bolts, i.e. their axial pull-out/drawn-in movements.

4. Bracket side-sway (if lateral translation occurred).

The locations of transducers for a typical joint are shown in Figure (2.6) and Plate (2.4).

### 2.7.2 Data Logger

A Solatron Orion data logger was used to record the readings measured by the transducers. The data logger provided an accurate conversion of the transducers' resistances in ohms to the required output in millimetres. A total of seven input connection cards for the 40 channels were used. All transducers were wired separately to the data logger using four-core insulated copper wires. A DC 110 cartridge tape recorder was used to save all the readings during the test so that the data could be transferred to the University computing facilities for post-processing.

All the operation parameters for scanning the transducers were set up and saved on the tape. Necessary information concerning the voltage, the channel numbers, the rate of scanning and the output device was input to the program.

A built-in printer gave a hard copy printout for all the measurement data. This printed readings at each load increment, allowed a continuous assessment of the joint behaviour to be made as the test progressed.

## 2.8 Installation of Transducers

The transducers had either 10mm or 15mm strokes. They were used extensively to determine the movement of the bolts, the brackets and the concrete around the joint under the applied load. According to the required quantities to be measured they can be divided into four groups:

### a) Group 1

This group of transducers was concerned with measuring the downward vertical deflection of each bracket's back plate. As have been described above, these measurements were taken as representative of the bolt's vertical deflection. Transducers with 15mm stroke were positioned vertically above each bolt in the top row, having their arms compressed against the top of the back plate. When there was more than one bolt, a horizontal distance of 65mm was adopted between the two transducers so that in all cases, each one was aligning with the centre line of a corresponding bolt. In the single bolt joint, in addition to the transducer positioned above the bolt, two additional transducers were provided, i.e., one at each edge of the back plate.

To mount the transducers on a bracket, both transducers were fixed with a purpose-made aluminium channel bolted to a steel

angle. The angle was running horizontally between, and clamped at both its ends to, two of the steel vertical rods which were part of the mounting frame.

The central bottom deflection of the back plate at its mid-span was also recorded for each joint during testing. This was measured by a transducer positioned vertically below the bracket. This transducer was fitted to a stand which had a magnetic base attached to the bottom stiffening closed frame.

b) Group 2

This group consisted of 24 transducers with strokes of 15mm. They were used to record the sideway movements of the concrete on both sides of the brackets. On each side, six transducers were vertically spaced in such a way that the second one from the top was located at the bolt's centreline level. The others were corresponding to the positions of the steel links above and below the joint. This arrangement was chosen because an earlier test [21] showed that the concrete movement above the level of top bolts is small compared with those below it. The six transducers forming a group on one side of the bracket were fixed with an aluminium channel held by the vertical mounting frame rods.

These positions were chosen to measure the concrete movement as it was expected to show a noticeable sideways movement when cracks start to form after yield of the steel links. The arms were partially compressed against the concrete to allow for recording either concrete expansion or contraction. Their points of contact with the concrete surface were only 25mm away from the column edges to avoid having them positioned over the virtually fixed column main bars.

c) Group 3

For each bolt in the top row, two transducers were used to

measure the axial pull-out or drawn-in movements. As the top bolt ends were hidden behind the vertical loading plate, these measurements could not be obtained directly. To overcome this problem, a 6mm deep hole was drilled and tapped in the centre of the bolt's end. A T-shaped flat thin steel plate was attached to the bolt end by a fixing into this hole. This allowed the axial movement of the bolt to be measured remotely. The transducer arm was half compressed to allow for movement to be recorded in either direction. All magnetic bases of the stands used in holding these transducers were firmly clamped by G-clamps to the mounting frame.

d) Group 4

In spite of having both brackets initially levelled horizontally, two transducers, one per bracket, were positioned to measure any lateral translation of the brackets during loading. They were located on the back plate's sides, at the level of the bolt's centreline.

Transducers used in all four groups were calibrated independently using a calibration micrometer.

## 2.9 Test Procedure

Before the loading plates came into contact with the machine fixed top platten, the input connection cards were connected to the data logger. Then the data logger was switched on and the saved program was loaded from the tape. A final inspection was made to ensure that all transducers were correctly and securely positioned and then the initial readings of all transducers were scanned.

The test procedure consisted simply of the gradual application of load. This continued until the joints were not capable of supporting any further load or for some reason no additional load

could be applied. The load was applied in initial increments of 50 KN and when the monitored deflections showed large increases, indicating onset of nonlinearity, the load increments were reduced to 25 KN. The load-deformations data were recorded for each load increment. Visual inspection of the joint surrounding was carried out throughout the test to record any visible crack formation.

To record any changes in deflection due to creep or yielding effect, the load was maintained constant over a period of two minutes, for each load increment, before another scan was taken.

After the end of each test, the transducers, the loading plates and the mounting frame were removed and kept for future use while the conditions of bolts and the brackets were examined. The column was lifted away from the test rig and a cover meter was used to detect steel links locations below the level of the tested joint. Then a level was specified for cutting off the affected column section. This check was done to avoid the difficulty in cutting through a steel link, and also to provide enough concrete height above the joint, to be tested, thus preventing any premature failure there.

A masonry saw was used to cut the column off at the marked level. The saw's cutting head was placed on a moving trolley in order to have the column laid on the ground during cutting as shown in Plate (2.5). The trolley was positioned in a way such that the machine blade would be cutting through a direction perpendicular to the sleeves axis. Guide wheels were used to have a precise cutting track. Wooden straight edges, orthogonal to the column edges, were also used to guide the wheels.

The cutting process started from one side of the column and continued vertically towards the column middle section. Cutting was stopped when the cutting efficiency of the blade was reduced due to the limitation of its radius. Then the saw was removed and

the column was turned upside down for cutting from the other side.

## 2.10 Material Properties

### 2.10.1 Concrete

As-mentioned earlier, twelve 100mm cubes were cast from the four batches. Four cubes, one from each batch, were cured with the test specimen under the same conditions. One of each was tested on the same day as testing. Tests were carried out at 33, 46, 53, and 73 days, respectively. The remaining cubes were water-cured until testing. Testing cubes was conducted in accordance with BS 1881:1983. Results obtained are shown below in Table 2.1, from which the average concrete cube strengths for the wet-cured and dry-cured cubes were 67.00 and 69.125 $N/mm^2$, respectively.

Assuming that the cubes' failing loads, for water-cured cubes, are normally distributed with only 5% probability that a result would fall below the mean value of these loads. A mean value of 61.9 $N/mm^2$ was obtained for the concrete material.

| Cube No. | Age at Test (days) | Batch No. | Curing Type | Failing Load (KN) | Compressive Strength (N/mm2) |
|---|---|---|---|---|---|
| 1 | 33 | 1 | Dry | 753 | 75.5 |
| 2 | 46 | 1 | Water | 646 | 65.0 |
| 3 | 46 | 2 | Water | 676 | 68.0 |
| 4 | 46 | 3 | Water | 728 | 73.0 |
| 5 | 46 | 4 | Water | 659 | 66.0 |
| 6 | 46 | 2 | Dry | 751 | 75.0 |
| 7 | 53 | 3 | Dry | 762 | 76.0 |
| 8 | 73 | 1 | Water | 679 | 68.0 |
| 9 | 73 | 2 | Water | 677 | 68.0 |
| 10 | 73 | 3 | Water | 646 | 65.0 |
| 11 | 73 | 4 | Water | 627 | 63.0 |
| 12 | 73 | 4 | Dry | 498 | 50.0 |

TABLE 2.1 : RESULTS OF CONCRETE CUBES TESTING.

All four cylinders were water cured and tested at an age of 46 days. As can be seen from Table 2.2, all four results obtained from indirect tensile strength tests are consistent, giving an average of 4.05 $N/mm^2$ for the concrete tensile strength.

The four prisms were tested at an age of 60 days. An average of 6.22 $N/mm^2$ was obtained for the concrete flexural strength.

| Cylinders 100 × 200 mm | | | | Prisms 500 × 100 × 100 mm | | | |
|---|---|---|---|---|---|---|---|
| Batch No. | Age at Test (days) | Failing Load (KN) | Tensile Strength (N/mm2) | Batch No. | Age at Test (days) | Failing Load (KN) | Flexural Strength (N/mm2) |
| 1 | 46 | 131.0 | 4.17 | 1 | 60 | 21.1 | 6.33 |
| 2 | 46 | 127.3 | 4.05 | 2 | 60 | 20.1 | 6.03 |
| 3 | 46 | 126.3 | 4.02 | 3 | 60 | 21.5 | 6.45 |
| 4 | 46 | 125.2 | 3.98 | 4 | 60 | 20.2 | 6.06 |

TABLE 2.2 : RESULTS OF CONCRETE CYLINDERS AND PRISMS TESTING.

### 2.10.2 Reinforcing Steel

Two tensile tests were carried out in accordance with BS 4449 : 1976 to get the yield stress for the deformed bars used as column main bars. Using a Demec strain gauge, a series of strain values was obtained up to the yield point. The steel proved to have a well defined yield point and its value was 448.0 $N/mm^2$. Both tests had to be stopped before obtaining the ultimate strength. This was due to the slipping of the ribbed samples in the testing machine jaws.

The 8mm mild steel bars used as steel links in the column had a remarkable high value of yield stress. An average value of 450.0 $N/mm^2$ was determined from four tensile tests.

### 2.10.3 Sleeve Material

As there was no available specification regarding the sleeve material properties, it was decided to carry out a simple tensile test to determine the relevant yield stress and elastic modulus. Having only a wall thickness of 3.0mm, there was a problem of applying a tensile load without damaging the sleeve cross section. A solid mild steel cylinder, 50mm in length, was fitted in each end of the sleeve to make sure that the testing machine's clamping jaws would not crush the sleeve ends at the early stages of loading.

The tested specimen had a length of 300mm. Two punched marks, 50mm apart, were made on the sleeve surface. These marks which were used as reference points for strain measurements, were near the sleeve mid-length to avoid areas of stress concentration close to the jaws. The scale of the loading machine was adjusted as the expected yield stress was around 250.0 $N/mm^2$. Then load was applied incrementally. The strain was measured for each load step by means of a Demec strain gauge. As the strain measurements were taken manually, three strain values were read for each load step up to the yield load. The average of these, with the exclusion of the outlying values, was used in obtaining the stress-strain curve for the material shown in Figure (2.7). The yield stress was found to be 274.0 $N/mm^2$.

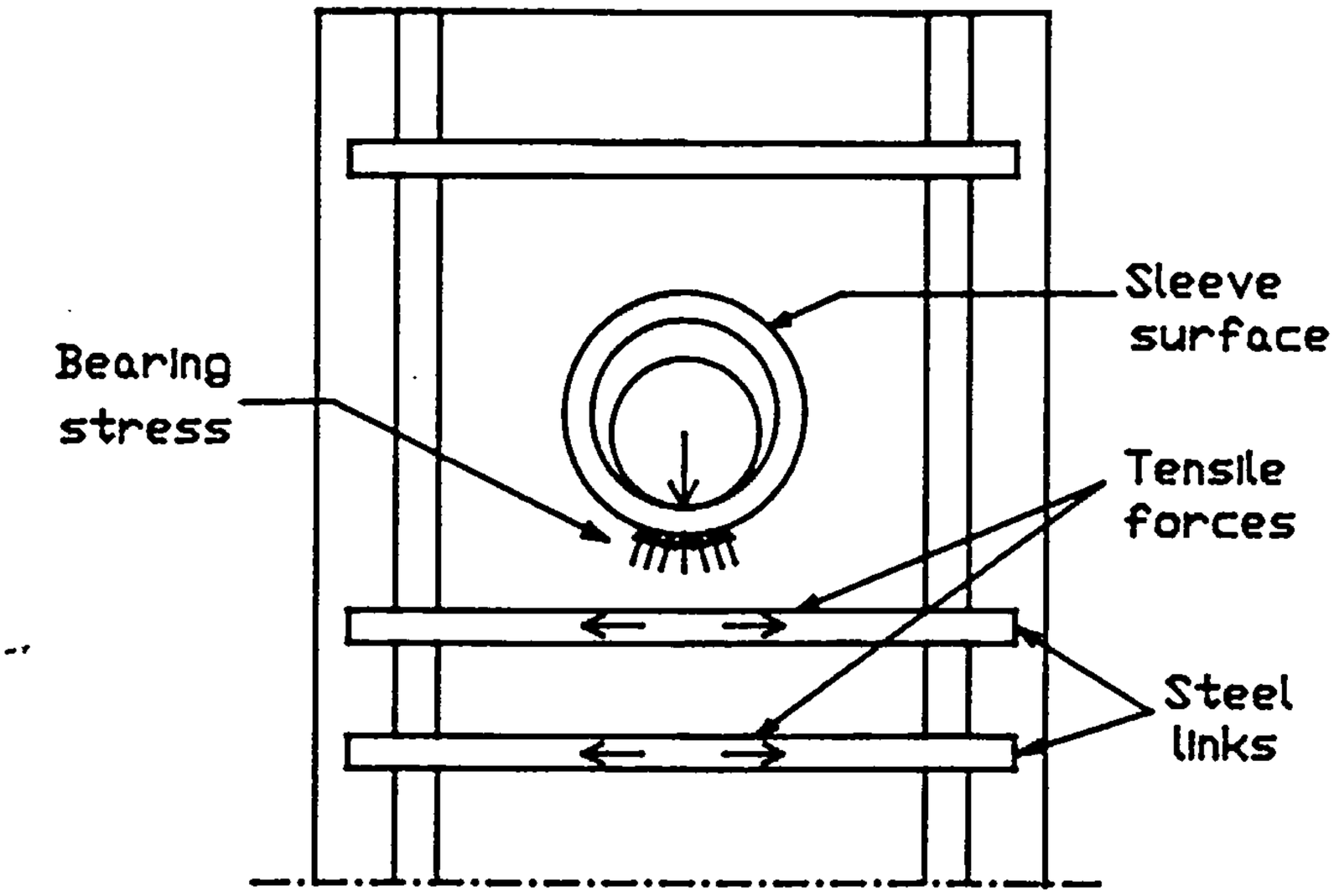


FIGURE (2.1) : FORCE DEVELOPMENT ALONG THE CURVED SLEEVE SURFACE AND IN THE STEEL LINKS AROUND THE JOINT.

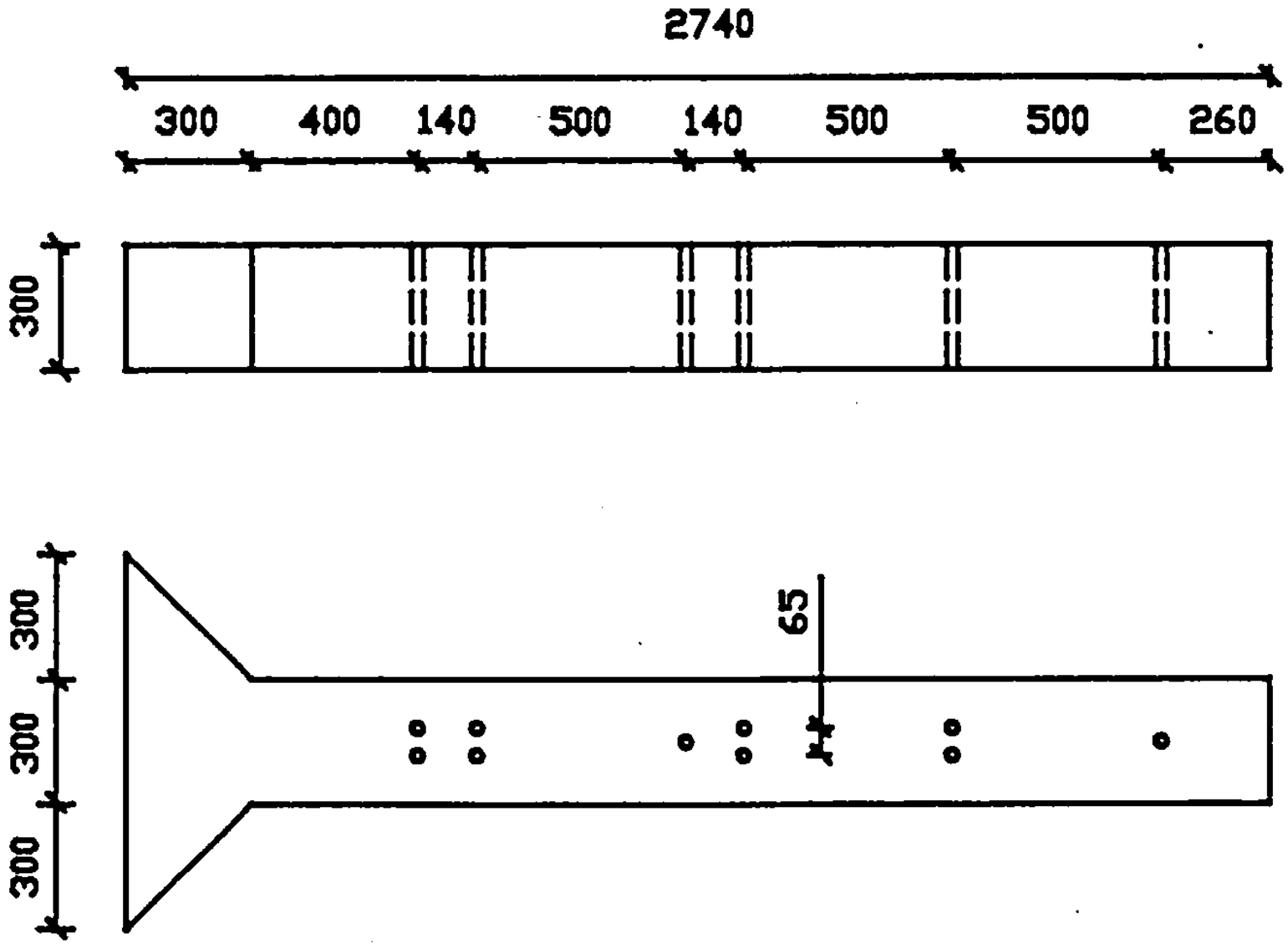


Dimensions are in millimetres

Diameter of holes = 27.0 mm

FIGURE (2.2) : DIMENSIONS OF THE TEST SPECIMEN WITH SLEEVES ARRANGEMENT.

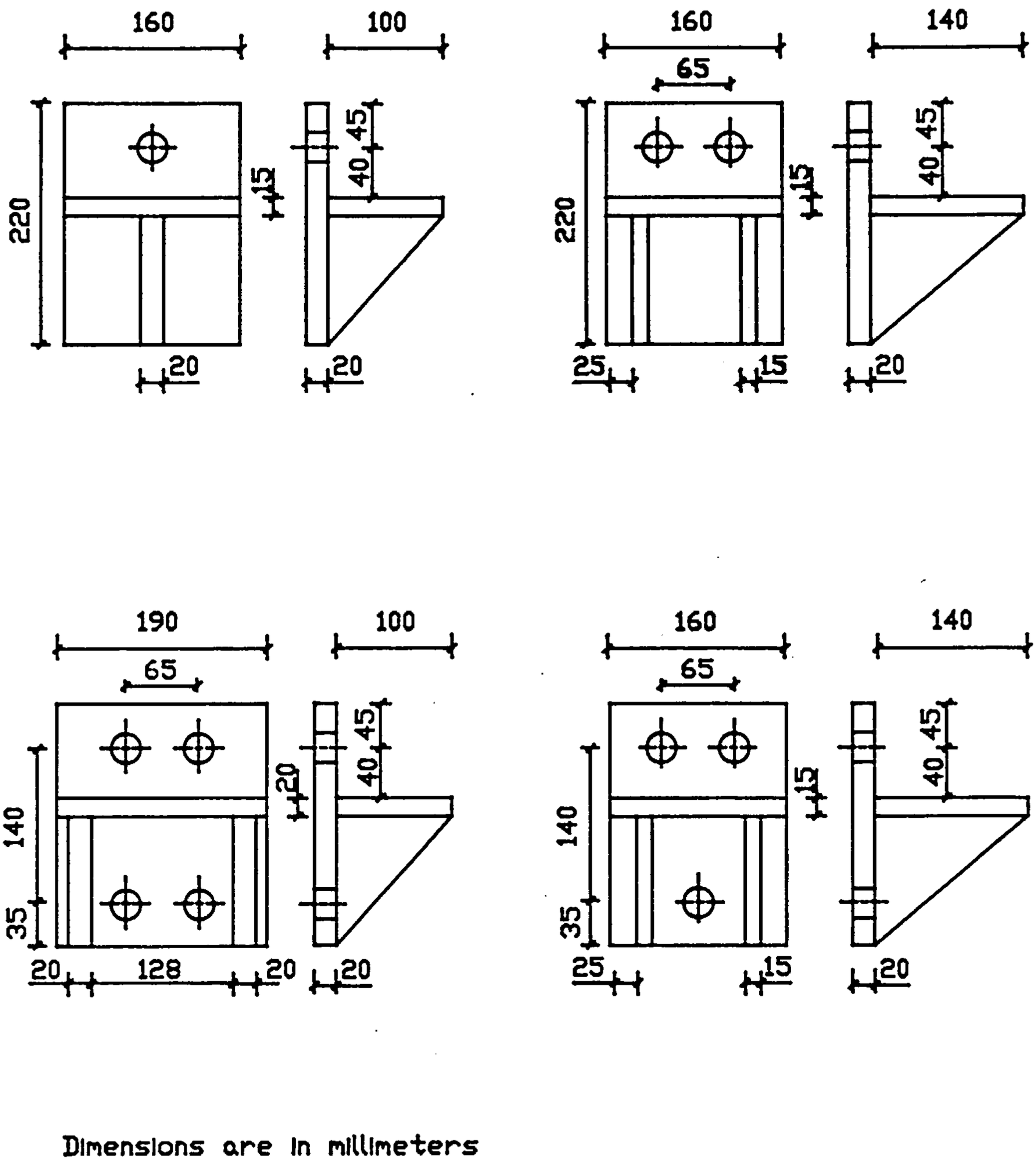


Dimensions are in millimeters

Diameter of holes = 27.0 mm

FIGURE (2.3) : GEOMETRICAL DETAILS OF THE STIFFENED STEEL BRACKETS USED THROUGHOUT THE TEST PROGRAMME.

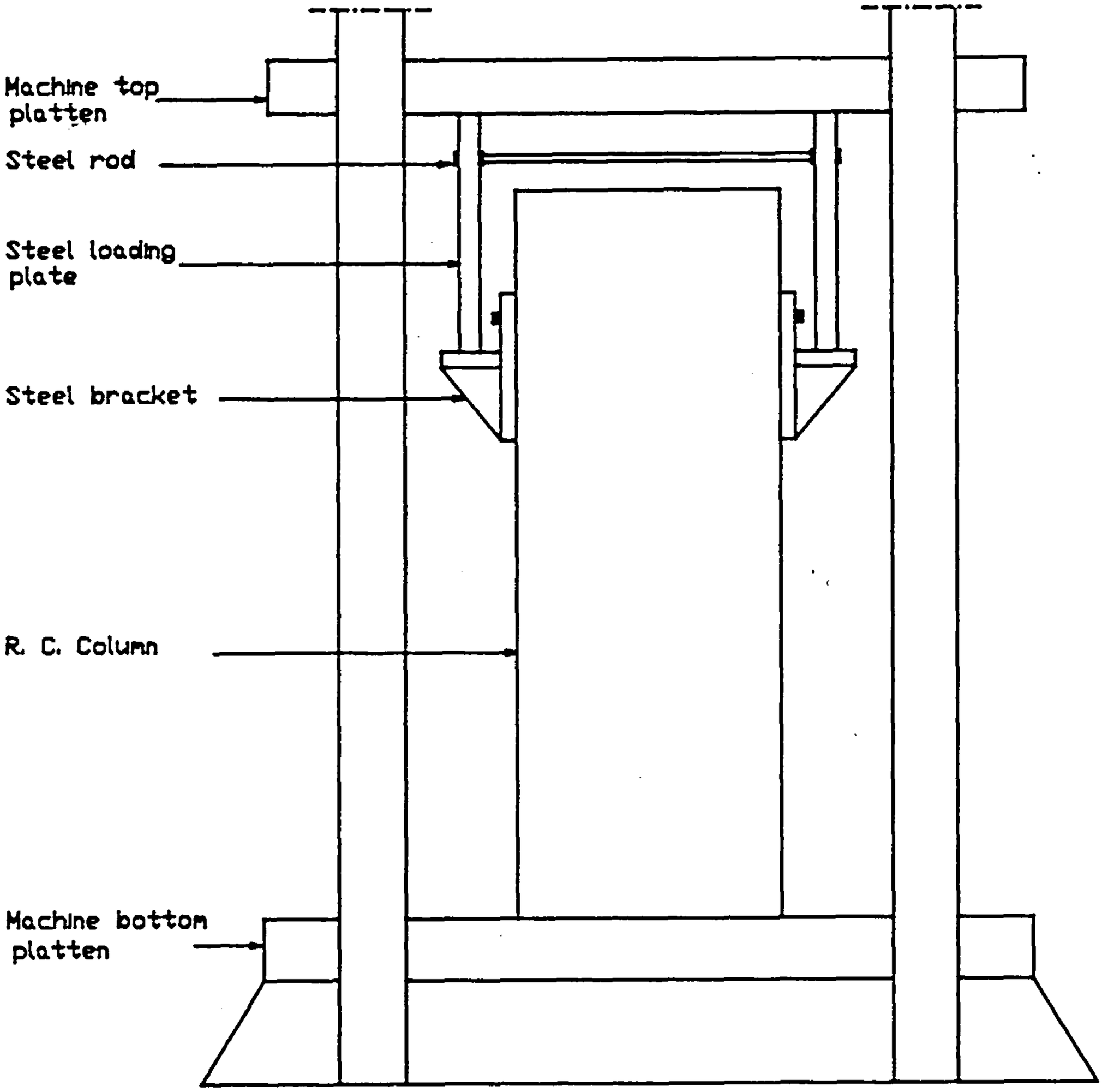


FIGURE (2.4) : GENERAL VIEW OF TEST SETUP ARRANGEMENT EXCLUDING DISPLACEMENT TRANSDUCER MOUNTING FRAME.

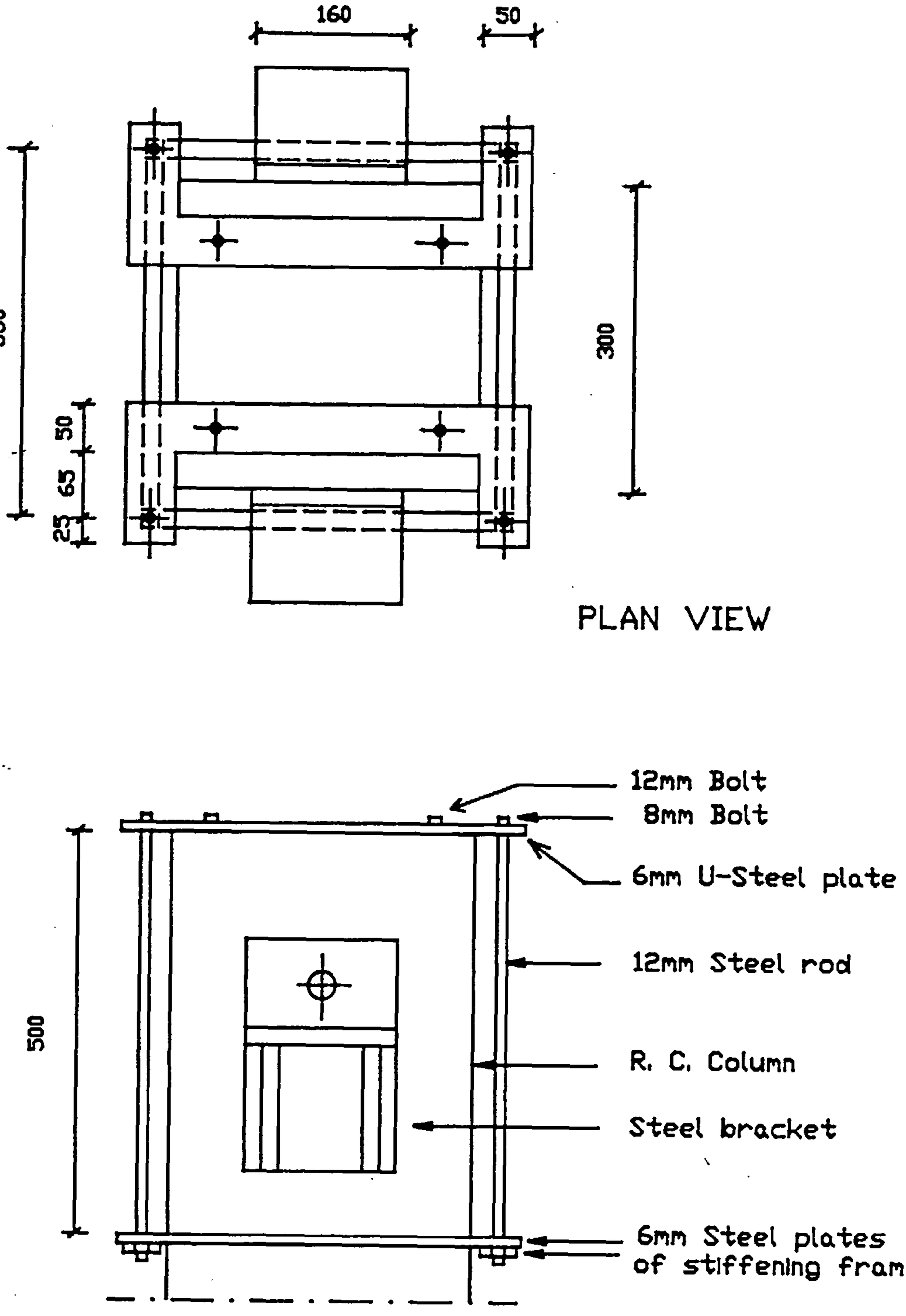


Dimensions are in millimeters

FIGURE (2.5) : DETAILS OF THE MOUNTING FRAME AROUND A TESTED JOINT.

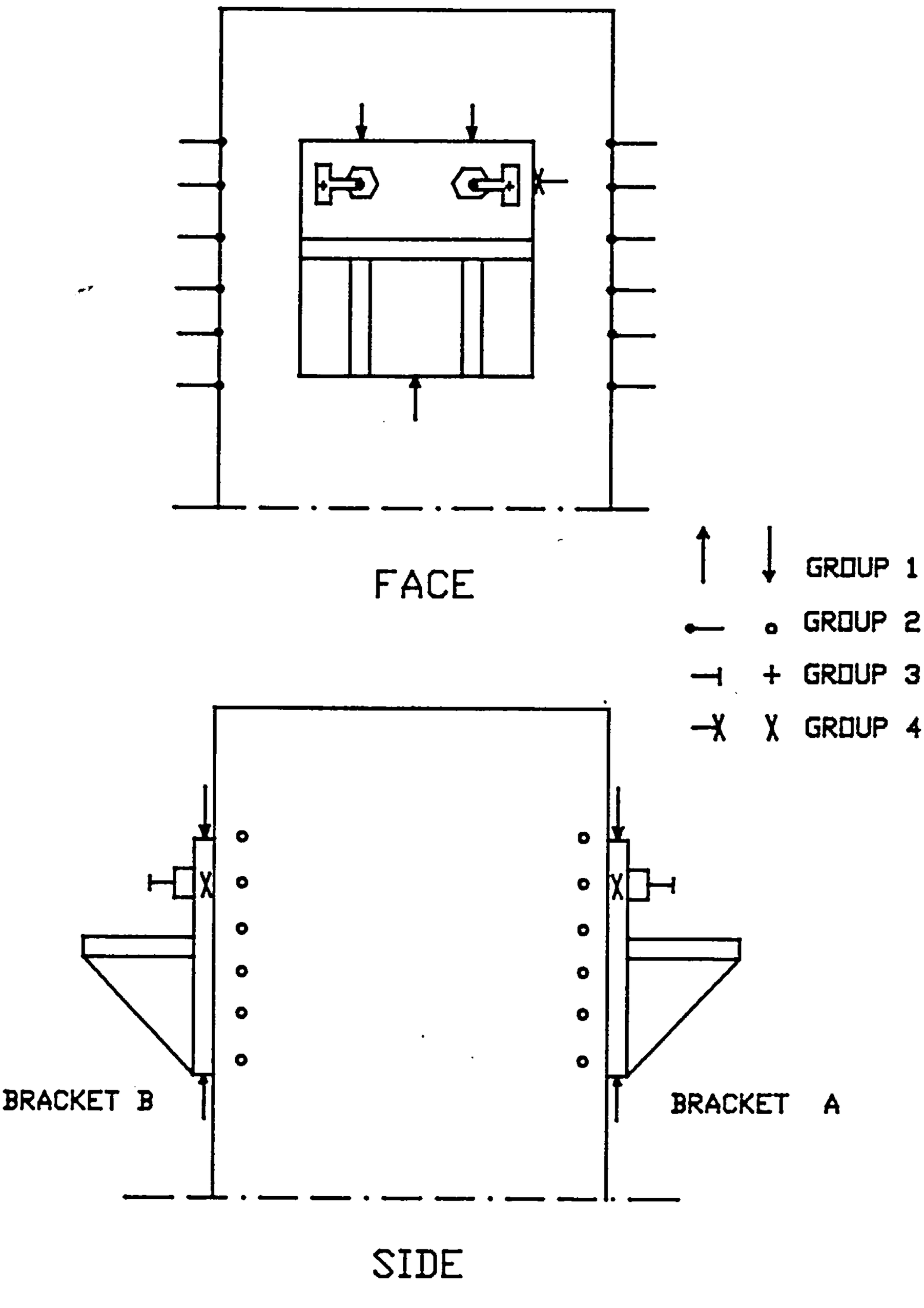


FIGURE (2.6) : A TYPICAL ARRANGEMENT OF TRANSDUCERS AROUND A TESTED JOINT.

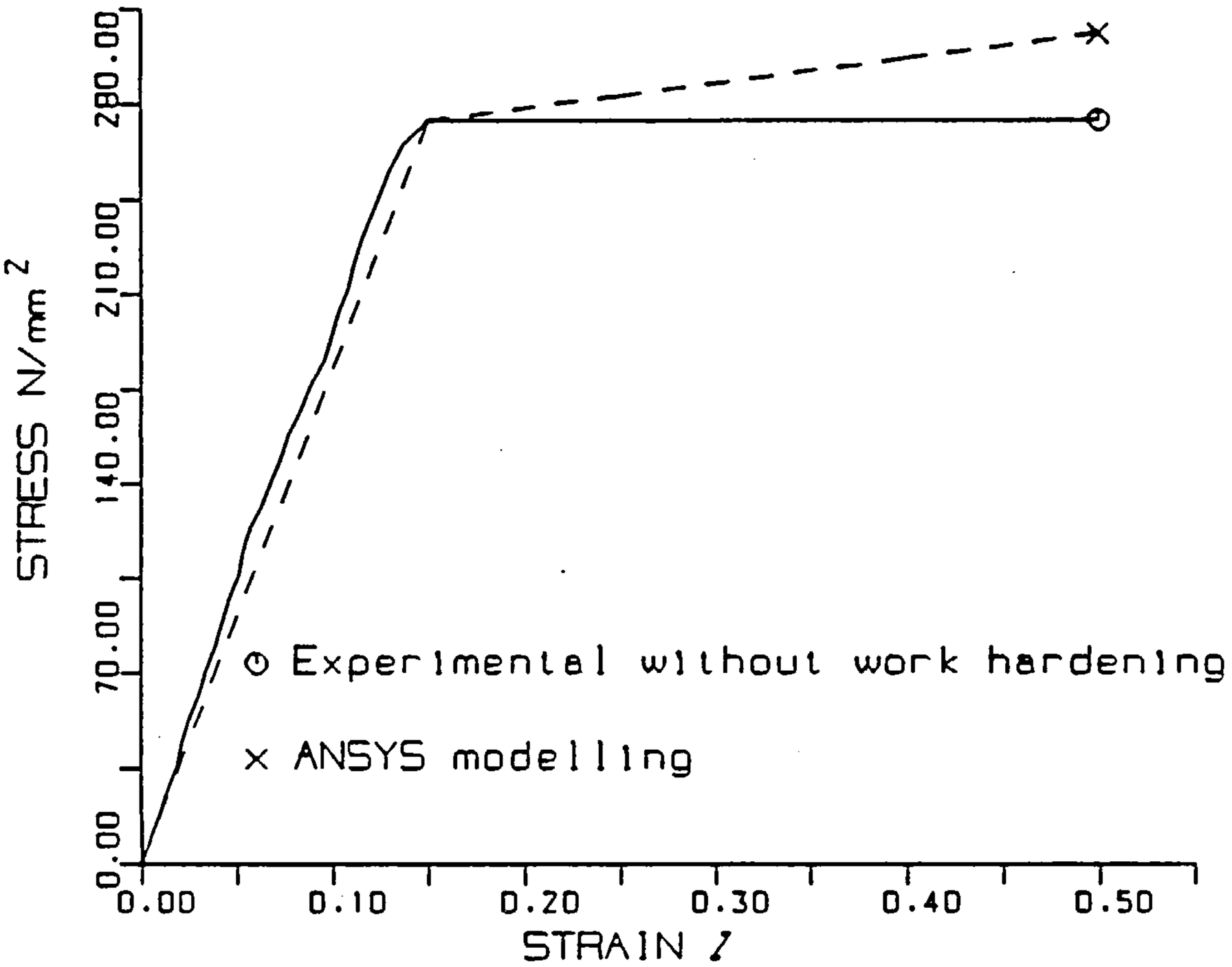


FIGURE (2.7) : STRESS-STRAIN CURVES FOR THE SLEEVE MATERIAL.

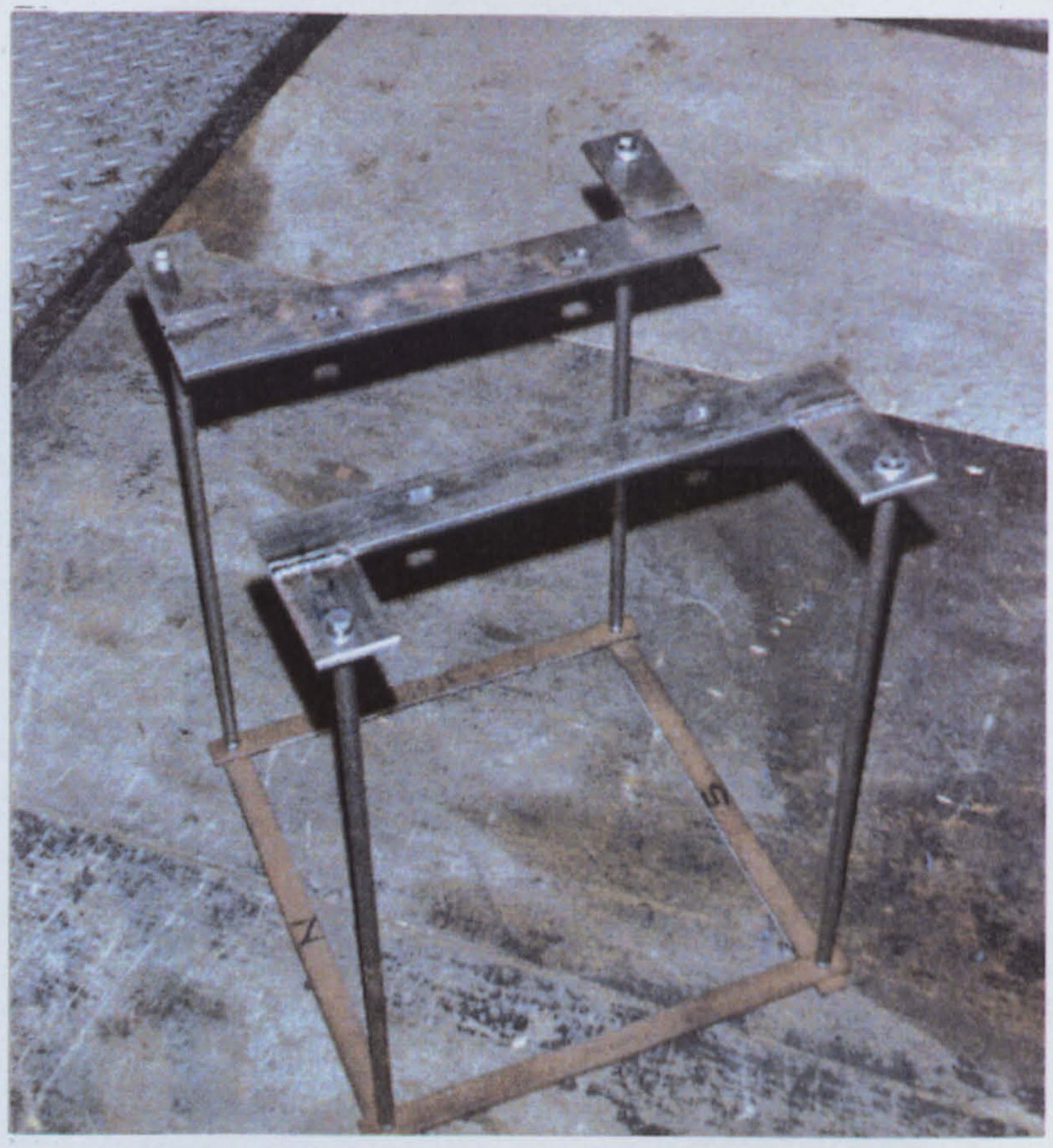

PLATE (2.1) : DETAILS OF THE STEEL MOUNTING FRAME USED FOR HOLDING THE TRANSDUCERS IN ALL TESTS.

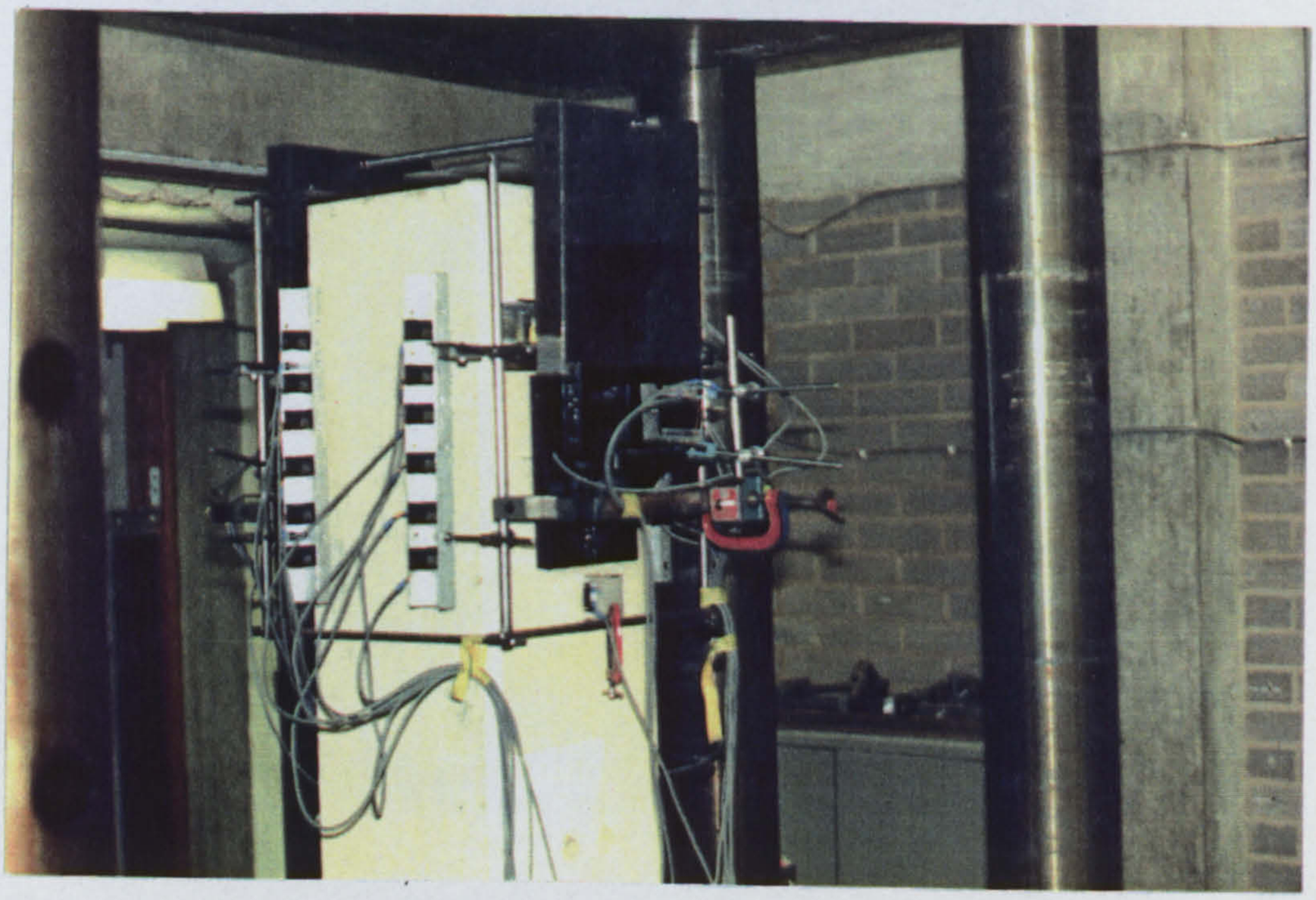

PLATE (2.2) : ILLUSTRATION OF TEST ASSEMBLY FOR A SINGLE-BOLTED JOINT WITH THE LOADING PLATES IN POSITION.

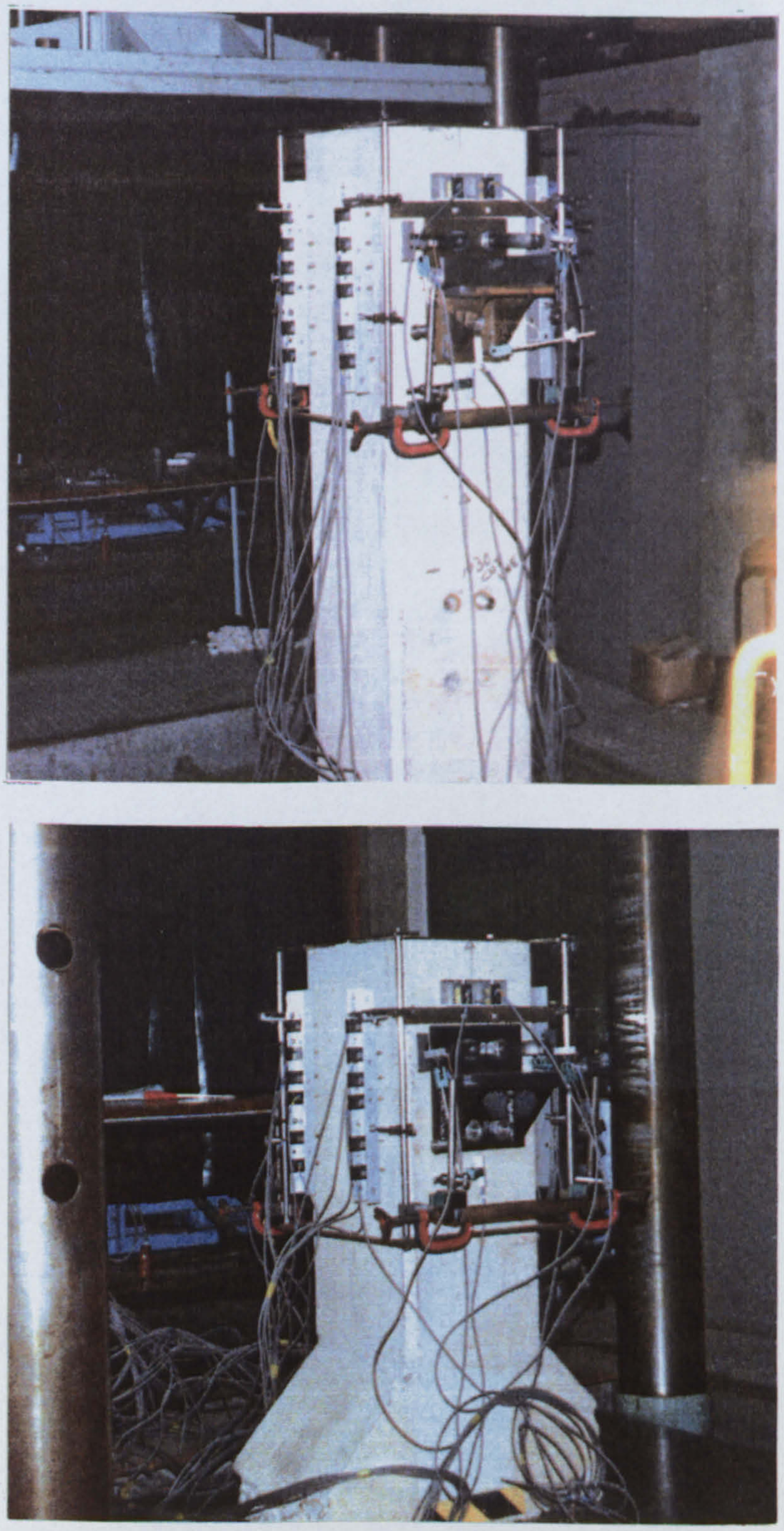

PLATE (2.3) : VIEWS OF TEST ASSEMBLY FOR THREE- AND FOUR-BOLTED JOINTS WITH THE LOADING PLATES REMOVED.

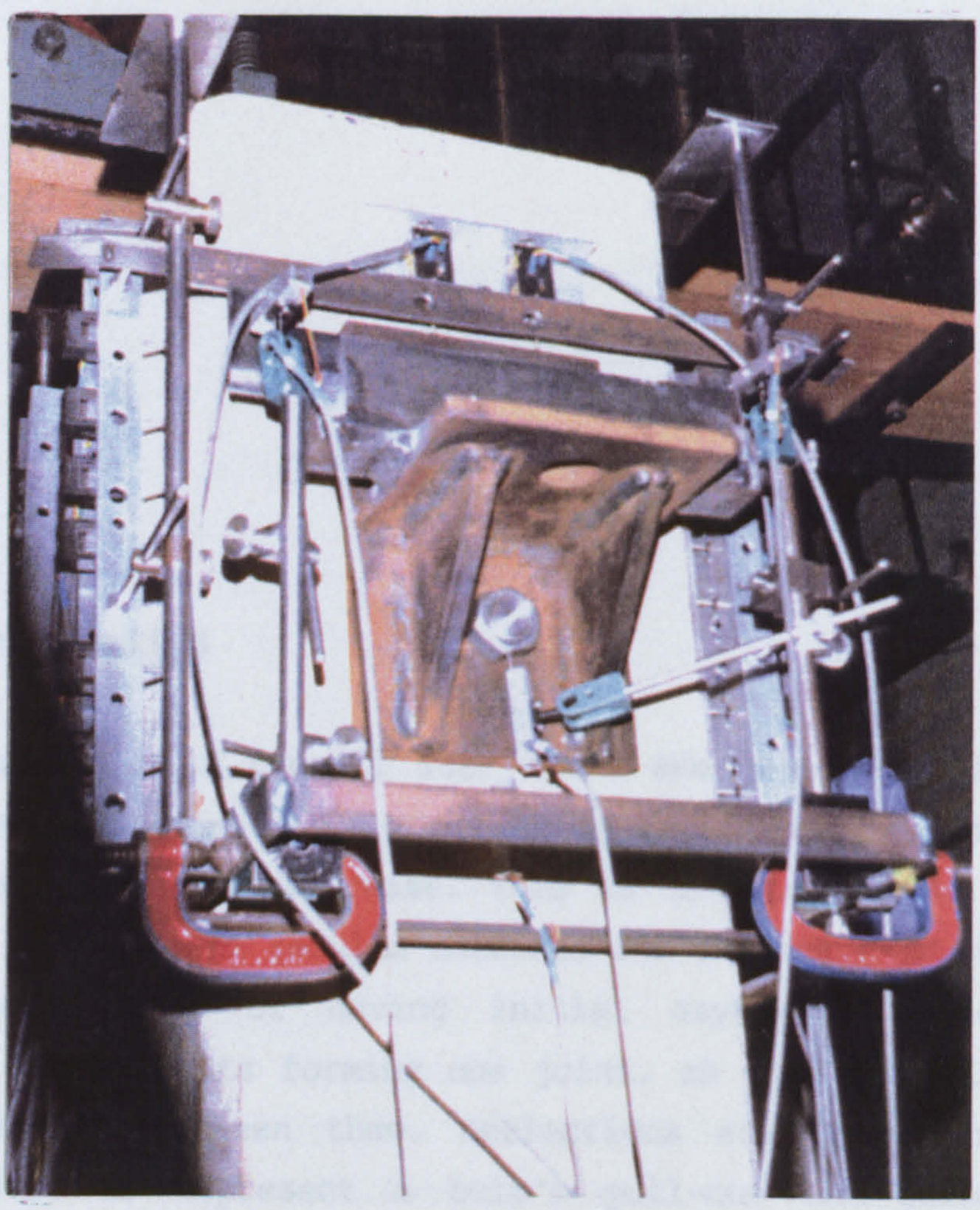

PLATE (2.4) : BRACKET CLOSE-UP SHOWING DETAILS OF THE TRANSDUCERS ARRANGEMENT FOR A THREE-BOLTED JOINT.

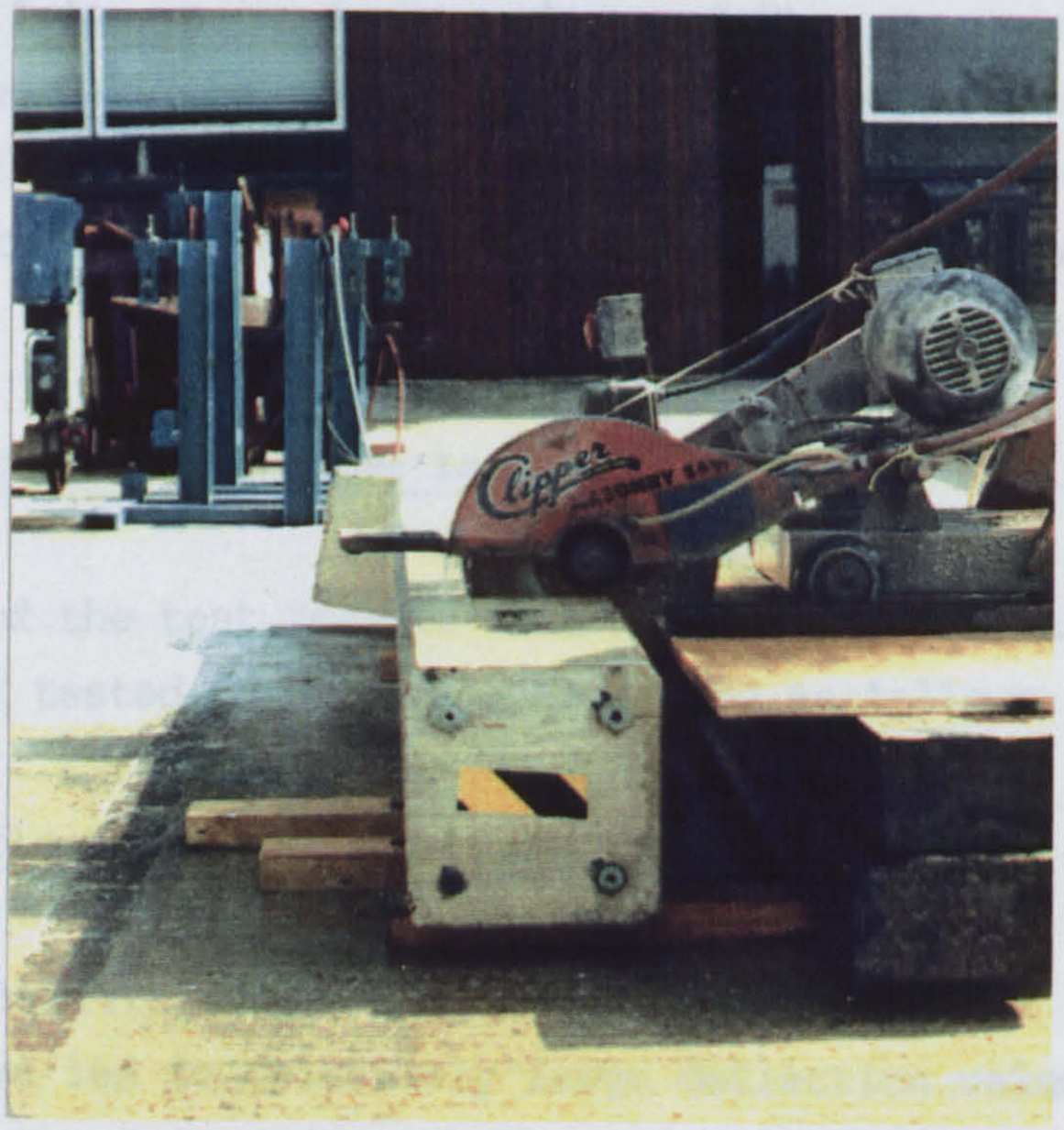


PLATE (2.5) : MASONRY SAW CUTTING THROUGH THE COLUMN AT A MARKED LEVEL.

# CHAPTER THREE

# DISCUSSION OF TEST RESULTS

## 3.1 Introduction

The main results for all four tests are given in this chapter. All loads used in the figures or in the discussion are per bolt end unless stated otherwise. This is to allow direct comparison to be made between results obtained for different joints. Despite the possibility of having initial asymmetry caused by the positions of bolts forming one joint, an even load distribution was assumed between them. Deflections are termed negative or positive, to represent a bolt's pull-out and drawn-in axial movement, respectively. Bolts are termed top and bottom when referring to their location in the joint. Also the bracket position is consistently indicated as A or B, as shown earlier in Figure (2.6). A number used to define a joint or a test corresponds to the number of bolts involved in the test, e.g. joint 2 indicates that there are two bolts forming this joint. At the end of this chapter, a summary of the important findings is given.

## 3.2 Joint Behaviour under Loading

In view of the test results obtained, the structural behaviour of a typical tested joint can be described as follows:

### 3.2.1 Deflections and Rotations

During the first load increments, the bedding of the bolt onto the sleeve led to relatively large deflection values. On further loading, the bolt became well seated against the sleeve invert giving rise to a steady increase in deflection up to failure.

Just before failure, the vertical deflection rate reached its maximum value.

During the initial stages of loading, the bolt was pulled out at one end and drawn in at its other end. As loading continued, a steady increase in the pull-out deflection could be seen. By the time significant bending moment had developed due to the small load eccentricity from the column face, the rotation of the back plate was obvious and resulted in a further increased pull-out deflection. The maximum value for drawn-in movement at the other end was extremely small due to the presence of the concrete face.

### 3.2.2 Developed Stresses

Considering the equilibrium of vertical forces for a loaded steel bracket, the applied load must be equal to the sum of the forces carried by the bolts and the frictional force acting at the column face as shown Figure (3.1). This force arrangement creates a tensile axial stress in the part of the back plates above the level of load application. In joints 3 and 4, where bottom bolts are introduced, a compressive stress acts below the load application level. At any stage of load application, the axial stresses acting in the back plate of a typical joint can be represented by the diagram shown in Figure (3.2).

Depending on the back plate's geometrical dimensions, the above stresses may stretch or compress the plate, thus affecting the recorded deflections at its top and bottom. However, calculated values of the net expansion of a typical loaded plate were found to be so small that they had an insignificant effect on the recorded deflections. This was due to the relatively large dimensions of the plate.

As a result of load eccentricity from the column face, top bolts in tested joints were subjected to a tensile force in addition to the applied shear force. This combination of forces should have

an influence upon the joint ultimate strength. However, within the range investigated, the ratio of the tensile force / tensile strength per bolt was small, i.e. not large enough to cause a significant reduction in the joint ultimate strength. This was due to the small load eccentricity maintained during the tests compared with the back plate height (and thus its lever arm). Therefore, the effect of the tensile force on the joint ultimate strength has been ignored.

### 3.2.3 Friction Effect

Friction occurs in the lower, compressive contact area between the back plate of the bracket and the column face. To obtain the actual shear forces carried by the bolts at any stages of loading, the value of the corresponding frictional force developed in the contact area has to be known. In attempt to achieve this, the following assumptions were made:

1. The moment developed due to the eccentricity of the applied load is mainly resisted by two equal and opposite forces T and C as shown in Figure (3.1).

a) T is a tensile force carried by the top set of bolts.

b) C is a compressive force acting at the lower part of the back plate. Its magnitude varies across the plate width due to the presence of the bracket stiffening webs which attract more load. However, to simplify the analysis, the compressive stress is assumed to be uniformly distributed across the plate width.

2. The applied vertical force is resisted by both the reactions from the bolts in shear $R_b$ and the tangential frictional force $R_f$. The latter is assumed to be a function of the compressive force C.

3. The contribution of $R_b$ to the resisting moment is negligible compared with those provided by the above forces. This is due to its small eccentricity from the column face.

All forces and different lengths given in Figure (3.1) are defined and described in detail in Appendix I. In this appendix, it can be seen that by satisfying the moment equilibrium conditions for a loaded bracket, a value for the developed compressive force can be obtained. Then, from the fundamentals of friction, a value for the frictional force could be estimated at any stage of loading. A value of 0.66 was obtained experimentally for the static coefficient of friction between the concrete surface and the steel plates used throughout Tests 1-4.

### 3.2.4 Asymmetrical Loading

With the exception of Test 4, the column base was carefully centralized in the test rig before load application. This was done to ensure that the applied load was equally shared between the two brackets. However, the recorded difference in the axial movement at both ends of top bolts suggests the possibility of asymmetrical loading being developed during the test. As described earlier, top bolts experienced a pull-out deflection at one end and a drawn-in deflection at its other end during the initial stages of loading. This deflection trend might have affected the magnitude of the frictional force acting at each bracket-column interface, leading to asymmetrical loading between the two brackets under test. Although separate load cells were not used on each bracket, the following facts reduce the possibility of having asymmetrical loading in Tests 1, 2, and 3.

1. The machine top platten was denied any free rotation after the application of the first load increment. As a result, any load difference between the tested joints must be a minimum.

2. If the two applied loads did differ by any significant amount, their resultant would have acted at a distance, s, from the column centre as shown in Figure (3.3). Since the column base was centralized, only experimental errors in the positioning of the column could have led to an eccentricity of the applied load. The calculation given in Appendix II shows that even if the resultant eccentricity, s, had a value of 10mm, this value would not introduce a load difference of more than 5.0%.

3. Failure was not obtained, as will be seen in this chapter, at both tested joints simultaneously. However, test results showed that the unfailed joints were themselves on the verge of failure. Bolt ends at these joints on both faces of the column exhibited severe deformation at the end of the test.

From the facts listed above, the effect of the asymmetry, induced at the initial stages of loading, may be ignored. That is, it may be assumed that each joint carries an equal share of the total applied load. Only in Test 4, the non-centralization of the column base has led to an obvious case of asymmetrical loading as will be seen in Section 3.6.

## 3.3 Test 1

In this test, a single bolt joint was tested until failure. The main observations can be summarised as follows:

### a) Mode of Failure

The joint failed by bolt shearing off on its end at bracket A. This failure happened with a loud noise at a load of 275 KN per joint. The failure load per bolt end was found to be 210 KN after deducting the calculated value of the frictional force $R_f$ as derived in Appendix I. The failed joint is shown in Plate (3.1). After failure, the condition of the bolt was examined and it was clear that the failure shear plane passed through the reduced

section at the root of the threads. Also it was obvious from the examination of the bolt that its other end had been severely distorted in shear.

b) Load-deflection Curves

From the graphs plotted in Figure (3.4), it seems that the load-vertical deflection curves for both brackets have the same trend. Apart from an edge curve at bracket B, all other curves for both brackets appear to curve in a similar pattern. Plotted deflection values were obtained after allowing for the bolt bedding onto the sleeve at the start of testing. By comparing curves of bracket A with those of bracket B, it can be seen that the ultimate recorded deflections are nearly equal. Also, the recorded bottom deflections, throughout the test, are less than those measured at the top edge for the same value of load. As there were no noticeable sharp increases in deflection values, a specific load value could not be obtained to represent the onset of yielding.

There should have been a linear variation in deflection across the width of the bracket's back plate. This is confirmed since the values recorded by transducer $T_1$ nearly represent the mid values between those recorded by both edge transducers throughout the test. This steady difference in deflection values between the edge curves supports the occurrence of small induced in-plane rotations of the bracket. This might have been caused by the existence of bolt tolerances at the early stages of loading.

$T_1$ and $T_b$ curves were compared for each side individually. Assuming that $\kappa$ represents a ratio between their corresponding values at a certain load, changes in $\kappa$ values throughout the test was examined. The examination revealed that this ratio, for both brackets, continued to increase steadily after the occurrence of bolt bedding. At failure, $\kappa$ was found to be 0.84 and 0.92 for brackets A and B, respectively. The change in $\kappa$ values may be attributed to the following facts:

1. The load eccentricity from the column face caused an out-of plane rotation of the bracket. This allowed the transducer connected to the top edge to record larger values than that connected to the bottom edge.

2. At the start of loading, the static frictional resistance between the back plate and column face can be considered high enough to cause a reduction in the recorded bottom deflection values. As the load increased, this resistance was overcome and the plate continued to move down reducing the difference between the recorded values at its top and bottom, i.e. $\kappa$ approaches unity.

3. In contrast to the way in which the transducer $T_1$ was held in position, $T_b$ was fitted to a stand which had a remote magnetic base. In the first load step, an initial settlement of the stand might have occurred preventing the transducer from recording the actual bracket's deflection. On applying more load, the plate continues to deflect downwards compressing the arm of the transducer, thus recording its deflection. This is highly reflected in the $T_b$ curve of bracket A at the first two load increments.

At bracket B, one edge deflection curve, following the trend of bracket A curves, having lower deflection values than those representing the bottom readings. However, it only showed increasing deflections up to 115 KN. From that load value and onwards, it showed a constant deflection value. This seems to be as a result of a measurement problem. It is felt that this end continued to move downwards but for some reason the transducer attached to it did not carry on measuring (loss of contact). Assuming that this end stopped sliding and remained fixed in position at 115 KN does not seem to be true due to the following reasons:

1. No remarkable translation was recorded by the group 4 transducer, attached to this bracket, at 150 KN onwards.

2. The relation between the $T_1$ curve and the other edge curve had followed the corresponding one at face A without a big change. This change would be expected if the other end was fixed.

The stiffness of the joint, characterised by the slope of the load-deflection curve, remained more or less constant up to the last stages of loading. At these stages, a gradual decrease in the stiffness value could be seen. This continued until maximum load was reached.

Figure (3.5) shows the axial deflection for the bolt. At the first load increment, there was hardly any axial movement for both ends. Then the bolt was pulled out at face A and drawn in at its other end. As loading continued, a steady increase in the negative deflection could be seen. Just before failure, the rotation of the back plate was obvious resulting in more pull-out deflection at bracket A. As stated earlier, due to the existence of the concrete face the maximum value for the drawn-in movement at bracket B was relatively small

c) Bearing Stress

As the applied load on the joint increased, the upper curved surface of the bracket's hole deformed with the bolt bearing on the hole's side material. Initially this bearing stress was concentrated at the point of contact between the bolt and the bracket. Further application of load caused yielding of the bracket material, developing the contact point into an area of contact. This allowed for more embedment of the bolt which should have resulted in a more uniform distribution of the bearing stress. Under increasing load, this bearing stress between the bolt and the top of the hole caused deformation of this part of the hole. Bracket examination has indicated that high bearing

pressure only existed in a small area on the top of each hole causing this part to be ovalized in shape.

Another type of bearing stress has been created by compressing the sleeve against the concrete beneath its end. As a result, the concrete in this area was crushed and some local spalling was observed on the column face after the removal of steel brackets.

d) Concrete Movement

During the test, the concrete movements were recorded at both sides of each bracket. The expansion or contraction of the concrete could be determined from the recorded readings of every two corresponding transducers at one level up the column. As there were no visible cracks around the joint at any stage in the test it was not surprising to have no appreciable concrete movement recorded at any monitored level. This is thought to be due to the remarkably high concrete strength obtained.

A further contribution to the concrete strength is that the region below the bolt was highly reinforced by having closely spaced steel links adding to the confinement of the concrete. The effect of concrete confinement on the joint behaviour is investigated experimentally in Chapter 7. The high value of the steel yield strength must also have delayed, or even prevented, the yielding of any link placed beneath the joint.

e) Creep Effect

Two reading scans were taken for each load step. Two minutes were the difference in timing between them. The purpose of the second scan was to monitor the change in deflections under sustained load. By comparing the corresponding deflection values in both scans, it was found that the difference between every two values, for the same load value, is of hardly any significance. This trend continued until ultimate load was reached. Just before

Having a very slight change in the rate of deflection increase, the load-deflection slope remained almost the same throughout the test.

Compared with the deflections obtained in Test 1, those obtained in Test 2 for individual bolts (i.e. not for the bracket as a whole) had slightly larger values at the same values of load. However, at 150 KN they became nearly equal and thereafter the Test 1 deflection had increased much more rapidly until failure. As in Test 1, it was difficult to deduce a specific load value at which bolt yielding had begun. This difficulty arises from the fact that no large increase in the rate of recorded deflections could be found near failure.

The axial movements recorded at both ends of each bolt are plotted in Figure (3.7). As in Test 1, from the start of loading, a bolt was pulled at one end and drawn in at its other end. Due to the dominance of the bracket vertical deflection, a relatively small axial deflection rate could be recorded until the last stages of loading. At bracket B, the large deflection values experienced by the bolts' ends at the early stages of loading had a small reduction in value just before failure. Both ends at this bracket had a similar behaviour with a slight difference in values. It seems that positive deflections took place in the first two load steps when a slight difference between the loads carried by each bracket might have occurred. At bracket A, the developed moment at the back plate increased the rate of deflection as can be seen from load value of 150 KN onwards. It is of interest to note that the maximum recorded negative value of 1.45mm occurred at the bolt's end which also had the maximum vertical deflection at bracket A.

From Figures (3.5) and (3.7), it can be noted that if the bolt end experienced a positive deflection at the start of loading it becomes non-recoverable and the bolt's end will not have any negative recorded value at any stage of the test.

At bracket B, curve $T_1$ could not be produced from the experimental data as a result of having an error in reading the transducer. This was due to bending of the transducer's arm, which occurred immediately after the start of testing. Following the trend obtained from Test 2, this curve should have had deflection values more than the corresponding ones in curve $T_2$. This is demonstrated by the dashed line curve in the figure.

Axial movements for top bolts are plotted in Figure (3.9). Two ends had clear negative deflections since the start of loading. As in Test 2, the deflection rate is small after the bolts' ends had their initial deflection values at the start of loading. This is a result of the vertical deflection dominance. At the late stages of loading, the bracket rotation became more obvious leading to a higher deflection rate. This is highly demonstrated by the trend of plotted curves after reaching a load level of 125 KN. It was also found, as in Test 2, that bolts which had the highest values of vertical deflection also had high values of pull-out deflection. 2.85mm was the maximum value of the pull-out deflection at failure. This value was the maximum recorded axial deflection for all tests so far.

In highly stressed regions, local concrete spalling below the bolt's centreline level was noticeable after brackets' removal. Also friction marks were found at the interface between the back of each bracket and its corresponding column face, especially at the area below the level of the bottom bolt. The visual observation of this region provided a qualitative evidence of high pressure.

From both the examination and measurement of sleeves diameters after testing, these observations can be made :

1. The maximum vertically measured diameter was 30.70mm, this value corresponds to the bolt at which the maximum recorded vertical deflection at bracket A.

2. At both faces, the measured diameters indicated that there is a difference in deflection experienced by top bolts.

3. Compared with the top bolts, the bottom one at face A had carried the least load value as its measured sleeve diameter, after testing, showed less value than all remaining sleeves.

## 3.6 Test 4

From the data obtained in the previous test, it was expected that failure load for the four bolts joint must exceed the testing machine capacity which is 1500 KN.

### a) Mode of Failure

At a load of 1150 KN on the machine's dial, the welds connecting both the horizontal plate and the webs to the back plate at face B fractured. Therefore, the test was terminated. By examining the welds after failure, it was discovered that the average value for the actual penetrations are 5.94 and 5.00mm instead of 8.0 and 10.0mm, as had been designed, respectively. Plate (3.3) shows the failed bracket. To have a representative value, a total of 16 readings were taken along the length of each weld. The measured values for the actual penetration are listed below in Table 3.1 while the actual values for weld loads are calculated in Appendix III.

| | | | | | | | | |
|---|---|---|---|---|---|---|---|---|
| Top Weld Measurements (mm) | 4.70 | 5.30 | 5.96 | 5.38 | 6.34 | 7.72 | 5.70 | 7.60 |
| | 5.64 | 4.46 | 5.76 | 5.42 | 5.54 | 8.16 | 5.86 | 5.60 |
| Web Weld Measurements (mm) | 5.12 | 5.26 | 5.18 | 4.92 | 4.80 | 5.08 | 4.84 | 4.84 |
| | 4.48 | 4.60 | 4.92 | 5.10 | 5.28 | 5.46 | 5.40 | 4.80 |

TABLE 3.1 : WELD MEASUREMENTS FOR THE FAILED BRACKET.

It was suggested that the test might be completed afterwards provided that new welds are provided for this particular bracket. However, it was felt that trying to reapply load on the bolts after releasing, then with the concrete already crushed beneath them would not give reliable measurements. Besides, it would be extremely difficult to fix the transducers back in their positions, just before failure, as they were shifted due to the bracket failure.

b) Load-deflection Curves

The curves shown in Figure (3.10), for each bracket, are almost identical, indicating that the top bolts, in each side, were sharing the bracket load almost equally. From the deflection rate, it can be seen that at the maximum recorded load the bolts were far from yielding.

From the start of loading and up to failure, the curves for top bolts are parallel for each bracket. The bottom deflection curves showed very small values of deflection in the early load steps. This may be attributed to an initial settlement experienced by the remote holders of transducers $T_b$ at this stage of loading. After reaching a load value of 25 KN per bolt, a steady increase in the bottom deflections was recorded for both brackets.

From the plotted curves, a wide margin can be seen between the deflections of both brackets. Throughout the test, bracket B was clearly moving vertically faster than bracket A. This was accompanied by noticeable local concrete spalling around bracket B. These observations suggest that there was a difference in load values carried by both brackets. This difference was due to the non-centralization of the column base in the test rig. Comparing the deflection values for both brackets led to the conclusion that the applied load was shared between brackets A and B in the ratio of 0.45 : 0.55. Allowing for the bracket-column friction

effect and assuming even load distribution among all four bolts, each bolt had a maximum load of 96.0 KN and 120.0 KN in bracket A and B, respectively. Deflection values versus the actual applied loads are plotted as dashed line curves in Figure (3.10). Despite the clear load difference between both brackets, the dashed line curves showed no apparent change in stiffness. This is mainly because bolt yielding has not occurred. From these plotted curves, it can be seen that the asymmetrical loading effect, in the joint's linear range, is not a very significant one.

Axial movements for the ends of top bolts are shown in Figure (3.11). No positive deflection had been recorded at either end. As in the previous joints, the steady small increase in deflection is recorded for most of the load increments. This is followed by a big increase just before the joint failure.

As has been reported in the previous tests, the bolt's end at the bracket which had the maximum value of pull-out deflection had also the maximum vertical deflection. This finding indicates that the column might have a tendency to rotate about one of its edges due to the compression of the soft board provided to eliminate stress concentration, see Figure (3.12). As the machine's top platten was rigid, one of the brackets had to experience more deflection to compensate for the column rotation. Thus there will be an increase in the load eccentricity from its corresponding column face. This deflection increase was reflected in both axial and vertical movements of the bolt's end.

In practice, when beams are mounted on the steel brackets, the first beam assembled will cause some sideways rotational deflection of one bracket. However, further sideways deflection under imposed load will be prevented by the very high rotational stiffness of the beams themselves. Consequently, the deflection values obtained from these tests should be higher than those likely to be achieved in a real building frame.

## 3.7 Bracket Vertical Deflection

In all tested joints, the vertical deflection curves demonstrated that the curves denoted by $T_b$ are showing less deflections than those recorded at the top (curves $T_1$ and $T_2$) throughout testing. In addition to the minimal effect of the axial stresses developed in the back plate, the difference in deflection can be attributed to two reasons, namely, transducer support settlement and geometrical imperfection of the back plates.

### 3.7.1 Transducer Support Settlement

As has been stated in the previous chapter, the transducers positioned vertically above the bolts in the top row were in direct contact with the top of the back plate. They were fixed in position in such a way to record any vertical deflection of the plate as soon as the load is applied. In contrast to this, the transducer positioned below the plate was remotely fixed by means of a stand connected to a magnetic base, which in turn is attached to the stiffening steel frame. Due to this way of setting up, the stand which acts as a support for the transducer becomes prone to an initial settlement at the first load step. If this settlement takes place, it will be also experienced by the transducer. As a result, the arm of the transducer may lose contact with the plate giving rise to very small recorded deflections as was seen in Tests 1 and 4. As the plate continues to deflect downwards the arm becomes compressed and deflection readings can be obtained.

### 3.7.2 Geometrical Imperfection

Another reason which might have had an effect on the difference between the top and the bottom readings is the geometrical imperfection found at the top edge of the back plates. It was found that the top edges which transducers were resting against had a slightly sloping face, i.e. the plate ends were not square.

This slope is towards the outer edge as shown in Figure (3.13).

At the start of loading the transducer arm was in contact with a point nearly at halfway of the back plate thickness. As the applied load increases and due to both the vertical deflection and rotation of the bracket, the transducer arm could not be in contact with the same point any longer. It came into contact with another point across the width of the edge. As a result of the edge slope, the level of the new point would be quite different from that of the initial one. Thus, the reading taken at this point would not be the same as if the bracket did not rotate. In Appendix IV, an attempt was made to calculate this difference in readings for a particular bracket depending on its measured geometrical dimensions and the deflections obtained.

## 3.8 Comparison of Joints Behaviour

Since the properties of all tested bolts are nominally identical, the data obtained for a single bolt in a joint can be compared with its counterpart in another joint. The specimen and loading being symmetrical, there should theoretically not be any unsymmetrical behaviour. However, occasionally imperfections in material or manufacture or different tolerances could lead to differences in deformations.

### 3.8.1 Strength

As the shear plane passed through the threaded portion of the bolt, the area based on the reduced diameter must be used in calculating the bolt stress at failure. For a standard 24mm bolt, the threaded cross section area is 0.7 times that of the bolt shank. Based on this area and the obtained failure loads for the tested bolts, the bolt shear stresses at failure of joints 1 and 2 were 663.1 $N/mm^2$ and 560.5 $N/mm^2$, respectively. The bolt shear stress at the end of Tests 3 was 557.3 $N/mm^2$.

From the obtained joints' failure loads, it can be concluded that the ultimate strength of a joint can be greatly affected by the density of the bolts. For the two-bolts joint, the ultimate strength was found to be about 1.7 times that of the single bolt. Also the three-bolts joint provided a capacity which is almost 2.6 times that of the single bolt joint. Such values of strength could not be compared with that recorded for joint 4 due to its premature failure by a different mechanism.

### 3.8.2 Stiffness

The stiffness of a joint is characterised by the slope of the load-deflection curve. The curves shown in Figure (3.14) illustrate the differences in stiffness for the four joints tested. Each curve, representing a joint, was obtained by taking an average of the top bolt deflections for the joint considered. The main features of the curves can be summarised as follows:

1. Compared with other joints, the single-bolted joint showed a lower stiffness at all stages of loading. The joint stiffness had its maximum value at the early stages of loading. On further loading, the curve exhibited continuous deterioration of stiffness up to the point of failure.

2. As expected, the addition of a bolt to a joint should make it stiffer. This is well pronounced at higher loads. As an example, at the ultimate load of joint 1 its deflection value was nearly 3.9 times that of joint 2 and 4.75 times that of joint 4. It is interesting to see that the effect of adding a bolt to the joint on its stiffness decreases with the increase of the original number of bolts per joint. This is clear by comparing curves of both joints 3 and 4 where the stiffness of the latter is only slightly higher.

3. Curve for joint 4 showed slight gain in stiffness after the application of a certain amount of load. The probable reason

for this change in stiffness is that bolt tolerances may have delayed having the full number of bolts, forming the joint, to be in contact with their mounting sleeves during the early stages of loading.

### 3.8.3 Rotational Rigidity

Under the application of a vertical load, the back plate of each bracket had gone through some rotation out of its original plane about a certain point. It is believed that this point is almost coincident with the bottom corner of the plate. This location was not obtained from readings. However, from the following facts it seems that this location is the most likely one.

1. The friction markings noticed on the concrete face, after testing, were developed with high intensity in the region close to the bottom edge of the back plate as shown in Plate (3.4).

2. By the time significant bending moment had developed, the bottom corners of the back plate had begun to press into the column face which provided a considerable support to the plate along the bottom edge. In consequence, the bracket appears to rotate around this point.

3. Under loading, the bracket pulls out at the top bolts level. In the meantime, the bottom edge is almost restricted from moving outwards by the compressive force acting at the lower part of the back plate.

It should be noted that by having more than two bolts per joint, this position of point of rotation can be changed. The point of rotation for joints 3 and 4 lies somewhere between the bottom corner of the back plate and the centreline of the bolts at the bottom level. The reason for this is that the bottom bolts take part in resisting the compressive force developed in this region.

Due to the eccentricity of the load from the column face, a moment is created at the concrete face. This moment which is responsible for the plate rotation tends to pull out the top bolts, creating an angle of rotation $\psi$, see Figures (3.1) and (3.13). Values of $\psi$ were computed and plotted against the induced moment values to represent the joint moment-rotation relationship. The M-$\psi$ curves for the tested joints are presented in Figure (3.15).

For a typical bracket, M values were given as the product of the applied load per bracket multiplied by the load eccentricity from the column face as shown in Figure (3.1). This was done to avoid any uneven load distribution between any top pair of bolts. On the other hand, $\psi$ values had to be calculated from the recorded axial deflections. A problem was faced at this stage as these deflections for individual bolts showed a positive deflection at one end and a negative one at the other end. To overcome this problem and to have more representative rotation values, it was decided to use the algebraic sum of deflections at both ends of a single bolt in computing the angle of rotation.

With respect to the behaviour of a joint under load, inspection of the plotted M-$\psi$ curves yields to the following observations :

1. As in joint stiffness, the curves show that the number of bolts per joint has an effect on its rotational rigidity. Compared with other joints, joint 1 has the lowest rotational rigidity while joint 4 has the highest one throughout all load values.

2. At the start of loading, joint 1 had a gradual increase in rotation. This was followed by an almost flat region indicating a continuous bracket pullout. High values of rotation were found just before failure. This was mainly due to the shear yielding of the bolt.

3. The small gap found between the back plate and the column face before loading commenced in Test 3, see Figure (3.16), might be the cause of having an inconsistent relationship between joints 2 and 3 up to a rotation 1.15/1000 radians. Obviously, as the load increased, the gap is reduced and the bottom bolt started to take part in resisting the moment, thus increasing the joint rigidity.

## 3.9 Summary

Although only a limited number of tests were performed it is felt that their results have indicated some points directly related to the effect of number of bolts per joint on its behaviour. Based on these results, the following conclusions can be drawn:

1. As a result of having a remarkably high concrete compressive strength and a heavy presence of steel links around the joints, the dominant mode of failure was bolt shear failure rather than concrete failure. The only exception to this was reported for joint 4 where a weld fracture failure took place. This incident showed how a different mode of failure can adversely affect the total strength of a joint.

2. As expected, the ultimate load capacity of a joint was greatly affected by the number of bolts per joint. For the two-bolts joint, the ultimate capacity was found to be about 1.7 times that of the single bolt joint. Furthermore, adding an additional bolt provided a capacity which is almost 2.6 times of that provided by the single bolt joint. Unfortunately the four-bolts joint strength could not be compared with these values as it had a premature failure.

3. Most of the bolts showed a significant shear deformation, at their loaded ends, prior to failure. Examining the bolt shanks against a flat surface, after testing, also indicated the

occurrence of some plastic bending about their longitudinal axes, see Plate (3.2). It was also clear that most sleeves had yielded at their ends forming ovoid cross sections.

4. The experimental load-deflection curves for brackets presented a reliable proof of increasing both the joint stiffness and rotational rigidity by having more bolts per joint. However, this effect became much less noticeable as the original number of bolts increased.

5. Finally, it should be mentioned that, throughout the tests, neither splitting cracks nor significant concrete expansion around the joint were observed although they could have been expected. This was mainly due to the high tensile strength of the concrete and the strong confinement provided by both the steel bracket and the surrounding steel links.

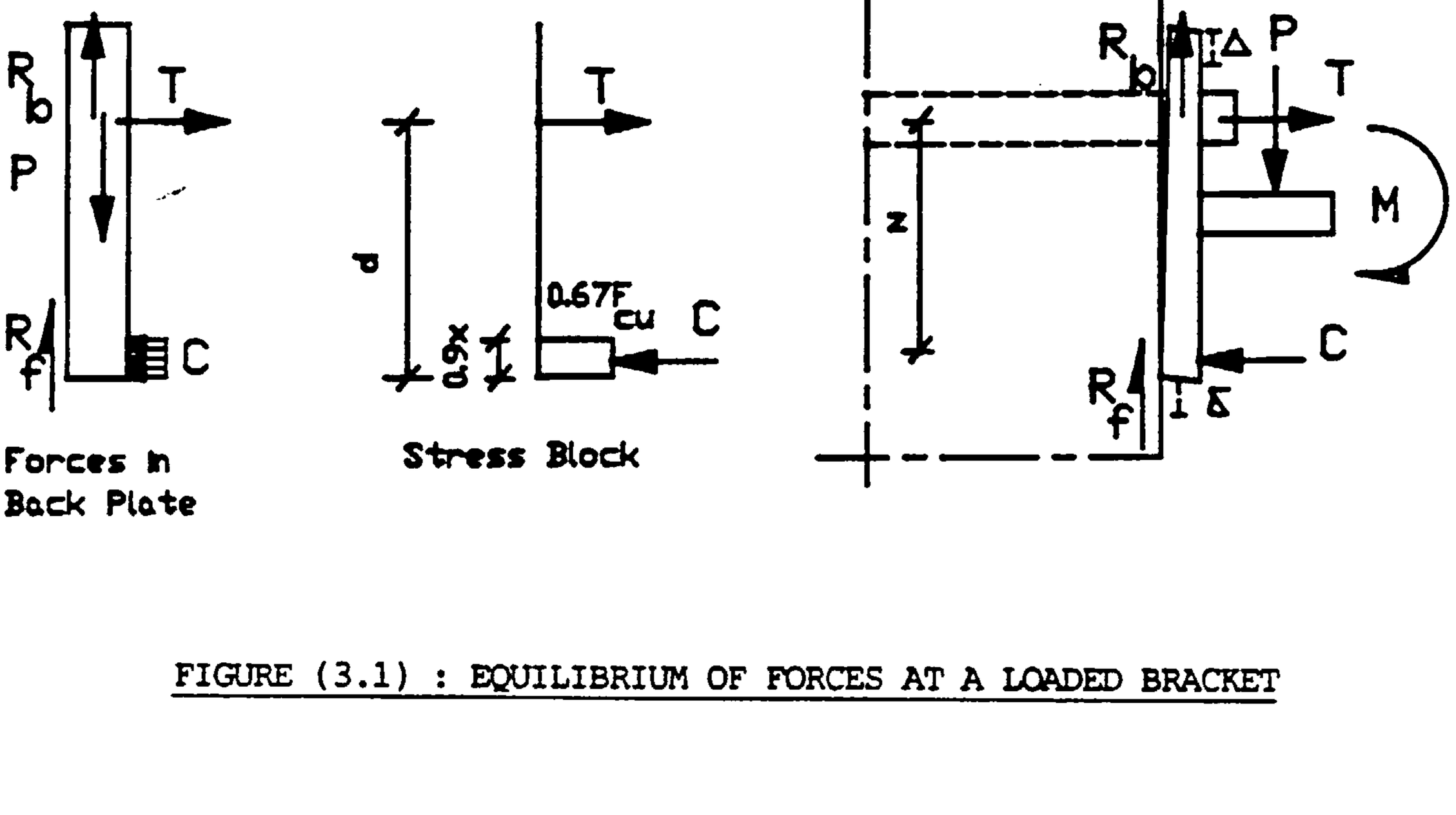


FIGURE (3.1) : EQUILIBRIUM OF FORCES AT A LOADED BRACKET

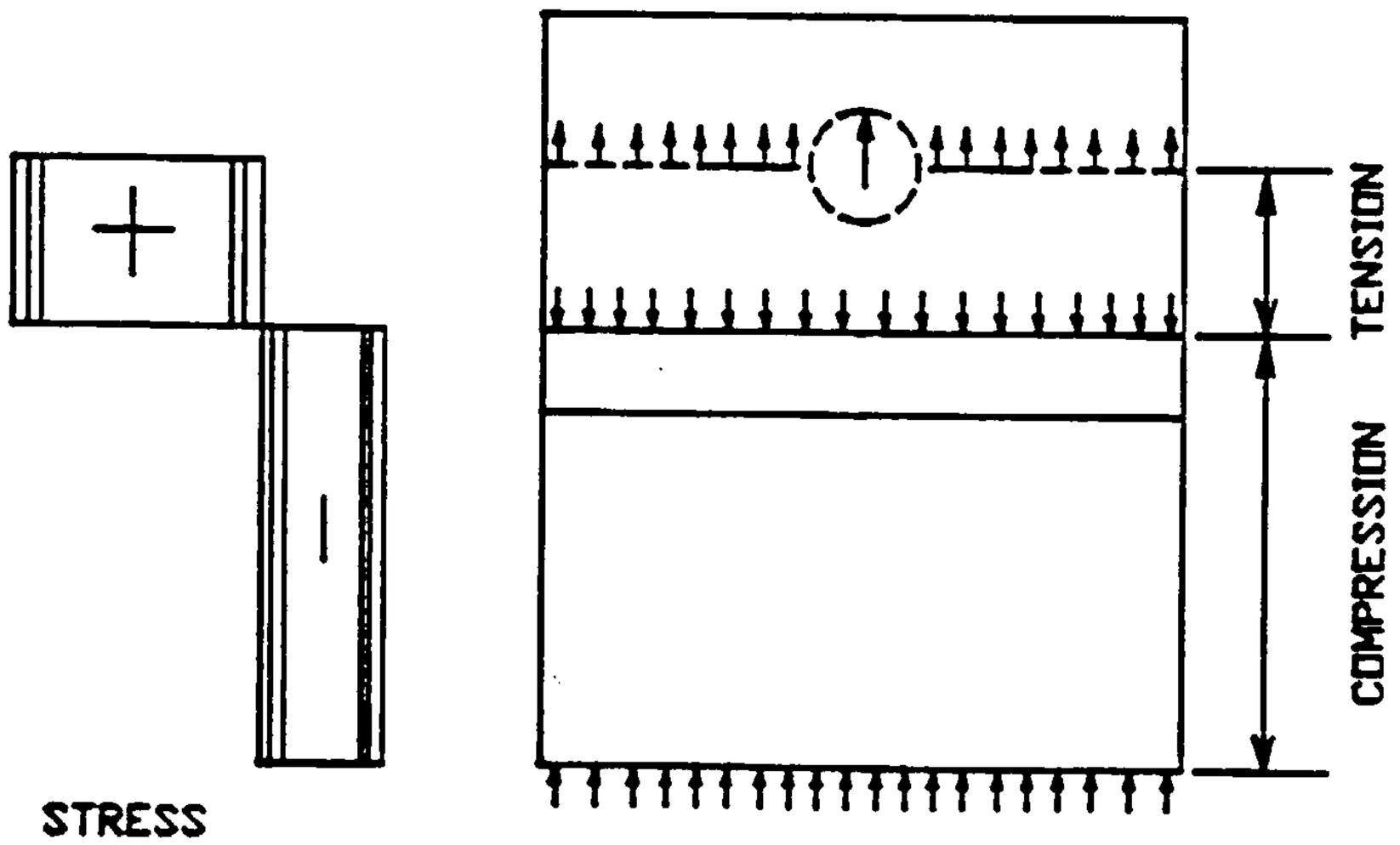


FIGURE (3.2) : AXIAL STRESSES ACTING IN THE BACK PLATE OF THE BRACKET.

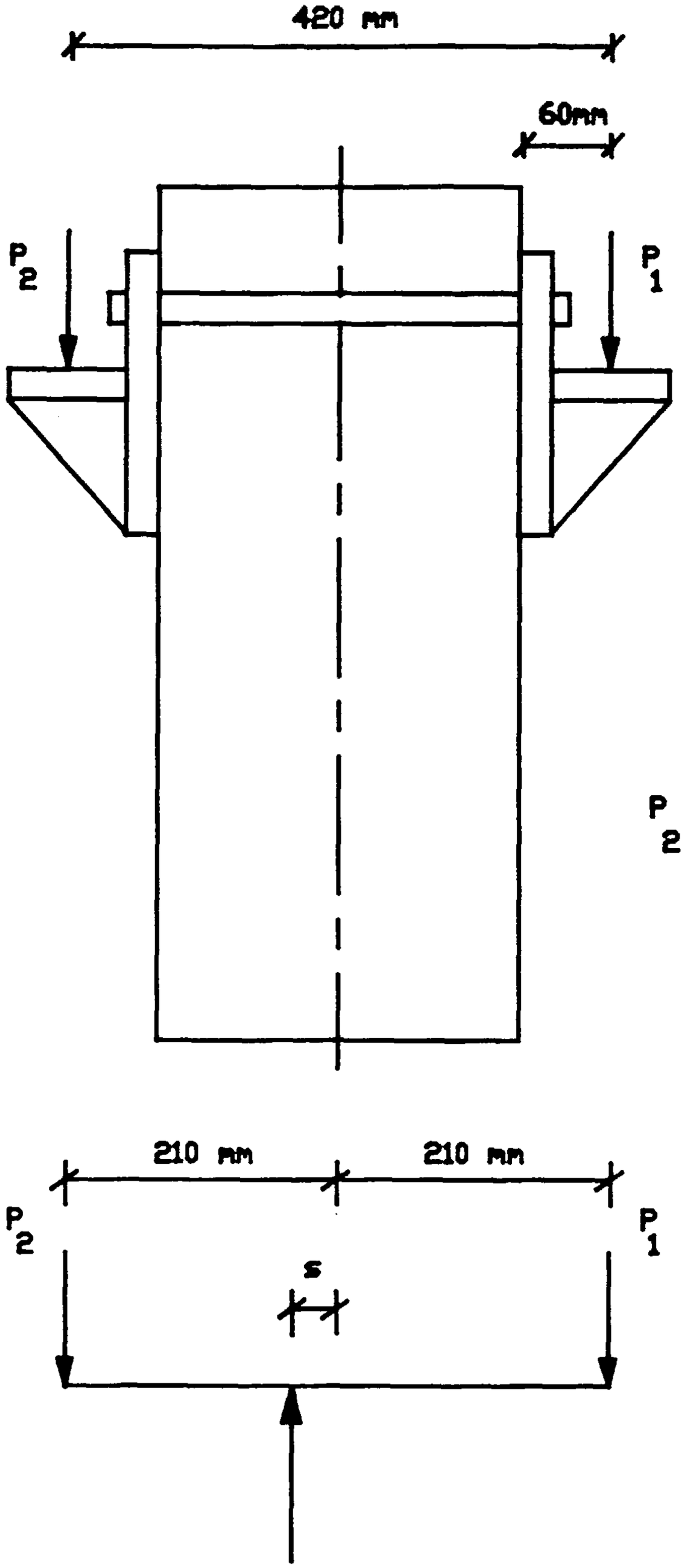


FIGURE (3.3) : EQUILIBRIUM OF VERTICAL FORCES DURING TEST.

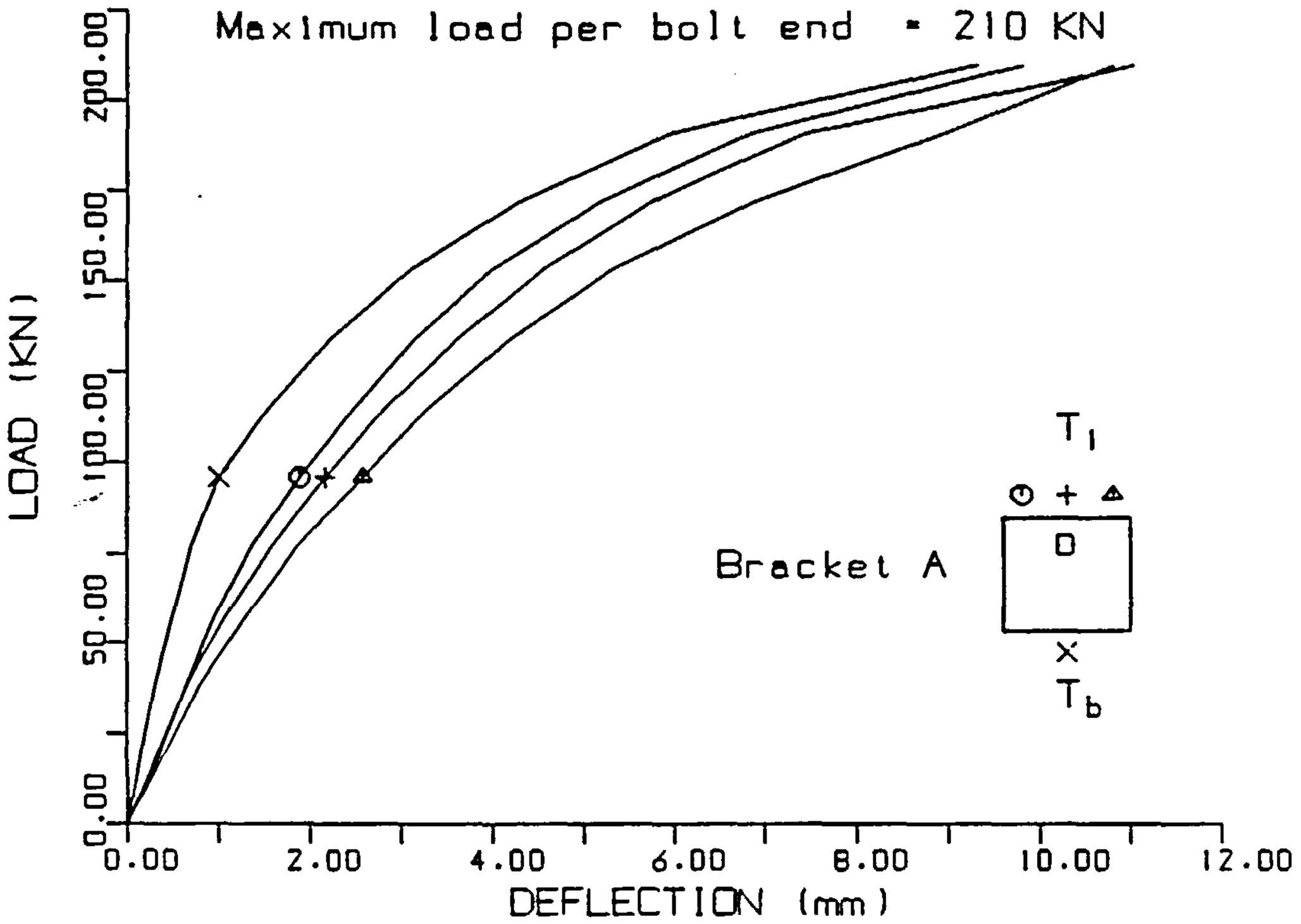


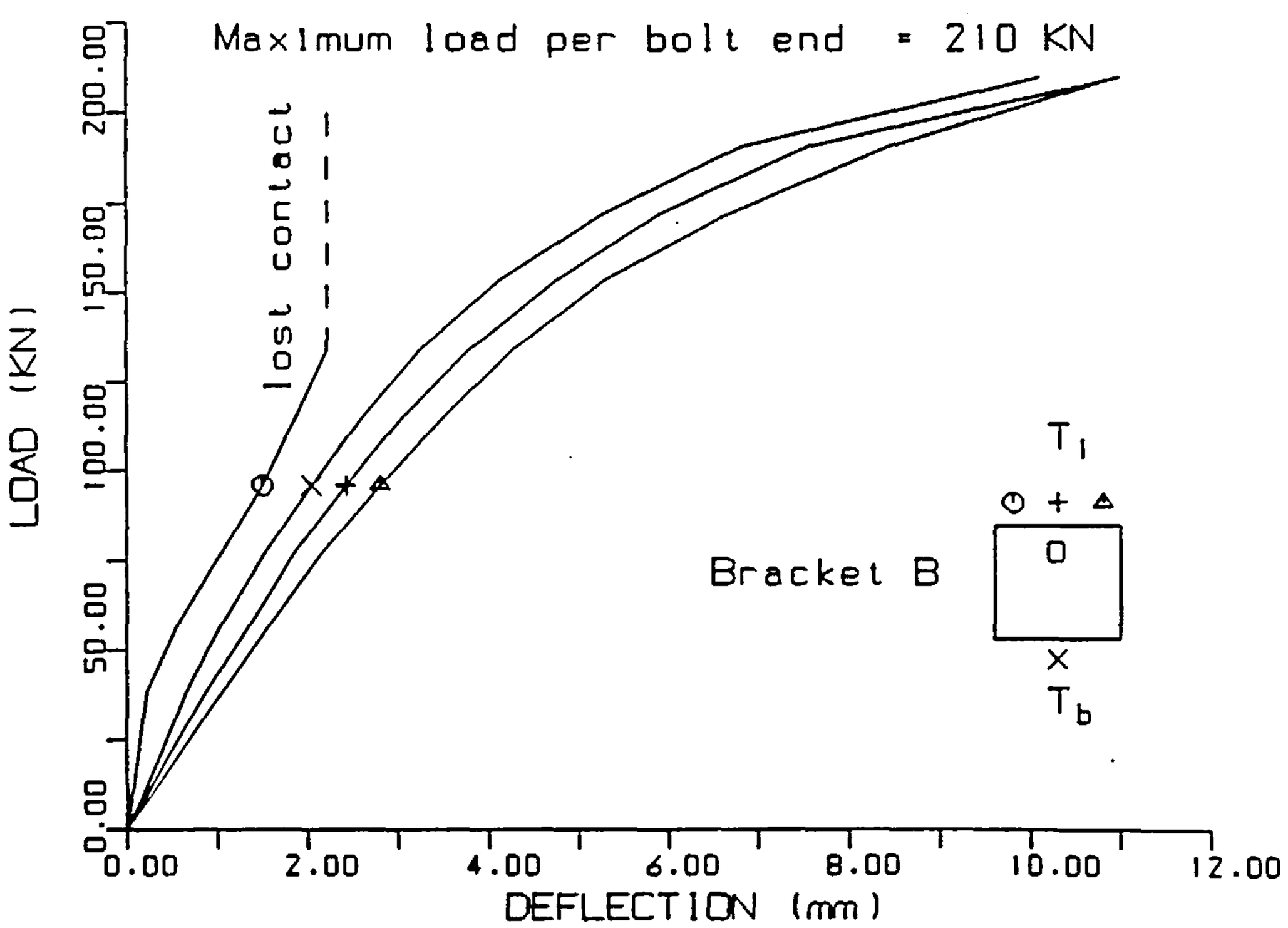


FIGURE (3.4) : VERTICAL DEFLECTIONS FOR THE SINGLE-BOLTED JOINT.

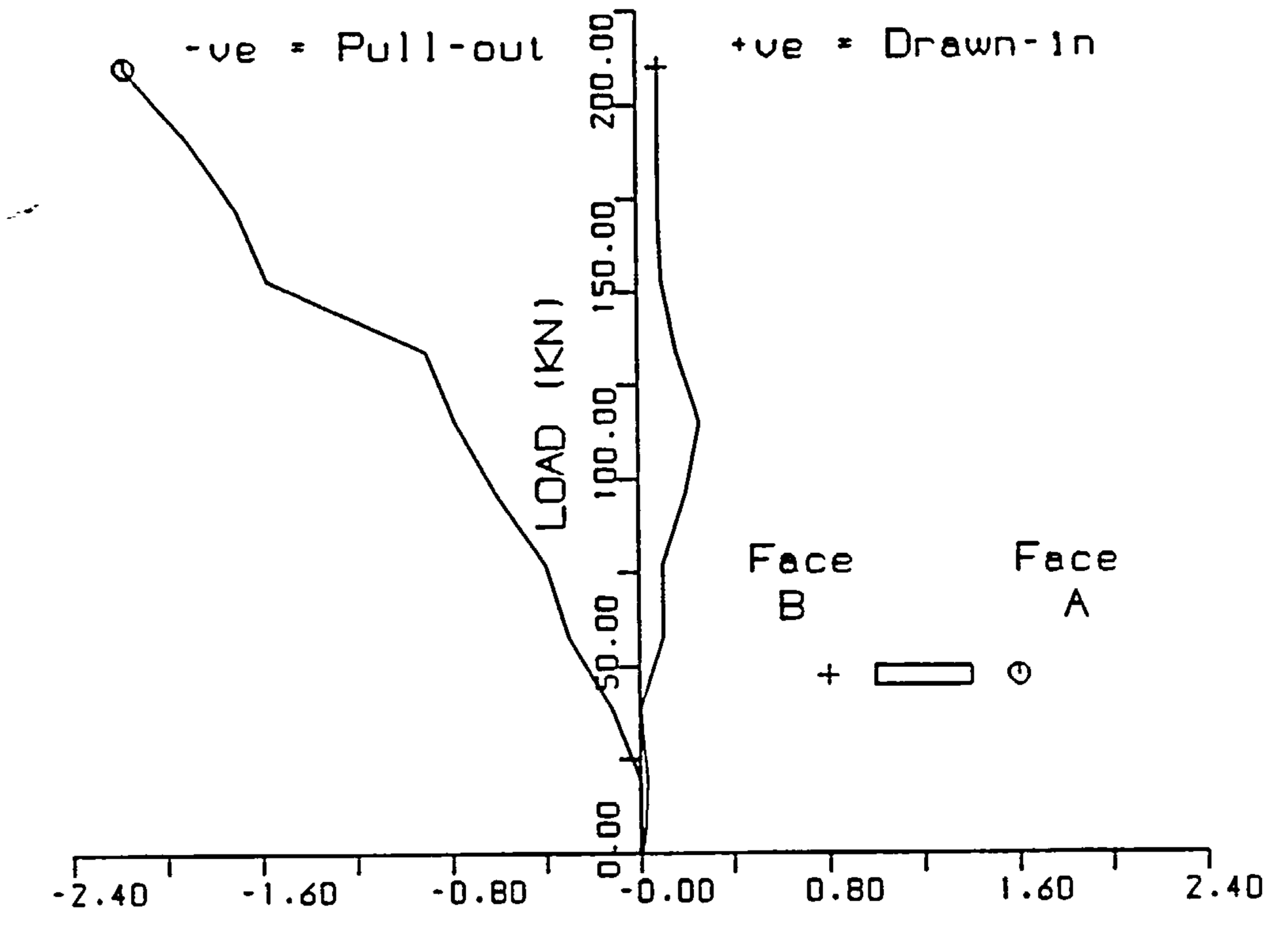


FIGURE (3.5) : AXIAL DEFLECTIONS AT BOTH ENDS OF THE SINGLE-BOLTED JOINT.

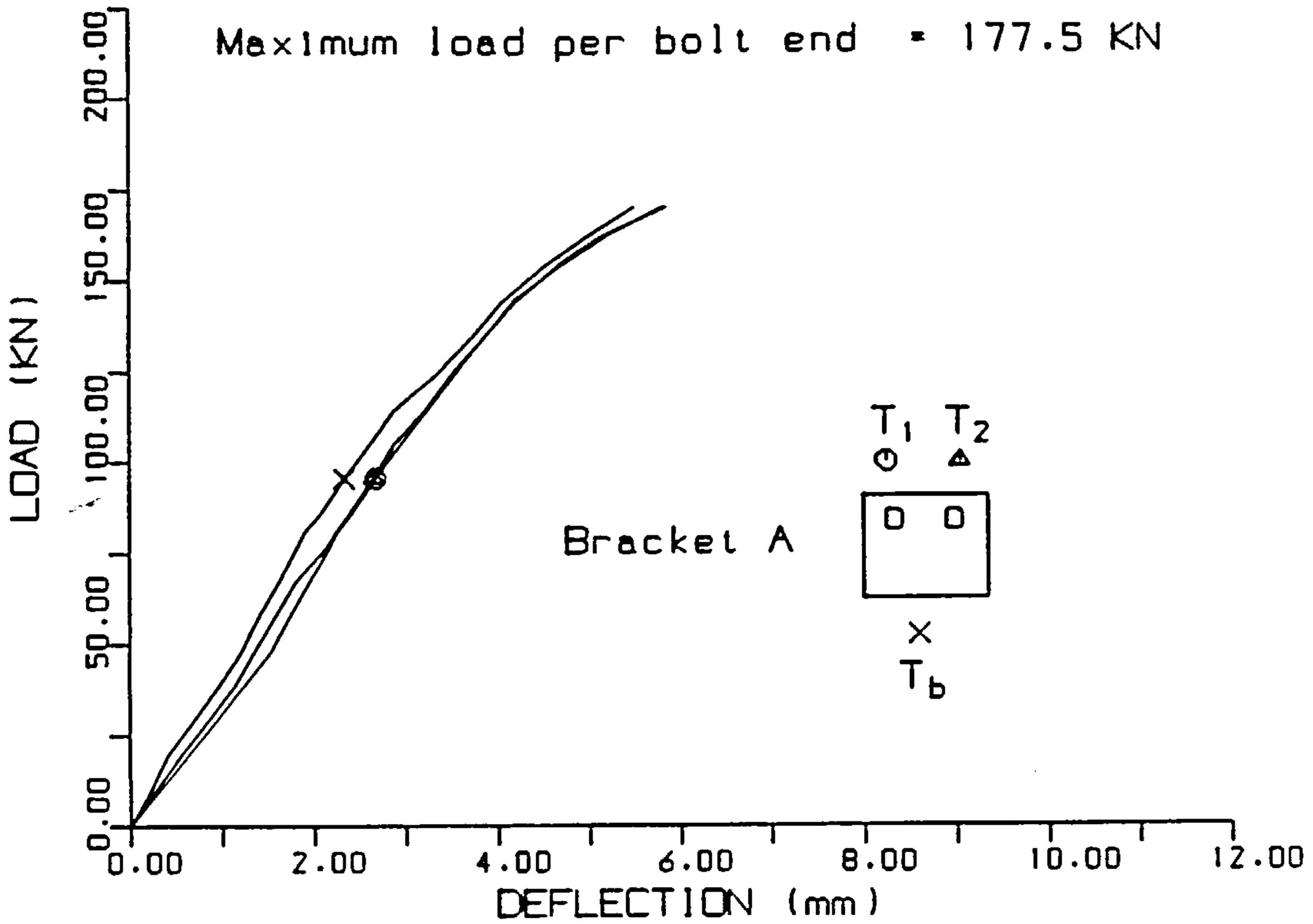


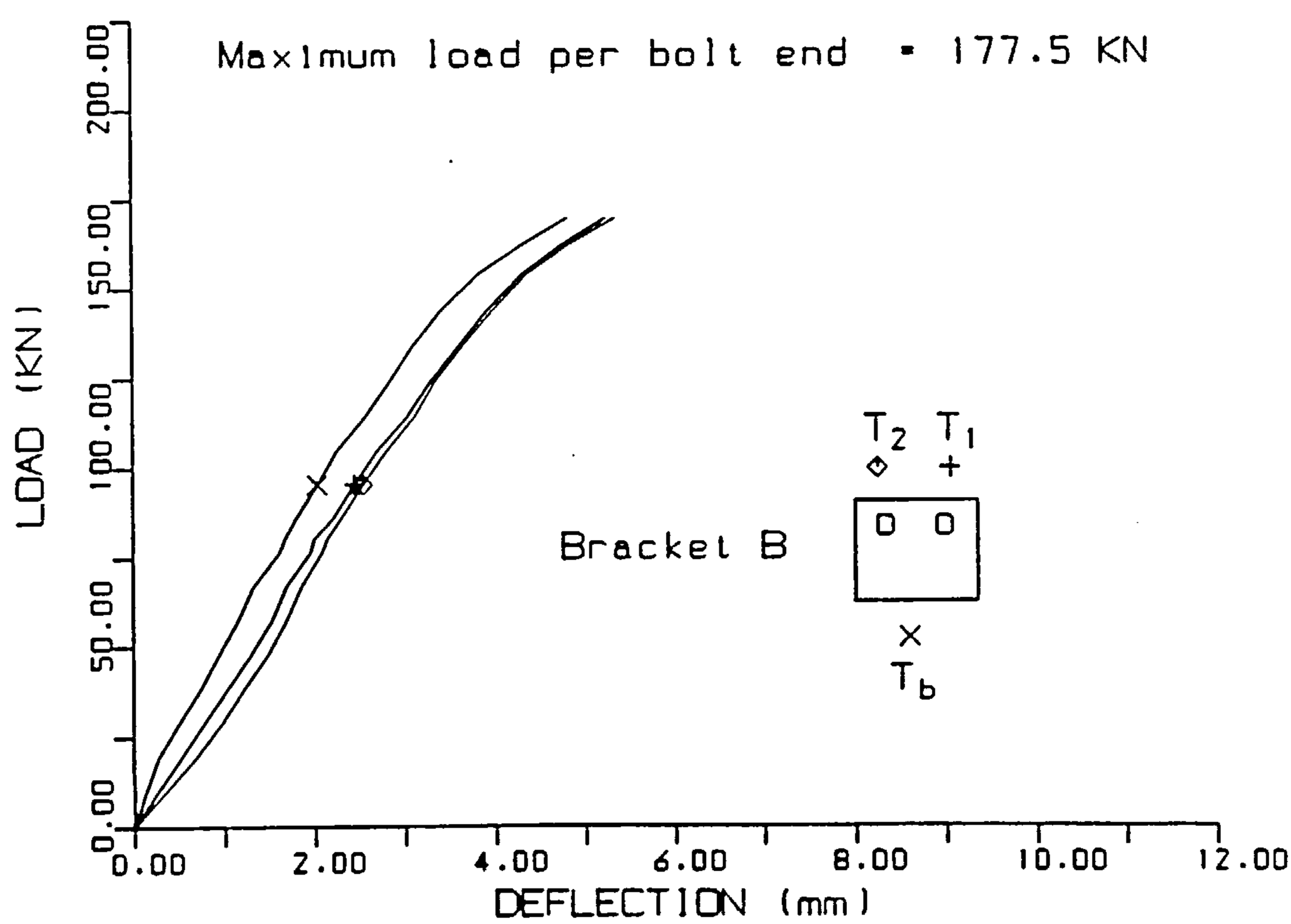


FIGURE (3.6) : VERTICAL DEFLECTIONS FOR THE TWO-BOLTS JOINT.

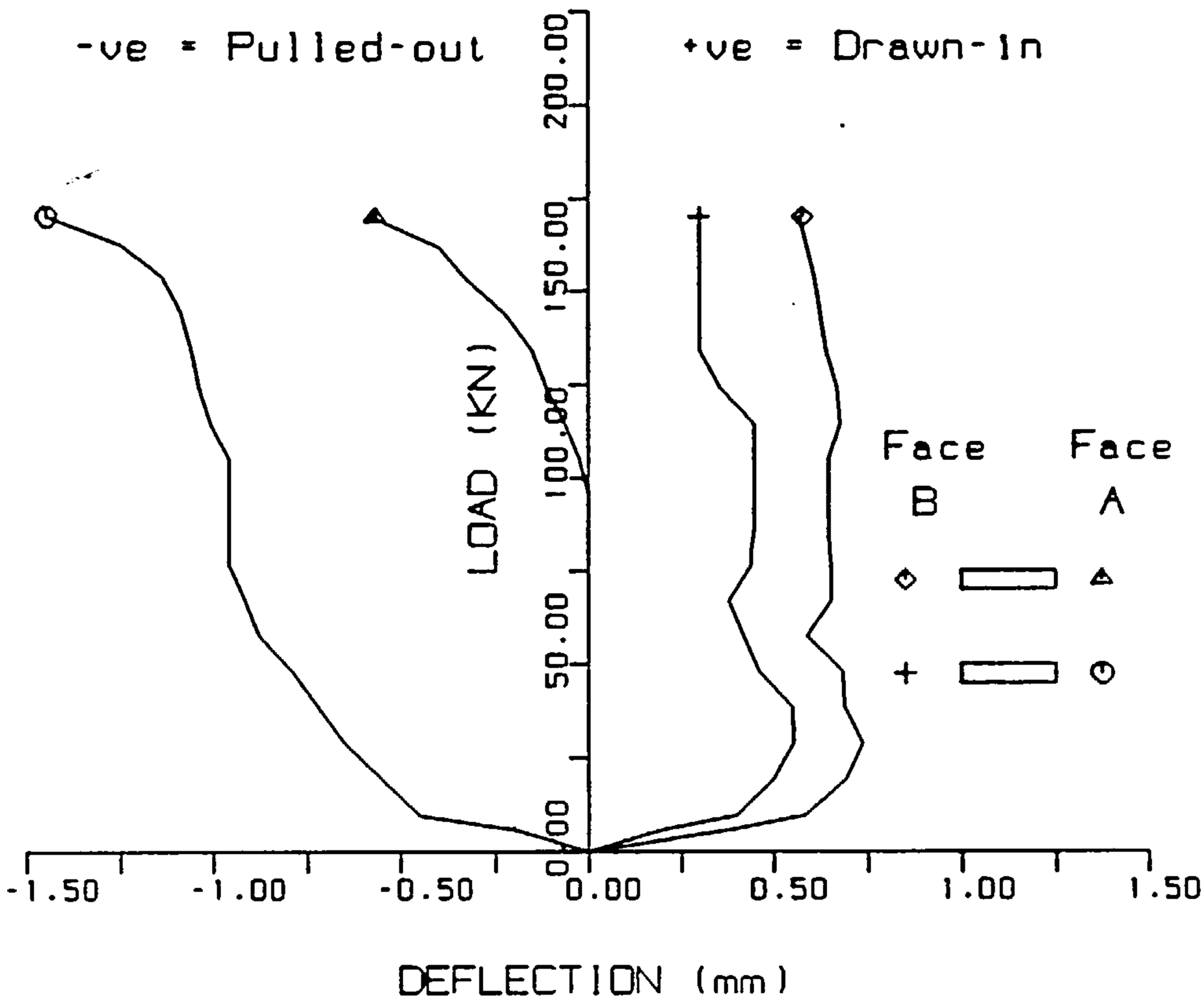


FIGURE (3.7) : AXIAL DEFLECTIONS AT BOTH ENDS OF THE TWO-BOLTS JOINT.

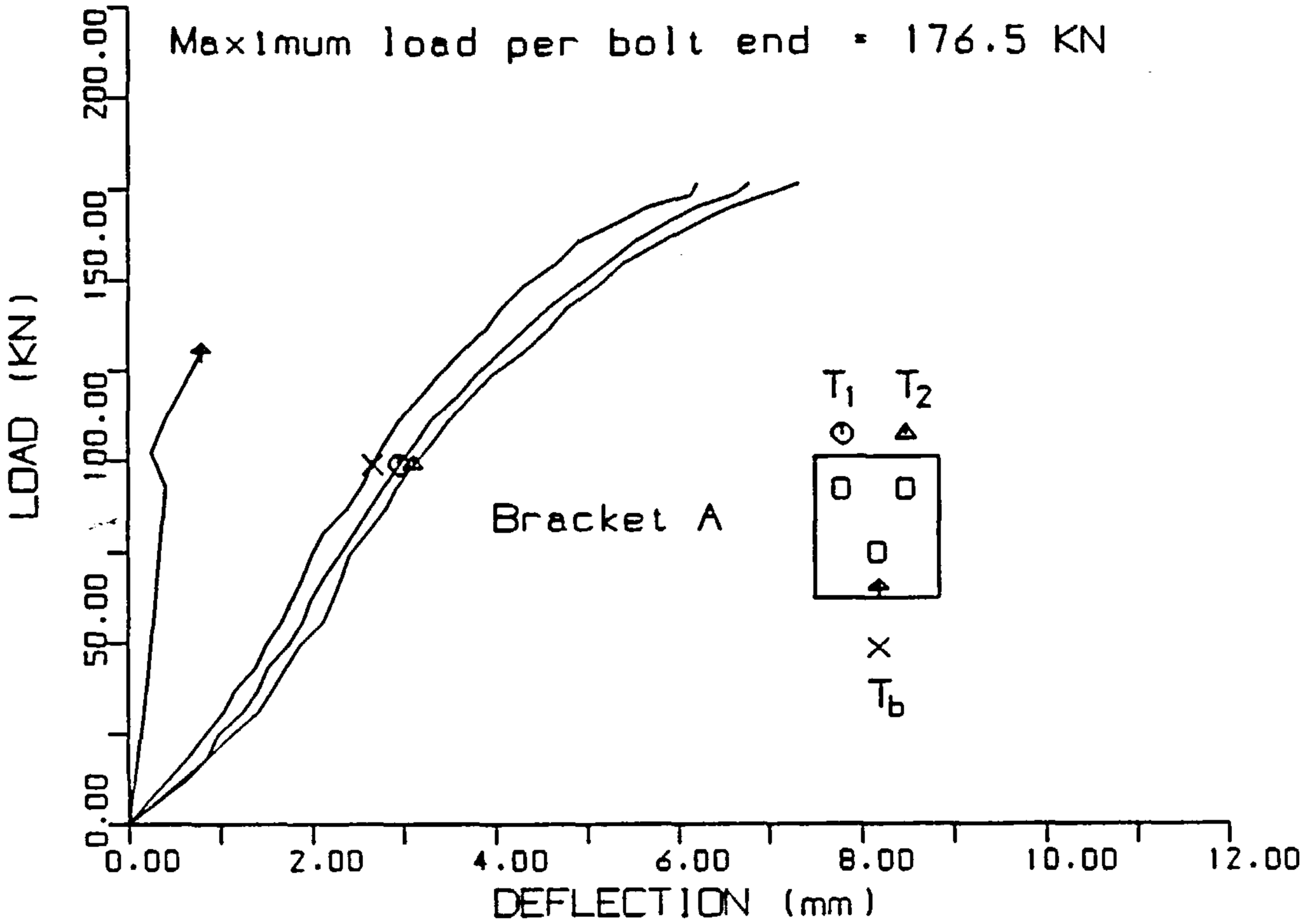


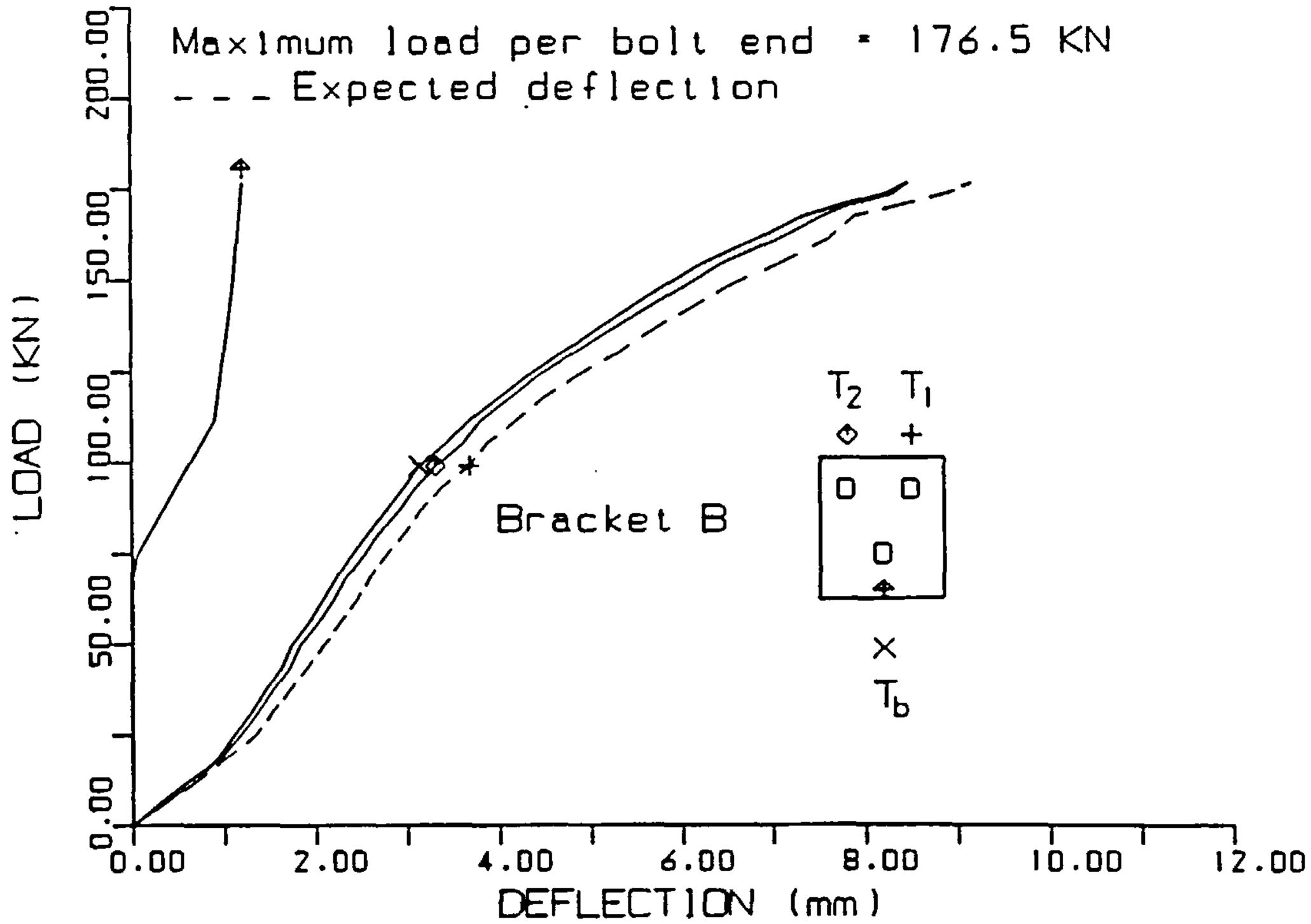


FIGURE (3.8) : VERTICAL DEFLECTIONS FOR THE THREE-BOLTS JOINT.

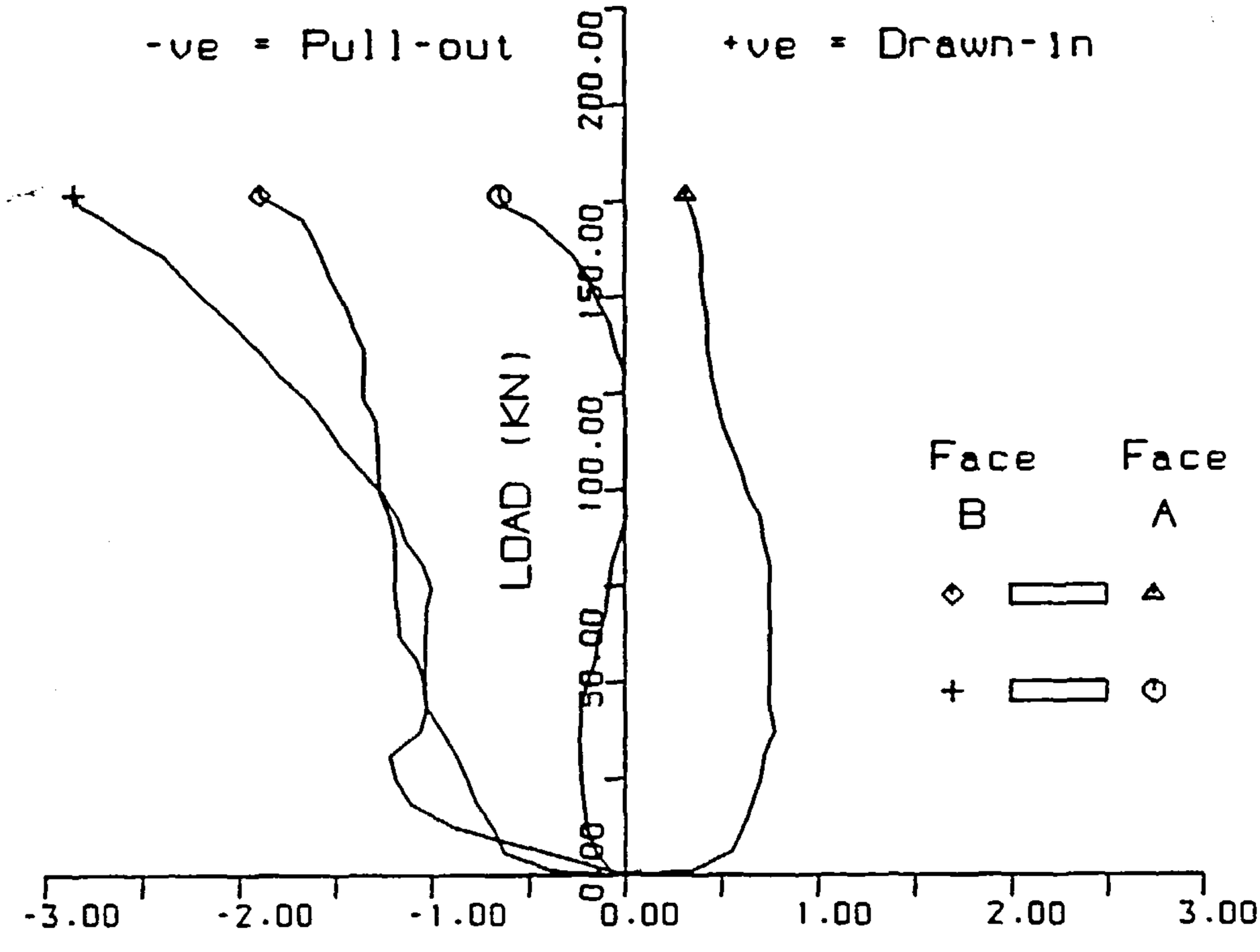


FIGURE (3.9) : AXIAL DEFLECTIONS AT BOTH ENDS OF THE TOP BOLTS IN THREE-BOLTS JOINT.

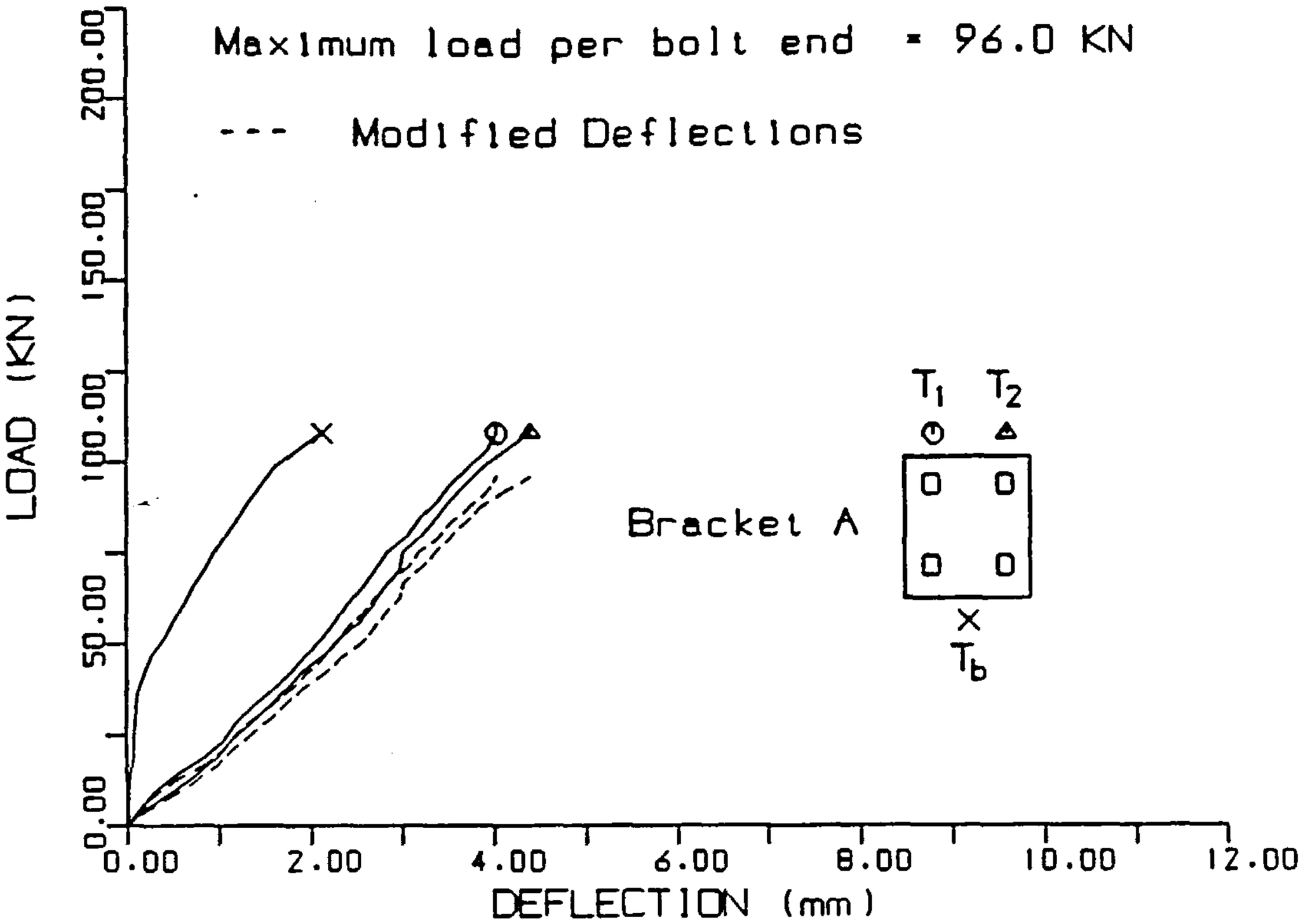


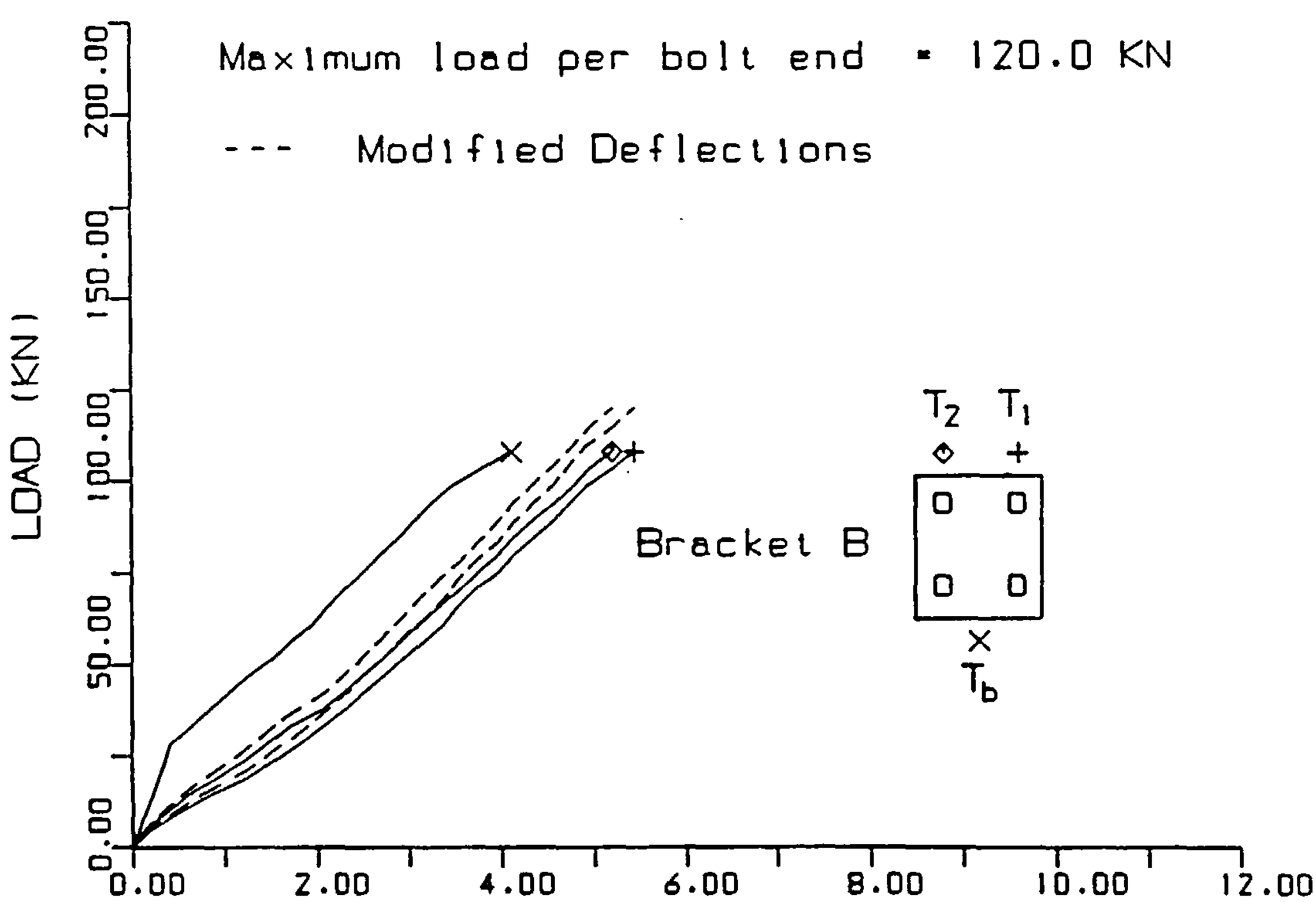


FIGURE (3.10) : VERTICAL DEFLECTIONS FOR THE FOUR-BOLTS JOINT.

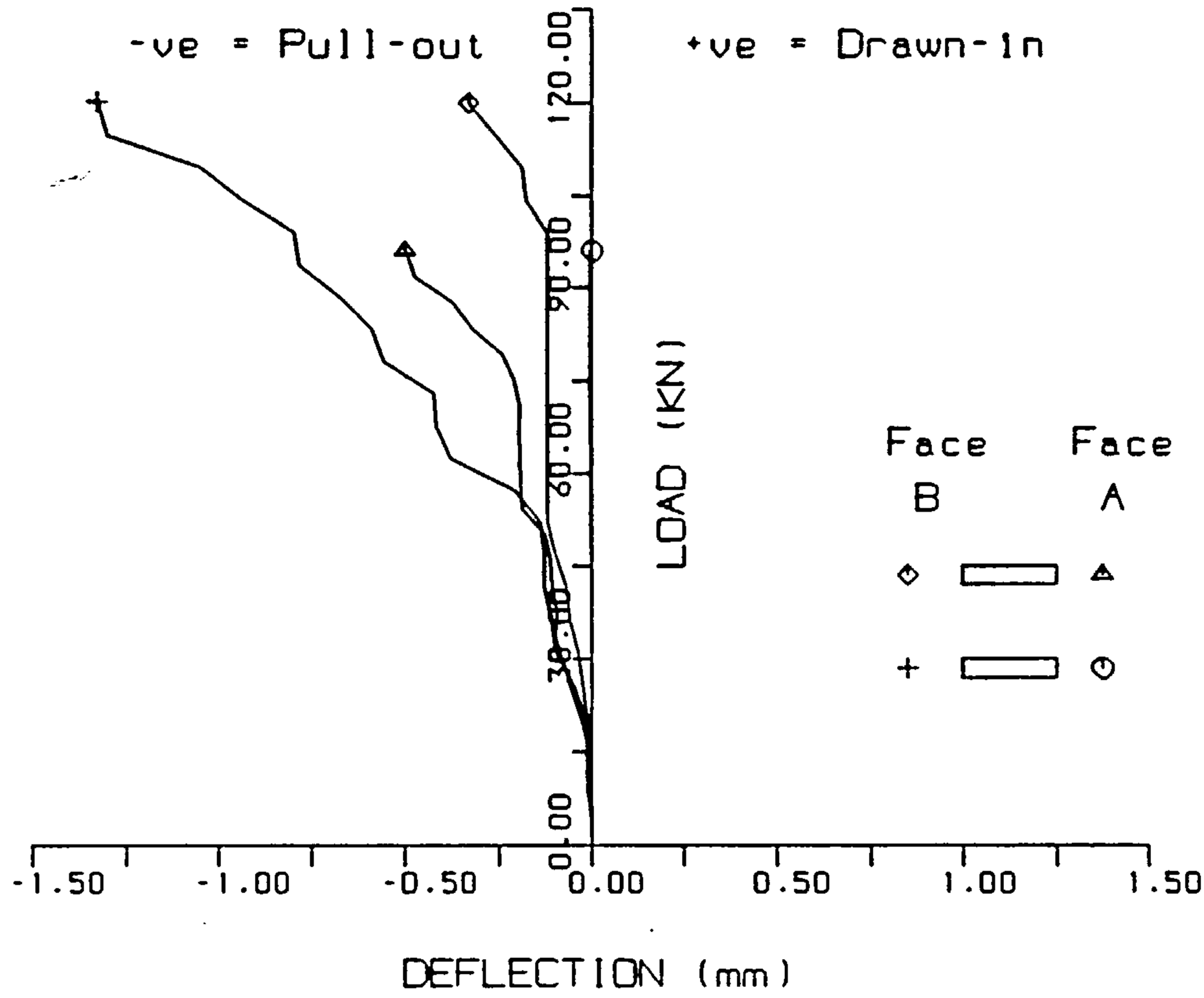


FIGURE (3.11) : AXIAL DEFLECTIONS AT BOTH ENDS OF THE TOP BOLTS IN THE FOUR-BOLTS JOINT.

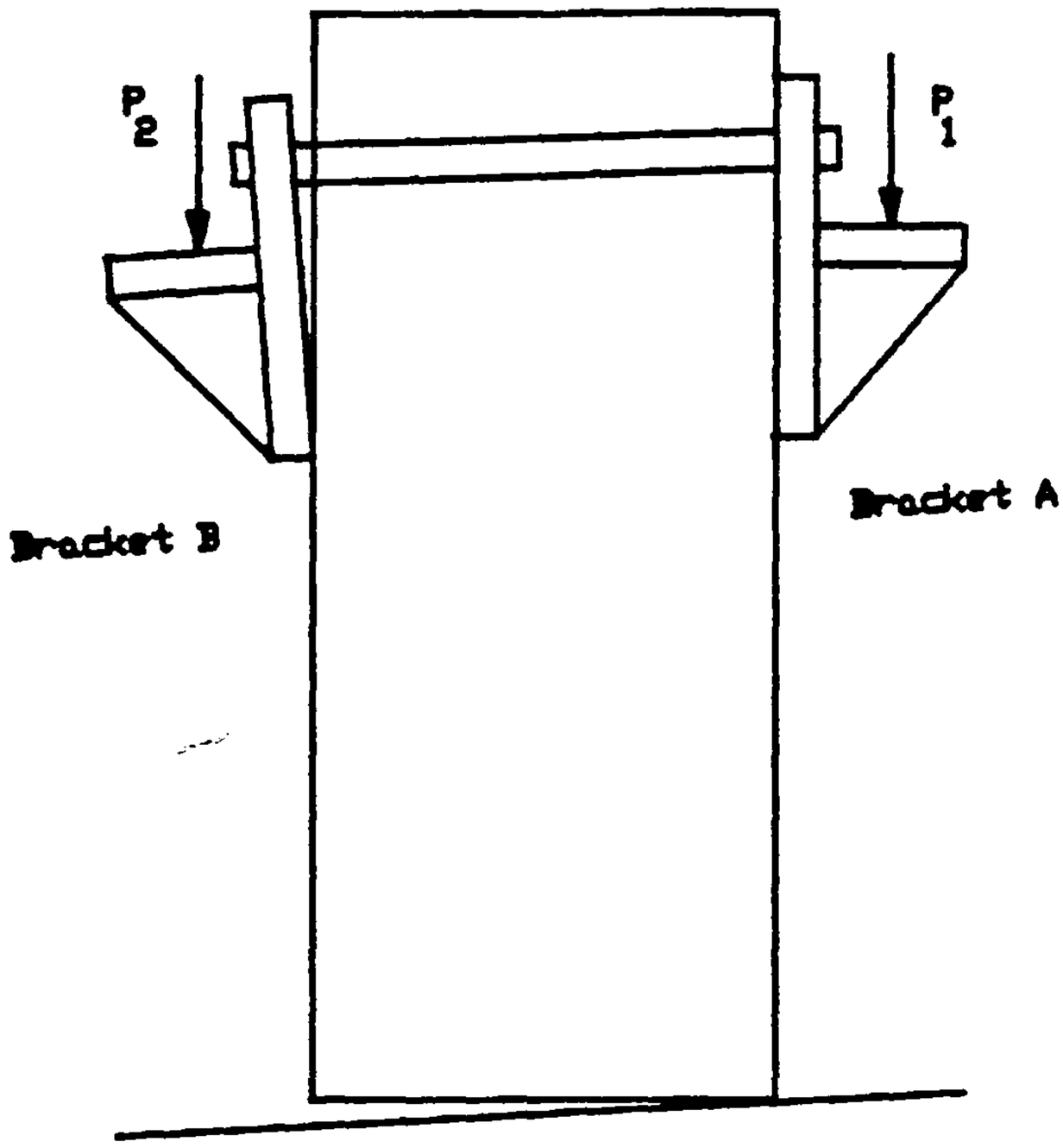


FIGURE (3.12) : EXPERIMENTAL BEHAVIOUR OF BRACKETS UNDER LOADING.

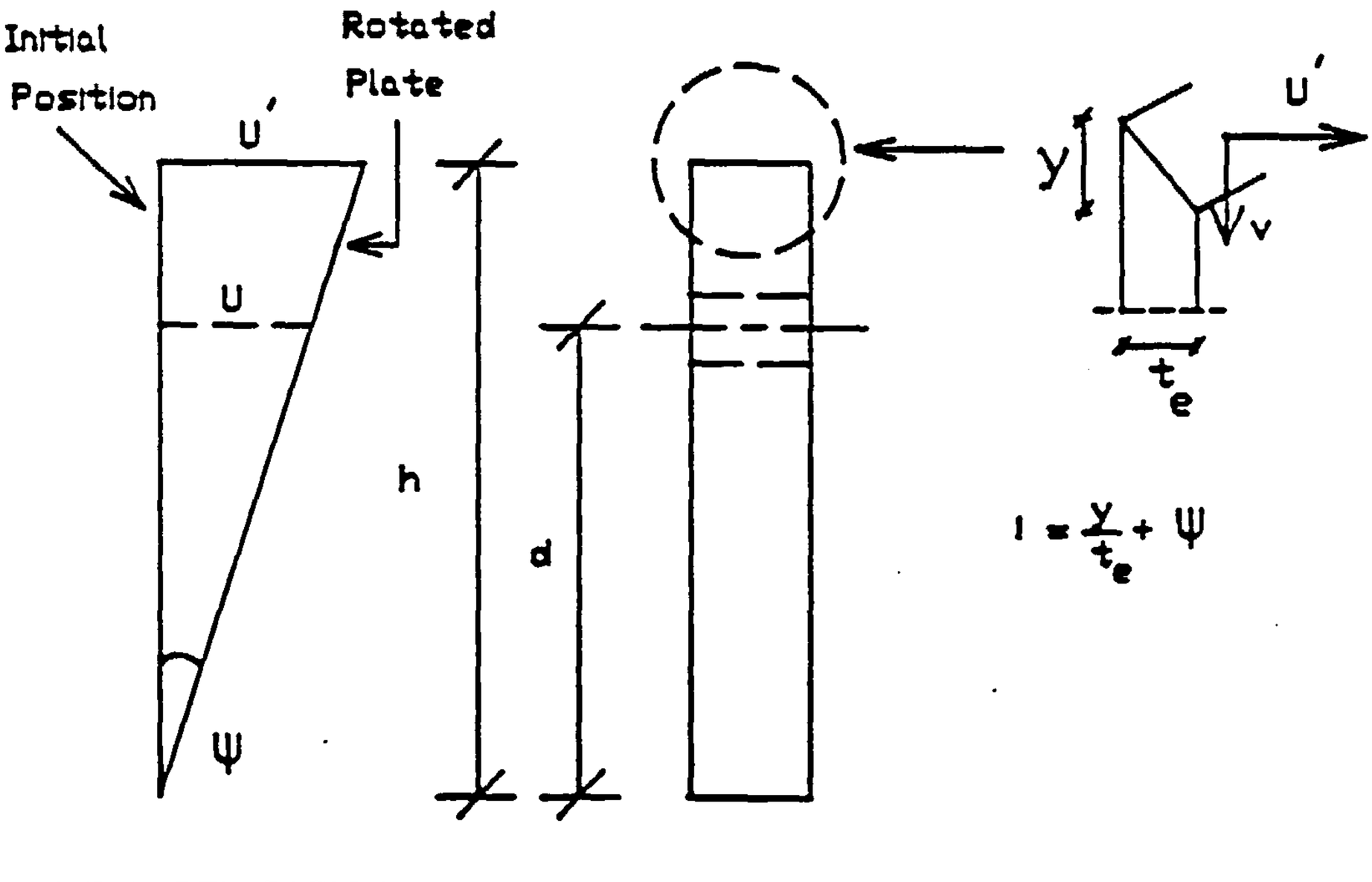


FIGURE (3.13) : VARIATION OF THE OUTWARD DEFLECTION UP THE HEIGHT OF A BACK PLATE.

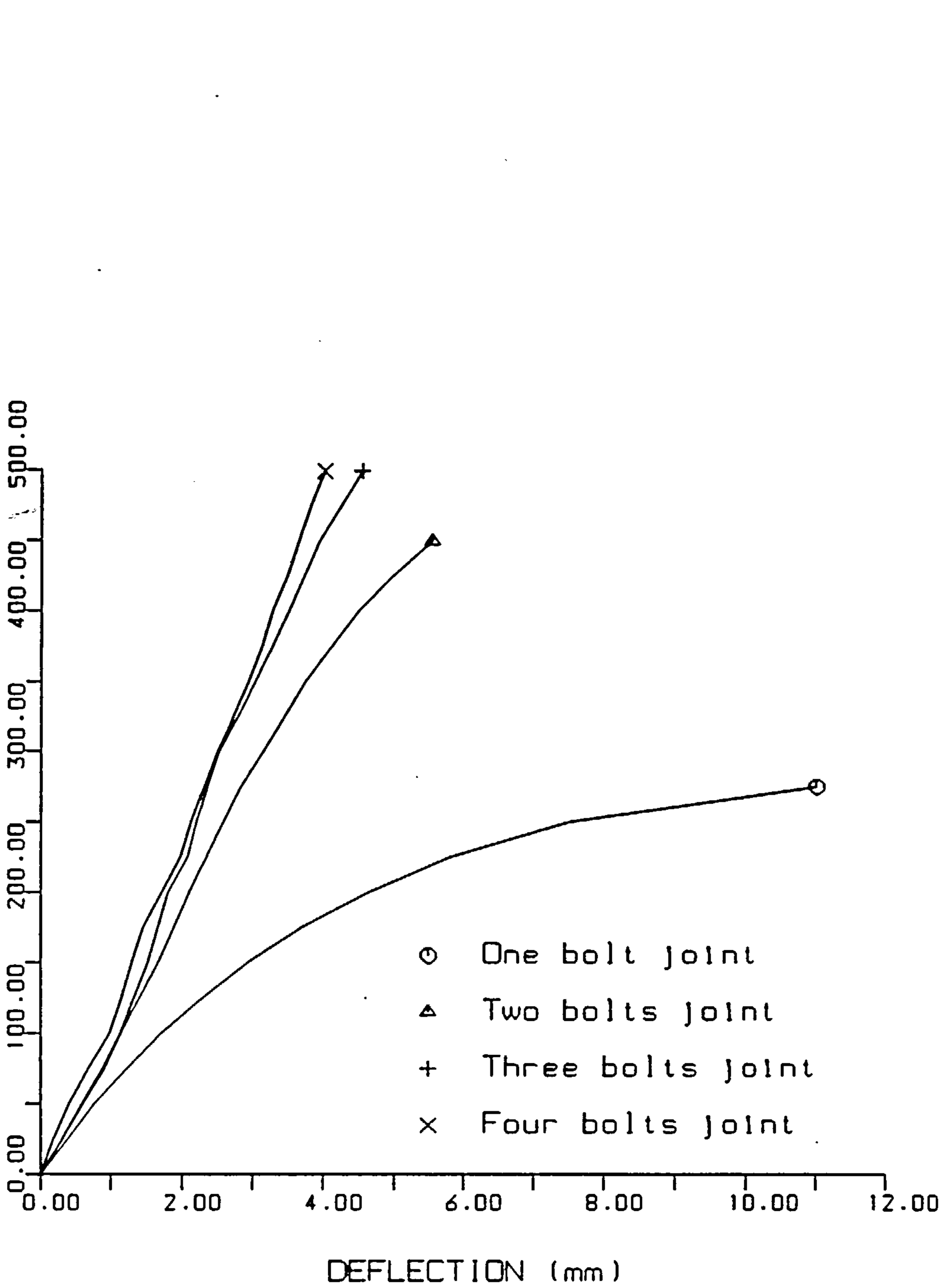


FIGURE (3.14) : LOAD-DEFLECTION CURVES FOR TESTED JOINTS.

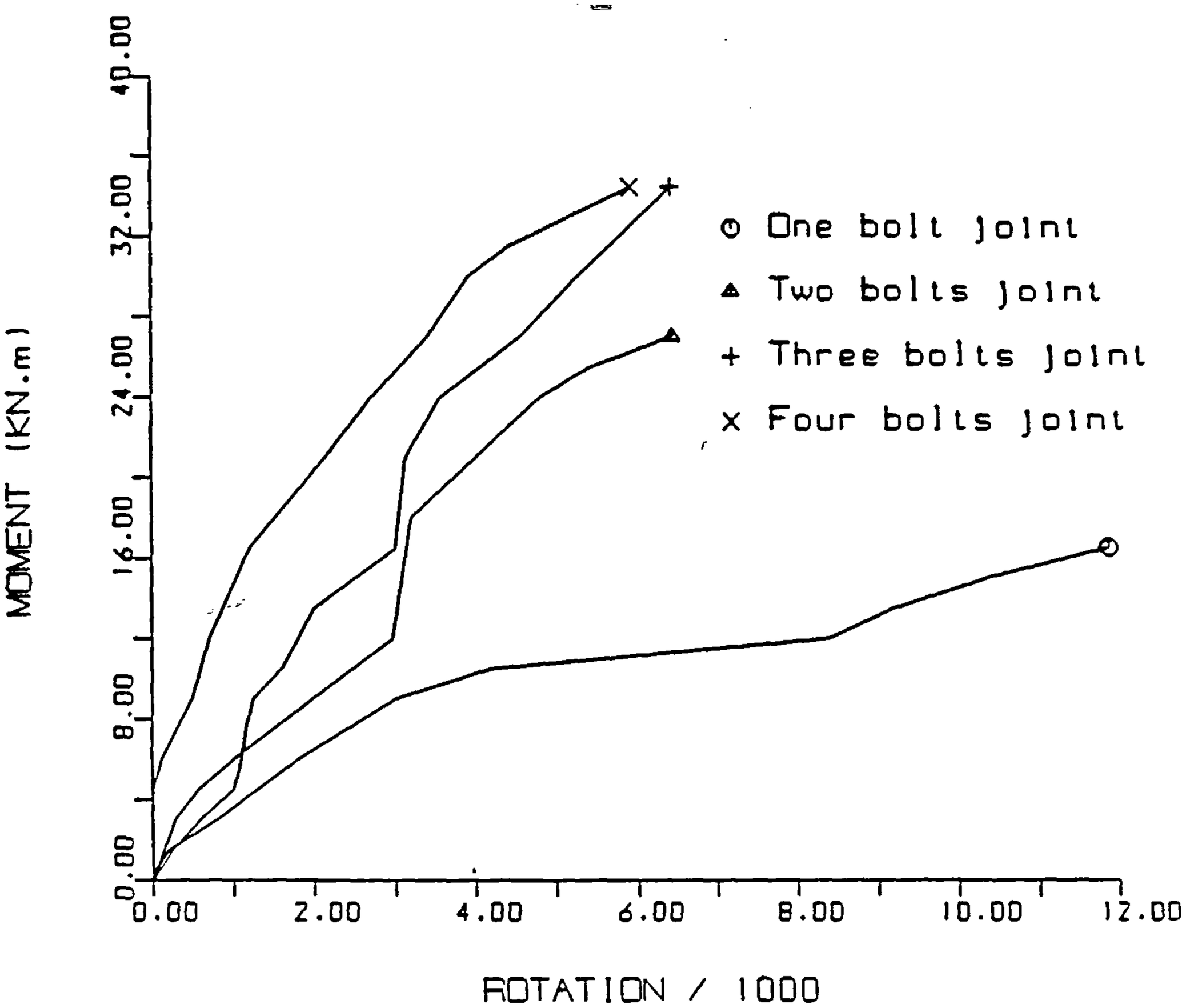


FIGURE (3.15) : MOMENT-ROTATION CURVES FOR TESTED JOINTS.

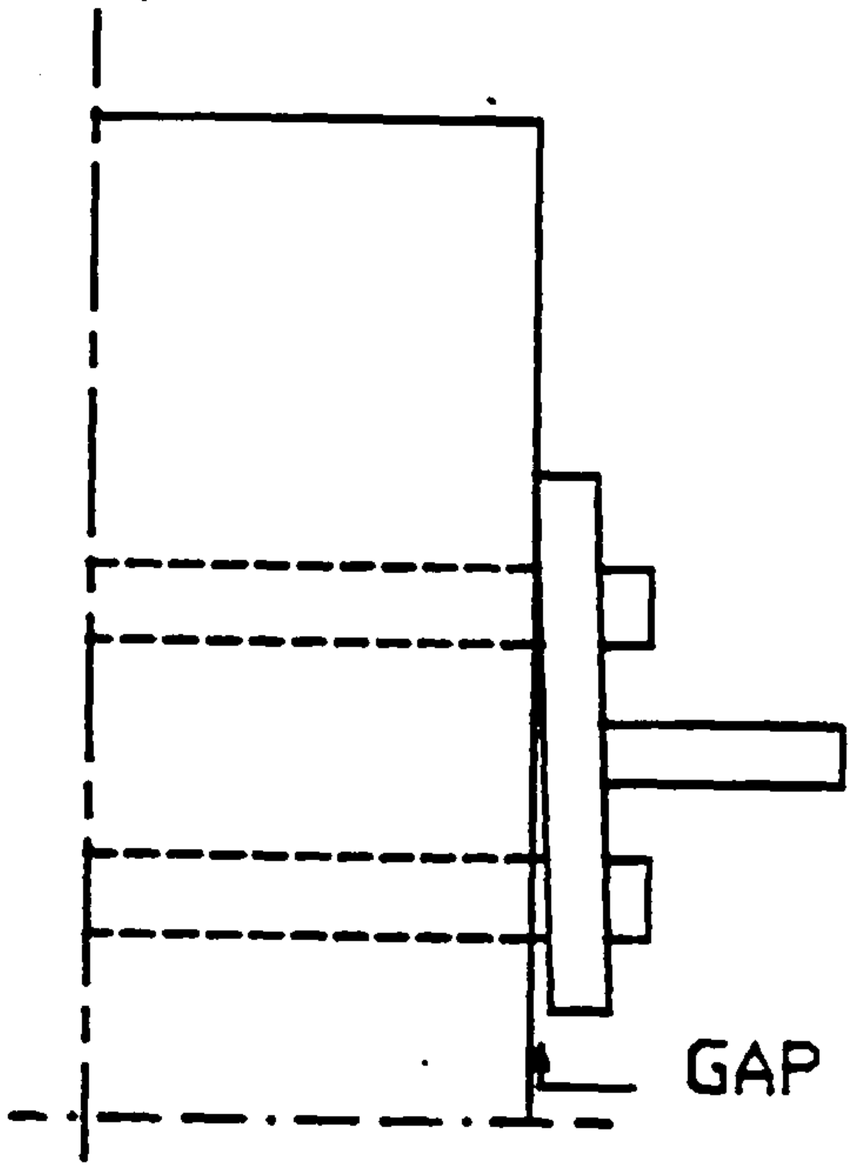


FIGURE (3.16) : INITIAL GAP BETWEEN CONCRETE FACE AND THE BACK PLATE IN TEST 3.

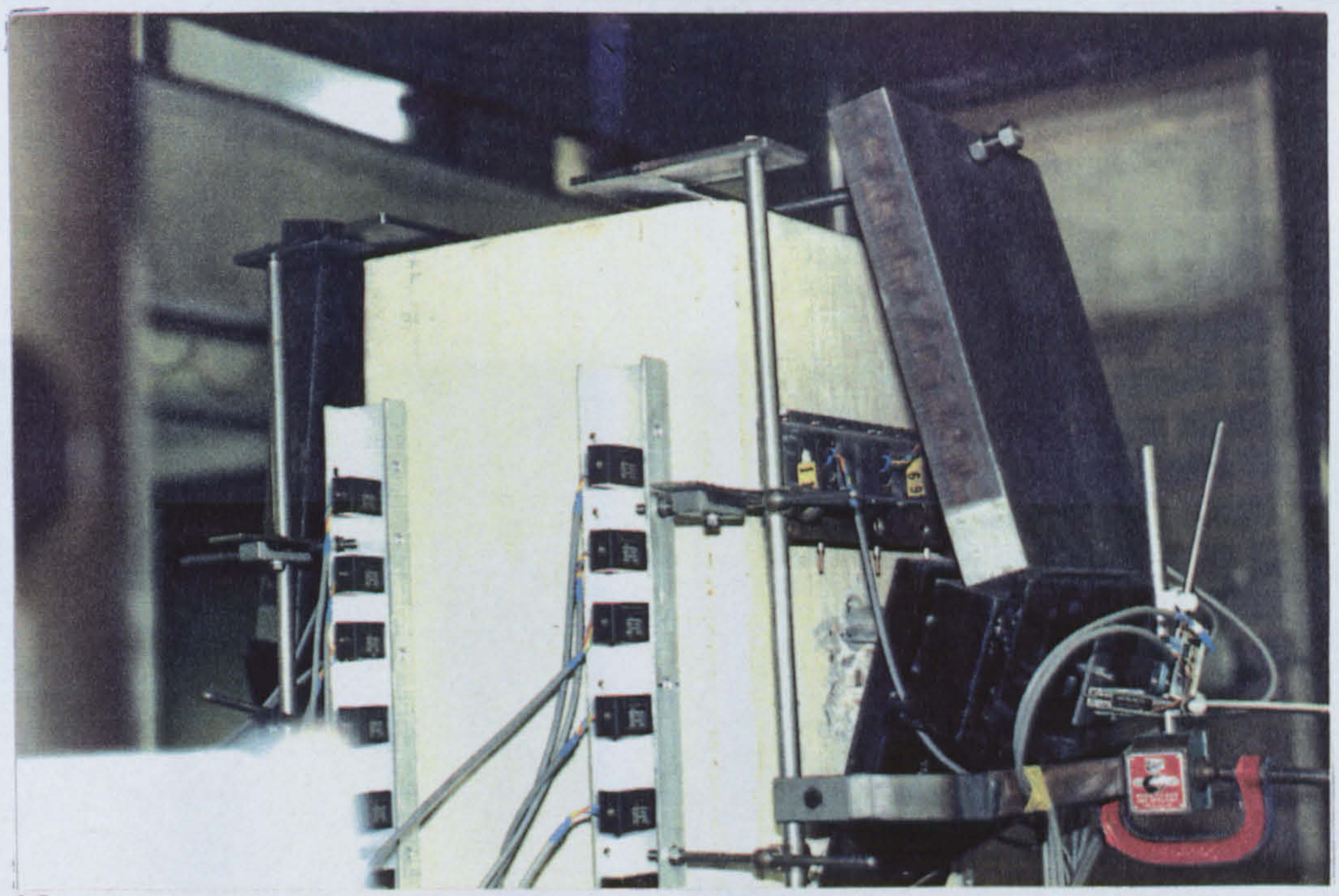

PLATE (3.1) : FAILED SINGLE-BOLTED JOINT BY BOLT SHEAR YIELDING.

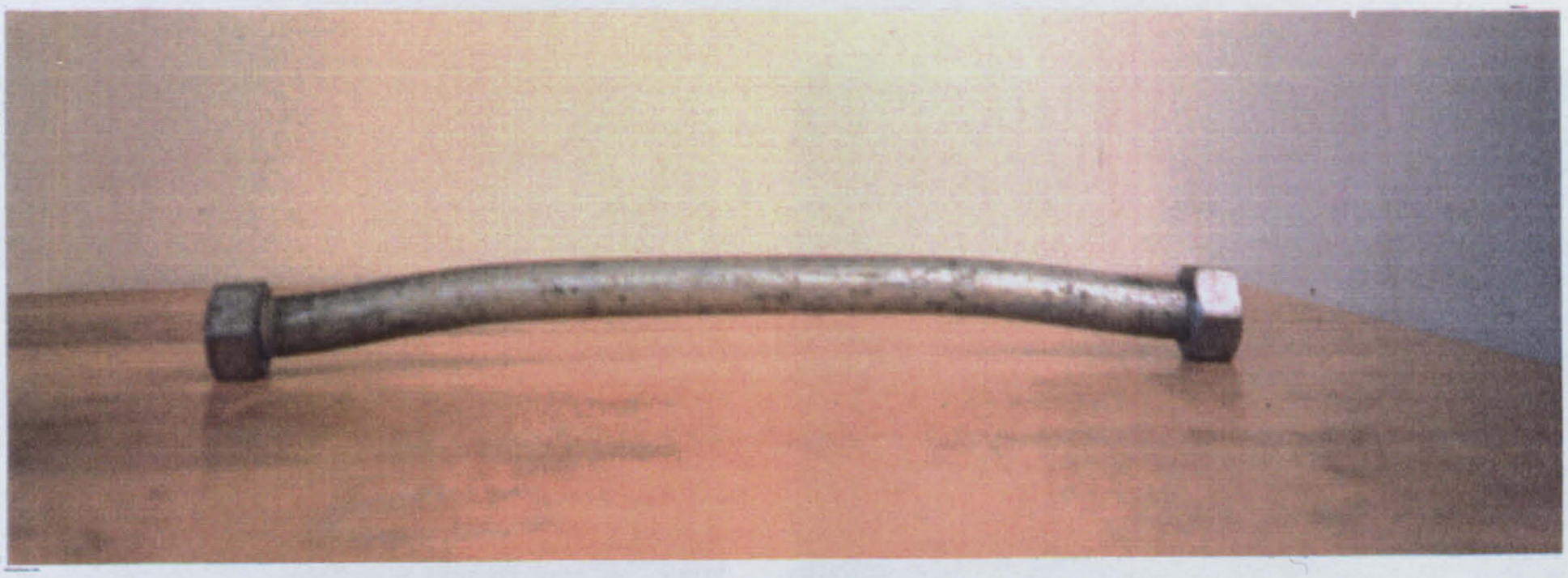

PLATE (3.2) : LARGE DEFORMATIONS EXPERIENCED BY A BOLT AFTER TESTING.

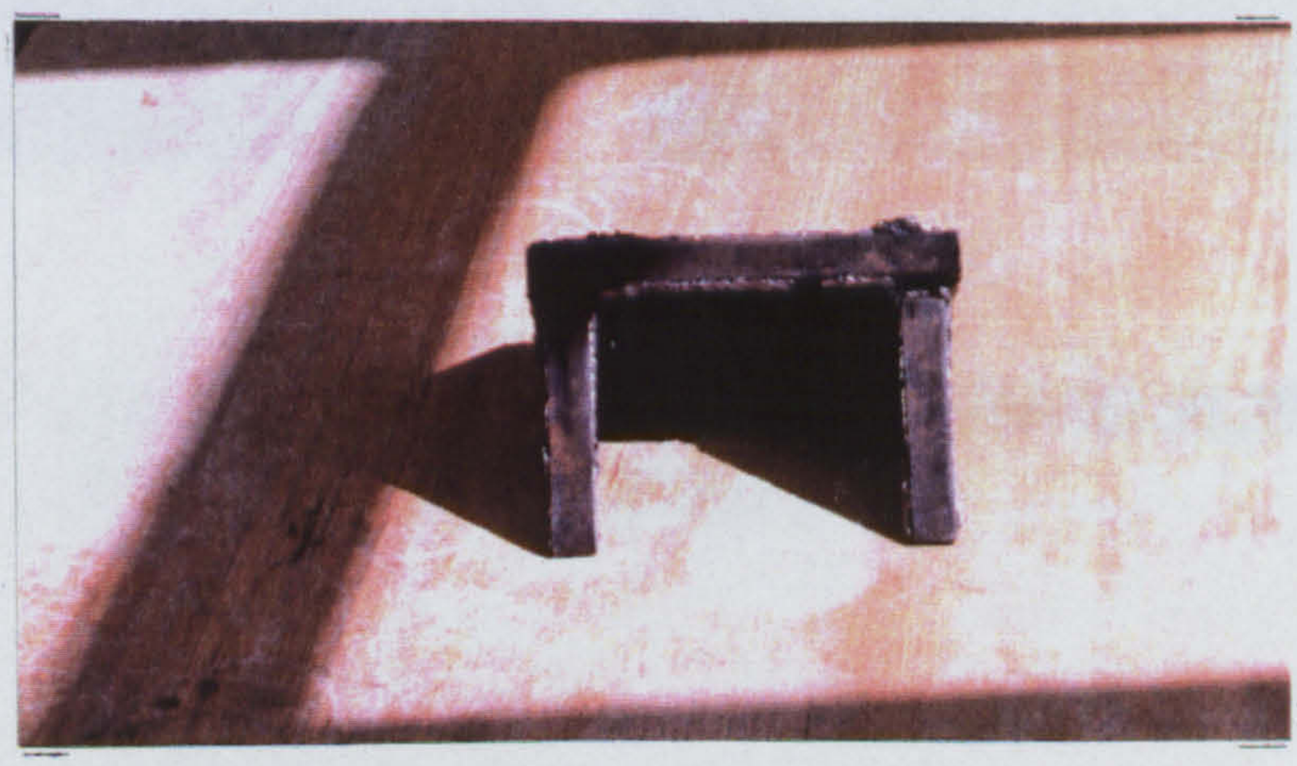

PLATE (3.3) : FAILED BRACKET BY WELD FRACTURE REPORTED IN TEST 4.

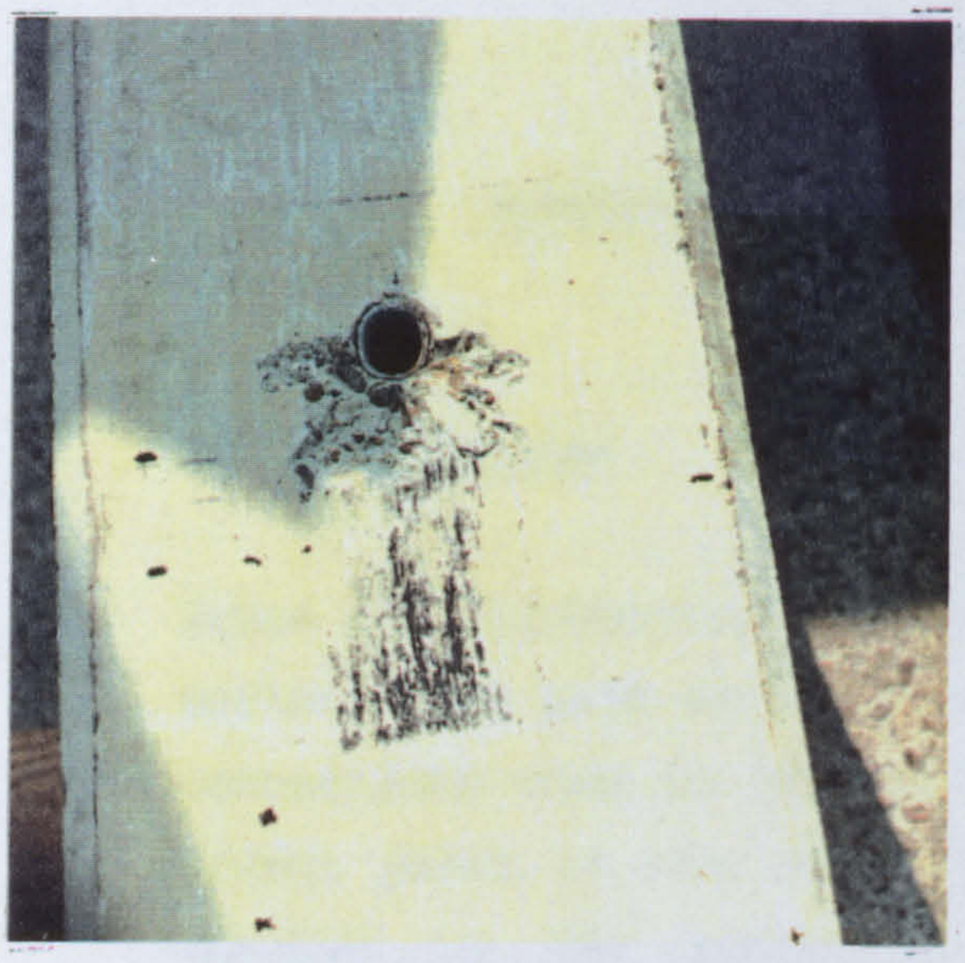

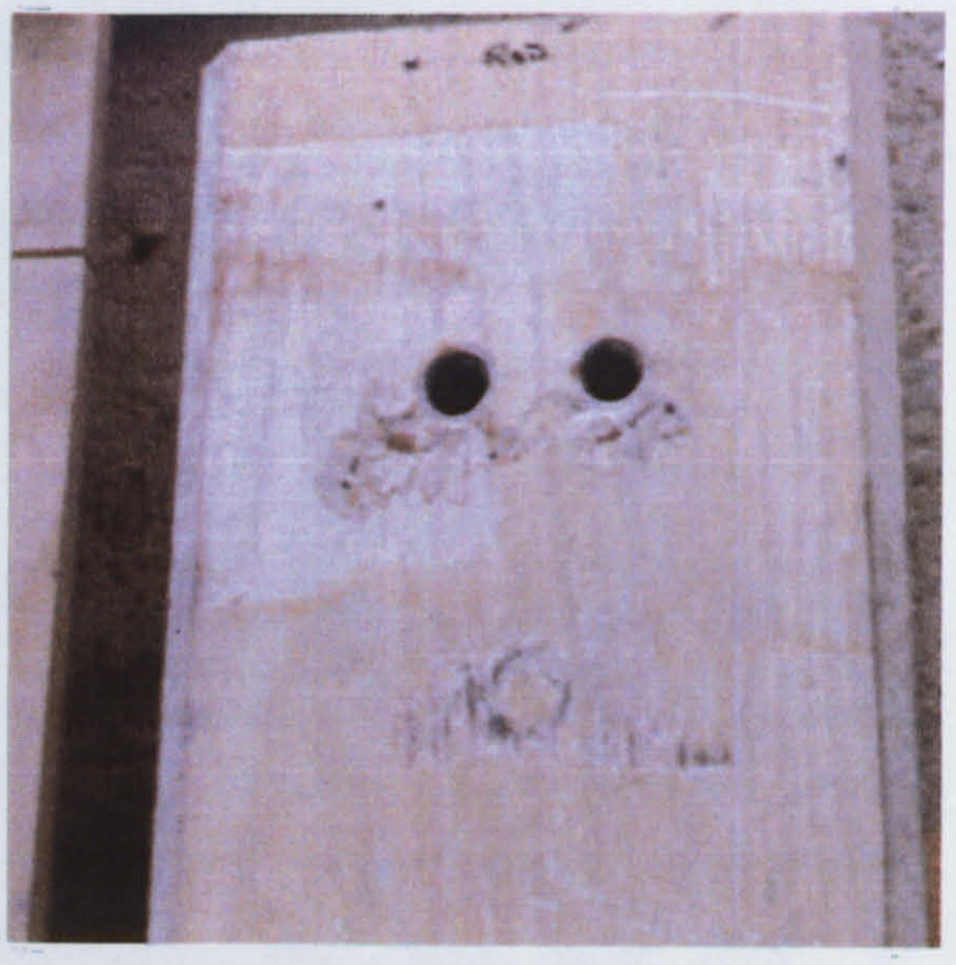

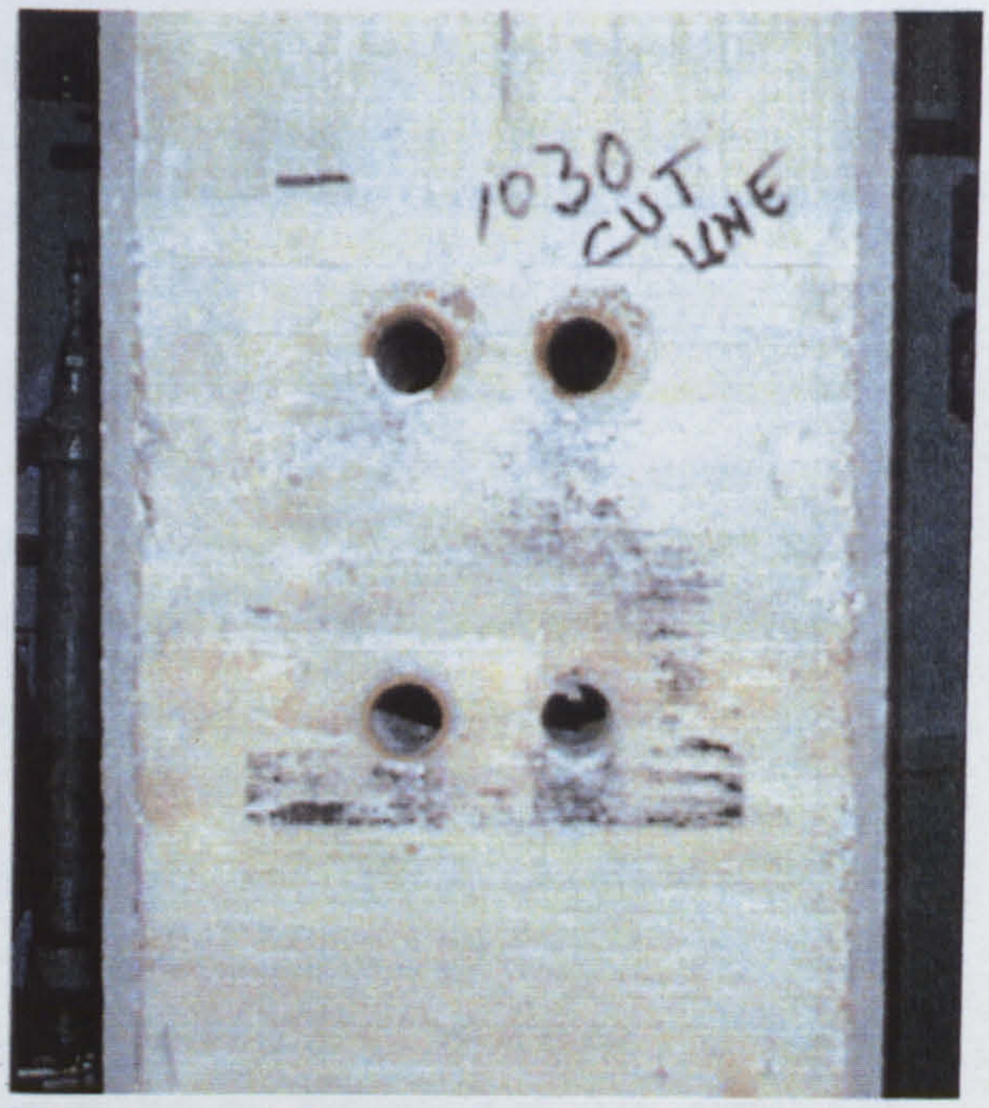


PLATE (3.4) : FRICTION MARKINGS AND CONCRETE SPALLING ON THE FACES OF DIFFERENT TESTED JOINTS.

# CHAPTER FOUR

# NUMERICAL MODELLING OF SLEEVED BOLT JOINTS

## 4.1 Introduction

Since the introduction of precast concrete construction, research workers have paid an increased attention to the behaviour of the connections used in joining different structural members. Until recent years it was recognised that the experimental approach, adopted in the preceding chapters, was the only way to investigate the behaviour of any connection designed to meet the requirement of a specific structure. This proved to be, and still is, the most popular way. However, due to the high costs involved, researchers are always looking for less costly but acceptable alternatives. Finite element modelling appears today as an attractive alternative. This arises from the fact that this method has a powerful numerical way for studying the response of complex structural systems. Also the rapid increase in the power of digital computers coupled with the decrease of their running cost has supported the selection of such alternative.

Structural connections are well known for their highly complex nature and the large number of parameters involved in their formation. As a result, numerous tests would be required before adequate information about a connection's behaviour was obtained. Therefore, it appears to be more rational and more economical to develop numerical models in which, one can vary the parameters involved in the connection. Evaluating results obtained from such models would lead to the development of better analysis and design specifications. The accuracy of the numerical models must always be checked against the results of an appropriate number of experimental tests.

In this chapter, modelling of single and double bolted joints, similar to those tested in Tests 1 and 2, is carried out. For convenience, the models will be defined as Model 1 and Model 2, respectively. The general purpose of these models is to gain information about the behaviour of the different joint components under vertical loading with special emphasis on the stresses developed in the steel links around the joint and the development of both cracking and crushing of the surrounding concrete.

A general introduction on modelling using the finite element package ANSYS with a brief description of of its main features is given. The details of the models geometry, material properties and the selected types of elements are also described.

Throughout this chapter, the details and discussion are general for both models. Any variances between the two models will be dealt with in the relevant sections.

## 4.2 Modelling Using ANSYS

ANSYS is a general-purpose finite element package for static, dynamic, buckling and thermal analyses. It can deal with both linear and nonlinear problems. It was developed at Swanson Inc., Houston, Pennsylvania, U.S.A. [52,53]. Its modular structure makes the implementation of models relatively straightforward. Its main program has efficient and reliable algorithms for the solution of nonlinear equations. Mainly because of these aforementioned features, it was decided to use ANSYS as the basis for this study.

The ANSYS program is constructed as a number of phases which is executed in a manner that progresses from pre-processor or input phases, through the process or solution phases, and on to the final post-processor phases. There is also a validation phase, in which the program attempts to identify any missing or conflicting data. In this particular phase, an estimate of the run-time and

file sizes is given. Warning and error messages (if any) may be also produced. In the input phase, ANSYS has the capability of data checking and geometry plotting during the generation of data. This allows a rapid verification of the input data prior to submitting the problem for execution.

Interactive ANSYS capability includes free format input in response to prompting commands displayed on the interactive terminal and immediate display of the current structural model. The graphic post-processor includes automatically scaled perspective deformation views, mode shape displays, zooming facility and arbitrary viewing direction.

ANSYS contains a library of over 90 standard elements including many specialised elements which can be used for most of the solid and structural mechanics applications. These elements can be used to solve a large variety of problems such as linear elastic and nonlinear e.g. plasticity and creep problems. Capabilities for stress stiffening and large deflection analyses can be also included with certain elements. ANSYS is also capable of dealing with problems which involves slip, contact and friction which are generally associated with structural connections.

In a numerical analysis based on the finite element method, the structure under investigation is divided into a large number of elements, which are interconnected by nodes. The nodes are generally situated in the corners of elements as shown in Figure (4.1). However, mid-side nodes can be introduced in some elements. Loads and supports are specified, and for the system a set of equilibrium and compatibility equations is set up, which can be solved numerically. Frontal solution is the numerical solution technique available in ANSYS. The available ANSYS program would run a wavefront of up to 500 degrees of freedom. Details about the wavefront limit are given in Section 4.13.

## 4.3 Model Development

One of the fundamental decisions taken at the planning stage was that the model should simulate, as realistically as possible, the actual conditions to which the bolted joint could be subjected. The solution was to develop a three-dimensional model which would allow for a more realistic degree of structural interaction between different components of the joint to be reproduced. This was of vital importance, as the main areas of interest were the effects of the applied load on both the bolt, sleeve and steel links materials and the surrounding concrete. In other words, the effect of the joint components on its overall integrity was to be studied.

### 4.3.1 Model Geometry

Taking an advantage of the dual symmetry, i.e. geometric and loading symmetry in Tests 1 and 2, only a quadrant of each joint needed to be idealised in the analysis. This was done to satisfy the limitation of the computer storage capacity and to save a substantial amount of CPU time. A cartesian coordinate system where the Z axis runs along the bolt's longitudinal axis is used. Figure (4.2) shows the geometry, dimensions and the coordinate system of the single bolted model. Since the geometry, loading, boundary conditions and material properties are symmetric, there are two planes of symmetry namely, XY and YZ planes.

Overall dimensions of the model were chosen according to match those of the tested column cross section. The total height was taken as 240mm to allow for locating a number of steel links around the joint, i.e. below and above the joint level. Plain concrete cover to the column vertical reinforcing bars was neglected in the analysis.

### 4.3.2 Model Parameters and Predictions

Based on the experimental work of this study and a previous test carried out on similar joints [21], the main parameters which would affect the connection behaviour could be divided into two groups. Firstly geometrical parameters, e.g. bolt and sleeve diameters, sleeve wall thickness, positions and size of steel links. Secondly material parameters, such as concrete compressive and tensile strengths, bolt, sleeve and steel links yield strengths. Most values of both groups of parameters, used as an input data for the model, were provided from the experimental data.

Solving for displacements, strains and stresses developed as a result of applying monotonically increasing loads on the bolt made the problem a static one. Therefore, a static analysis was adopted throughout the solution phase. The determination of the deformations and stress distributions in the critical regions is difficult and essentially nonlinear, because of the following considerations:

1. Under the application of a vertical load, the bolt experiences a vertical deflection at its loaded end. In the meantime, it has an axial and a horizontal deflection as well. In addition to these deflections, it may also exhibits some bending. As a result of these deformations, a large deflection analysis was chosen to account for the bolt's deformation under successive load steps.

2. The nominally point contact problem between the bolt and sleeve inner surface constitutes a major source of nonlinear behaviour under working conditions, i.e. contact or interface nonlinearity.

3. The loading and reactions are distributed over various regions and dispersed through the sleeve and concrete in varying

patterns. Due to the expected high stress concentration under the loaded bolt's end, plastic deformation leading to local yielding takes place in the critical elements, e.g. sleeve elements. This contributes to the nonlinearity of the problem even before high value of load is reached or overall yielding of the joint is initiated.

4. The behaviour of reinforced concrete is essentially nonlinear due to the nonlinear stress-strain relation of concrete, cracking of concrete and yielding of reinforcing bars, i.e. material nonlinearity.

From the above considerations, it is clear that the main types of nonlinearity are considered in the present model. The model would be expected to have a series of cracks in the most highly stressed region. It was decided to have a mesh pattern which had the same trend as the expected crack direction for the diagonal members. It was also hoped that by doing this, the successive cracks would appear as near to continuous lines as possible.

## 4.4 Mesh Generation

It is well known that the design and fineness of a mesh may critically affect the accuracy of the analysis. To provide a satisfactory model for the bolted connection analysis, the finite element mesh should exhibit the following properties:

1. Since the highest stress gradients are most likely to occur in the area where the bolt shank is expected to come in contact with the sleeve, the smallest elements should be concentrated in this region.

2. In areas where small uniform stresses are expected, i.e. areas away from the loaded end, mesh elements may be considerably larger, though not to such an extent that the curved surface of either the bolt or the sleeve is poorly described.

3. For best numerical conditioning of the stiffness equations, it was recommended that aspect ratio (height/width) for an individual element should preferably be within the range of 1 to 3 [52]. This condition has been met in most of the mesh elements, especially in the fine mesh region. However, in some places where transition between fine and coarse regions was made, it was not to possible to keep the aspect ratio below the required upper limit. The already pre-defined positions of the steel links around the joint added more difficulty in satisfying this requirement for certain elements.

4. While it is recognised that wedge elements are necessary to achieve transition from regions of small elements to regions of larger elements, their use was kept to a minimum. A warning message appeared during the checking phase supporting the avoidance of such elements.

To design a mesh incorporating all these features, the boundaries controlling the geometry were isolated. The bolt, the sleeve and the reinforced concrete solid were assessed independently. Then a mesh pattern was developed with two levels of refinement: fine and coarse as follows:

a) Fine Region:

This region represented both the expected sleeve yield area and the concrete most highly-stressed under the bolt shank. It starts from the bolt's loaded end in the XY plane and extends a distance of 50.0mm along the Z axis while its width almost covers the bottom surface of the bolt. This length was chosen as it is equal to the yield surface observed on the inverts of some sleeves after testing. Observation indicated that the maximum deformation of a sleeve took place at its loaded edge and gradually decreased along a distance not more than 50.0mm.

b) Coarse Region:

This region covers the elements which were believed to have lower stress concentrations in the region -50.0 > z > -150.0mm. The size of elements is larger than those of the previous region. Concrete elements at top and bottom of the model are also included in this region.

## 4.5 Selection of Main Element Types

ANSYS has a wide selection of element types. An element was required for each material zone which would be able to predict the behaviour of this zone up to the connection failure. In this section, a description is given of each chosen element to be used in the model with its corresponding capabilities and properties. Special requirements and restrictions concerning their choice are also given.

### 4.5.1 The Bolt

It was required to have an element to represent a 24mm diameter steel bolt shank capable of carrying a shear force at one of its ends. The element found to satisfy this condition is the "8-node isoparametric solid" known as STIF45 in the ANSYS element library. The element has eight nodes, and three translational degrees of freedom per node.

A 2x2x2 lattice of integration points is used with the numerical integration procedure. This means that the element stiffness matrix is calculated as the sum of weighted contributions from 8 points suitably located inside the element as shown in Figure (4.1). The shape functions used with the element define a linear displacement field over the element. In addition to shear loading, the element can be subjected to bending. This ensures realistic modes of deformation in flexure. The general shape of

the element is a cubic one. However, a prism or tetrahedron shape can be obtained by duplicating one or two nodes when entering the element connectivity in the input data file. Figure (4.3) shows the bolt discretisation.

### 4.5.2 The Sleeve

The element described above can generally be used to model any solid material. It was decided to use it, after accounting for the difference in their material properties, to represent the sleeve material as well. The sleeve mesh, for Model 1, is shown in Figure (4.4).

### 4.5.3 The Concrete

In modelling a highly-stressed reinforced concrete member, it is important to check cracking and crushing of the element. For this reason it was obvious to choose the "three dimensional reinforced concrete solid" provided in the ANSYS element library to represent the concrete solid. The choice of the element by ANSYS was based on the recommendations given by Suidan and Schnobrich [54] who introduced a three dimensional, 20-node isoparametric element. To reduce the amount of the computations associated with this element, it was substituted with an element having a 2×2×2 lattice of integration points. A previous work [55] showed that such substitution would lead to numerical results with only minor differences.

As in STIF45, this element which is known as STIF65 has eight nodes and eight integration points used for the computation of the element stiffness matrix. Three translational degrees of freedom are also associated with each node. The element is capable of cracking in tension and crushing in compression.
Although this element has the capability of accommodating three reinforcing bars in different directions, it was decided not to use this facility for the following reasons:

1. The element deals with the reinforcement as if it is smeared, i.e. distributed into an equivalent layer within the element. This is clearly not an exact way to represent the actual reinforcing bars used in the column.

2. Using such facility in an earlier work [41] indicated that the reinforcement provided in this way would highly stiffen the concrete element. If the steel to concrete ratio is increased the element will behave more similar to a steel element. As a result, crushing of any of its integration points would occur at higher loads.

By suppressing this facility, STIF65 is used in this work only to represent the solid plain concrete.

The concrete material behaves isotropically. The most important feature of this element is that it can represent both the linear and non-linear behaviour of the concrete. In the linear part, the concrete is assumed to be an isotropic material up to cracking. In the non-linear behaviour, the concrete may undergo plasticity and/or creep. The concrete solid mesh, for Models 1 and 2, are shown in Figures (4.5) and (4.6), respectively.

### 4.5.4 Steel Links

As STIF65 was only used to represent a three dimensional plain concrete solid, it was required to model the reinforcing bars separately. This was achieved by using the three-dimensional spar element. It was used to represent both the steel links and the main vertical steel bar of the column. The element can only be geometrically defined by two nodes, each of them has three degrees of freedom. The element is capable of being subjected to an axial force in either compression or tension as if it is a member in a pin-jointed structure. It is not capable of carrying bending stresses. The stress is assumed to be uniform over the

entire element.

Care was taken in adding steel links in position, see Figures (4.5) and (4.6), so that a link size should not be larger than that of the concrete element it is coincident with one of its sides. Simplicity is the main advantage of adopting such modelling of steel bars.

## 4.6 Contact Area Modelling

Initially, and before applying any load to the model, it was assumed that centres of both the bolt and the sleeve cross sections lie in the same vertical plane as shown in Figure (4.7). Due to the difference in their diameters, the bolt's centre, O, is located at a level 1.50mm below that of the sleeve, O'. As a result of this difference in centre locations, and due to the curved nature of both bodies, a geometrical gap is created between their surfaces. The size of this gap ranges from 0.00mm at the bottom edge of the bolt, i.e. where it must be in contact with the sleeve, to 3.00mm at the top of the bolt surface. To allow for a zero length gap in the model along the invert where x=0.0mm, two similar sets of nodes occupying the same space along the Z axis were provided. These nodes represent the initial line of contact between the bolt and the sleeve.

Having modelled both the bolt and sleeve bodies, it was required to allow the bolt to act independently inside the sleeve through which it passes. Meanwhile, it was not allowed to have downward vertical nodal displacements on the bolt's bottom surface which exceeded that of the corresponding nodes on the sleeve inner surface. Details of this can be explained as follows:

Due to the initial existence of the gap, the bolt is at first free to deflect without any constraint imposed by the sleeve. This deflection causes the gap size to possibly increase in certain places, and to decrease or close in other places. Once

the load is applied to the bolt body, its loaded end at z=0.0mm would experience a downward deflection. As the load is increased, this deflection causes the gap to decrease in size in the region close to the loaded end. Eventually the gap closes, allowing more bolt material to come into contact with the sleeve internal surface. In other words, by applying an external load the initial line of contact would be developed into an area of contact through which the load can be transmitted from the bolt to the sleeve. Naturally, the size of this area would increase by increasing the value of the applied load. It should also be expected that such an increase in area would be accompanied with local yielding of the sleeve material in this region.

From the description above, the importance of getting precise information about how this contact area develops under successive loading is obvious. To satisfy this requirement, special elements were used to represent the geometric gap. A one-to-one mapping of the nodes on the bolt external surface to those on the sleeve internal surface is used to facilitate the modelling of the contact region by these gap 'link' elements.

A gap element is used to connect each two corresponding nodes. If a gap closes under a certain load, this would mean that the bolt had come into contact with the sleeve at this particular point, and a load is transmitted between them. In addition to the zero gap along the sleeve invert, five nodes along the bolt bottom external surface were chosen to represent the possible contact area, with the final one being the closest to the bolt centreline. This was chosen as it was thought unlikely to have the corresponding two nodes at the centreline in contact with each other, even at the maximum load. Therefore, the nodal configuration used to discretise this part of the bolt is also used to discretise the corresponding part of the sleeve.

Both bolt and sleeve nodes in this region had identical X-axis locations on the interface around the bolt shank, see Figure

(4.8).

Having inadequate information about how this area would propagate in the direction of the Z axis, these gap elements were introduced all along the bolt shank, i.e. from z =0.0mm to z = -150.0mm. Additional gap elements were also used to represent the gap at the bolt's remote end. This was done to examine the possibility of having the remote end coming up to be in direct contact with the corresponding sleeve soffit surface.

Introducing the gap elements in the model caused all lower edge nodes of the bolt, and their corresponding ones situated on the sleeve surface, to act as if tied together. This is only true if they come in contact. It should be emphasised that if they do not come in contact, or in regions where no gap elements are introduced, the displacements are uncoupled and the two bodies act independently.

## 4.7 Gap Elements

The "three-dimensional interface" element which is called STIF52 in the ANSYS element library was introduced to the model to represent the gap elements described in the previous section. It is capable of representing discontinuous connection between two surfaces which may come in contact with each other. The element could be defined by two nodes, each has three degrees of freedom i.e. translations in the nodal X, Y,and Z directions. The nodes should be read in a way that a positive gap should be in the element x direction as shown in Figure (4.9). Each node belongs to a different substructure, i.e. either bolt or sleeve as explained earlier. The element has a linear shape function with no integration points.

The element can be thought of as three independent linear springs, each with its own stiffness value, that are oriented in the normal and tangential directions. These springs "connect" the

two surfaces at the nodes. Infinitesimal displacements in all directions are independent. The element is oriented so that the normal force associated with the element $F_n$ is in line with the two nodes, i.e. the element x direction. When it has a negative value, i.e. compressive force, both the interface and the normal displacement remains in contact. In other words, a negative value for $F_n$ indicates a gap closure between the two connected nodes. In this case, the normal displacement and force respond as a linear spring. A full description of the element is given in the ANSYS manuals [52,53].

The associated stiffness with the elements were chosen to be of high values to create very stiff elements in the direction of the gap, forcing the two nodes to move together in this direction. A typical value used as an input data for a spring stiffness was calculated as follows:

$$K = (E \times A) / L$$

where E is the Young's modulus of steel.

A is the surface area of an adjacent element.

L is the element thickness.

It should be noted that different values for K have been used in the model as the corresponding surface area, A, involved with gap elements differs along the Z axis. Figure (4.10) shows different areas used in calculating these stiffness values. For each interface element, the force is updated based upon a current displacement value in order to predict a new displacement. For a certain load step, the iteration is continued until the gap status remains unchanged for two successive iterations.

Element STIF52 has proved to be suitable for gap representation due to the following reasons:

1. It is capable of supporting only compression in the direction normal to the surfaces which is what is expected in the case of compressing the sleeve material under the bolt shank. It can also be used to resist shear (if any) caused by friction in the tangential directions.

2. The facility to examine the gap status, before and after applying a certain value of load, contributed much to the understanding of the gap closure under loading, as will be seen later.

3. As two nodes come into contact with each other the normal force can be transferred across the gap while the two nodes move together. In other words, the contact region is therefore discreetly modelled by these springs which couple the displacements and force the nodes to act together.

This element proved to be successful in joining two separate nodes having different locations together, as long as they had an initial gap between them, i.e. the two nodes must not occupy the same location in space. As this was not the case at the symmetric edge (at x=0.0mm where both the bolt and the sleeve are in physical contact before applying any load), it was not possible to use STIF52 to transmit the load from the bolt to the sleeve through this edge. Thus, another element had to be introduced to the model. STIF12 was the obvious alternative as its orientation is defined by an angle rather than by its nodal coordinates [52]. This allowed the two connected nodes to be initially coincident. This element is a two dimensional gap element which works in a way similar to that of STIF52, except that each node has only two degrees of freedom instead of three [53,56].

## 4.8 Final Remarks on The Mesh

a) Although care was taken in the design of the model mesh, and special attention was given to the areas of interest described

in section 4.4, certain simplifications were unavoidable. These can be described as follows:

1. As STIF45 was not capable of accommodating curved boundaries (each edge is defined by two nodes only), a small angle 12° was used for approximating the circular boundary with straight-sided elements. This was adopted for the bottom part of both the bolt and the sleeve in a way that made the segmented flat edge appear curved.

2. Having modelled the major components of the joint, both the steel bracket and the bolt thread were omitted from the mesh to minimise the finite element idealisation.

b) Along the Z axis, the size of the bolt elements was set equal to that of the sleeve elements to enable an accurate stress distribution to develop under the bolt shank.

c) The sleeve wall thickness should be kept constant all around its circumference. To maintain this, thickness was defined by having two identical sets of nodes in cylindrical coordinates, 3.00mm apart, representing both the external and internal diameters, respectively.

d) No link elements were used between the sleeve external surface and the first ring of concrete. The sleeve was unable to separate from the concrete surface after deformation.

e) The compatibility which should be satisfied between the elements was achieved by making sure that the elements are well connected at the joining nodes and no nodes are left unconnected. The strain compatibility between sleeve and concrete materials was maintained as the two different types of elements have the same shape functions.

f) All grid points are located in the cartesian coordinate

system, but a local cylindrical coordinate system was specified for the bolt and sleeve. The centre of the sleeve cross section is the origin of the global axes and will be referred to as the joint level.

## 4.9 Material Properties

Material properties are defined for each element. In contrast to a linear elastic analysis, where only Young's modulus E and Poisson's ratio $\nu$ have to be specified, a nonlinear analysis requires the knowledge of several more parameters. Parameters controlling the nonlinear behaviour of steel members, i.e. the bolt, sleeve and steel links, are discussed in this section. While those controlling the concrete nonlinearity will be discussed separately in the following chapter.

As the bolt material was high tensile steel, typical standard values of 205 $KN/mm^2$ and 0.25 were used for the elastic modulus and Poisson's ratio, respectively. Stress values specified by BS3692 [57], for grade 8.8 bolts, are also used. These are 628.0 $N/mm^2$ and 784.0 $N/mm^2$ for tensile yield stress and ultimate stress, respectively.

In ANSYS input data, a simplified curve can be used to represent the stress-strain relationship for a material instead of using that obtained experimentally. This is a simplification of the requirement to allow for the nonlinearity of the material behaviour once it has passed the yield point. Stress-strain curve obtained from simple tensile tests and its corresponding simplified version for sleeve material was shown earlier in Figures (2.7).

For the sleeve material, the curve consisted of two straight lines connected together at the yield point. The first of these has an elastic modulus equal to that obtained experimentally, i.e. 182.6 $KN/mm^2$. As the failure point was not obtained

experimentally, there was not enough information concerning the behaviour after yielding. As a result, reasonable values of 500 $N/mm^2$ and 0.05 were assumed for ultimate stress and strain, respectively.

Three straight lines were used to represent the stress-strain curve for the steel links, up to failure. The slope of the first line is assumed to be 205.0 $KN/mm^2$ while the other two slopes have reduced values to satisfy the requirement of the ANSYS program, see Figure (4.11).

## 4.10 Solution Convergence

It has been mentioned earlier that plasticity is a nonlinear property associated with the steel and concrete materials. It is characterized by the instantaneous, unrecoverable straining process. This dictates that the solution will not converge from the first iteration. So an iterative solution is required until convergence is obtained. However, a purely iterative method would not be the suitable solution to choose as it would fail to produce information about the intermediate stages of loading. A mixed incremental-iterative technique was essential, in which the total load is subdivided into smaller increments and the solution corresponding to each load increment is obtained by iterating until convergence is achieved. See Section 4.12 for the details of load application.

For a static analysis, a load step is said to be converged if the changes in plastic strain increments compared with their corresponding elastic strains are less than a preset value. This should be satisfied at all integration points in the structure from one iteration to the next one. This preset value is defined as input data in the convergence command and was taken as 0.10. It should be noted that this value reflects the most erroneous integration point, i.e. all other points have the same or less error. Convergence can be affected by other factors such as

deflection increment and status of either type of gap elements, or integration points in concrete elements. These can be described as follows:

1. A solution is considered unconverged if there is a change in deflection at a particular node between two successive iterations which exceeds a certain limit. This limit was taken in the input data as $0.1 \times 10^{-2}$ mm.

2. If a gap element in either 2-D or 3-D changes its status from open to closed (or vice versa) during a certain iteration, the solution needs an additional iteration to converge under the same value of load.

3. Convergence is incomplete if the status of an integration point in any concrete element changes from one state to another, regardless of the plasticity criterion limit or the deflection increment. In other words, if crushing occurs, or a new crack appears, or an existing crack opens during a certain iteration, then another iteration is needed to have a converged solution.

The full Newton-Raphson method is the iterative process adopted by ANSYS in solving the set of nonlinear equations created by the mesh. In this method, for each iteration the stiffness matrix is modified to take the effect of plastic strain increments, computed at integration points, into account. This successive updating of the stiffness matrix leads to a converged solution when the resulting stresses satisfy the materials' stress-strain relationship at a certain load step. The general algorithm of the method is described in detail in References [53,58].

The analysis of the joint at a particular load was terminated automatically by the program if no convergence was obtained even after a selected maximum number of iterations. This situation was most likely to happen when some regions yielded so much that the

results diverged. It must be noted that such a termination does not correspond to the failure of the joint, but means that a relatively large increment of load had been imposed. Usually a restart of the analysis with a smaller load increment proved to be successful.

## 4.11 Boundary Conditions

It was required to apply a system of boundary supports to the models simulating as realistically as possible those constraints provided by their geometry and by the testing techniques. As mentioned earlier, each node had three translational degrees of freedom, i.e. Ux,Uy and Uz. The boundary conditions applied to either model can be divided into the following three sections:

1. Symmetry conditions: Appropriate boundary conditions were imposed to account for the symmetry, e.g. the suppression of the translation in the X direction all over the entire YZ face at x = 0.0mm, while it is free in both Y and Z directions. Also at z = -150.0mm, where another plane of symmetry exists, translation in the Z direction was suppressed.

2. Support conditions: At both top and bottom of the concrete solid, where the expansion is believed to be negligible due to the confinement provided by the steel links, translations in the X and Z directions were suppressed. The translation in the Y direction was also suppressed at the bottom face. This may be not the precise condition in the test, as the vertical reaction at the bottom of the column induces a very small amount of axial compression in the Y direction. Concrete shortening was ignored as the absolute deflection of the bolt was of interest rather than the relative one.

3. Control of concrete spalling: After testing, spalling of concrete was observed on the column face after the removal of steel brackets. Although the steel bracket was omitted from

the mesh, it is felt that its restraining effect upon the column face had to be included in the numerical analysis. This was achieved by imposing boundary conditions across the XY face as follows:

The analysis was started with the assumption that the XY face (excluding the lowest edge) was free in the Z direction. After solution, the outward displacements, $U_z$, at the nodes on this face were checked. A linear variation of $U_z$ along the height of the back plate, as shown in Figure (4.12), was assumed with a maximum value at the bolt's top node. At each node on the XY face, a comparison was made between the computed $U_z$ values and the allowed $U'_z$ values. If $U_z$ had a value exceeded the allowed value $U'_z$, implying that the concrete tended to be pulled away more than the back plate, the value of $U'_z$ was used as an imposed boundary condition for the next load step.

## 4.12 Load Application

### 4.12.1 Model 1

Having only modelled a quadrant of the joint, a shear stress was required to act on the bolt's XY plane at z = 0.0mm. This type of pressure was not allowed in ANSYS as it allows only a pressure acting perpendicular and not parallel to the loaded plane.

To overcome this problem without having the bolt shank protruding out of the concrete solid, the load was first applied to the model in the form of a concentrated force at the bolt's centre. This proved to be unsuccessful as the load concentration at one node had the inevitable effect of greatly increasing the stresses in the elements connected directly to this node. This led to the use of a group of concentrated nodal forces. These forces acted over all nodes on the bolt cross-section in the XY plane to give rise to the mean value of shear stress. Assuming that the shear stress is uniformly applied along the loaded plane, the nodal

forces had different magnitudes at a certain value of load. The magnitude of a nodal force equals the value of shear stress corresponding to the applied load times the bolt's surface area associated with this particular node.

At higher load values, this loading technique proved to be inefficient as the load concentration had an undesirable effect on the rate of convergence. This has led to the use of a displacement controlled technique. A vertical displacement value for the bolt nodes in the 'loaded plane' was imposed at each load step. By adopting this technique, rapid convergence was achieved. The only disadvantage about this technique is that it assumes an artificial high rigidity for the bolt's loaded end. At any displacement value, the applied load was taken as the total of computed reaction forces at these nodes.

The bolt's self weight was ignored in the analysis as it was going to contribute negligibly to the total applied load. A typical imposed displacement increment was of an order of 0.03-0.05mm. This small value was chosen due to the complex effect of the nonlinearity of the concrete elements, especially those immediately surrounding the sleeve.

### 4.12.2 Model 2

The predicted displacements for sleeve nodes in contact with the bolt in Model 1 were saved and later used, after accounting for symmetry, as input data for the corresponding nodes in Model 2. This made it possible to eliminate the bolt and the gap elements from the mesh of Model 2. Thus, saving both storage capacity and computational time. Sleeve nodes with zero imposed horizontal displacement at the initial line of contact in Model 1 were released in Model 2. In addition, their computed horizontal deflections, at every load step, were added algebraically to those of the nodes lying in the same XY plane.

## 4.13 Wavefront Reduction

As has been mentioned earlier in Section 4.2, the frontal solution [59] is the solution technique adopted by ANSYS to solve the set of the simultaneous equations formed in the pre-processor phase. In this technique, the sequence in which the elements are generated is crucial to minimise the wavefront size of the model.

In Models 1 and 2, it was found that the easiest way to generate elements in the input phase is to generate a group of elements in the XY plane at z = 0.0mm then proceed along the Z direction until z = -150.0mm then another group is created and so on. Although this was simple enough in the input phase, it did not satisfy the wavefront requirement. So attempts had to be made to minimise the wavefront for the mesh.

ANSYS has a facility which allows for element re-sequencing according to their geometrical locations. It was found that the wavefront was greatly reduced by reordering all elements of the mesh according to their centroid locations along the Z axis. At this stage, the final wavefront had reached a value less than 500 and the model was ready to be submitted for execution.

## 4.14 Preliminary Runs

Some preliminary running trials were carried out to verify the function of different element types. From these runs, the following features were either added to or deleted from the input data file:

1. A very small force was initially introduced across and along the interface for each gap element. This was done to ensure that the bolt would not be separated from the structural model at early stage of loading, i.e. increase the stability of the model. The value of each force corresponds to a stiffness value which is nearly equal to $10^{-6}$ times the normal stiffness

associated with the element input data. The accuracy of the solution would be not affected by adding such small forces.

2. A value of 0.2 was initially used as a coefficient of friction between both bolt and sleeve bodies. However, this proved to have of a great effect on the rate of convergence of the gap elements. Removing friction, i.e. assuming both surfaces to be smooth, increased the rate of convergence considerably.

## 4.15 Summary

As stated in section 4.1, the main objectives of the present study is to develop realistic models for the analysis of bolted joints using the finite element package ANSYS. In this section, the models' main features and properties are briefly summarised.

The objective of the models is to predict the different aspects of the structural behaviour such as deformations and internal stresses for the joint main components. Also, to gain information about the development of both cracking and crushing of the surrounding concrete.

Almost all nonlinear properties were considered in the solution phase. Material nonlinearity is associated with the plastic deformations of the bolt, sleeve and steel links materials. It is also included with the crushing and cracking of concrete. Interface nonlinearity arises from the change in the size of the geometric gap between the bolt and the sleeve. Large deflection analysis was also adopted in the solution phase.

Eight-node isoparametric elements were used in representing both the bolt and the sleeve. A special eight-node element was used to represent the concrete solid, while separate bar elements were used for simulating the steel links and the column main steel bars. Gap elements were used extensively to model the development of the contact area between the loaded bolt and the sleeve under

successive loading.

Imposed incremental vertical displacements at the loaded end was adopted. Convergence had to be achieved at each load step before applying the next one.

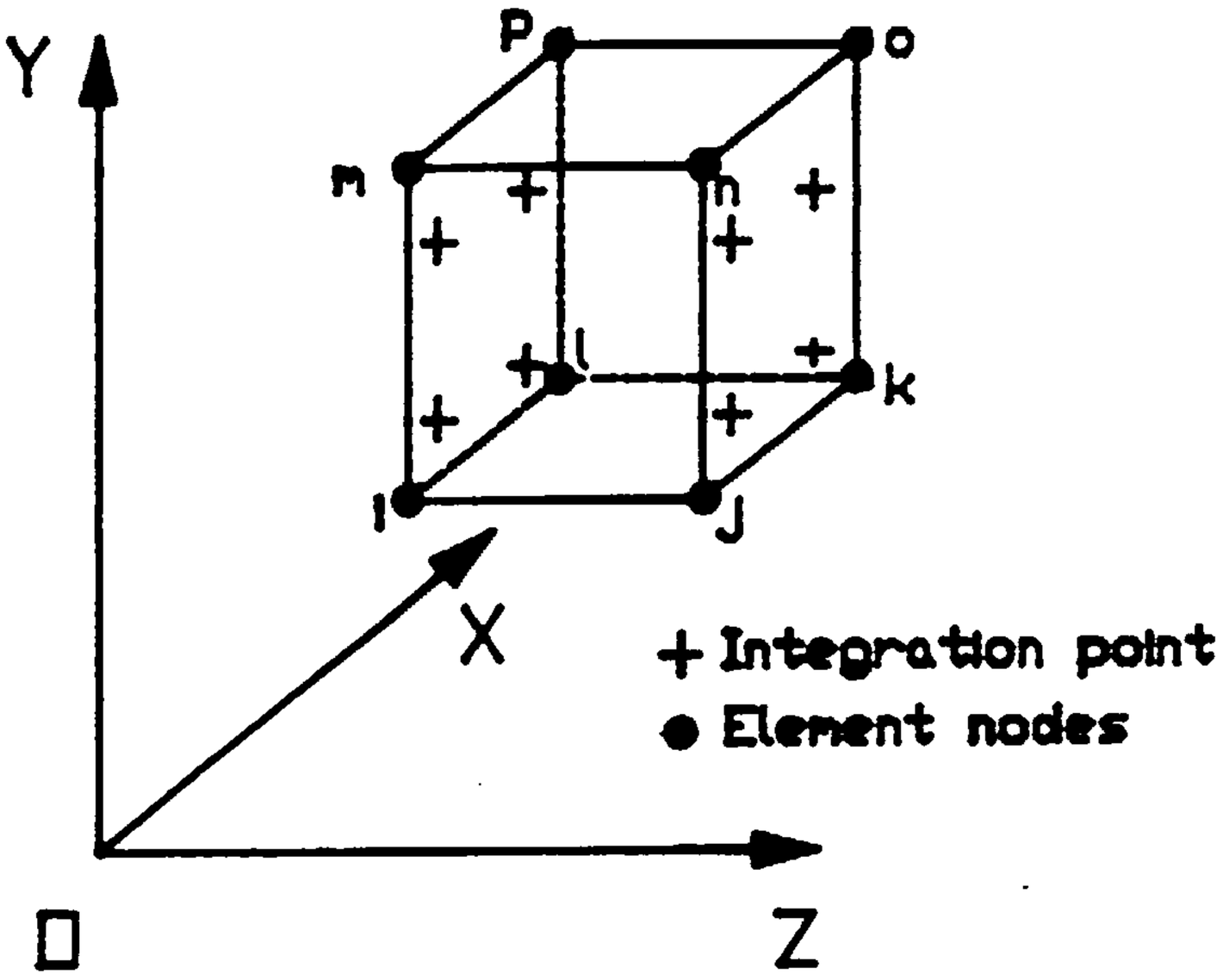


FIGURE (4.1) : A TYPICAL EIGHT NODED THREE-DIMENSIONAL ELEMENT.

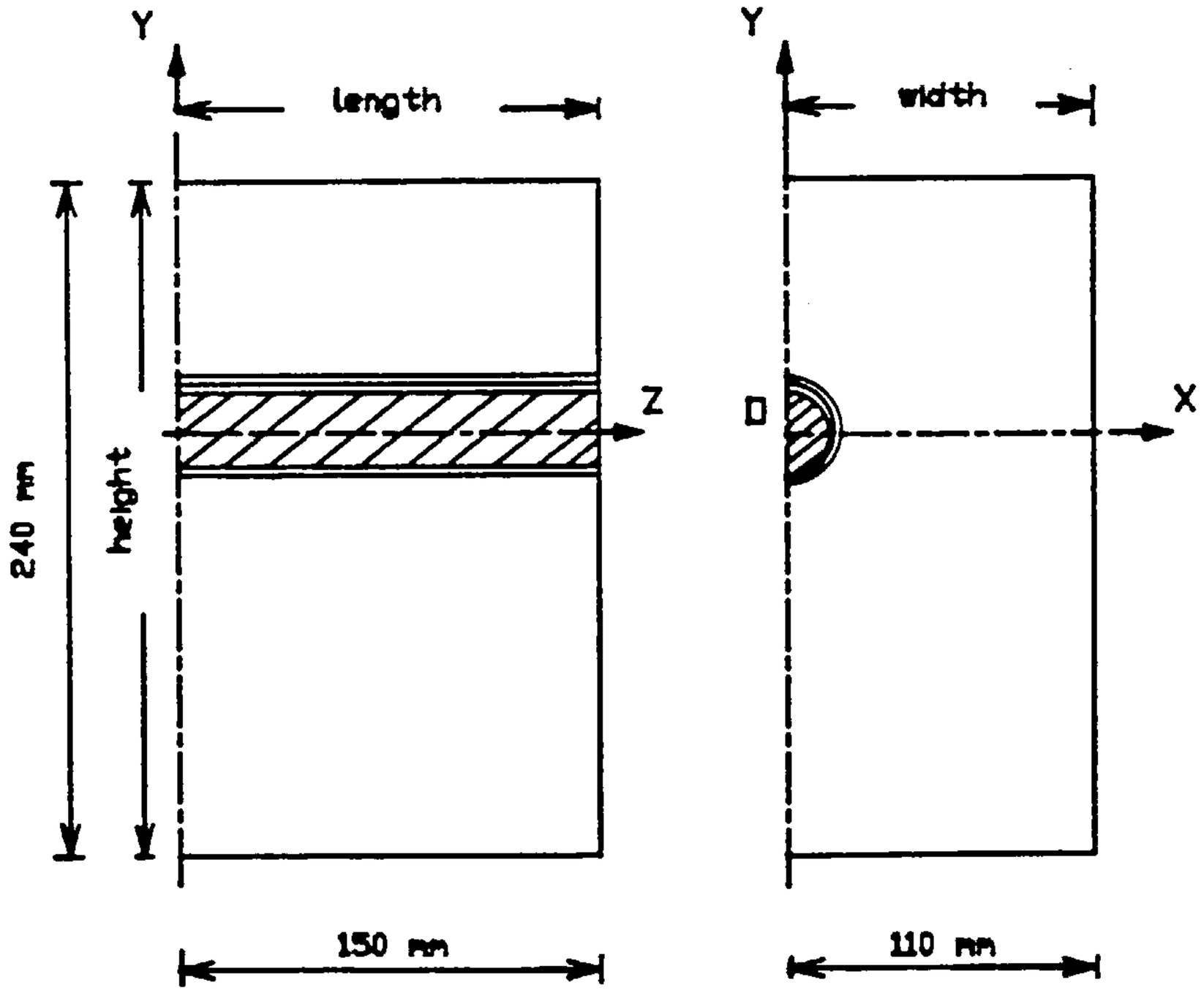


FIGURE (4.2) : GEOMETRY AND DIMENSIONS OF THE MODELLED JOINT.

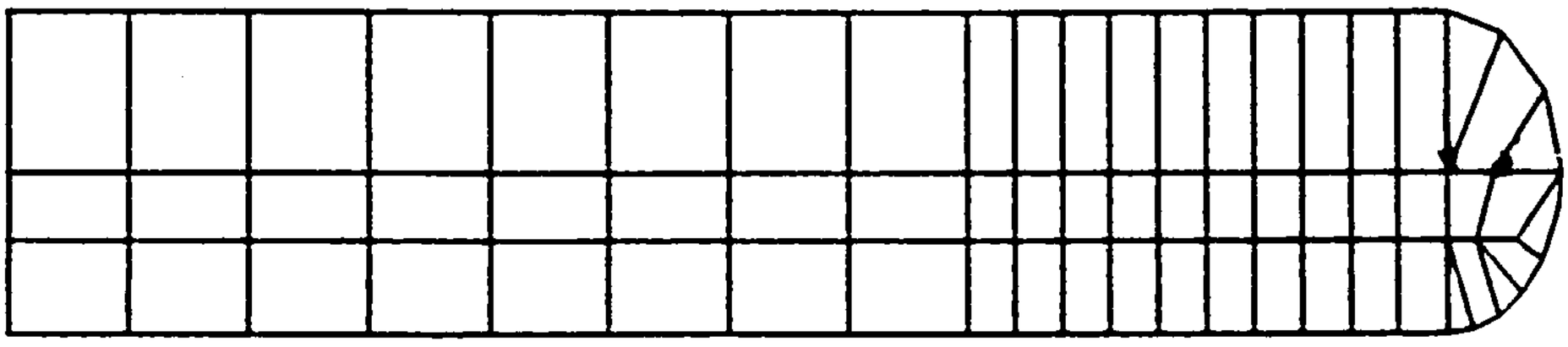

FIGURE (4.3) : FINITE ELEMENT DISCRETISATION OF THE BOLT SHANK.

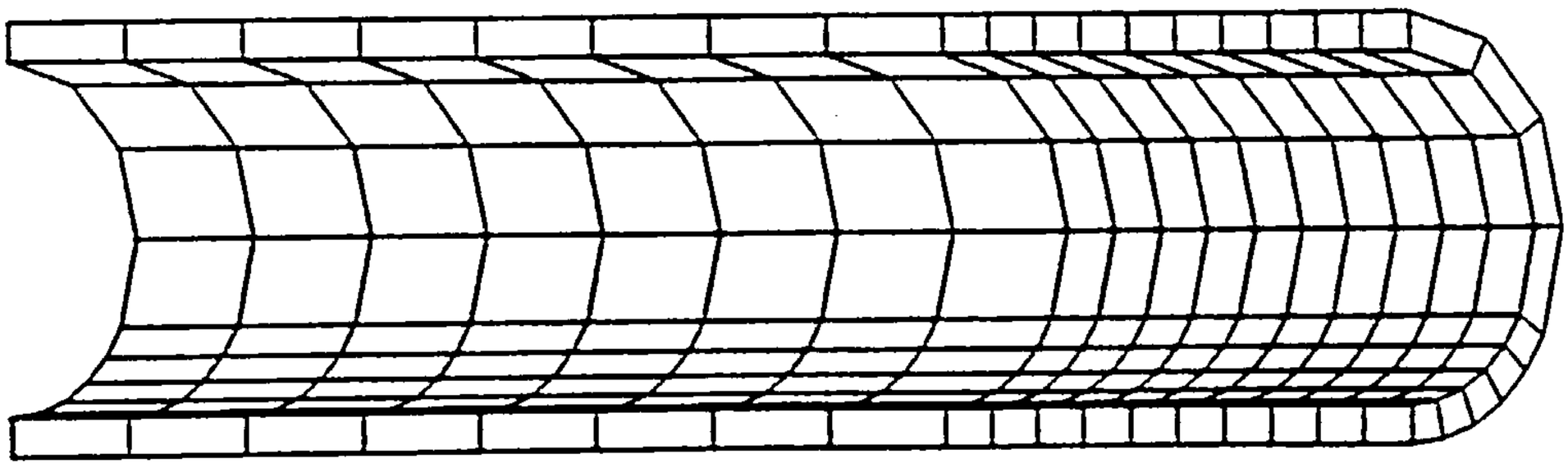

FIGURE (4.4) : FINITE ELEMENT DISCRETISATION OF THE SLEEVE.

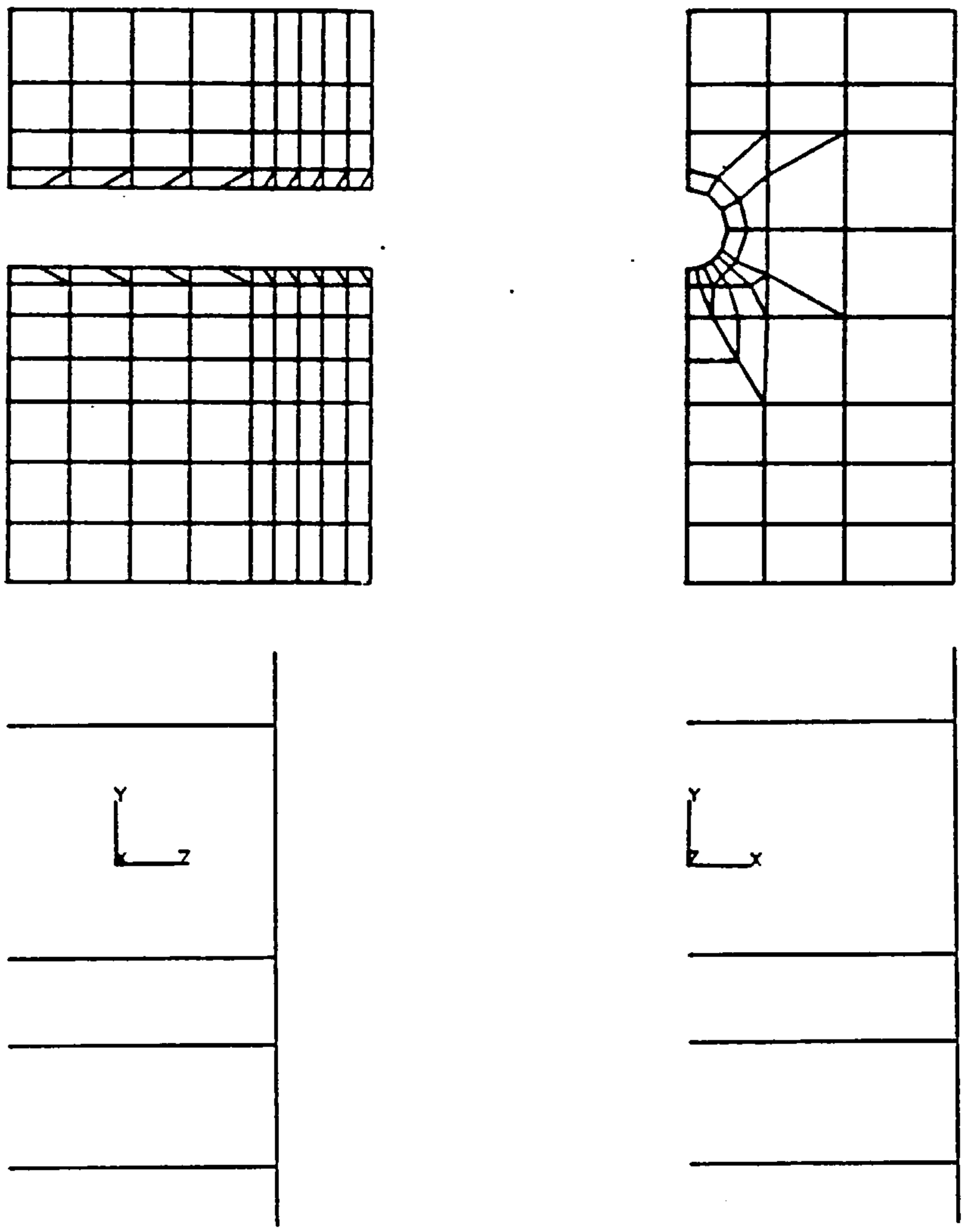


Left : Vertical section through plane containing sleeve axis.

Right : Face elevation.

Top : Concrete elements.

Bottom : Reinforcement elements.

A line of symmetry is located at the left of each view.

FIGURE (4.5) : FINITE ELEMENT DISCRETISATION OF THE CONCRETE SOLID WITH DETAILS OF REINFORCING BARS 'MODEL 1'.

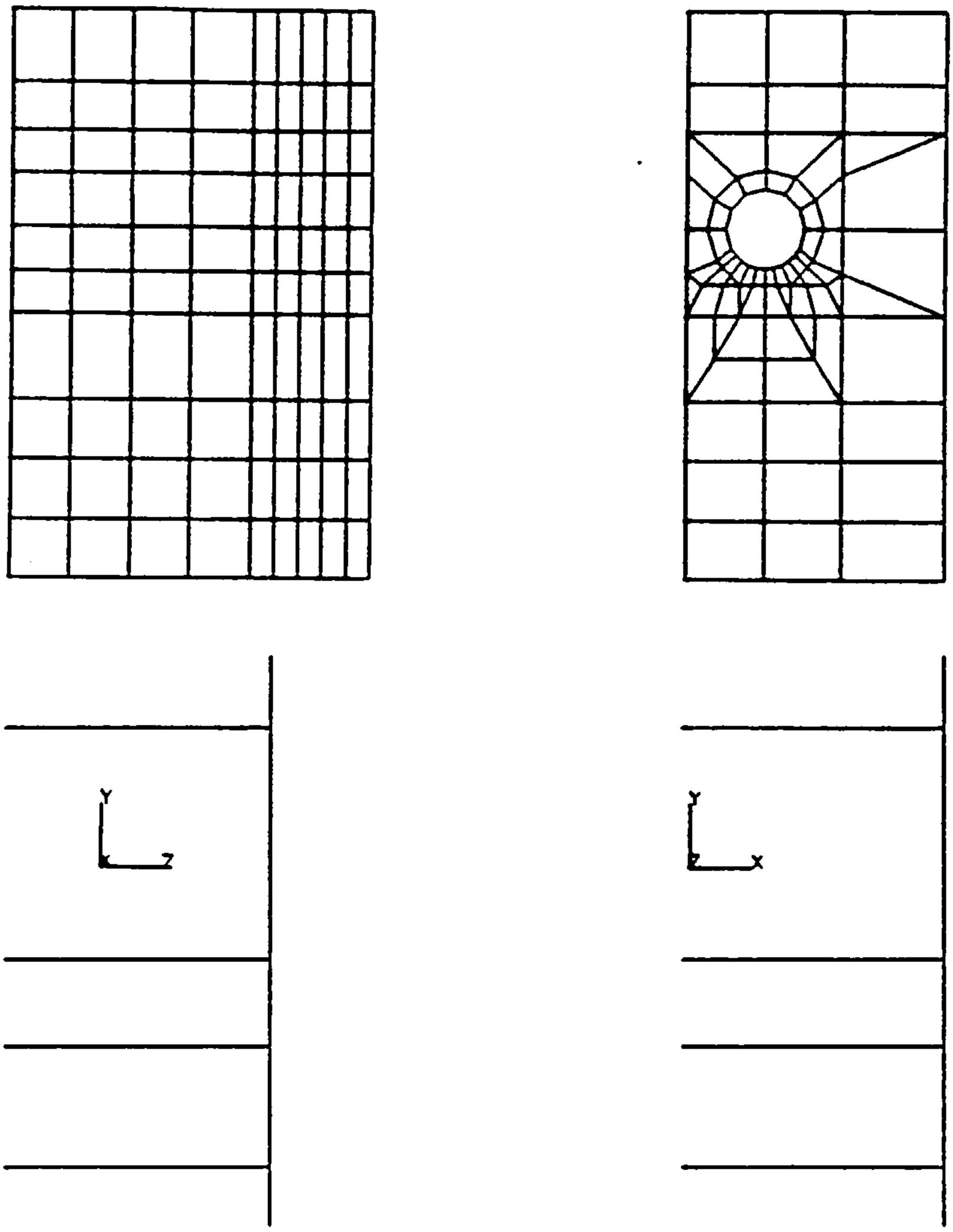


Left : Vertical section through plane containing sleeve axis.

Right : Face elevation.

Top : Concrete elements.

Bottom : Reinforcement elements.

A line of symmetry is located at the left of each view.

FIGURE (4.6) : FINITE ELEMENT DISCRETISATION OF THE CONCRETE SOLID WITH DETAILS OF REINFORCING BARS 'MODEL 2'.

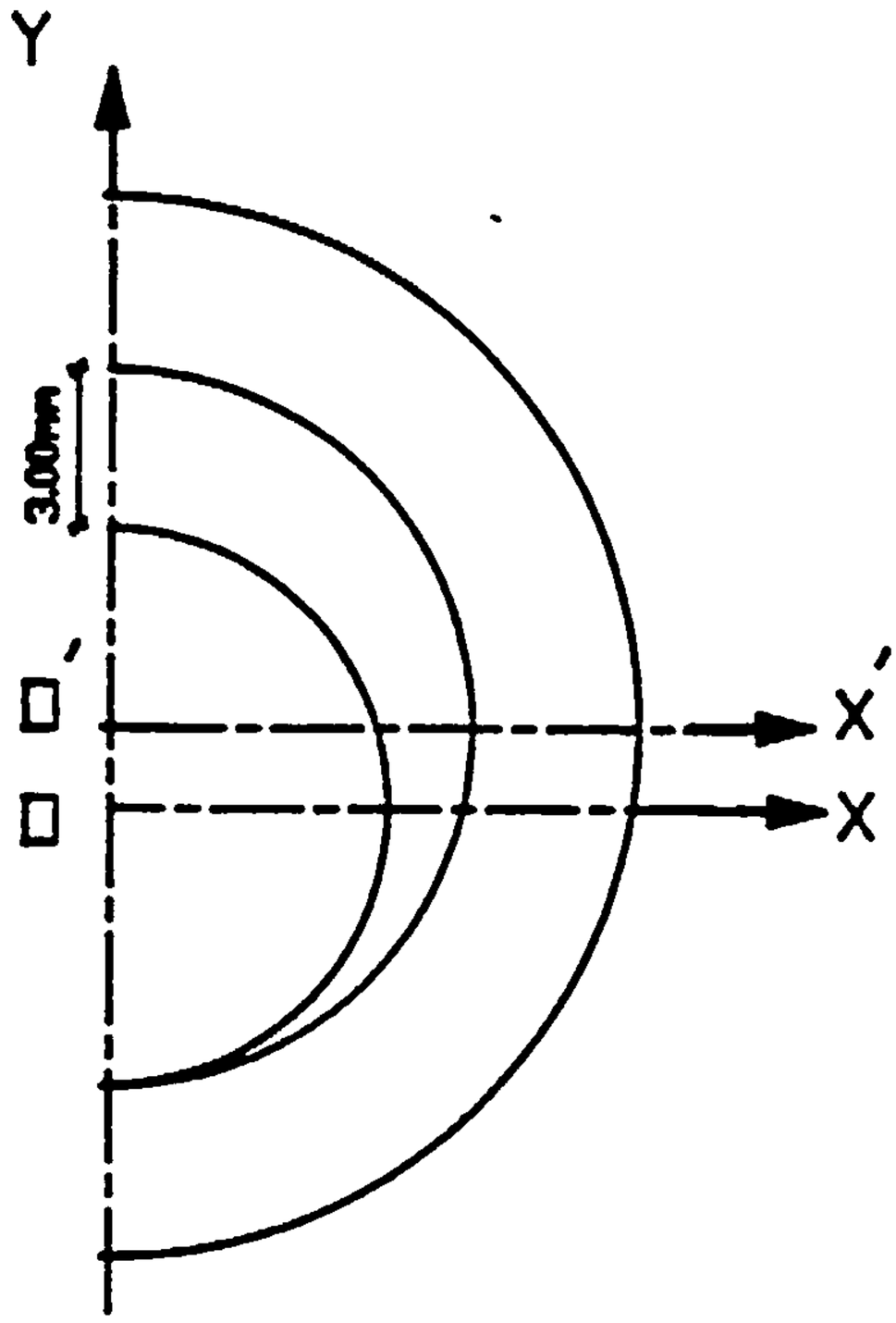


FIGURE (4.7) : INITIAL CONFIGURATION OF THE GEOMETRIC GAP BETWEEN THE BOLT AND THE SLEEVE IN THE XY PLANE.

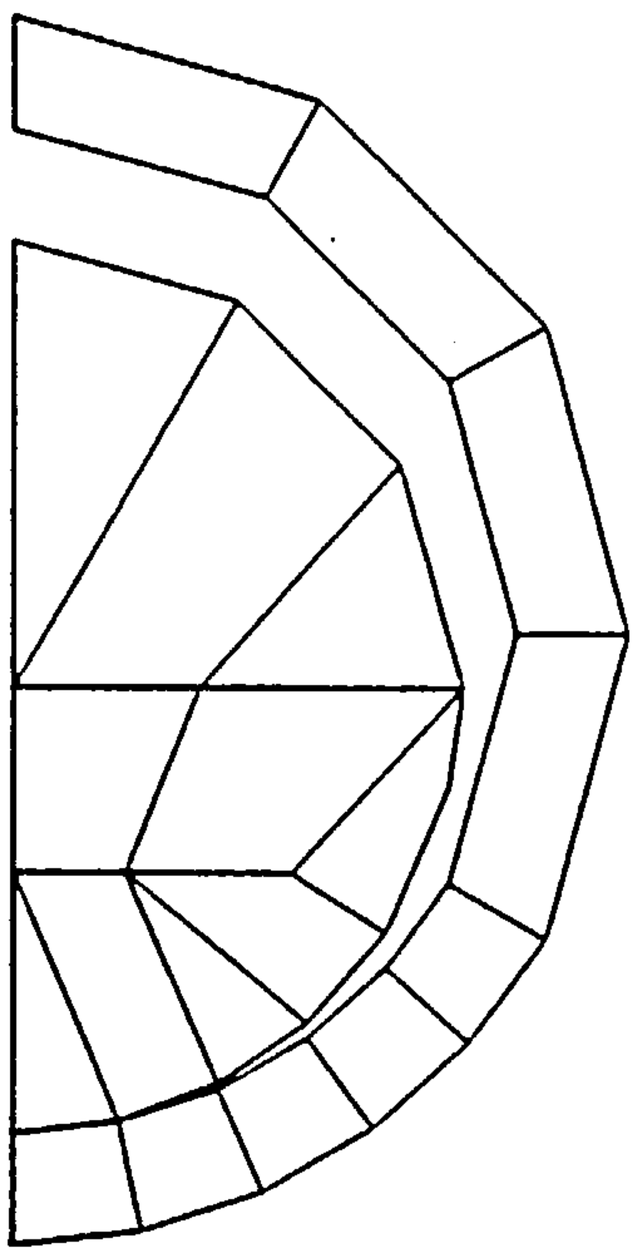

FIGURE (4.8) : A ONE-TO-ONE MAPPING OF THE NODES TO FACILITATE THE MODELLING OF THE CONTACT REGION BETWEEN THE BOLT AND SLEEVE.

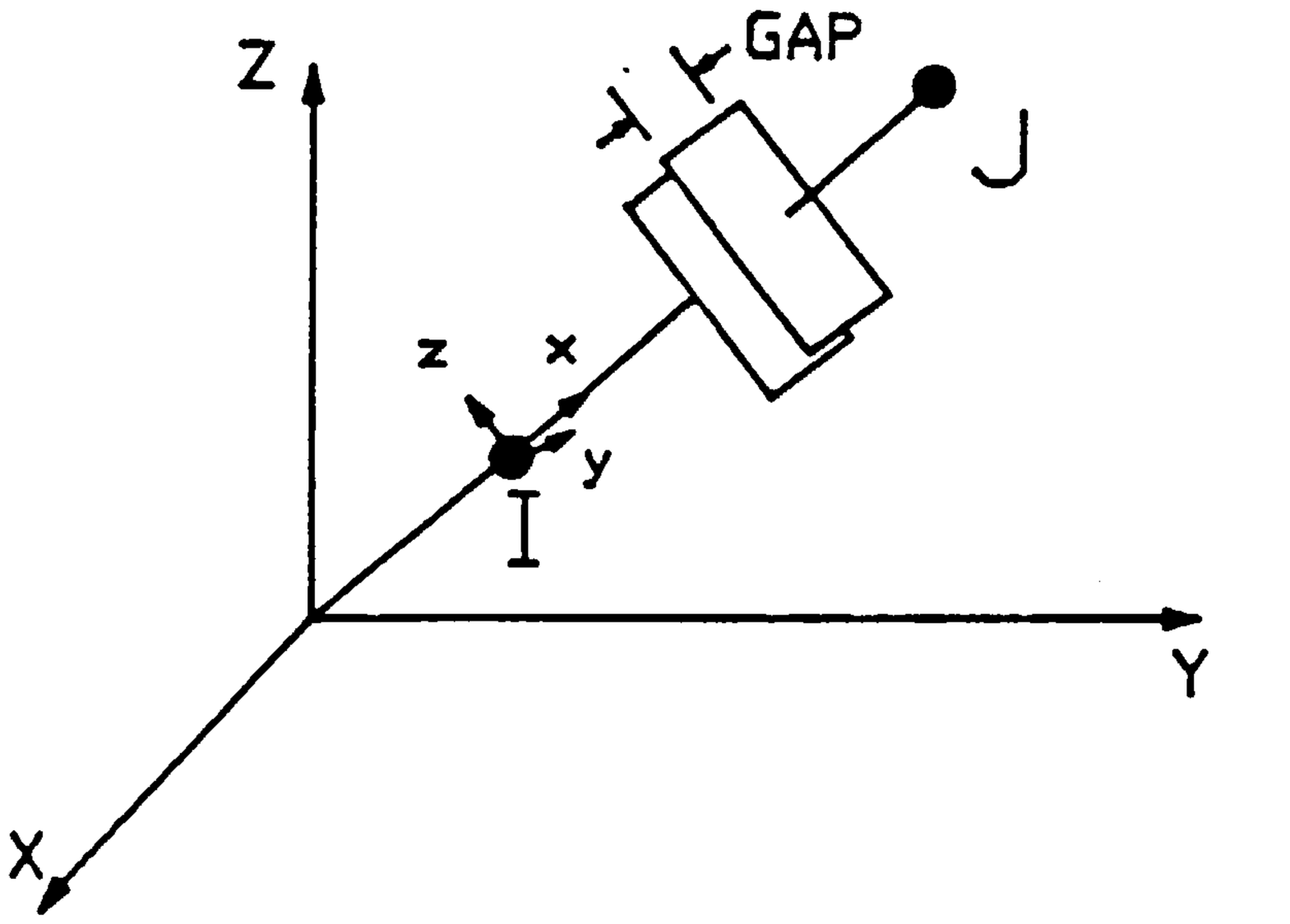


FIGURE (4.9) : A THREE-DIMENSIONAL INTERFACE ELEMENT WITH ITS BOTH GLOBAL AND LOCAL COORDINATE SYSTEM.

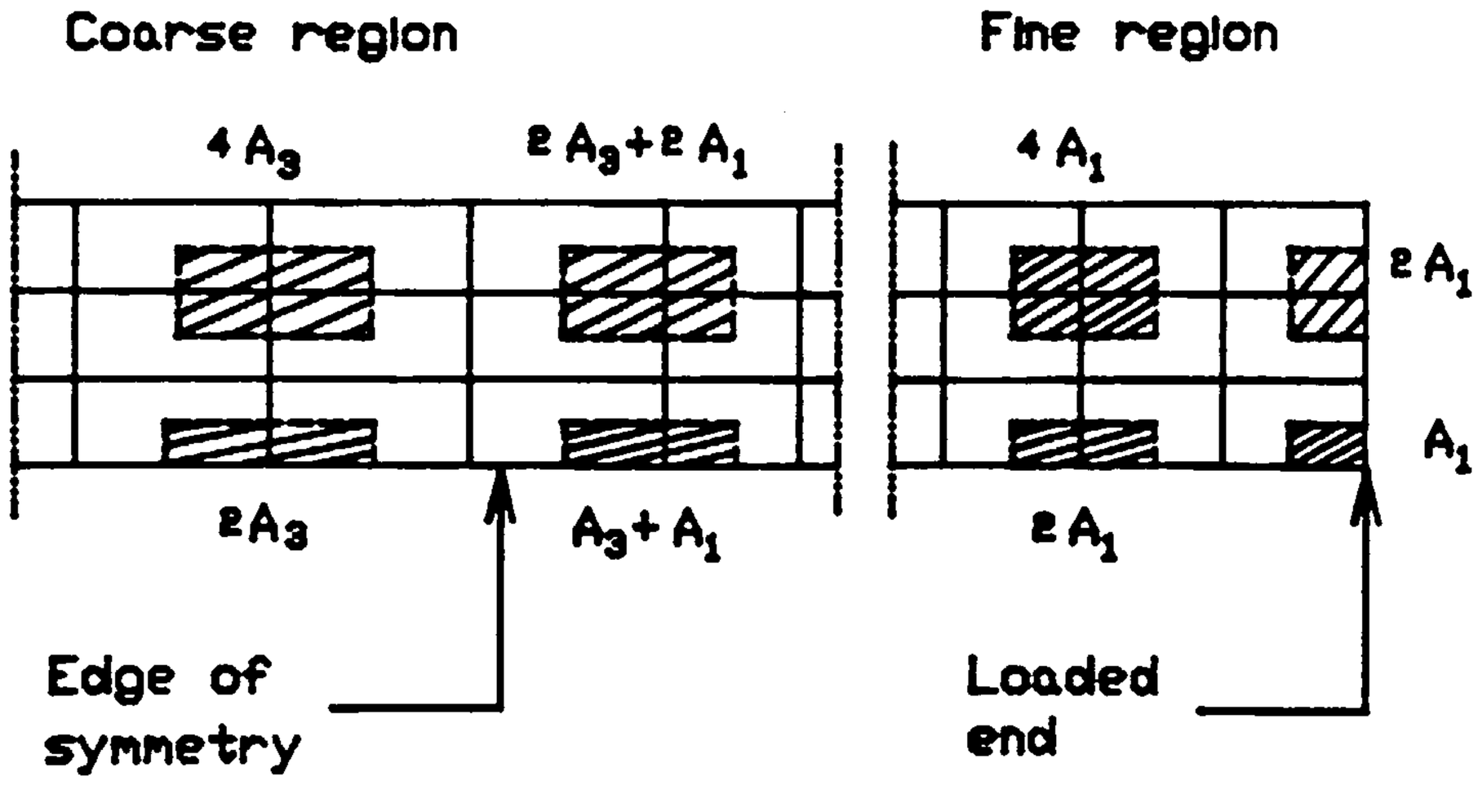


FIGURE (4.10) : PLAN VIEW SHOWING DIFFERENT SURFACE AREAS USED IN CALCULATING SPRING STIFFNESS VALUES.

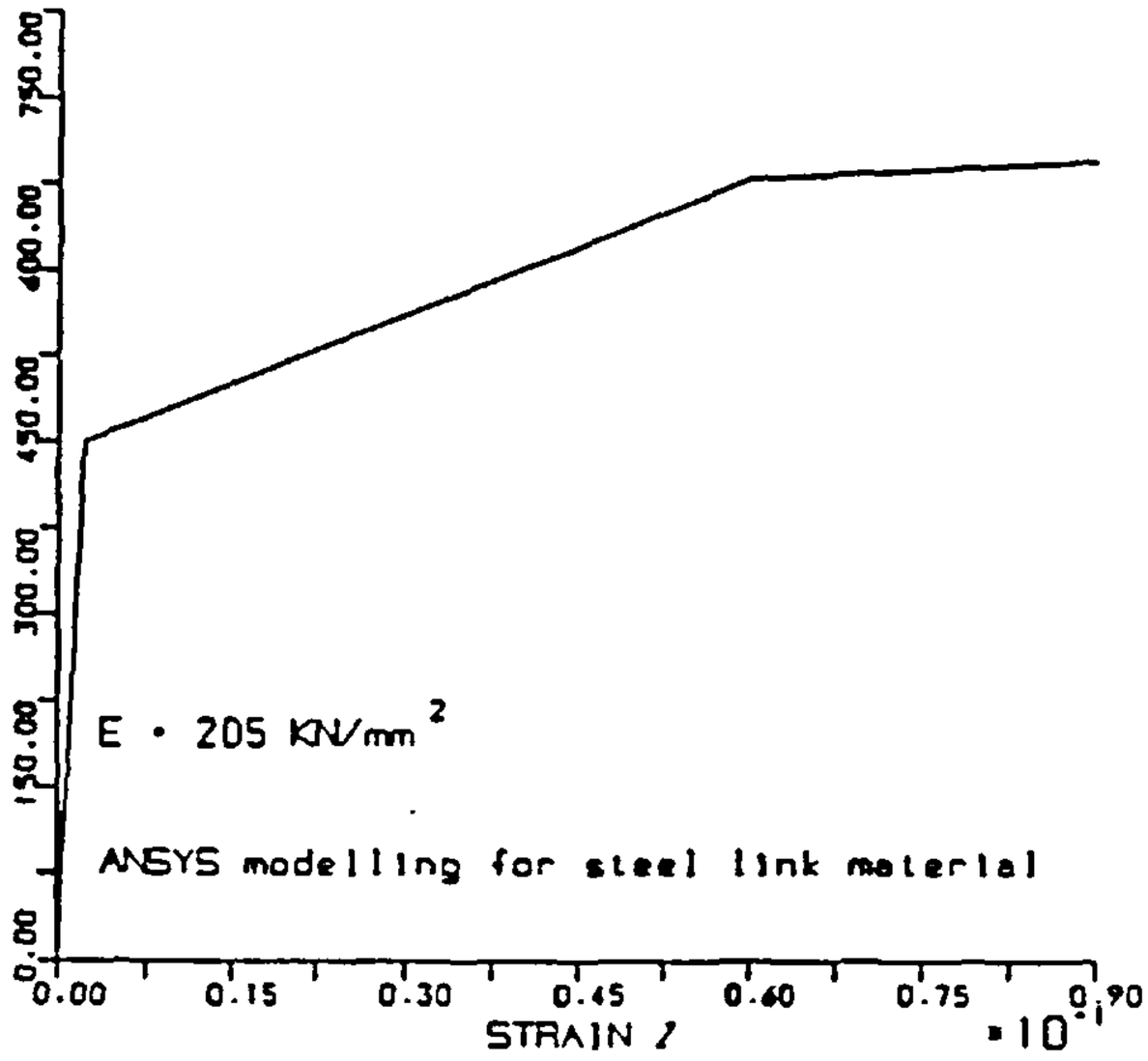


FIGURE (4.11) : STRESS-STRAIN CURVE FOR THE STEEL LINKS

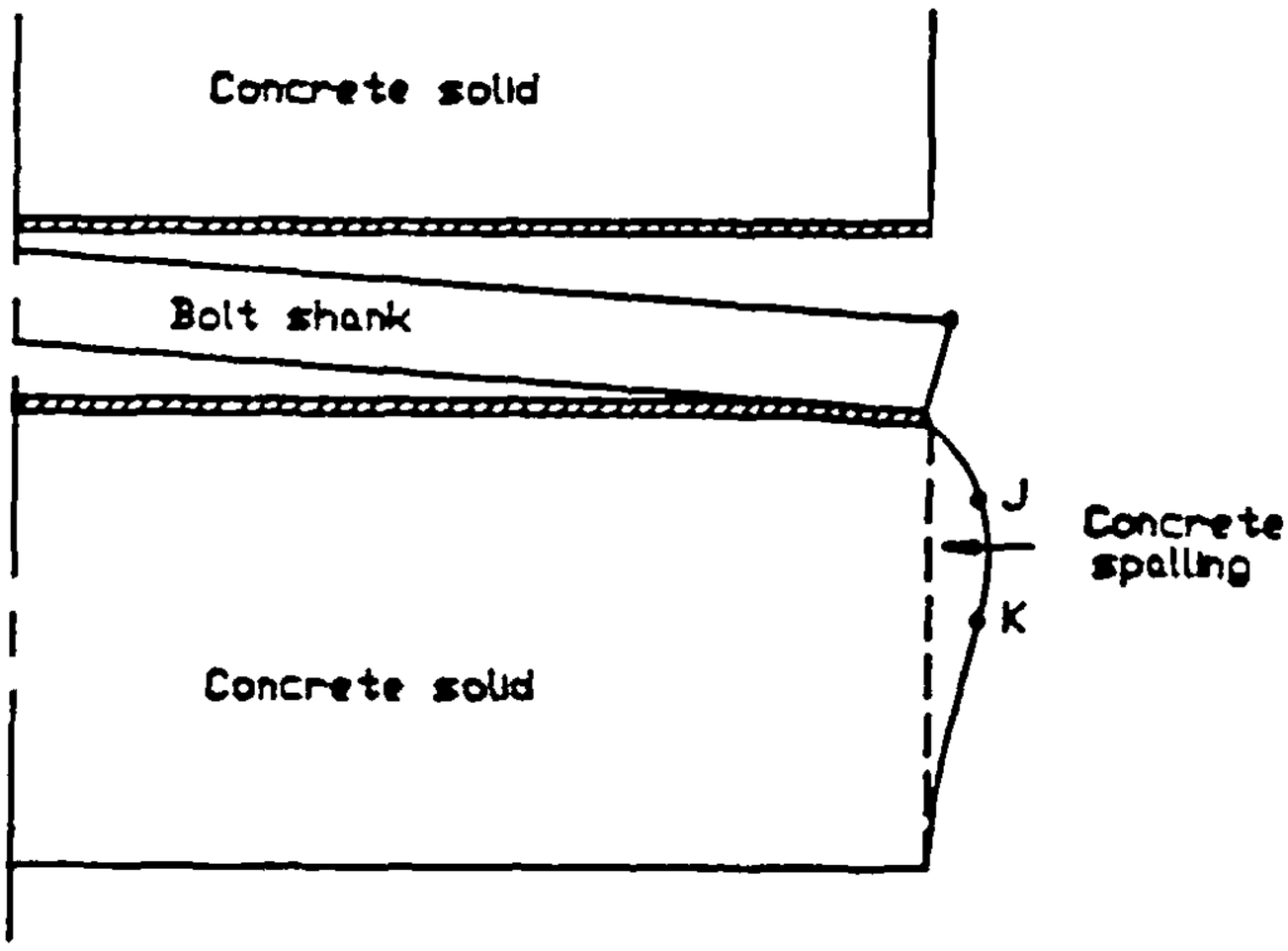


Plane of symmetry (YZ) for Model 1

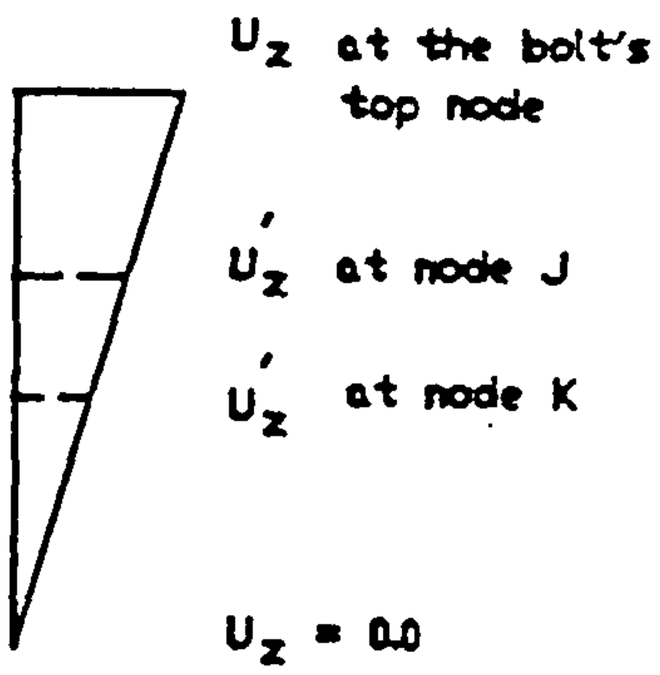


Assumed variation of outward deflection at load step n

FIGURE (4.12) : MODELLING THE RESTRAINT EFFECT PROVIDED BY THE BACK PLATE UPON THE COLUMN FACE.

# CHAPTER FIVE

# PRESENTATION AND ASSESSMENT OF CONCRETE MATERIAL MODELLING IN THE ANSYS PROGRAM

## 5.1 Introduction

Numerical modelling of concrete has the potential to play an increasingly important role in all areas of reinforced concrete research, analysis and design. It has been in use as tool for gaining better insight into the behaviour of concrete structures for the last twenty years. Comprehensive lists of reported works employing concrete modelling can be found in References [60-62]. However, its applicability is limited to some extent by the lack of a universally accepted model, which can be used in any general reinforced concrete structure. Moreover, the numerical prediction of the behaviour of a concrete structure is expected to be highly sensitive towards the basic input of the concrete material properties. This chapter sets out a summary of these properties with reference to the three-dimensional element STIF65 which is incorporated in the ANSYS program to model the concrete material. This is followed by three sample results given to calibrate the element under the application of loading.

## 5.2 Concrete Behaviour Under Axial Loading

Concrete exhibits a complex structural response with various important nonlinearities; namely a non-linear stress-strain behaviour, tensile cracking and compression crushing failures [63]. Also its behaviour under loading is highly affected by many variables such as nature of applied stress, rate of loading, mechanical strengths (compressive and tensile) and degree of

confinement. Concrete behaviour under axial, biaxial and multiaxial loading is well documented in References [60-62] and will, therefore, be discussed briefly in this section.

A typical stress-strain relationship for concrete subjected to monotonic uniaxial compressive load is shown in Figure (5.1). The curve is linearly elastic up to 30% of the maximum compressive stress $f_c$. This limit was proposed by Kotsovos and Newman [64] as a limit of elasticity. For stresses above this point, the concrete starts to behave nonlinearly up to about 70-90% of $f_c$ value where the curve bends until the peak stress is reached. Beyond the peak stress, the curve descends, indicating concrete strain softening. The curve continues to descend until failure is reached at the ultimate compressive strain $e_u$.

It is widely common practice to use the value of $f_c'$ obtained from testing either cubes or cylinders as a measure for assessing the quality of concrete. However, this value, on its own, is not sufficient to define a complete stress-strain curve representing the concrete's behaviour during all stages of loading.

The shape of the stress-strain curve is almost similar for different grades of concrete, with more pronounced brittle behaviour at higher strengths [65,66]. This fact attracted many researchers [67-70] to develop a numerical expression to describe both ascending and descending parts of the curve. Naturally, the accuracy of each of these expressions depends greatly on the number of parameters involved in its formation.

A more recent mathematical description of the curve proposed by Tsai [71] was found to be appealing because of its simplicity. Experimental data obtained by Kupfer et al. [72] was used in this study to examine its validity as shown in Figure (5.2). This figure demonstrates that Tsai's formula can successfully represent the uniaxial behaviour of concrete under short term monotonic loading. Hence, it was adopted in the present work. In

Tsai's formula, given below, the ratio Y of the concrete stress to the maximum compressive strength $f_c$ is given by

$$Y = \frac{m\ X}{1 + \left[m - \frac{n}{n-1}\right] X + \frac{X^n}{n-1}}$$

Where X = the ratio of the concrete strain e to the strain $e_p$ at the stress $f_c$.

m = the ratio of the initial modulus of elasticity $E_c$ to the secant modulus $E_o$ at y =1 , see Figure (5.3).

n = a factor to control the steepness rate of the descending part of the curve.

From the above formula, it is clear that some controlling material parameters have to be known in advance to trace a complete stress-strain curve for a given $f_c$. These parameters are listed below.

a) <u>The Initial Modulus of Elasticity</u> $E_c$

In the absence of direct measurement of the concrete stiffness, a reasonable value of the initial Young's modulus, $E_c$, had to be assumed. In the literature, a number of empirical equations were proposed for its calculation. These are listed in Reference [62] and plotted in Figure (5.4). In most of these, $E_c$ is taken to be a function of the square root of $f_c$. Using the average value of 61.90 $N/mm^2$, obtained earlier for $f_c$, values of $E_c$ appeared to vary between 33.3 and 47.2 $KN/mm^2$. It is worth pointing out that a factor of 1.3 was taken as a material factor $\Upsilon$ in the formula provided in BS8110 (serviceability limit state requirement). Based on these values and those recommended by BS8110, a representative value

of 37.0 KN/mm$^2$ was chosen to be employed in Tsai's formula. This value of $E_c$ had been also used for an almost similar concrete strength in a previous reported work [73].

b) The Compressive Strain $e_p$

The peak stress under short-time loading is attained at a strain value between 0.0015 and 0.002 for normal strength concretes[66]. As relatively higher strength concretes exhibit a slightly higher strain at the peak stress [60,61], a value of 0.002 was adopted for the strain $e_p$ corresponding with $f_c$.

c) The Ultimate Compressive Strain $e_u$

In concrete testing, the test specimen neither yields nor fails when maximum stress is reached; but a gradual decrease of stress at an increasing strain, called strain softening, is observed [74]. Since the softening branch of the curve is test-dependent, viewing it as a material property is questionable [75]. However, in the present work it will be treated as a material property to have a better representation of concrete in the post-peak stress range.

The strain value $e_u$ and the corresponding stress, at which failure is defined, have a strong dependence on the value of $f_c$. Visible cracks were reported to occur at a strain value of 0.0035 [62]. For design purposes, the same value of strain is set by BS8110 to limit the degree of crushing failure allowed in the concrete. As will be seen later in this chapter, ANSYS adopts a stress dependent crushing criterion and allows only for the ascending branch of the stress-strain curve to be modelled. Though, a value of n had to be employed in Tsai's formula to give rise to a curve similar to that reported by Wischers [76] for a similar concrete strength. Figure (5.5) shows the complete proposed 'target' stress-strain curve for the concrete material used in this work.

At this stage, it is worth emphasising that $f_c$ = 61.90 N/mm$^2$ was taken as the uniaxial compressive strength. The author is aware of the fact that a reduction factor of 0.7-0.9 should have been applied to $f_c$ to have a more representative uniaxial compressive strength, i.e. a cylinder strength rather than a cube strength. However, it was observed from preliminary trials carried out to verify element STIF65 that using an unreduced value of fc led to much better correlation with the experimental data.

Under uniaxial tension, concrete has a remarkably low ultimate strength. For practical purposes, it can be taken as 0.08 to 0.125 of the crushing strength [77]. In this work, the tensile strength was taken as the average strength of the four cylinder splitting tests, $f_t$ = 4.05 N/mm$^2$.

Experimental data indicated that concrete Poisson's ratio $\nu$ lies in the range between 0.15 and 0.22 [60]. Since a value of 0.2 was considered quite effective for normal concrete [61], it was used in this work. ANSYS assumes that $\nu$ has a constant value under all stress stages. Hence, any volume increase in concrete at and near peak stress will not be predicted by the element.

Under different combinations of proportional biaxial and multiaxial loading, concrete exhibits strength and stress-strain behaviour somewhat different from that under uniaxial conditions. A reduction or an increase in the concrete compressive strength is dependent on the nature of the applied stress (either tension or compression)[72].

## 5.3 Constitutive Modelling Capabilities in The ANSYS Program

### 5.3.1 Constitutive Model

In recent years, a large number of material models have been proposed to characterise the behaviour of concrete material.

Nevertheless, each model has its own advantages and limitations, which depend on the application, numerical implementation and stability. Some models are based on the classical elastic theory (recoverable strain during unloading) while others are plasticity-based (irrecoverable strain). In ANSYS, an elastic hardening plastic model is implemented to represent the behaviour of concrete. This assumption is more general than that of perfectly plastic material because it takes into account the material hardening up to the the peak stress, see Figure (5.6). In the literature, similar models based on this approach have been successfully used [78-81].

Following the incremental theory of plasticity, the total strain increments are decomposed into the elastic and plastic strain components. The elastic response is governed by a linear isotropic stress-strain law while the plastic one depends on the selected yield function, hardening and flow rules. All of these are addressed individually below.

a) Yield Function

For strain-hardening concrete, the initial yield surface is the limiting surface for concrete elastic behaviour. So if the state of stress lies within this surface, only linear-elastic constitutive equations are applied. On continuing straining beyond the initial yield surface, subsequent yield surfaces develop accompanied by irrecoverable plastic strains. In ANSYS, both the initial and subsequent yield surfaces (loading surfaces) are defined by the same yield function [53].

Figure (5.7) shows the projections of concrete yield surfaces in a two-dimensional principal stress space. From this figure, it can be seen that a yield function exists for any stress combination, i.e. biaxial compression, biaxial tension or combined compression-tension. In the biaxial compression zone, the von Mises yield function is used to define the elastic

limit and the flow function. Previous works [54,82] used this yield function successfully in concrete numerical analyses. In the biaxial tension, it is assumed that the initial yield surface coincides with the failure surface. Under this assumption, concrete behaves in a purely linear elastic manner up to failure without plastic deformation. The reader is referred to the ANSYS manual [53] for the definitions of all used yield functions.

b) Hardening Rule

The motion of the subsequent yield surfaces, described above, during plastic loading is described by the hardening rule. ANSYS provides a kinematic hardening rule which assumes that during plastic flow the yield surface translates as a rigid body in the stress space, maintaining the size and shape of the initial yield surface, see Figure (5.8).

c) Flow Rule

The flow rule relates the plastic strain increments to the corresponding stress increments at a certain load step. It can be either an associated or a non-associated are depending whether the incremental plastic strains are connected with the yield function or not. The former is adopted in this work as it gives rise to a symmetrical elastic-plastic matrix which is more efficient from the computational point of view. Also, it has been satisfactory implemented with concrete modelling in many reported works [78,79,83].

Explicit matrix constitutive equations relating the strain to the stress are given in the ANSYS theoretical manual [53].

### 5.3.2 Failure Criterion

The strength of concrete under multiaxial stresses is a function

of the state of stress and can not be predicted by limitations of simple tensile and compressive stresses independently of each other [61]. Therefore, a failure criterion is always needed to determine the concrete strength by considering the interaction of the various components of the state of stress. Many failure criteria for concrete have been proposed in the past. A comprehensive review of these can be found in References [60-62].

In ANSYS, the elastic strain-hardening plasticity-based model, described above, is combined with a five parameter failure criterion [84] for a complete characterisation of the concrete material behaviour. This particular failure criterion has provided a very good fit to experimental data [62]. However, its main disadvantage is that it requires a considerable amount of computational time [80].

To represent the failure criterion, two values must be explicitly defined in the input data. These are the uniaxial tensile and compressive strengths. Then the program generalises the given value of the latter creating three additional parameters to take biaxial and triaxial stress conditions into account.

At this stage, it is necessary to explain that a failure of a concrete element will be defined, in the present work, as the element's ultimate load-carrying capacity. Two types of failures are accounted for, these are tensile cracking and compression crushing failures.

## 5.4 Special Features of Element STIF65

### 5.4.1 Cracking and Post Cracking Behaviour

The cracking of concrete is the most significant factor that dominates the behaviour of concrete structures. The response of STIF65 under tensile stresses is assumed to be linear elastic until the cracking surface is reached. This surface is governed

by the prescribed concrete tensile strength $f_t$. In this element, a smeared crack approach is adopted. This approach, introduced by Rashid [85], represents cracks as a change in the material property of the element over which the the cracks are assumed to be smeared. The distributed cracking representation is based on the concept of a stress discontinuity while it maintains the displacement continuity across the crack. This concept fits the nature of the finite element displacement method, as the continuity of the displacement field remains intact.

A crack appears at an integration point when any principal tensile stress exceeds the given $f_t$. The crack direction is perpendicular to this principal stress. A plane of weakness, in a direction normal to the crack face, is introduced and the normal stress at the crack drops to zero. With this approach, cracked concrete material is assumed to be orthotropic with principal axes being normal and parallel to the crack direction, see Figure (5.9). According to the type of strain across the crack (compressive or tensile), the status of crack becomes closed or open respectively. Once a crack is formed, its direction is assumed to be fixed for all subsequent loading. Cracks orientation can be obtained directly in the post-processor phase. Upon further loading of singly cracked element, up to two additional sets of cracks might be formed in orthogonal directions to the first set at the same integration point. Crack representation is given in details in the ANSYS manual [53].

As cracked concrete can partially transmit shear across the crack due to the aggregate interlock, a positive shear retention factor was used to reduce the shear modulus of the uncracked concrete. A constant value of 0.5 was used to achieve this reduction. This value was successfully used elsewhere [86,87]. Beside the realism of the aggregate interlock representation, having a reduced shear modulus proved to remove any numerical difficulties caused by the singularity of the material's constitutive matrix if it had a zero value [60].

The major shortcomings of crack representation in ANSYS can be listed as follows:

1. As cracks are represented as infinite numbers of parallel fissures across the area associated with the cracked integration point, their exact positions, widths and spacing are not available from the analysis.

2. Near ultimate loads, propagation rate of cracks increases with a marked tendency to join together. This may lead to a change in their initial directions, predicted by the fixed crack model. A rotating crack model would have been probably better in this aspect [88].

3. The smeared crack approach has been criticised by Bazant [89] for being a mesh size dependent.

4. Cracked concrete can still carry some tensile stress in the direction normal to the crack, i.e. tension stiffening. Numerical predicted behaviour was reported to be much improved by applying the tension stiffening stress to the cracked concrete [81]. In ANSYS, tension stiffening is not accounted for as the modulus of elasticity, normal to the crack direction, drops immediately to zero as shown in Figure(5.10).

5. ANSYS only offers the use of a constant shear retention factor. The use of a variable reduced shear modulus has been found to offer a more realistic modelling of the post-crack behaviour [90].

### 5.4.2 Crushing and Post Crushing Behaviour

Within a concrete element, crushing occurs at an integration point when the state of stress is multiaxial compression and the stress level is beyond the von Mises failure surface, shown in

Figure (5.7). Under this condition, the material associated with this point loses its strength completely and all its stresses are released and distributed among other integration points. This is reflected by a drop in the element's equivalent stress.

A crushed element whose all eight integration points are crushed has no contribution in the global stiffness matrix. As previously mentioned, a major shortcoming in the input of STIF65 is that there is no strain criterion (limiting value) combined with the crushing strength to give more general crushing simulation. To prevent the numerical difficulty associated with negative tangent moduli, once the peak stress has been reached, the unbalanced stresses are released in a stepwise fashion with a zero tangent modulus value assuming perfectly plastic behaviour, see Figure (5.11).

### 5.4.3 Post-Crushing Stability

Crushing of some concrete elements in the heavily stressed region was expected to occur at early stages of loading. This would give rise to a stress redistribution which could be so high as to locally upset the numerical stability of the model even with employing small load increments. To overcome this problem, it was required to keep the crushed elements numerically effective with a minimum strength capacity. It was not possible, due to the limitations of the software, to allocate new material properties to these elements after being crushed.

One way of averting the problem was to stiffen-up the concrete elements by taking full advantage of their smeared nature. A percentage of the element's volume was introduced as smeared material within the element. This material has strength in its direction only and exhibits the same stress-strain curve but with an infinite much reduced slope beyond the peak stress, see Figure (5.12). Thus as the element gets crushed, the smeared material continues to transfer load to the surrounding elements. Within an

element, a very small percentage of the volume was used in all three orthogonal directions (X,Y,Z). A value of 0.01% was found to be numerically satisfactory. Also, the ductility of the element was significantly improved by adding this 'reinforcing material' as will be seen shortly in Section 5.5.

### 5.4.4 Concrete-Steel Interaction

The behaviour of concrete and steel materials were modelled separately through their stress-strain relationships. Values for yielding, cracking and crushing strengths were given as material input data. However, the bond between the concrete and steel was not modelled in detail. It is assumed in this work that there is a sufficiently strong bond between the links and concrete so that no relative movement of the steel and the surrounding concrete can occur. The facts listed below ruled out the adoption of bond detailed modelling.

1. In the literature, bond has been modelled by using either two or three-dimensional linkage elements [91,92]. These elements have a similar behaviour to the gap elements used in the present work. The adding of these elements would mean introducing additional nodes occupying the same space of the original nodes. As a result, the total number of degrees of freedom would increase leading to an increase of the model wavefront. This increase would not agree with the software limitation of the wavefront.

2. The use of the smeared-crack approach spreads the effect of cracking over a large region which far exceeds the localised region where bond slip actually occurs. Therefore, the use of this approach appears to be incompatible with a detailed modelling of the interaction between steel and concrete [93].

With the above facts in mind, the interaction can be considered to be adequately described by the assumption of perfect bond.

### 5.4.5 Creep Effect

Test results, reported in Chapter 3, indicated that no significant creep effect was observed. As a result, it was felt that it is not necessary to include such effect in the numerical analysis.

## 5.5 Element Verification

A previous work [41] had verified element STIF65 in shear through modelling simply supported beams with different reinforcement distributions and material properties. In that work, comparing the numerical results with its experimental counterpart had led to the conclusion that the multilinear stress-strain relation is a more realistic way to model plain concrete behaviour. However, in order to have more confidence in the use of this element under the application of axial loading, there was a need for more verification. In this section, the adequacy of STIF65 is verified by comparing numerical predictions against theoretical and experimental data obtained from standard cube and cylinder splitting tests similar to those reported in Chapter 2.

### 5.5.1 Kupfer's Concrete Prism

A plain concrete prism 200x200x50 mm tested by Kupfer et al.[72] was modelled with 25 mm cubic elements as shown in Figure (5.13). A uniform uniaxial loading was applied to the model by displacing the top and bottom faces towards each other. As brush bearing plattens were used in the test producing only little friction on the concrete-steel interface [94], the top nodes were not restrained in any direction. The material properties adopted are based on Kupfer's data [72]. Also no reinforcing material was used within the elements' volume. Figure (5.14) shows a very close correlation between predicted and the ascending portion of the reported stress-strain curve (which is input to the program). Failure was spontaneous as soon as the peak stress was reached.

### 5.5.2 Standard Cube Test

A 100 mm cube was modelled by 125 cubic elements as shown in Figure (5.15). Boundary conditions were imposed to simulate those existing in a cube testing. The top of the cube was laterally constrained to simulate the friction effect of the stiff top platten at the platten-specimen interface. The top nodes were displaced equally in the vertical direction. The stress-strain response predicted numerically is compared with the target curve in Figure (5.16). The peak stress obtained numerically represented 96% of the maximum input peak stress. This was obtained at strain value of 0.002 which agrees very well with that given in the input data.

For comparison purpose, the curve representing the unreinforced concrete material is also shown in the same figure. It is interesting to note that adding the 'reinforcing material' to the elements made it possible to trace out the softening branch numerically up to failure. Oscillatory behaviour in stress was observed at high strains before failure, while convergence was still well maintained. It is suspected that the cause of this behaviour was due to the high confining stress at the top boundary elements which increased the residual strength in the cube.

### 5.5.3 Cylinder Splitting Test

Using symmetry, one quarter of a 100x200mm cylinder was modelled with 93 concrete elements. The finite element mesh is shown in Figure (5.17) where the load is applied through two stiff steel elements forming a half loading strip of 8.00mm total width. Symmetry boundary conditions were imposed at the vertical and horizontal planes of symmetry. A plane strain analysis was adopted in this model, i.e. no strain in the longitudinal direction. This type of analysis was believed to be adequate as

previous works have demonstrated its capability to simulate similar models [95,96]. For concrete, the material adopted in the cube model was used while a linear behaviour is assumed for the steel. Perfect bond was assumed between steel and concrete. The cylinder failed at an ultimate load of 140.0 KN, at which no solution could be obtained for a very small load increment. This value is 1.12 times the average experimental value. During loading, an almost uniform horizontal tensile stress existed over about 0.75 of the diameter as shown in Figure (5.18).

## 5.6 Concrete Input Data in The Program

Based on the results of the analytical investigations, described in the previous section, the concrete input data was considered reliable enough for estimating the concrete behaviour during all loading stages. In the program, the following material model parameters were adopted:

1. The ascending branch of the uniaxial stress-strain curve is represented as a series of four data points as shown in Figure (5.5).

2. The value of the initial Young's modulus taken as 37.0 KN/mm$^2$.

3. A constant value for Poisson's ratio 0.20.

4. A constant value for the shear retention factor 0.50.

5. Values for the crushing and tensile strengths under uniaxial conditions taken as 61.90 N/mm$^2$ and 4.05 N/mm$^2$ respectively.

6. A 0.01% of the volume of concrete elements was represented in a smeared fashion, having similar stress-strain curve to that of the concrete but with a much reduced slope beyond the peak stress.

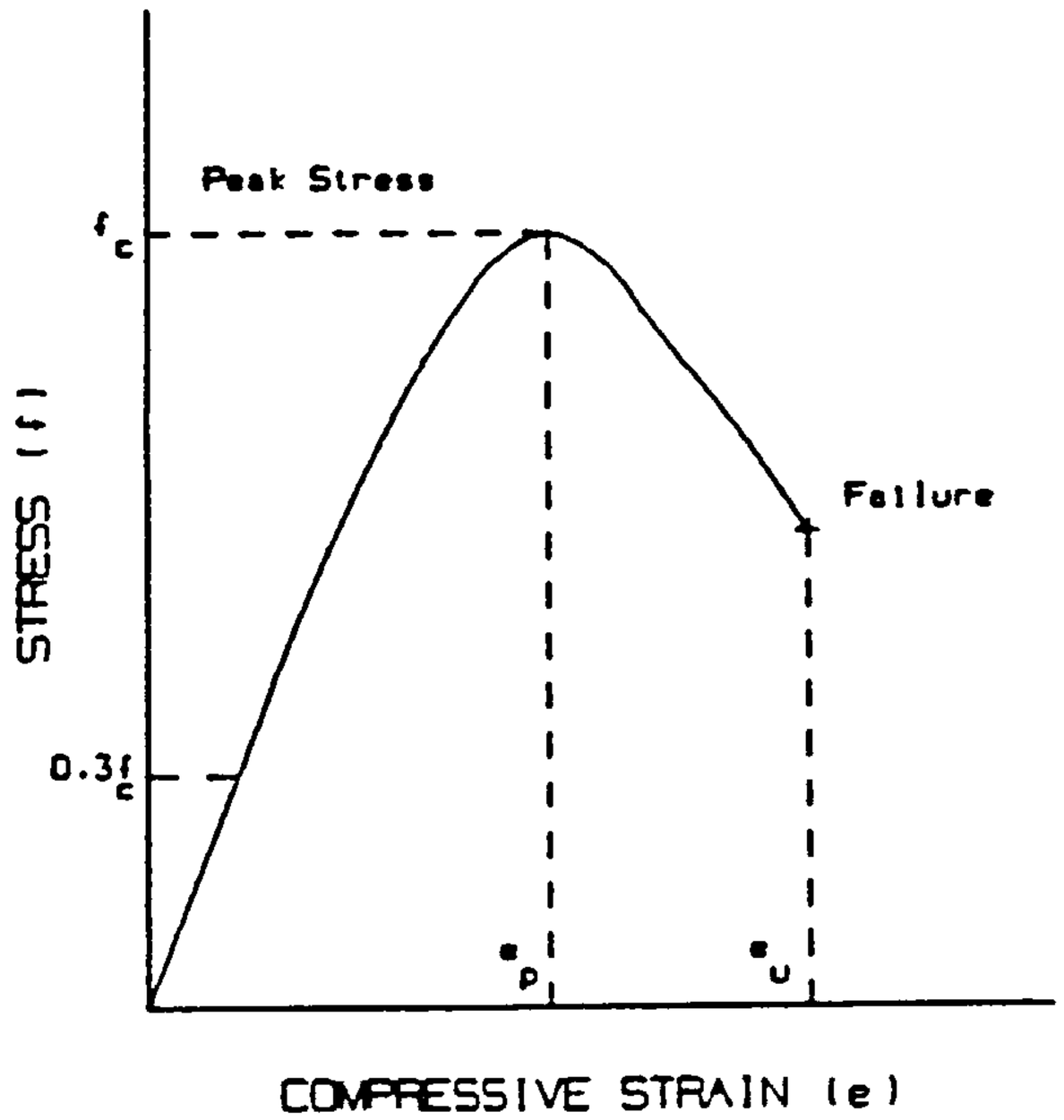


FIGURE (5.1) : CONCRETE STRESS-STRAIN RELATIONSHIP IN UNIAXIAL COMPRESSION.

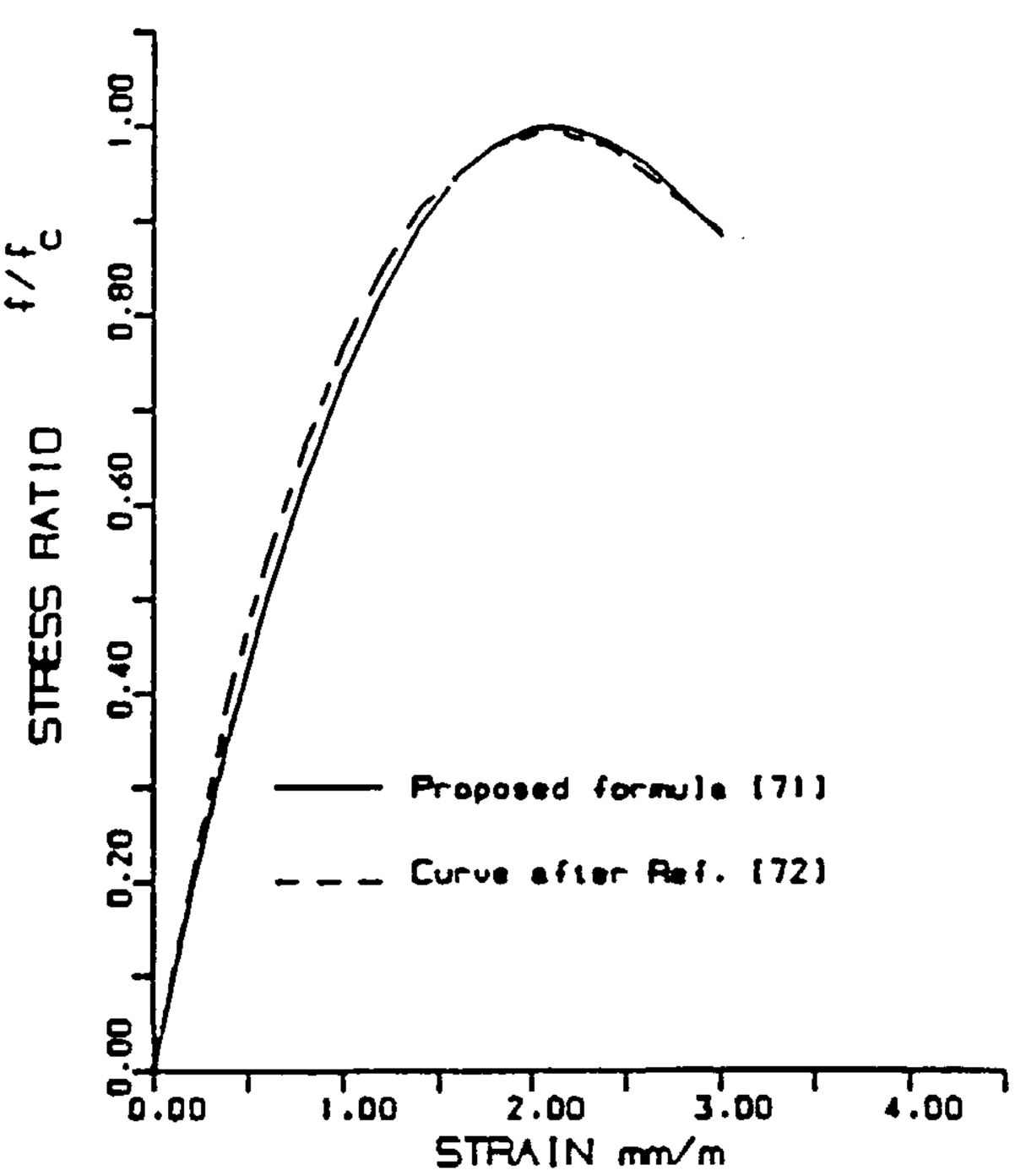


FIGURE (5.2) : VERIFICATION OF TSAI FORMULA USING KUPFER DATA.

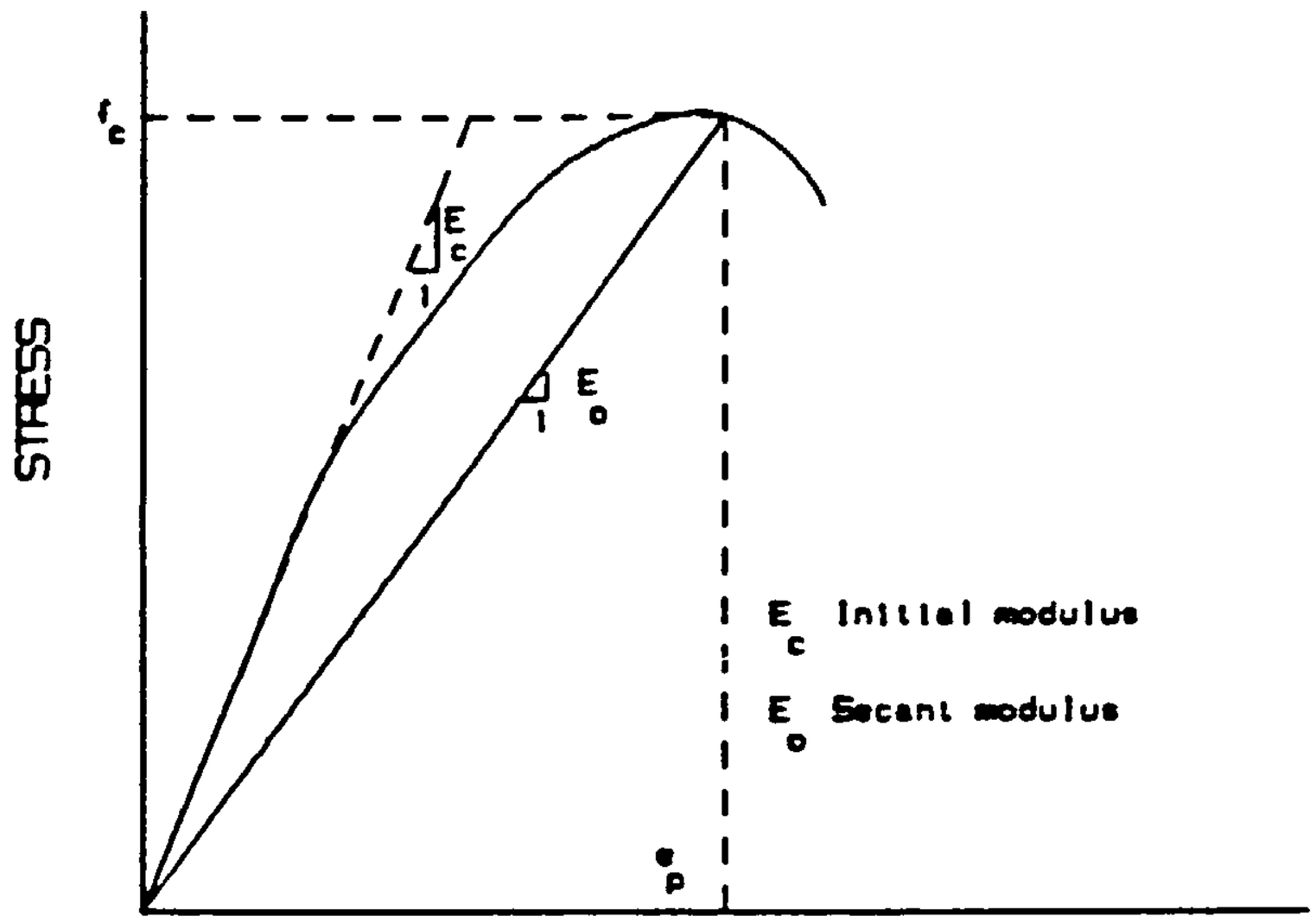


FIGURE (5.3) : INITIAL AND SECANT MODULI OF CONCRETE.

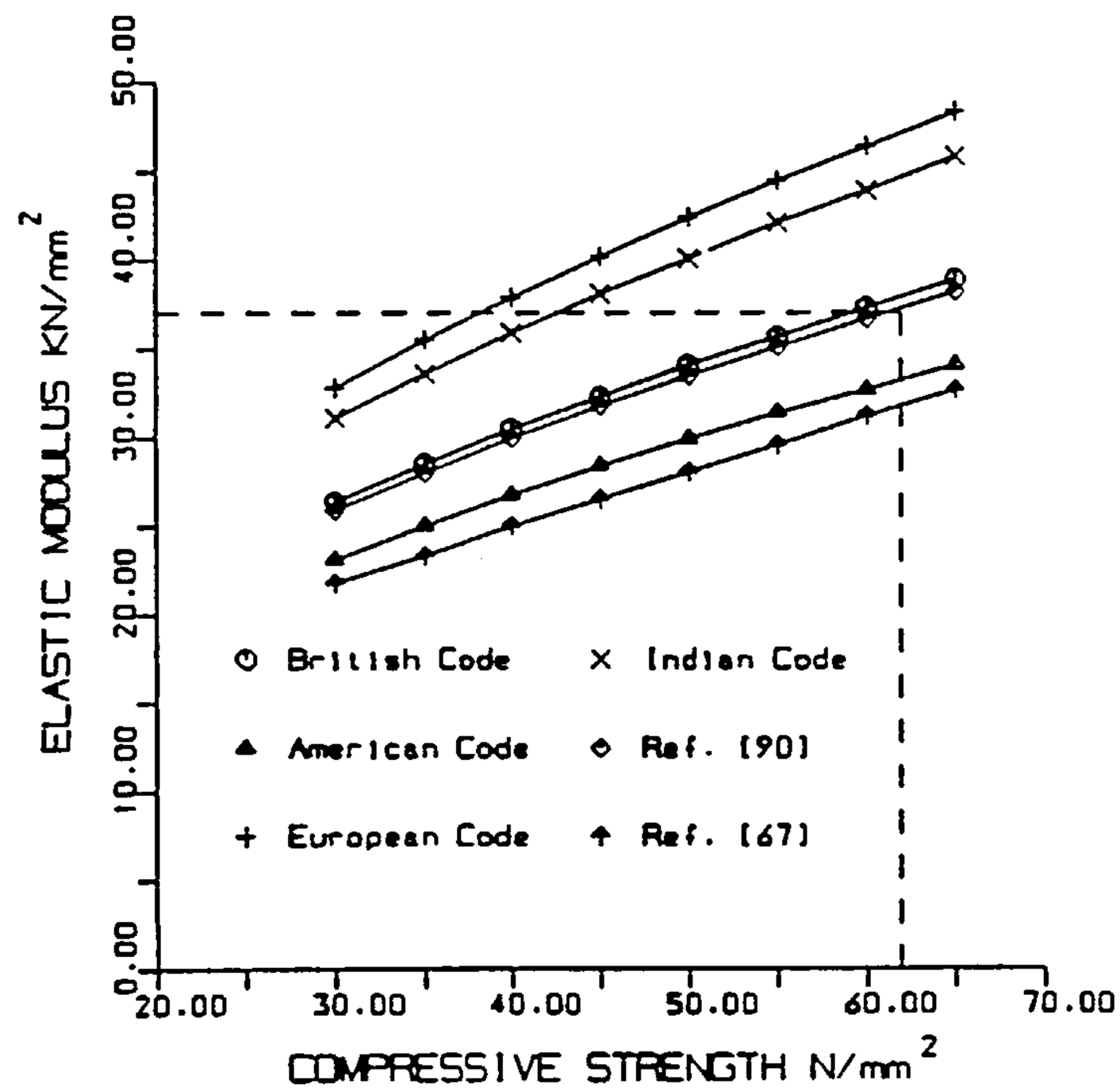


FIGURE (5.4) : PROPOSED RELATIONSHIPS FOR CALCULATING THE INITIAL STIFFNESS VALUE OF CONCRETE.

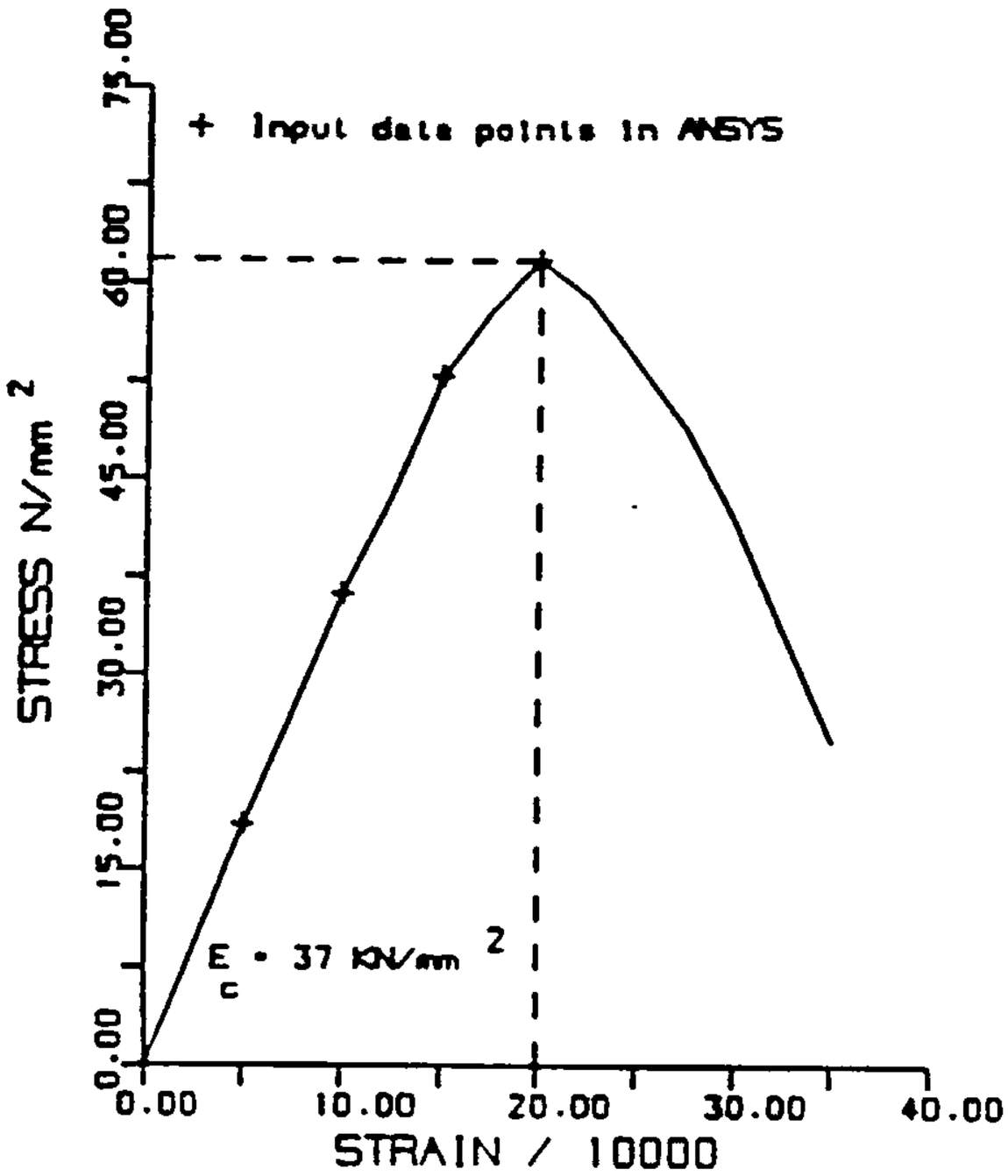


FIGURE (5.5) : MULTILINEAR IDEALISATION OF THE CONCRETE STRESS-STRAIN CURVE USED IN THE ANALYSIS.

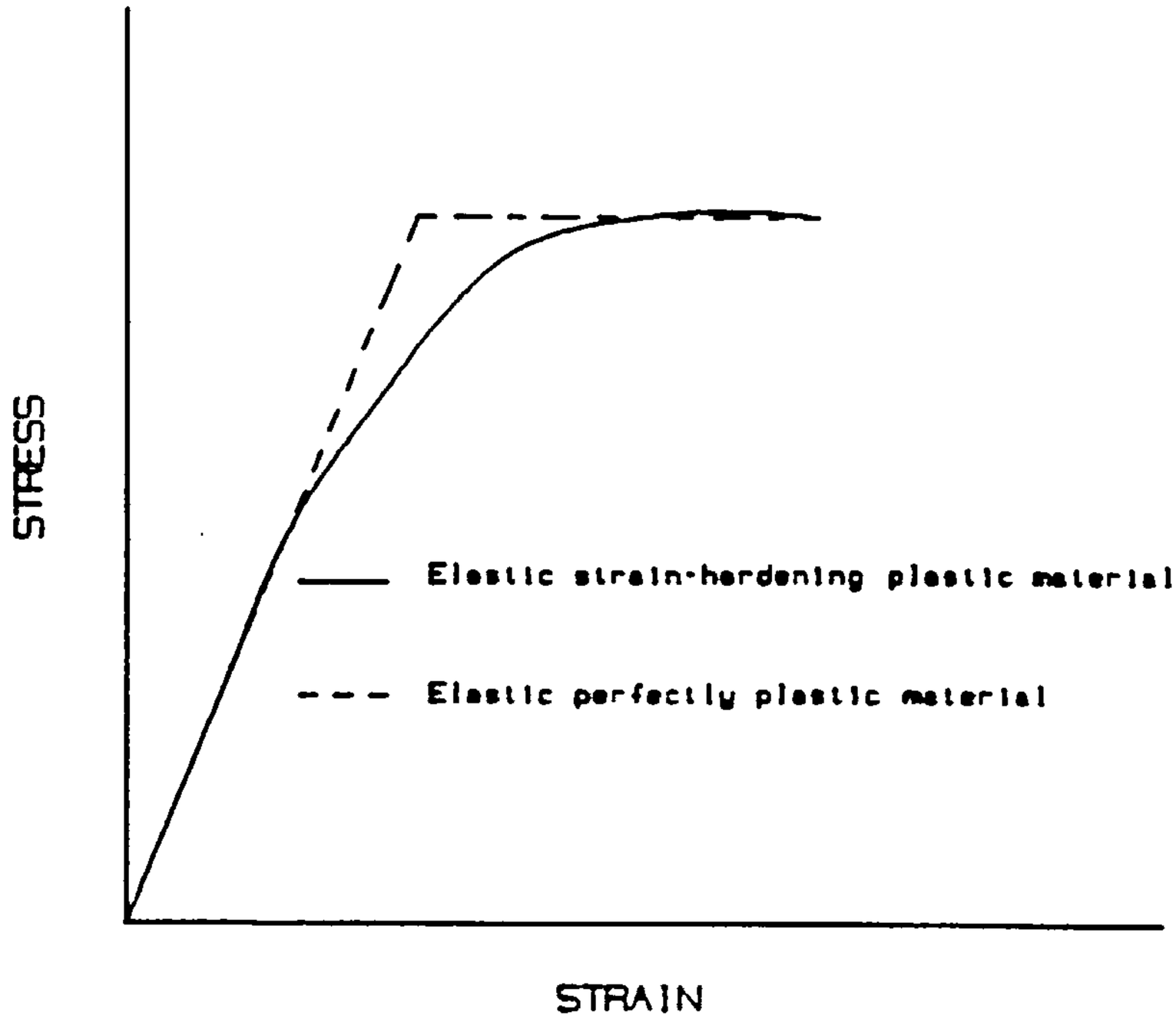


FIGURE (5.6) : SCHEMATIC REPRESENTATION OF MATERIAL BEHAVIOUR.

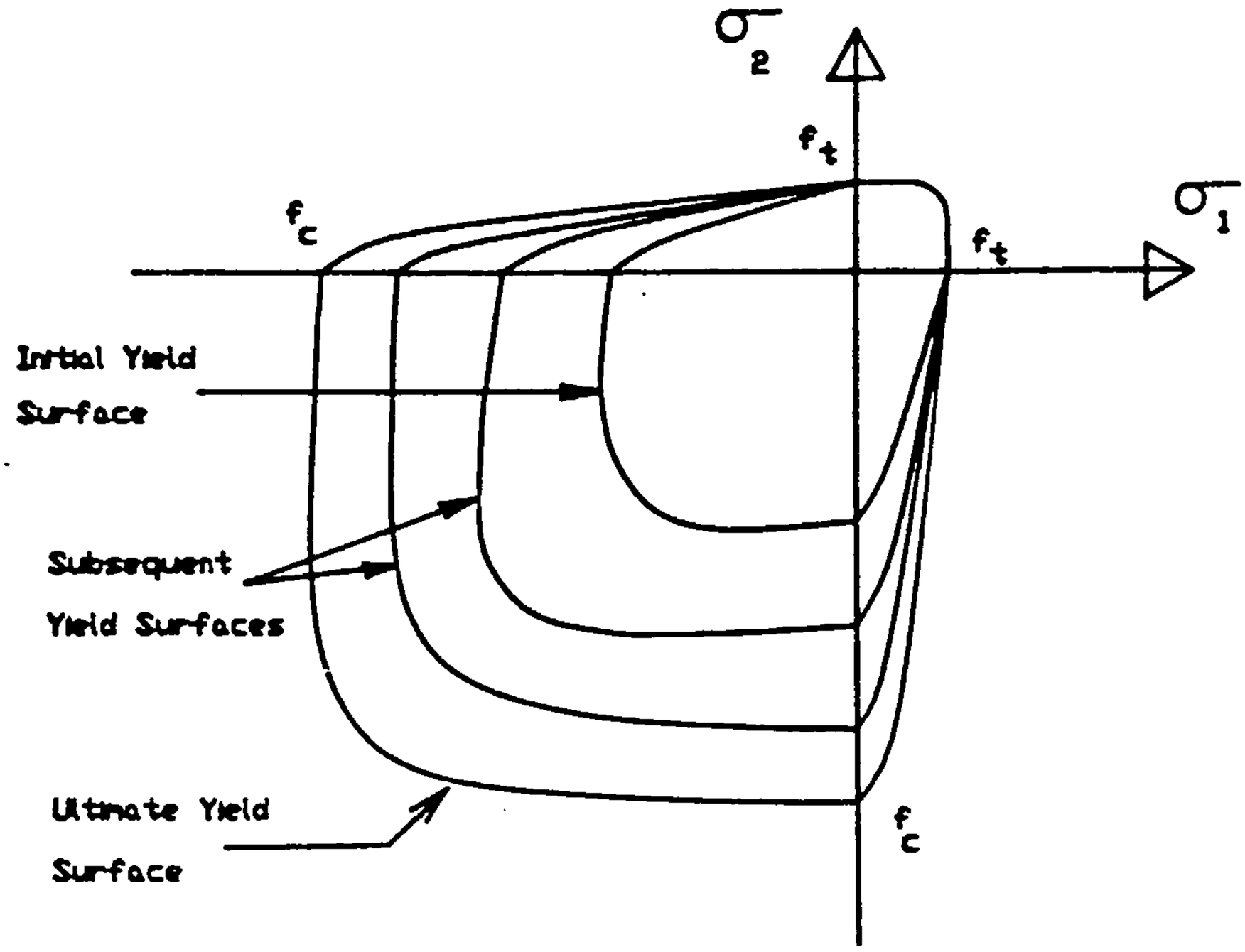


FIGURE (5.7) : YIELD SURFACE OF CONCRETE IN TWO-DIMENSIONAL PRINCIPAL STRESS PLANE.

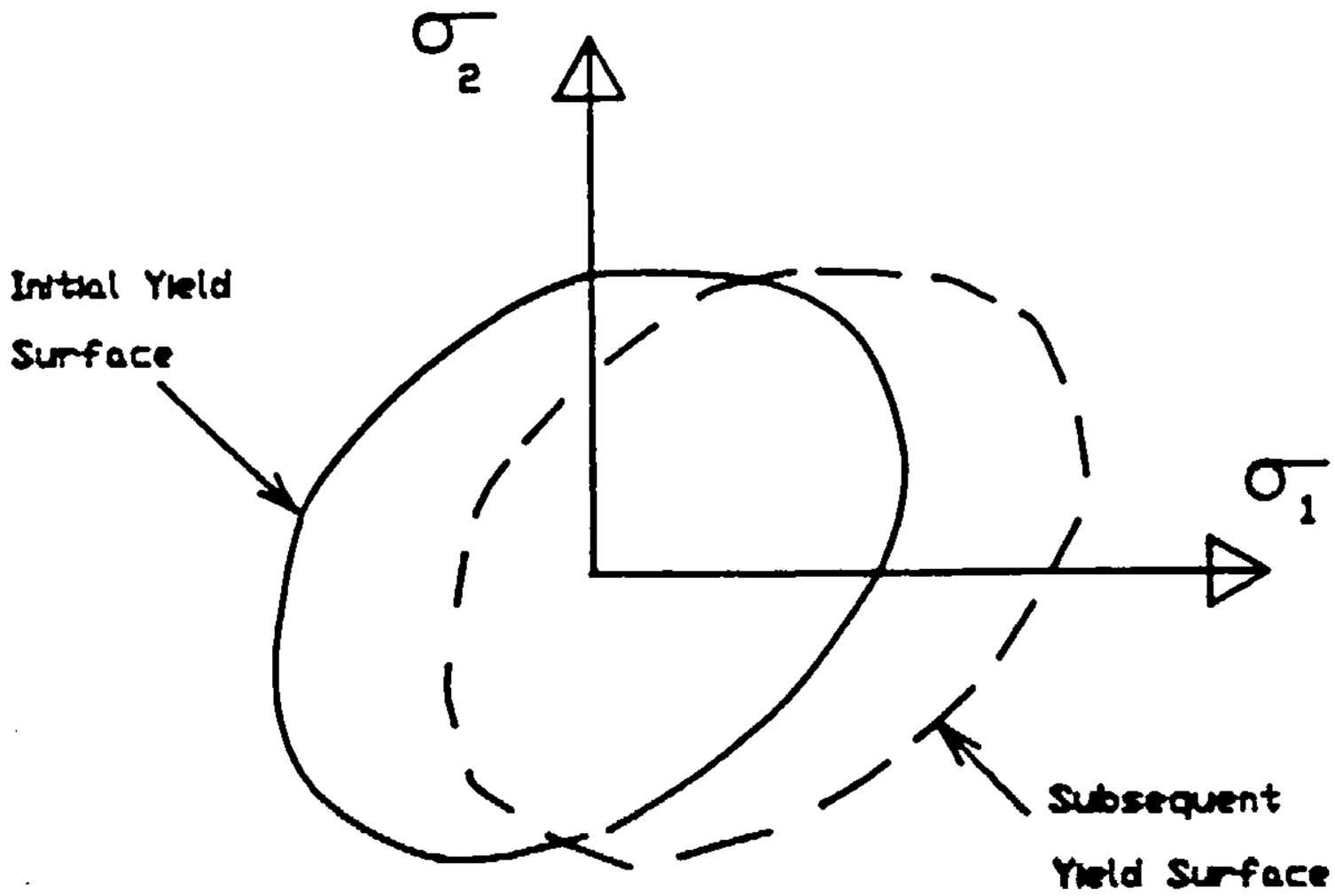


FIGURE (5.8) : KINEMATIC HARDENING RULE.

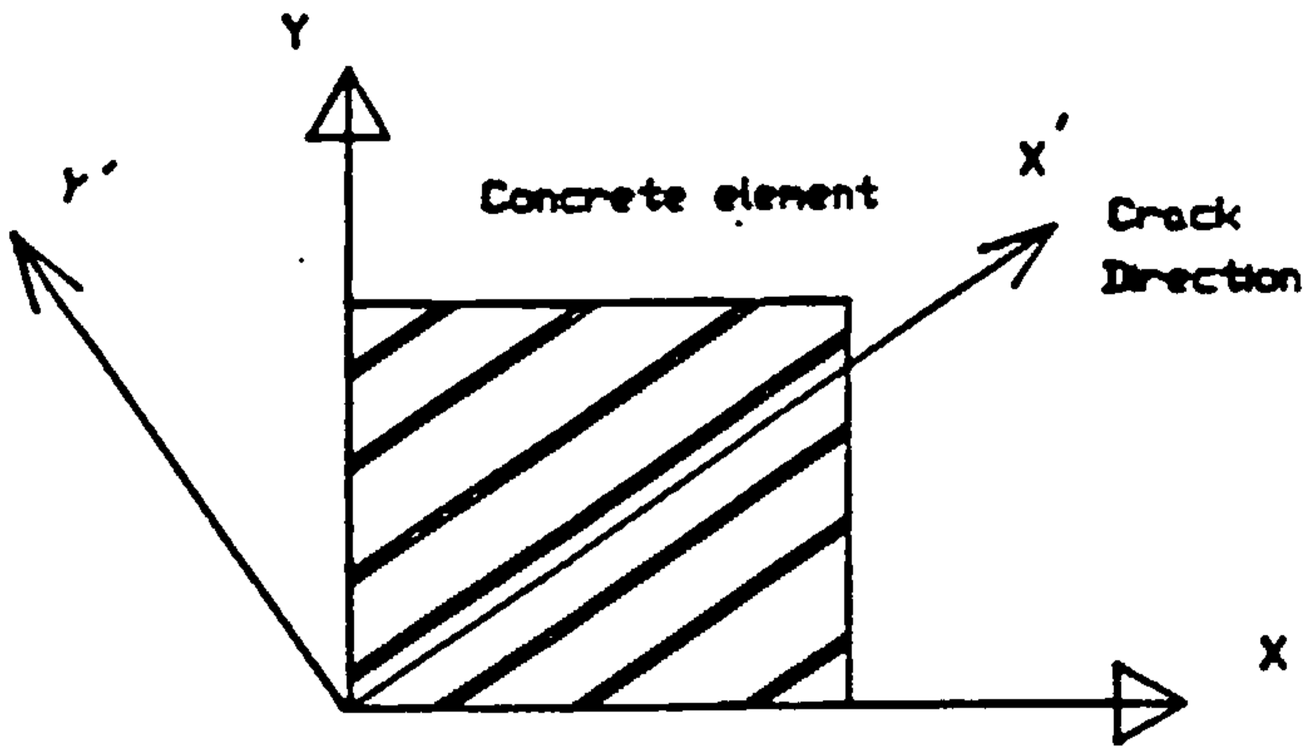


X Y Initial axes before cracking

X'Y' Axes after cracking

FIGURE (5.9) : INITIAL AND TRANSFORMED AXES FOR A CRACKED CONCRETE ELEMENT IN SMEARED CRACK MODELLING.

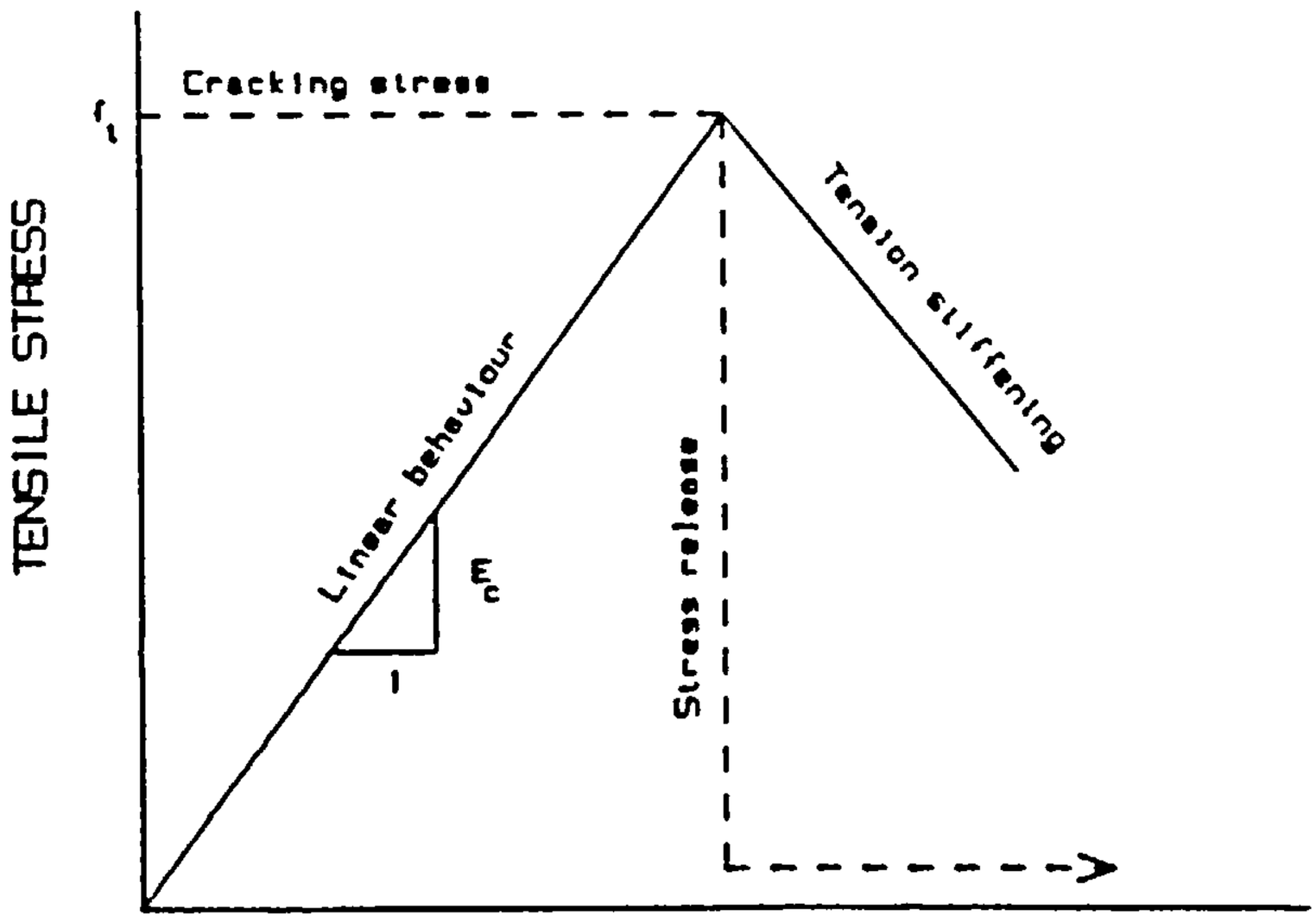


FIGURE (5.10) : SOLUTION PROCEDURE FOR POST-CRACKING ANALYSIS.

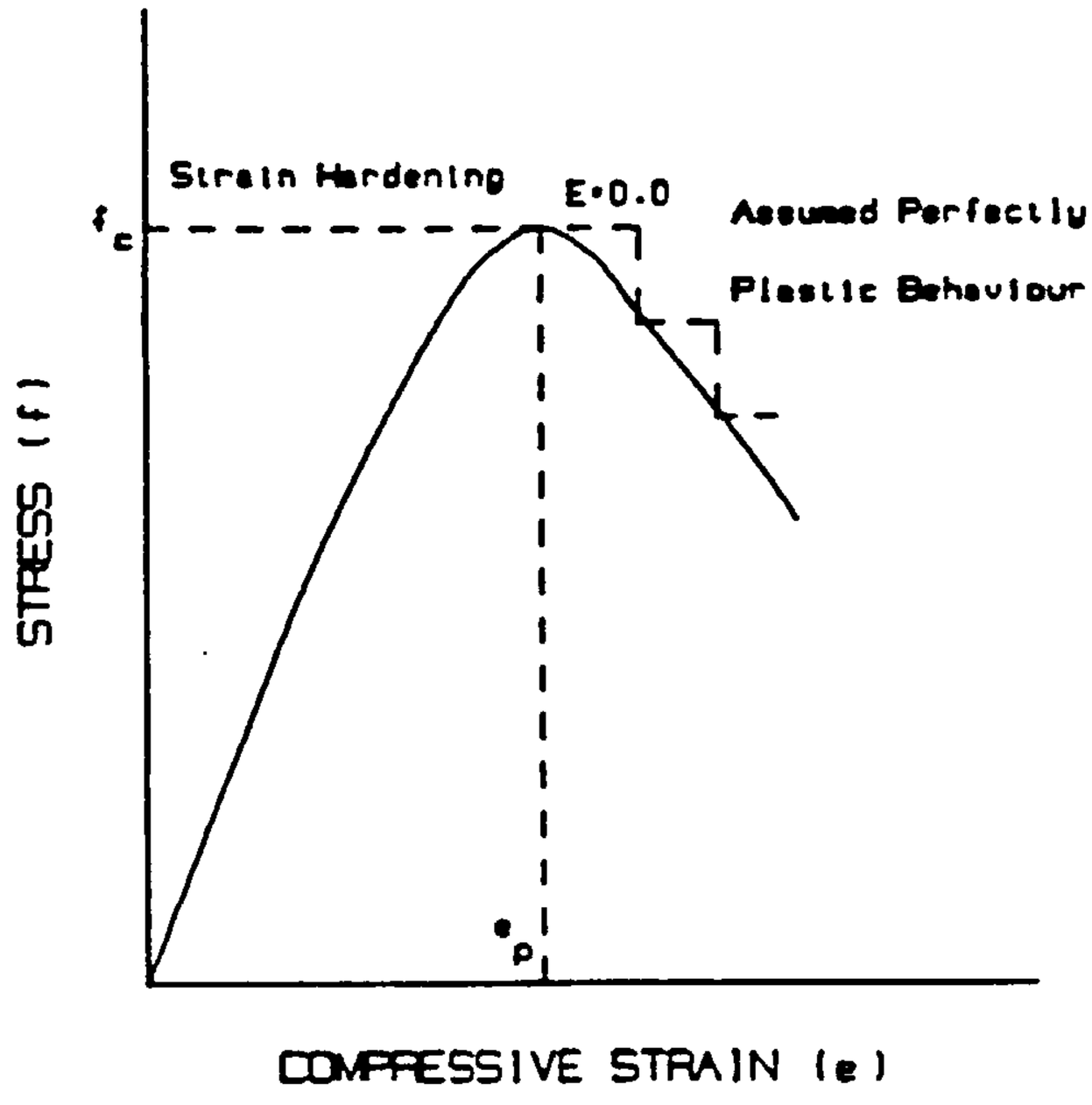


FIGURE (5.11) : SOLUTION PROCEDURE FOR POST-CRUSHING ANALYSIS.

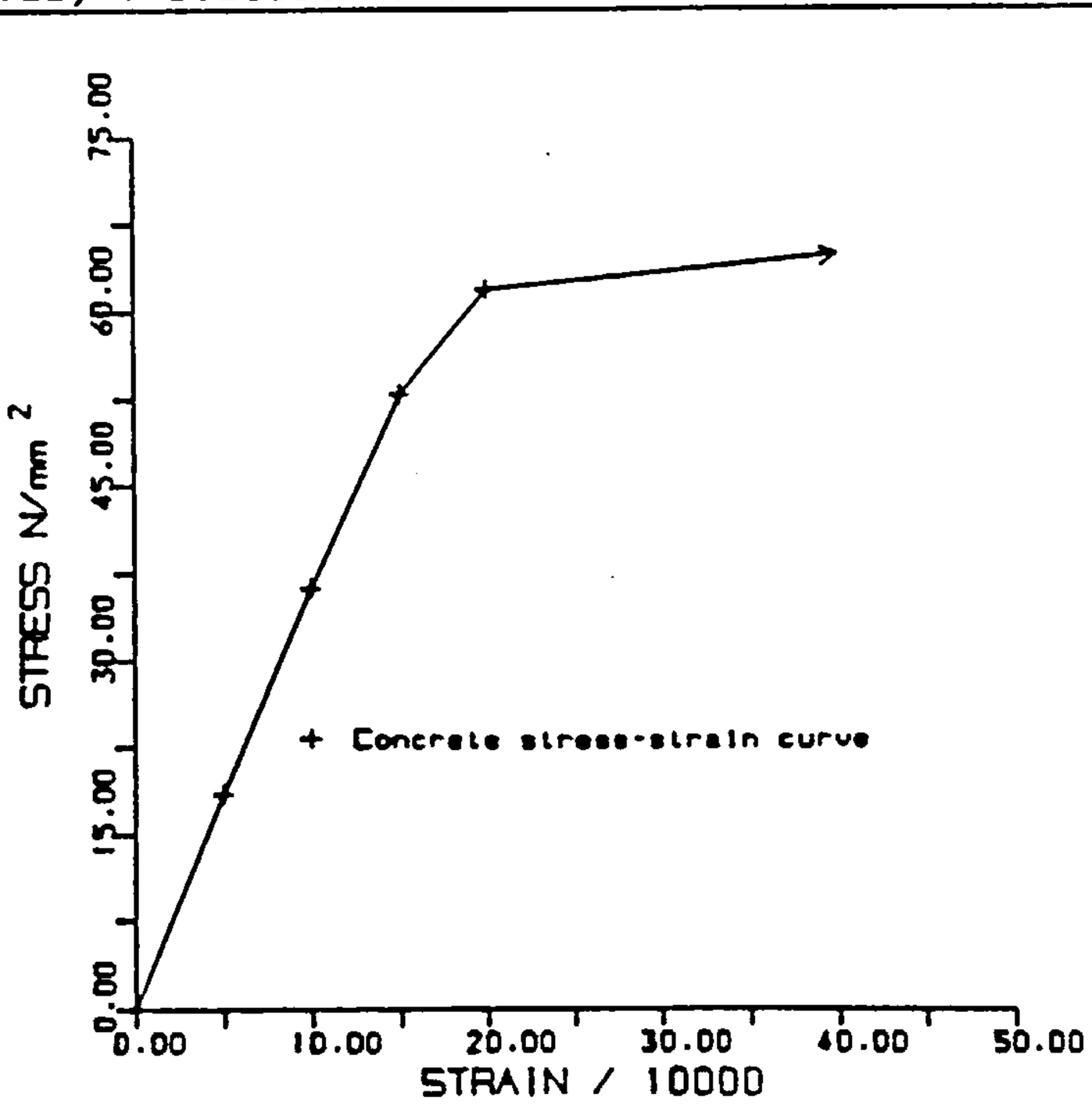


FIGURE (5.12) : ADOPTED STRESS-STRAIN CURVE FOR THE SMEARED REINFORCING MATERIAL.

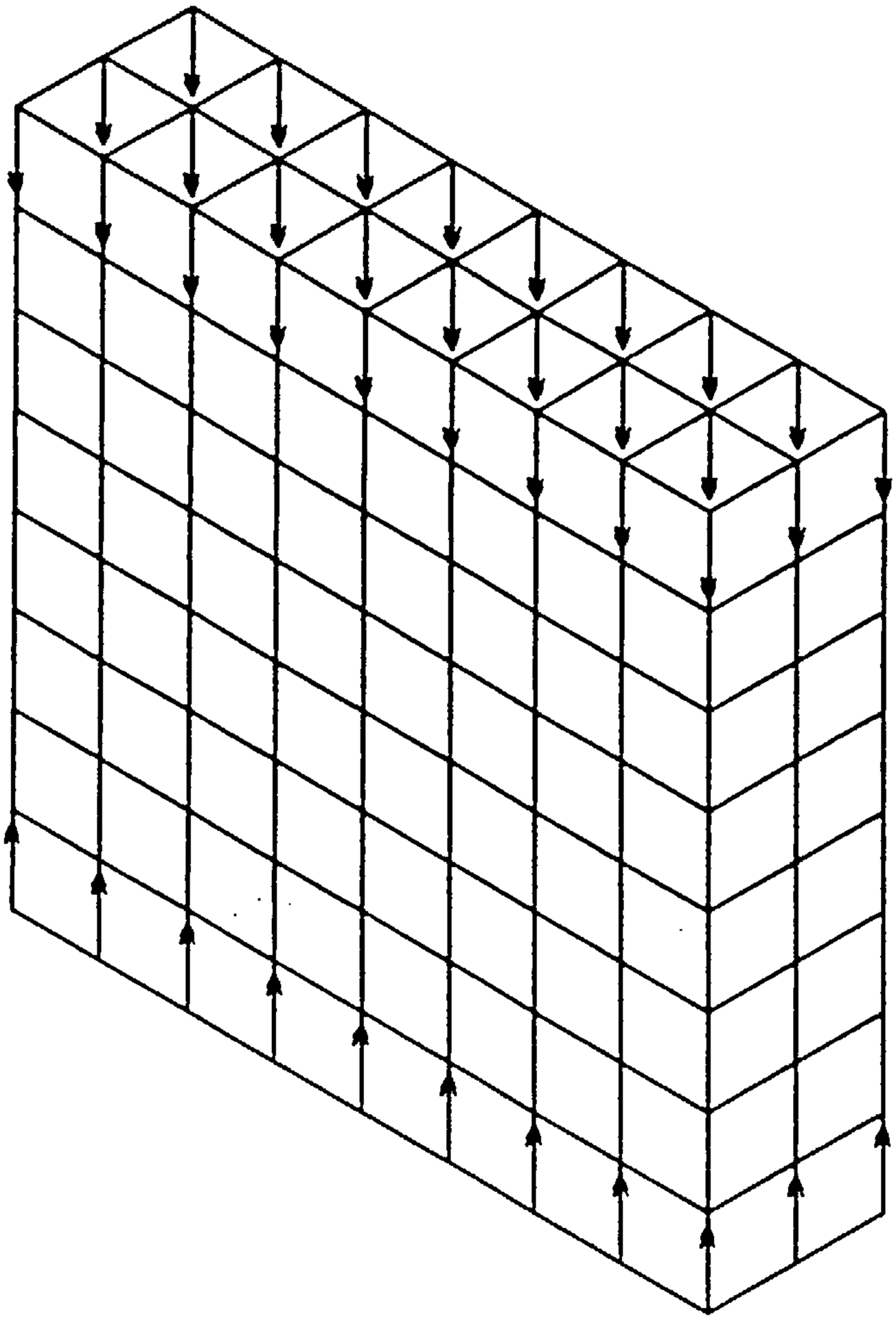

FIGURE (5.13) : FINITE ELEMENT IDEALISATION OF KUPFER PRISM.

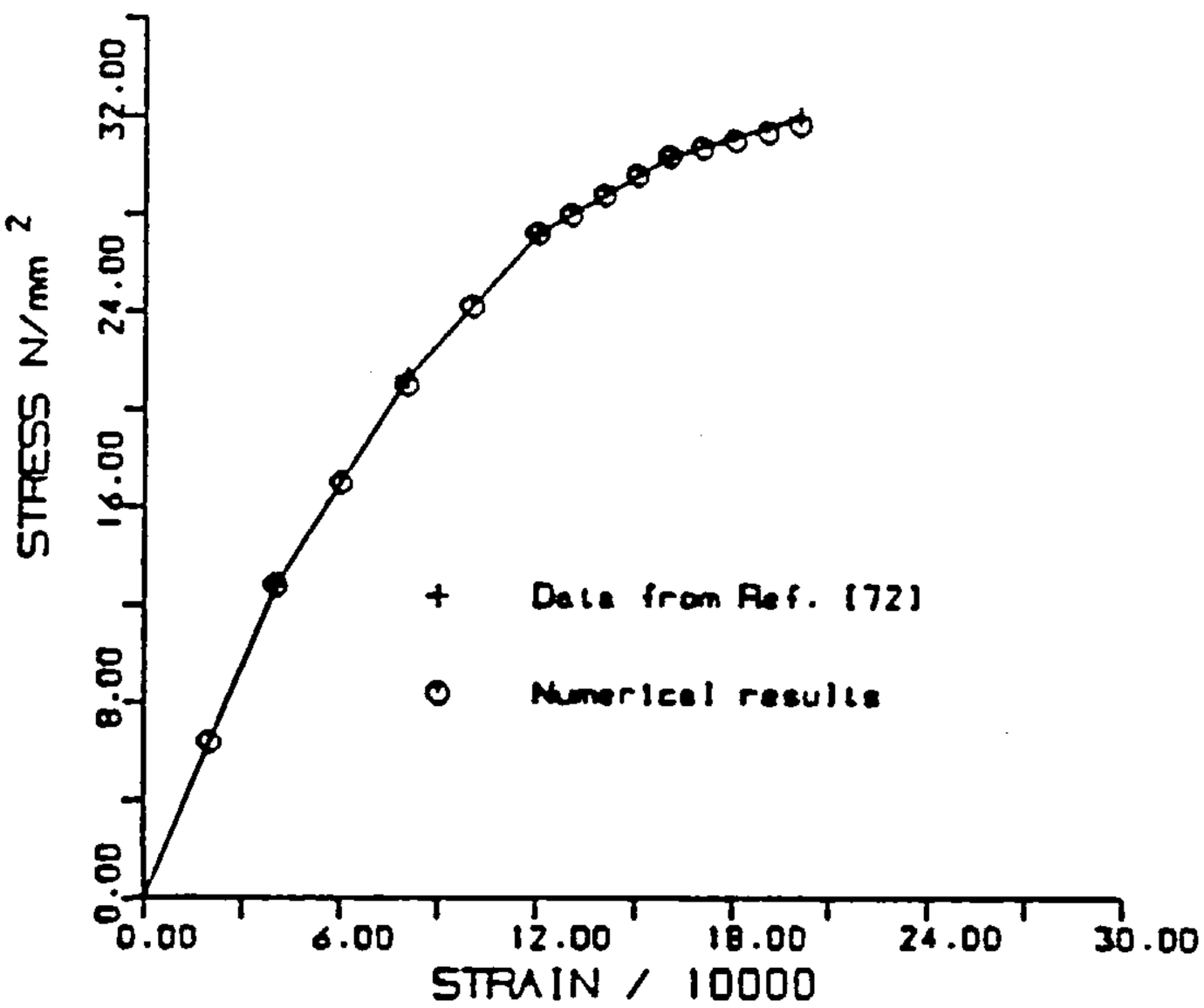


FIGURE (5.14) : COMPARISON OF PREDICTED STRESS-STRAIN CURVE WITH KUPFER DATA.

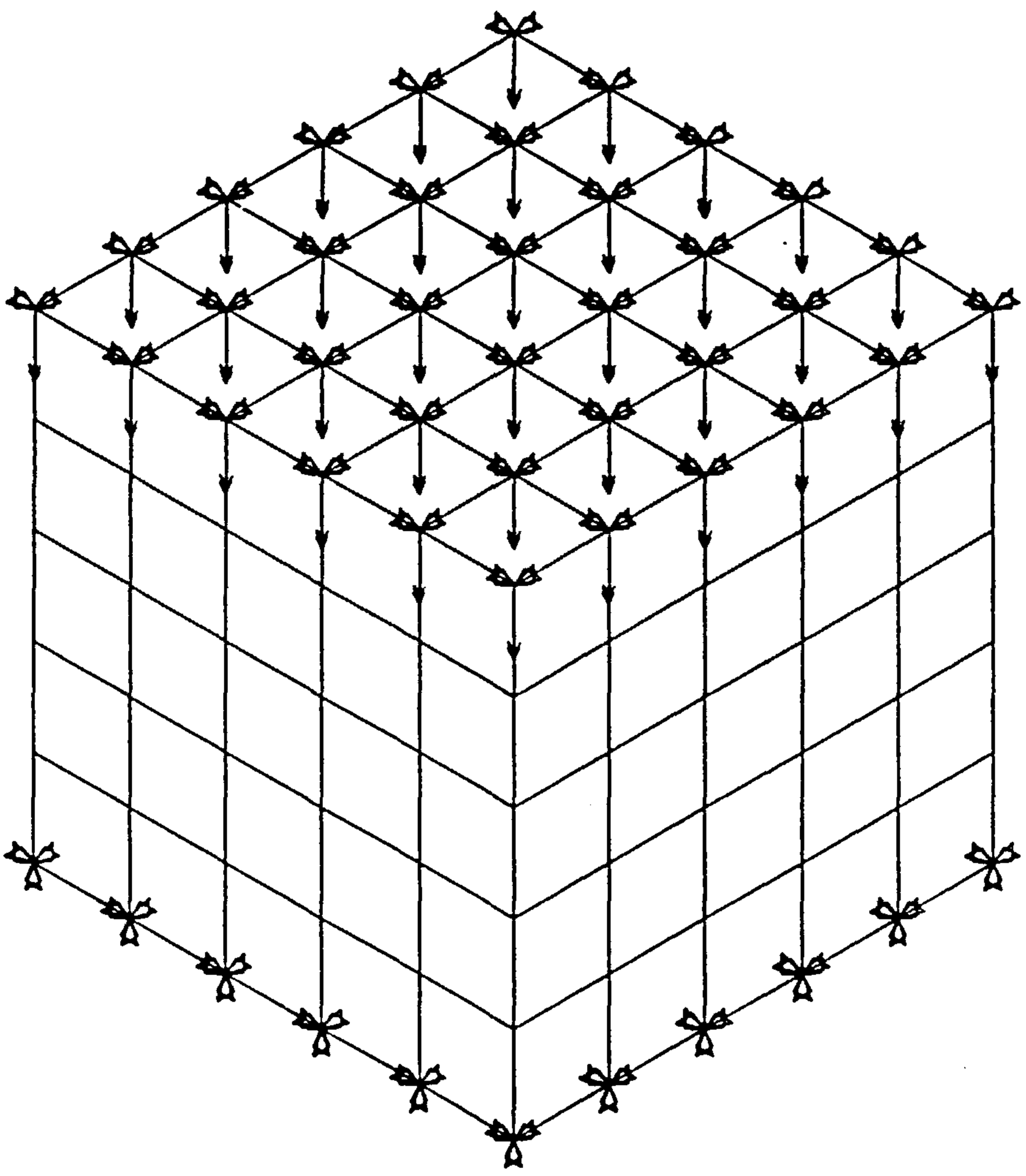

FIGURE (5.15) : FINITE ELEMENT MESH OF A 100mm CUBE WITH BOUNDARY CONSTRAINTS.

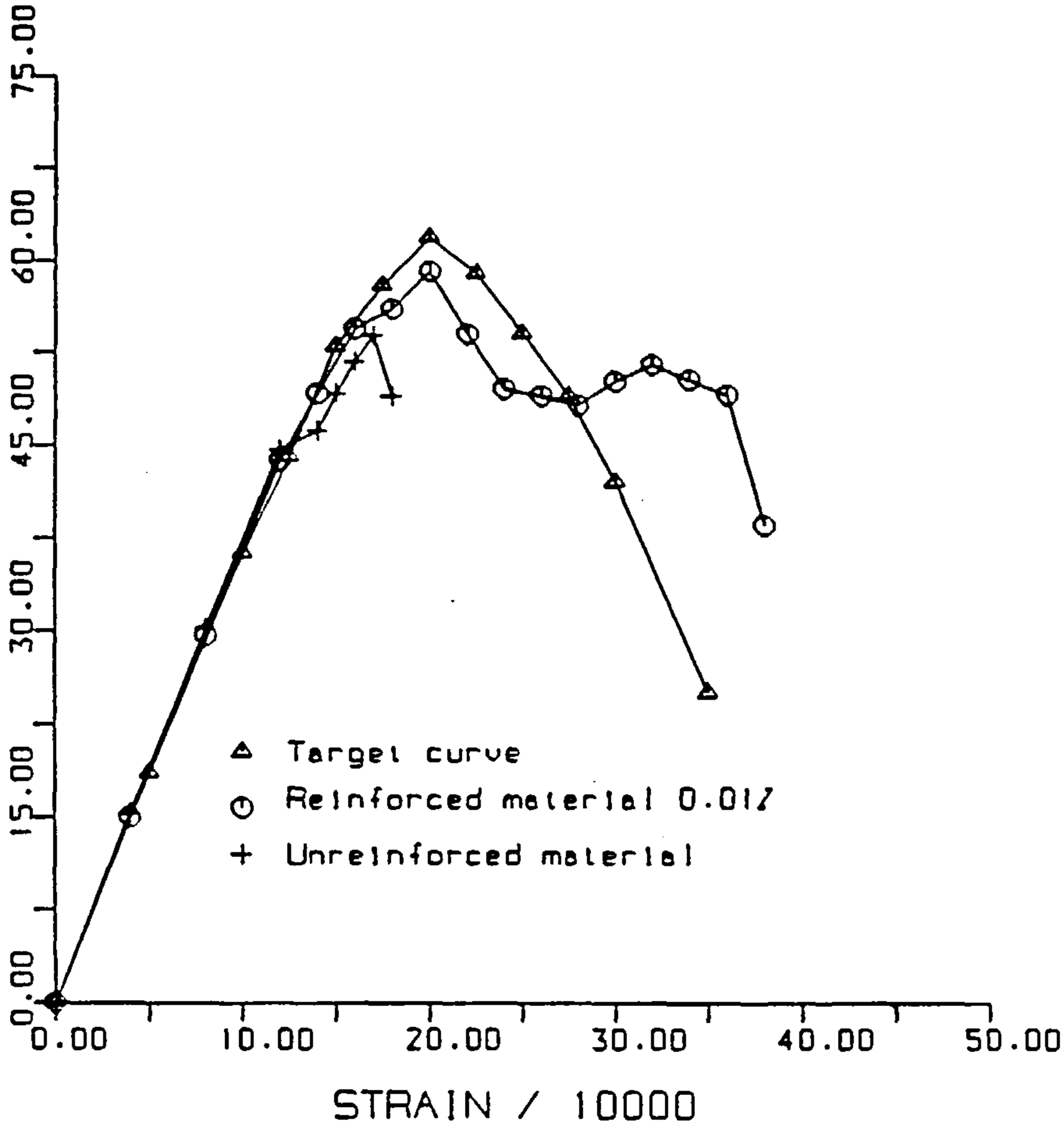


FIGURE (5.16) : PREDICTED RESPONSES FOR THE CUBE STRENGTH COMPARED WITH THE TARGET CURVE.

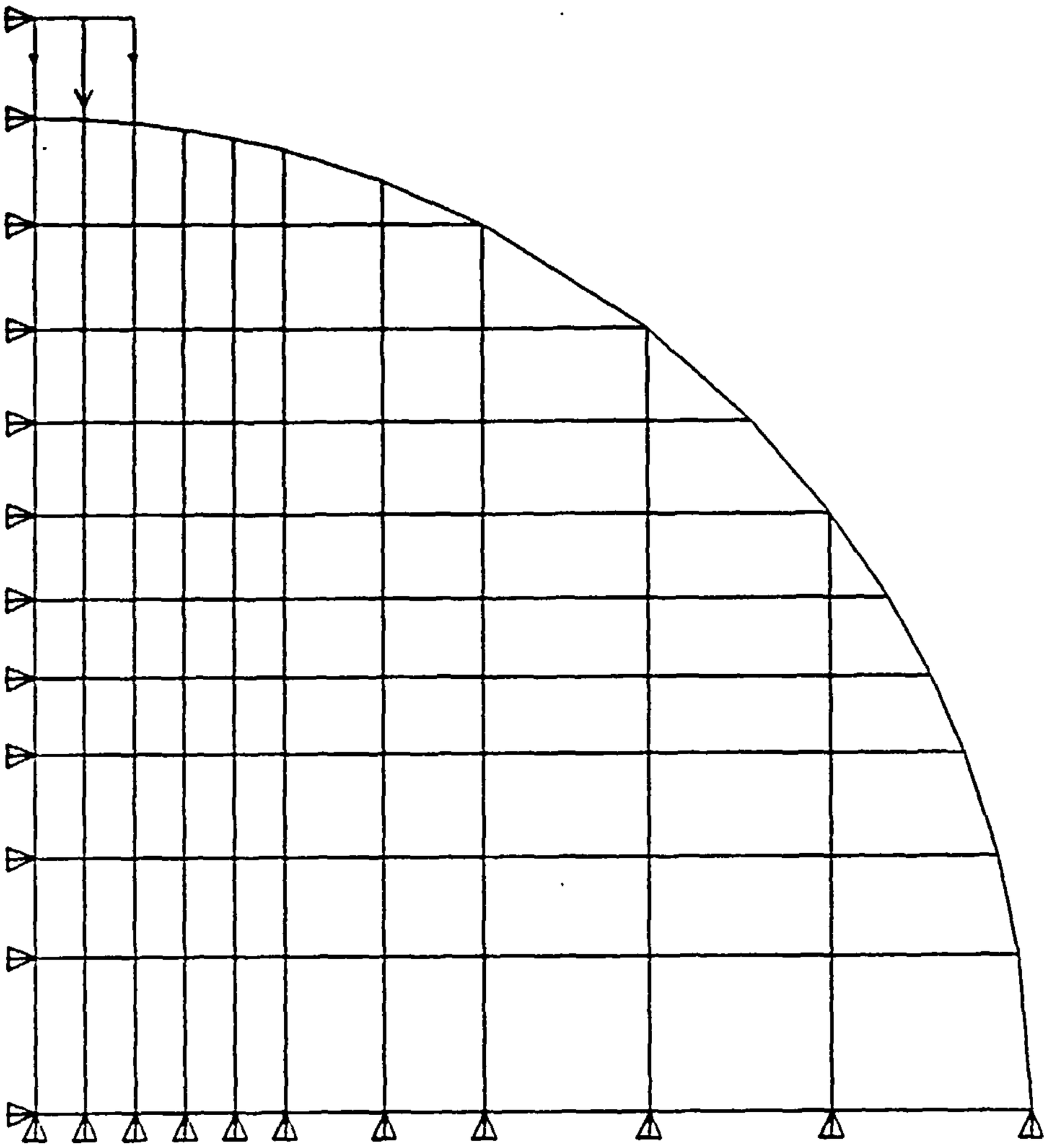

FIGURE (5.17) : FINITE ELEMENT MESH OF A CONCRETE CYLINDER WITH BOUNDARY CONSTRAINTS.

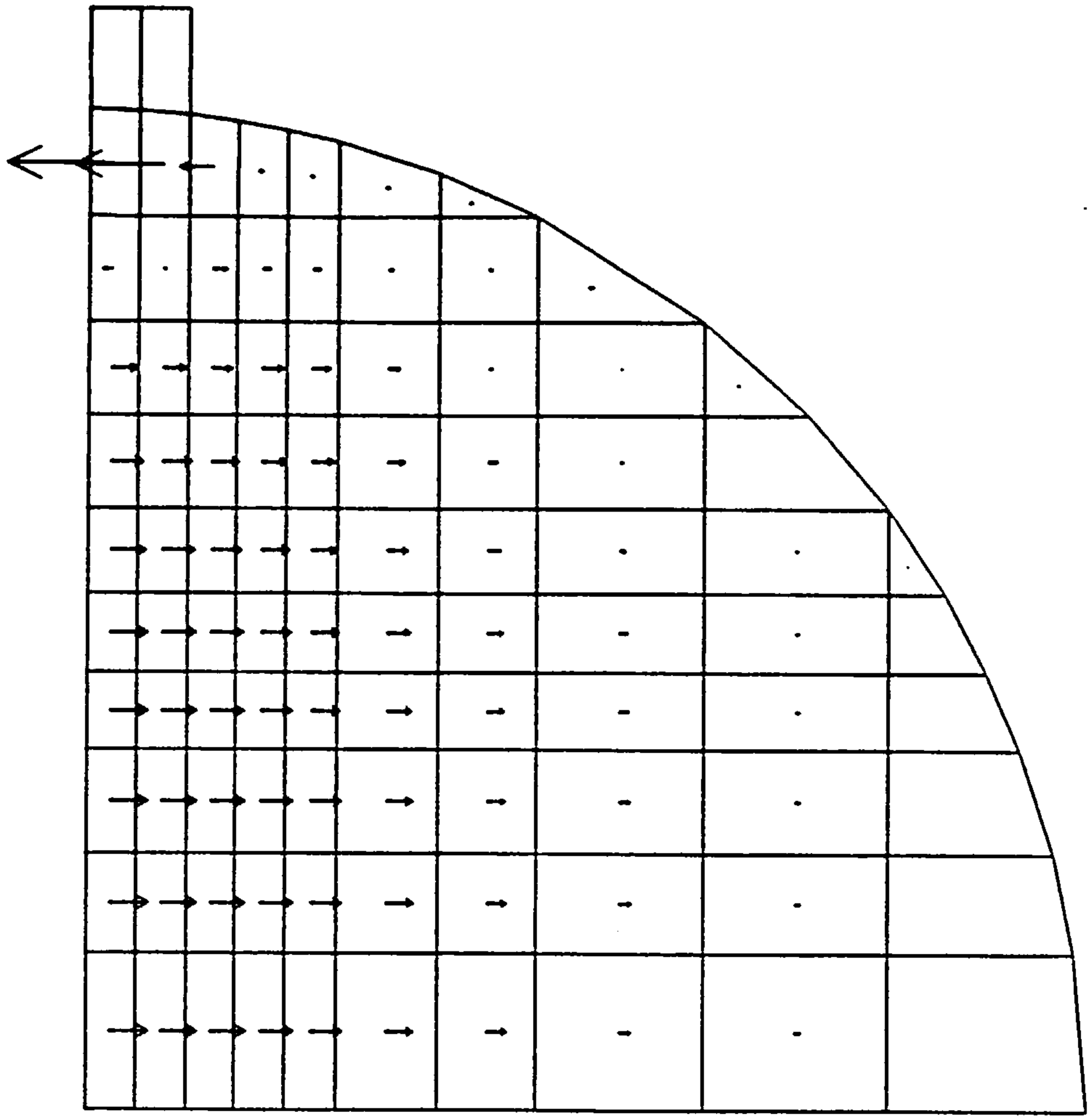

Arrow length represents stress magnitude.

FIGURE (5.18) : PREDICTED TENSILE STRESSES FOR THE CYLINDER AT A TYPICAL LOAD STEP.

# CHAPTER SIX

# NUMERICAL PREDICTIONS

## 6.1 INTRODUCTION

Having discussed the main features of both the ANSYS program and the models' components in Chapter 4, the basic results of Models 1 and 2, i.e. the single- and double-bolted joints respectively, are presented in this chapter. Special emphasis is given to the data which could not be obtained experimentally, in particular, the stresses in the cross sections of steel members, i.e. bolt, sleeve and steel links.

In the following sections, both displacement and stress distributions for individual components of the models are discussed in detail. Development of the contact area between the bolt and the sleeve, throughout the loading range, is traced. This is followed by a full description of the propagation of crushing and cracking in the surrounding concrete. The variation of tensile stresses along the steel links, up to the ultimate load, is also examined.

To have a measure of the models' accuracy, verification of the numerical results against the corresponding experimental values is presented at the end of the chapter. Throughout the discussion, care was taken to represent the behaviour of any joint component at load values related to its experimental ultimate loads.

Finally, the attention of the reader is drawn to the fact that load values, used in this chapter, are twice the sum of computed vertical forces at the nodes with prescribed deflections. This is due to the symmetry accounted for in both models.

## 6.2 The Bolt

The general behaviour of the bolt, and consequently its effect on other joint components, represents the chief goal of the joint modelling. For this reason, it was felt that it would be appropriate to make its numerical results serve as a starting point for the discussion in this chapter. This section highlights the main features of the bolt load-displacement curves in an attempt to understand its behaviour under direct loading. For ease of discussion, some terms are defined to describe certain parts of the bolt finite element mesh. These terms, the bolt mesh and the global axes are all shown in Figure (6.1). Each type of displacement is dealt with separately below.

### 6.2.1 Vertical Displacement

Imposed vertical deflections at the bolt's loaded end in Model 1 are plotted versus the computed load values in Figure (6.2). The importance of this curve arises from fact that it does not only represent the bolt's vertical deflection at the column face (the joint stiffness) but it can be used in a direct comparison with that obtained experimentally. The comparison which is given in Section 6.7 acts as a check on the accuracy of the model.

From the load-vertical deflection curve, it can be seen that the joint stiffness had its maximum value at the early stages of loading. This was due to the high resistance to movement given to the bolt from both the sleeve and concrete beneath. As the load increased, a few sleeve elements in the fine mesh region reached their yield stress, reducing the resistance to the bolt's vertical movement. In addition, minor cracks also started to develop in the concrete elements immediately beneath the sleeve. On further load increase these cracks became more extensive. This caused a reduction of the concrete strength in this area. Such a reduction appeared directly in the form of a gradually decreasing slope of the curve.

By the time more gap elements reached a closed status, a greater distribution of the transferred load was obtained, i.e. distribution over a larger area of the concrete solid. This was accompanied by an increase of both the length and width of the sleeve yield area reflecting the weak concrete found beneath. Thus the loaded end and its contact area with the sleeve moved steadily into the crushed concrete found beneath. Each application of deflection increment caused a decreasingly smaller increment of the load sustained by the model as a result of the nonlinear behaviour of concrete and steel. This trend continued until failure of the model occurred. For the whole range of deflection, the trend in the incremental load was fairly regular and no abrupt change in load values between any two deflection increments was found.

The experimental failure load of the bolt in Test 1, that is, 210.0 KN was obtained at a vertical deflection value of 4.20mm. This load value represents 75% of the joint failure load which will be referred to as the ultimate load in this chapter.

As expected, the remote end kept moving upward, reducing the size of the corresponding gap until it came into contact with the sleeve soffit. This occurred at a load value equal to 52% of the ultimate load. Following this gap closure, the rate of vertical deflection was substantially reduced at the remote end.

The variation of the bolt's vertical deflection along its longitudinal axis, at different load values, is shown in Figure (6.3). It can be seen that each plotted curve has two well pronounced zones. The first zone covers the distance where the bolt is in contact with the sleeve. Naturally, both the length and value of this zone increase as the load increases. The second zone covers the remainder of the bolt's length where the deflection values are positive. In this zone, curvature of the bolt is clear due to the induced bending, especially after the remote end became in contact with the sleeve.

### 6.2.2 Axial Displacement

From the start of loading, the induced moment caused an elastic bending of the bolt. As a result, the bolt was in compression at the bottom edge while in tension at the top. This is demonstrated by the displacement contours shown in Figure (6.4). From this figure, it can be seen that axial negative and positive deflections are below and above the level of the bolt's centreline, respectively. The contour line at the centreline works almost as a mirror line reflecting the negative contour lines below it to positive ones above it.

Figure (6.5) shows the variation of the axial deflection at the loaded end down the bolt's vertical diameter for different load values. From this figure, the following remarks can be made:

a) All curves have the form of an inclined straight Line. This shows that the axial displacement varies almost linearly down the vertical diameter of the bolt.

b) Up to 20% of the ultimate load, the ratio between both maximum positive and negative displacement values is almost unity. This indicates that the bolt's cross section remained almost plane under loading. On further load increase, the negative deflections started to increase at a higher rate. This can be attributed to the gradual shift of the spring force concentration from the loaded end.

### 6.2.3 Lateral Displacement

Under loading, the bolt shank experienced a lateral displacement. Lateral displacement contours of the bolt's loaded end at 50% of the ultimate load are shown in Figure (6.6). From this figure, it can be seen that there is no lateral displacement where the bolt's elements are in contact with the sleeve. This is due to

the movement restriction provided by the deformed sleeve in this region. Due to the Poisson effect, the lateral flow of the bolt's material creates positive and negative deflection values at the bottom and top right hand corners, respectively. Compared with the vertical and axial deflections, the lateral deflection had very small values.

### 6.2.4 Stress and Strain Distributions

Calculated element stresses at integration points were in the elastic region up to 60% of the ultimate load, where local plastic strains started to form in the bottom elements of the loaded end. Figure (6.7) shows the principal stress distribution in vector plots where the length of a vector is directly proportional to the stress value. From this figure, it can be seen that stress vectors are parallel to the Z direction in most of the bolt shank indicating a uniform bending. Tensile and compressive stresses have been developed along the length of the top and bottom edges, respectively. As expected, high compressive stresses were found in the elements in contact with the sleeve. The figure clearly demonstrates the existence of a transition zone in stresses between the top and bottom edges close to the loaded end.

Figure (6.8) shows the longitudinal stress distribution in terms of contour lines in the YZ plane at 50% of the ultimate load. The constancy of the stress contours along the bolt is notable. However, a deviation in the stress pattern can be seen in the area close to the loaded end, where higher values of stress were found. This was expected, as the bolt embeds itself into the sleeve invert creating a high localised bearing stress. This area which increased by increasing the load, was found to be bounded by the the highly affected concrete elements beneath the bolt. The constancy of stress contours has led to a regular strain pattern as shown in Figure (6.9). In the XY plane, relatively high strains were concentrated locally at the lower right corner

of the loaded end.

## 6.3 Development of Contact Area

In Model 1, the computed applied load was completely transferred to the sleeve as the sum of the spring forces in the closed 2-D and 3-D gap elements. As the loading increased, more 2-D and 3-D gap elements reached a closed status thus increasing both the length and width of the contact area. Due to the surface curvature of both bolt and sleeve, the contact area was of semi-elliptical shape. Using computed displacement values, status of gap elements and symmetry, Figure (6.10) shows best fitted curves drawn to represent the development of contact area with the increase of loading.

From this figure, it can be seen that the width of the contact area increased rapidly in the early stages of loading. This increase continued until most of the sleeve's invert, at the loaded end, came in contact with the bolt. In physical terms, the bolt became well seated against the sleeve invert. Also, the progress of sleeve yielding under loading was accompanied by a continuous increase in the length of the contact area in the Z direction. As was expected, the maximum depth, at any stage of loading, occurred at the initial contact edge which represents a line of symmetry. Once a gap element became closed, its status remained unchanged until the ultimate load was reached.

## 6.4 The Sleeve

### 6.4.1 Sleeve Deformation

The sleeve's cross section at the loaded end was much affected by the high stress concentration. This was accompanied by a noticeable sleeve deformation in the area close to this region. Figure (6.11) shows the progress of sleeve deformation at different load values. Sleeve elements at the loaded end were

severely distorted at the late stages of loading. This was demonstrated by the reduction of their original thickness.

Figure (6.12) shows the variation of the sleeve vertical deflection for Model 1 along the edge of symmetry, i.e. at x = 0.0mm. In this figure, curves are plotted at load values equal to those adopted in Figure (6.3). From both figures, it is clear that every two tied nodes have almost the same value of vertical deflection. At nodes, where bolt and sleeve were no longer in contact, the sleeve had insignificant vertical deflection.

Figures (6.13) and (6.14) show vertical displacement contours for the sleeve and the surrounding concrete elements of Model 1 and 2, respectively. These were plotted at 50% of the corresponding ultimate loads. From these contours, the displacement consistency can be seen. In Model 1, the maximum value of displacement takes place at the bolt's bottom corner which lies on the line of symmetry. In Model 2, the vertical deflection values are almost equal at both sides of the sleeve's vertical centreline with their maximum values lying at this centreline. At later stages of loading, the deflection rate increased at the nodes beneath the sleeve and close to the line of symmetry. This was due to the combined effect of highly-stressed zones in this area.

In both models, on proceeding away from the sleeve, the deflection values decrease gradually until they become a minimum. Also, the vertical deflection values above the joint level were negligible.

Figures (6.15) and (6.16) show lateral displacement contours for the sleeve and the surrounding concrete elements of Models 1 and 2, respectively. These were plotted at 50% of the corresponding ultimate loads. Expansion of concrete beneath the bolt in Model 1 is reflected by the positive lateral deflections. Negative values were found close to the X axis. This can be attributed to the force concentration at the sleeve lower elements which pulls the

side of sleeve downward allowing its nodes (unconnected to the bolt) to adopt a line of reduced curvature and thus move laterally towards the vertical line of symmetry.

In Model 2, a noticeable concrete expansion beneath the sleeve was found at both sides of the sleeve's vertical centreline. Due to the existence of the right-hand free vertical edge, sleeve bottom nodes tended to move laterally towards this edge, creating larger values of expansion in this region. As a result of this expansion, nodes at the sleeve's horizontal centreline were pulled towards the vertical centreline creating some contraction at this region.

### 6.4.2 Sleeve Yield Area

A sleeve yield element can be defined as the element at which the computed strain is larger than the assumed yield strain of the sleeve material. Due to the high load concentration, plastic strains started to develop in the elements close to the loaded end at relatively low load values. Figure (6.17) shows the development of the sleeve yield area, shown marked, at different load values. Closing more 3-D gap elements, the line bounding the yield area increases in depth as well as in width. Due to the stress spread in the sleeve elements, it was found that the yield area is always larger than the contact area obtained at the same load value.

Sleeve principal stress contours for Model 1, at 50% of the ultimate load, are shown in Figure (6.18). The stress contours have a fairly regular pattern with the highest compressive stress values occurring at the sleeve loaded end. By increasing the load, the most highly stressed zone was found to move away from the edge of symmetry. This may be attributed to the closure of more gap elements across the sleeve's curved surface and the formation of weak concrete zones close to that edge.

1. Up to the ultimate loads, all links had a gradually increasing tensile stress in their legs lying in the XY plane while insignificant compressive stresses were found in those lying in the YZ plane.

2. In Model 1, the maximum values occurred where the members were attached to the plane of symmetry, i.e. the mid-span of links. Then the stress decreased gradually until it reached minimum values at the rightmost members. This was expected as the maximum deflection of steel links nodes took place at those located vertically below the bolt.

3. It was expected that there would be a stress variation down the different levels, i.e. stresses with larger values would be found in links closer to the bolt level. However, the obtained numerical results, for Model 1, suggest that the maximum stress values obtained at successive levels below the bolt level, decrease only slowly. This was due to the tendency of concrete splitting in the column along the model's symmetry plane.

4. From the early stages of loading, the highest stresses were developed in links (a) and (b) of Model 2 at the vertical bolt centreline, with slightly higher values in link (a). On proceeding away from this centreline, the value of stresses decreased for both links.

5. Following the expansion trend of concrete beneath the sleeve in Model 2, the stresses in lower links, links (b) and (c) increased notably at their edge elements especially those connected to the vertical edge of symmetry, i.e. the column centreline. This can be attributed to the accumulation of developed stress, which caused a substantial increase in number of cracks in this area.

internal stresses and deformation in the highly stressed zone. At the early stages of loading, local cracks were discontinuous, causing no significant effect on the elastic deflection. On further loading, they started to develop and propagate in large numbers resulting in an increase of the bolt's deflection rate.

In the XY face, cracks were initiated almost vertically in elements close to the bolt's vertical centreline. With further increase in load, new cracks appeared in adjacent elements. These cracks were found to be at an inclined angle to that vertical centreline. This was accompanied by the formation of cracks in the YZ face, penetrating to a distance equal to half of the concrete cover. In the final stages of loading, predicted cracks stabilised in the highly-stressed region and no further increase in their numbers was observed. In both models, no cracks were predicted in concrete elements located above the joint level.

### 6.6.2 Concrete Crushing

Below the joint level, concrete crushing has a particularly strong influence on its resistance to the sleeve deformation. The numerical results showed that the region of the loaded end was subjected to a wholly compressive state of stress. This helped crushing to initiate in the elements which were in contact with the sleeve in this region. Although the first element to be completely crushed did so at 25% of the ultimate load, the onset of crushing took place at much lower value. As the applied load increased, the crushed area under the deformed sleeve edge developed. It increased not only in depth but vertically in the XY plane as well. The crushed zone immediately beneath the sleeve propagated up to a depth of 40.0mm in the Z direction for both models. This length is equal to the plain concrete cover.

The spalling of concrete on the surface can be seen as the phenomena created by the complete crushing of concrete elements found at this surface. In testing, concrete spalling was clearly

observed in the region immediately beneath the bolt's level. The numerical results suggest that spalling occurred in a localised area below the bolt level in the XY face. Area of spalling increased with the load increase. However, the associated outward deflections were always controlled by the upper limits laid by the assumed movement of the bracket's back plate. Concrete nodes located at z < -40.0mm were confined by the steel links. Thus, much smaller outward deflections were computed at these nodes.

### 6.6.3 Stress Distribution

Concrete located beneath the loaded end was stressed by the bearing of the bolt shank. Stress contours in the XY plane are shown side-by-side with those in the YZ plane in Figure (6.23). The contours represent the equivalent stresses of the elements. It is clear that continuity has not been broken at the vertical edge of symmetry. On proceeding away from the loaded end, the stress values decrease gradually until they become a minimum. Other parts of the concrete model, especially those which are above the joint level proved to have insignificant stress values. Also minimal stress values were found at elements located at distance 50.0mm or more below the X axis.

The whole of the load applied to the bolt was transferred to the concrete by bearing. As a result, compressive and tensile principal stresses were developed beneath the joint level in an equivalent way to that obtained in an indirect splitting test. The compressive stresses flow inside the concrete solid at an inclined angle, with maximum values at the elements connected to the sleeve as shown in Figure (6.24). The transverse tensile stresses were responsible for the development and propagation of cracks in the concrete solid. However, the adequately confined concrete prevented the splitting of the concrete solid, even at the ultimate load. This fact was numerically supported by the development of axial tensile stresses in the steel links during all load stages.

## 6.7 Assessment of Models

A numerical model can be considered reliable if its predicted behaviour is consistent with both the expected and experimentally predetermined values. However, some allowance should be made due to the fact that a numerical model always assumes a perfect structure and homogeneous materials. In the previous sections, the interpretation of the numerical results was given. In this section, an assessment is made of the models' accuracy.

### 6.7.1 Ultimate Loads

Once the experimental maximum loads were reached for both models, the models' main elements were examined in an attempt to predict the corresponding failure modes. In Model 1, the average vertical stress obtained in the bolt's elements in the XY face was 496.2 $N/mm^2$ at a maximum load of 210.0 KN. Applying this value to the reduced cross section at the bolt thread where the area is 0.7 of the bolt's cross section gives rise to a stress of 708.85 $N/mm^2$ which is only 6.9% higher than the obtained experimental value. As the bolt shank was not modelled in Model 2, a value for the shear stress at its thread could not be obtained. Examination of the concrete elements in both models revealed that weak cracked and crushed concrete zones were developed beneath the sleeve. However, the axial tensile stresses in the steel links were found to be in the elastic region. From the above findings, the possibility of having a joint concrete failure at the experimental maximum loads was ruled out for both models.

After carrying out the above comparison, further load was applied to both models to determine the loads at which they would fail. On reaching a load value of 315.0KN, the extent of concrete damage in Model 1 was obvious and the model could no longer accommodate any load increase. The maximum vertical deflection was 8.20mm. At failure, steel links (a), (b) and (c) had maximum stress values of 348.0, 331.4 and 298.2 $N/mm^2$, respectively.

In Model 2, failure was obtained at a load value of 273.0 KN. Failure was characterised by the development of weak concrete zone at the symmetry plane and the propagation of cracks towards the free column edge and the column side. No plastic strain was developed in the steel links up to failure.

### 6.7.2 Deflections

Both the experimental and numerical load-vertical deflection curves are shown for comparison in Figure (6.25). The former was obtained as the average of both $T_1$ curves shown earlier in Figure (3.4). Since the early start of loading there is a clear difference in values between the experimental and numerical deflections, the numerical deflection being smaller throughout the entire loading history. This difference can be attributed to the following reasons:

1. Occurrence of grout settlement under the bolt shank and within the sleeve as soon as the load was applied. This settlement which was not modelled within the finite element analysis, accounts for the early divergence of the curves.

2. The numerical deflections were computed at the column face while the experimental ones were measured at 10.0mm away from the face. This value represents half the thickness of the bracket's back plate. At higher loads, shear deformation of the bolt outside the column face accounts for the curves' progressive divergence as the maximum load is approached.

Up to a load value of 200.0 KN, the numerical deflection curve remained parallel to the experimental one. Then the gap between them started to increase due to the rapid increase in the experimental deflection. The yield of the bolt's threaded end contributed much to this experimental deflection increase.

The vertical deflection, at the bolt's remote end, had not been measured experimentally, leaving in question the possible closing of the gap at this end. The numerical results successfully provided an answer to this question.

Although the vertical deflection has a similar trend to that obtained experimentally, the axial deflections differ in magnitude. The computed deflections at the bolt's centre are much smaller. The only explanation that can be offered is that the load was applied at the column face in the model, while it had an eccentricity value of 60mm in the test. The induced moment created by this eccentricity at the column face had a bigger contribution in the bolt's pullout tendency. The rate of the bolt's pullout was later increased by the bolt thread yield at the last stages of loading. As a result, relatively high values were recorded for the axial deflection in the test. Load eccentricity could not be included in the model due to the limitation of the ANSYS program.

The numerically obtained lateral deflections at the column's far edge have very small values. However, their trend of expansion below the joint level is positive. This is in a good agreement with the those obtained experimentally.

The sleeve cross section at the loaded end has been deformed in the model to an ovoid section similar to that obtained in the tests. Also the numerical results provided information about the development of sleeve yield area and its contact area with the bolt at intermediate load stages. The maximum values agree very well with those found experimentally at the ultimate loads.

### 6.7.3 Stresses and Strains

The numerical results suggested the development of plastic strains in the bolt shank after reaching 60% of the joint ultimate load. On reaching the ultimate load, these strains were

only limited to the top and bottom edges while the central portion of the bolt shank remained elastic. In most tests, the examination of the bolts after testing revealed the occurrence of some plastic bending about their longitudinal axes.

Since axial strains in the steel links were not measured, no comparison could be made with the numerical results. However, elastic tensile stresses computed in the links indicated the development of a lateral force beneath the sleeve.

The cracks which started in the highly stressed regions when the local concrete strength was exceeded were insufficient to cause a numerical collapse of the joint. This is in compliance with the experimental findings. It is worth pointing out that these cracks could not be monitored experimentally as the steel brackets covered most of these regions. Crushing and spalling of concrete have been predicted in areas which correspond reasonably with those observed experimentally after the bracket's removal.

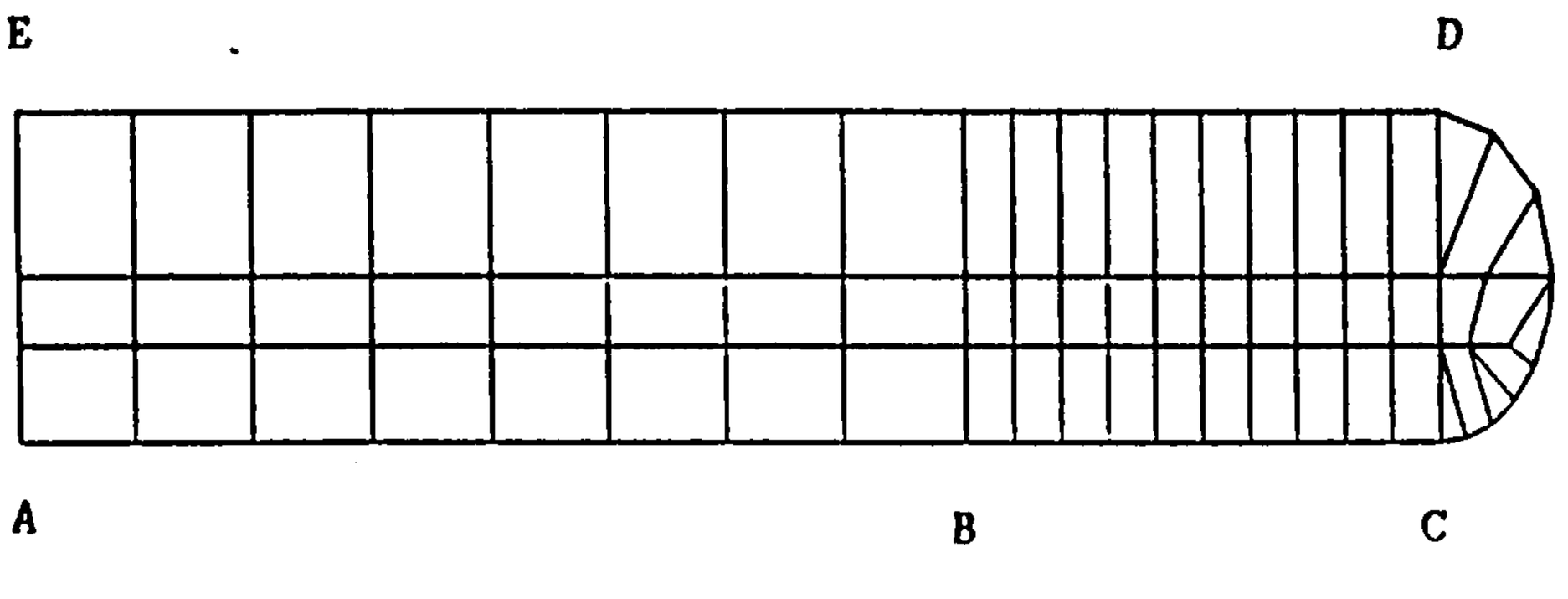


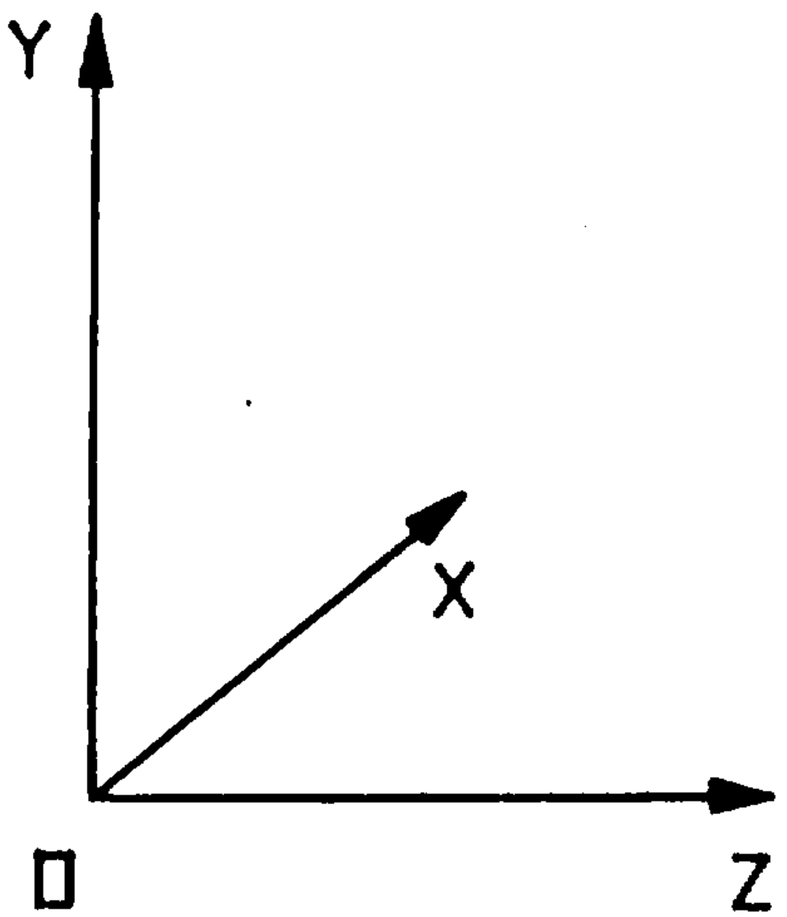


AB : Coarse Mesh

DE : Top Edge

AE : Remote End

BC : Fine Mesh

AC : Bottom Edge

CD : Loaded End

FIGURE (6.1) : DEFINITION OF DIFFERENT PARTS OF THE BOLT FINITE ELEMENT MESH.

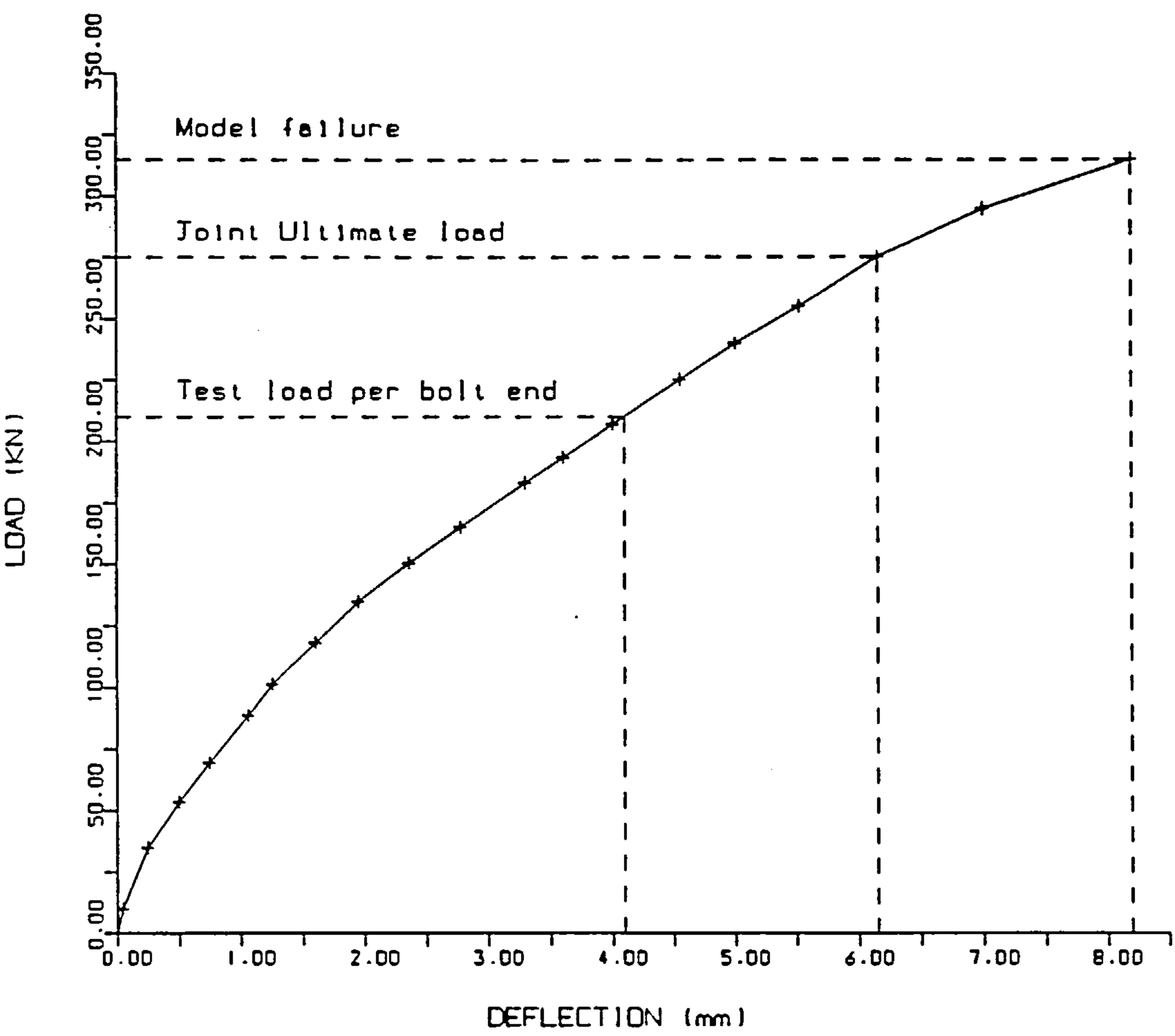


FIGURE (6.2) : PREDICTED LOAD-DEFLECTION RESPONSE AT THE LOADED END OF THE BOLT.

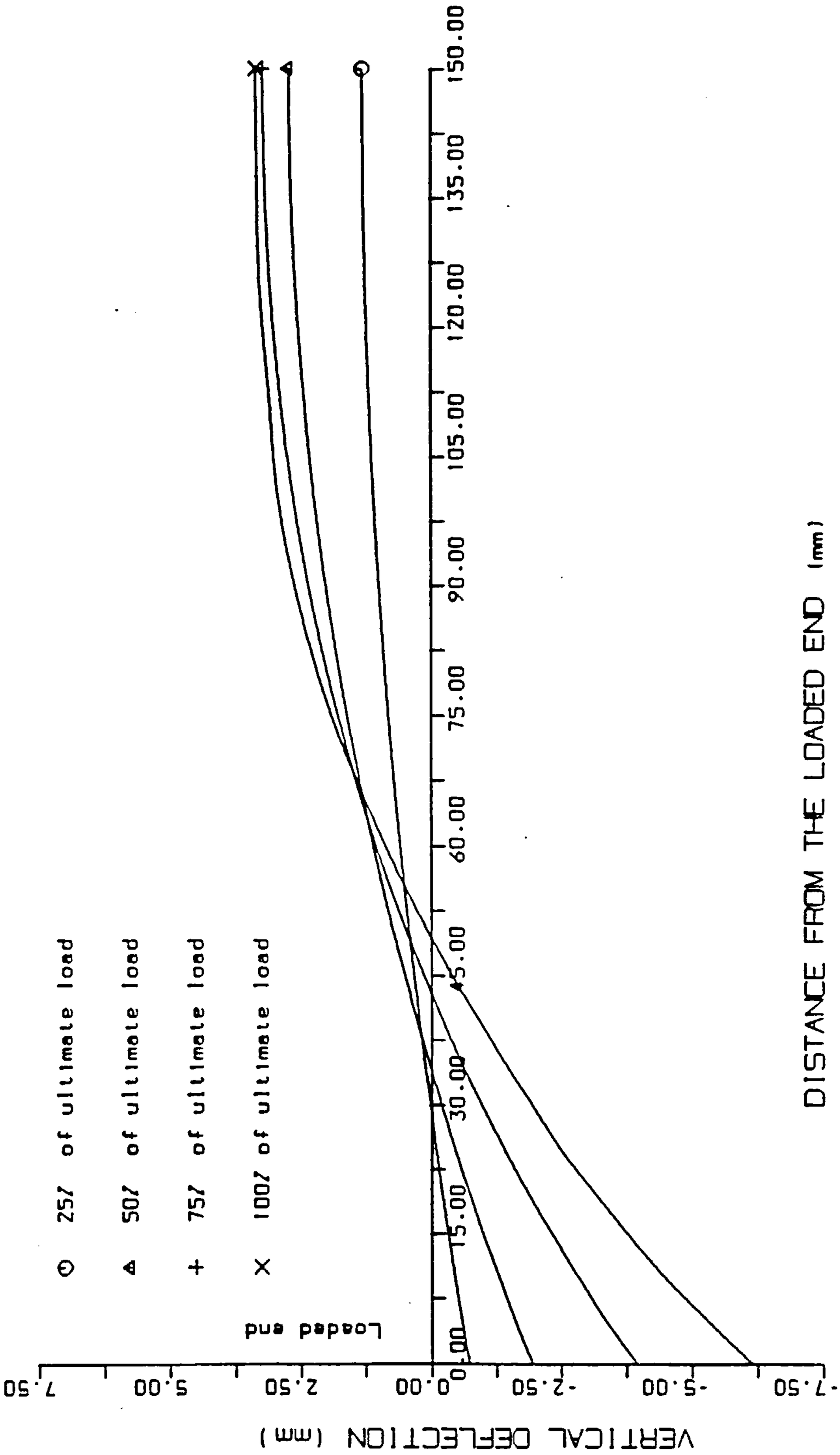


**FIGURE (6.3) : VARIATION OF THE VERTICAL DEFLECTION ALONG THE LONGITUDINAL AXIS AT VARIOUS LOAD VALUES.**

Positive values = Bolt in tension
Negative values = Bolt in compression

I = 0.627mm
H = 0.450mm
G = 0.273mm
F = 0.097mm
E = -0.087mm
D = -0.275mm
C = -0.461mm
B = -0.648mm
A = -0.835mm

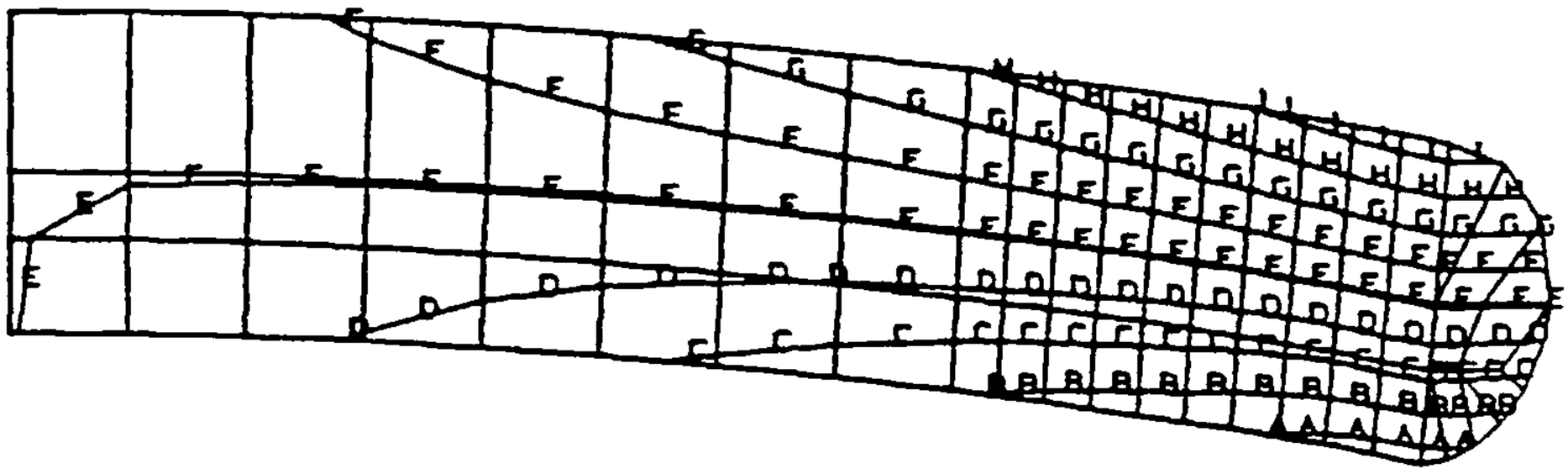

FIGURE (6.4) : BOLT AXIAL DEFLECTION CONTOURS AT 50% OF THE ULTIMATE LOAD.

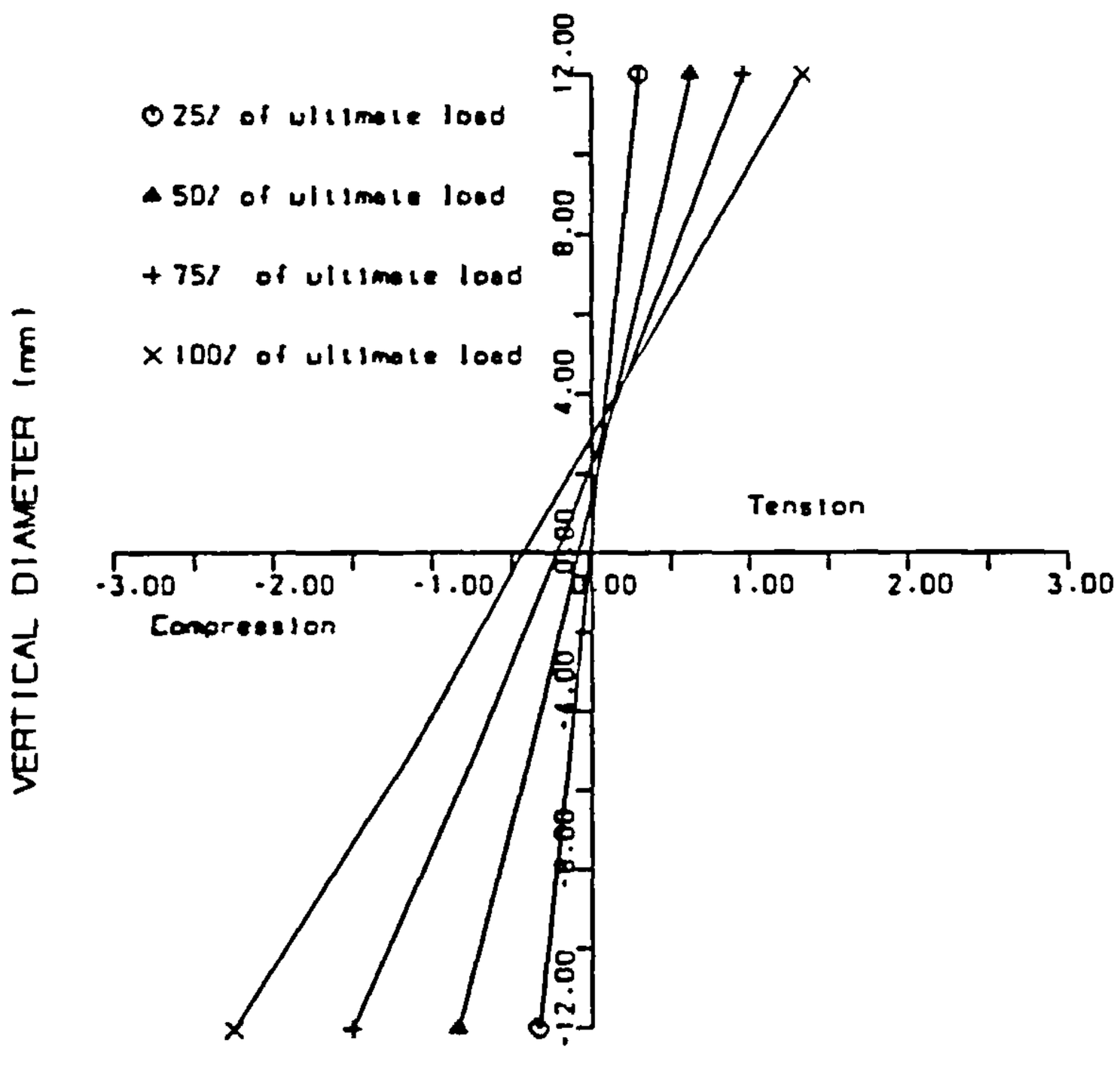


FIGURE (6.5) : VARIATION OF THE AXIAL DEFLECTION AT THE LOADED END DOWN THE BOLT'S VERTICAL DIAMETER.

Positive values = Moving away from the vertical diameter

Negative values = Moving towards the vertical diameter

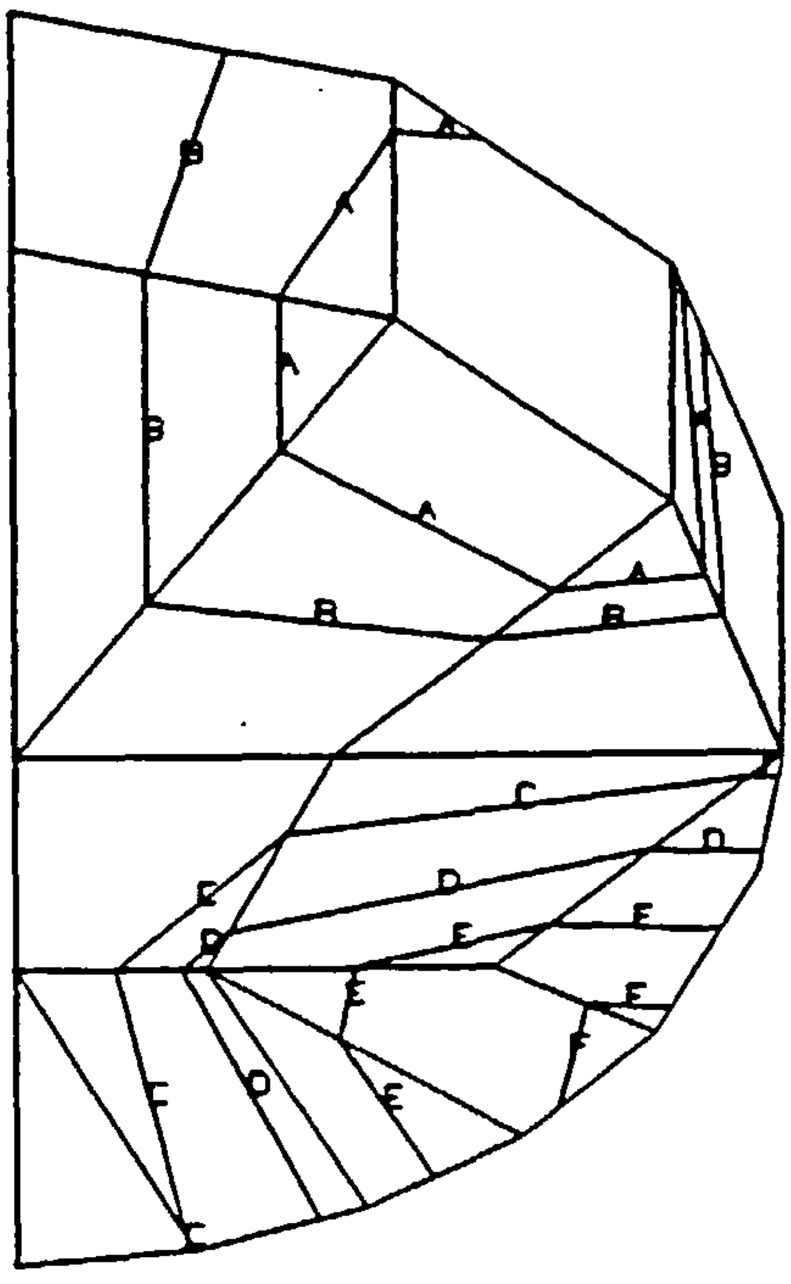


A = -0.55E-2mm
B = -0.40E-2mm
C = 0.90E-3mm
D = 0.10E-2mm
E = 0.12E-2mm
F = 0.13E-2mm

FIGURE (6.6) : LATERAL DEFLECTION CONTOURS AT THE LOADED END AT 50% OF THE ULTIMATE LOAD.

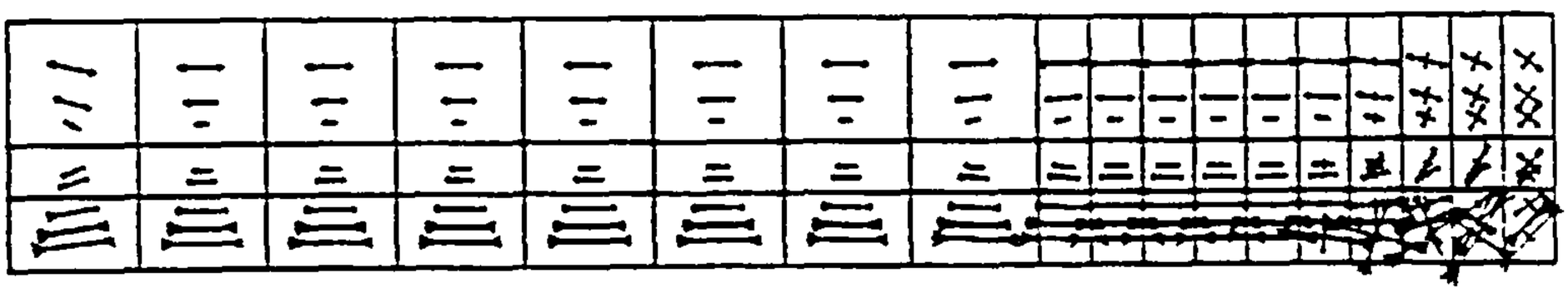

Arrow length represents stress magnitude.

FIGURE (6.7) : PRINCIPAL STRESS DISTRIBUTION FOR THE BOLT SHANK AT 50% OF THE ULTIMATE LOAD.

Positive values = Tensile stress
Negative values = compressive stress

A = -550.0 $N/mm^2$
B = -500.0 $N/mm^2$
C = -450.0 $N/mm^2$
D = -350.0 $N/mm^2$
E = -250.0 $N/mm^2$
F = -100.0 $N/mm^2$
G = 250.0 $N/mm^2$
H = 350.0 $N/mm^2$
I = 450.0 $N/mm^2$

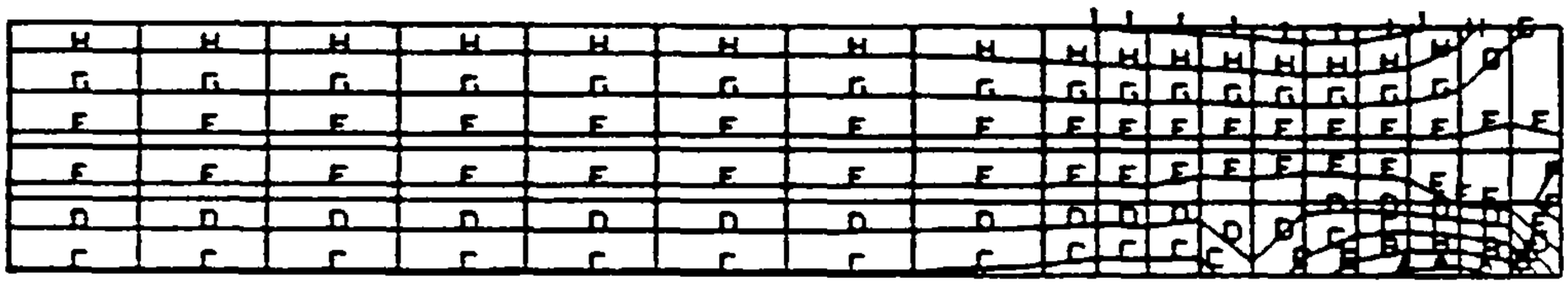

FIGURE (6.8) : LONGITUDINAL STRESS DISTRIBUTION FOR THE BOLT SHANK AT 50% OF THE ULTIMATE LOAD.

Positive values = Bolt in tension
Negative values = Bolt in compression

A = -2.2E-3
B = -1.5E-3
C = -1.0E-3
D = -0.5E-4
E = 0.5E-4
F = 1.0E-3
G = 2.0E-3

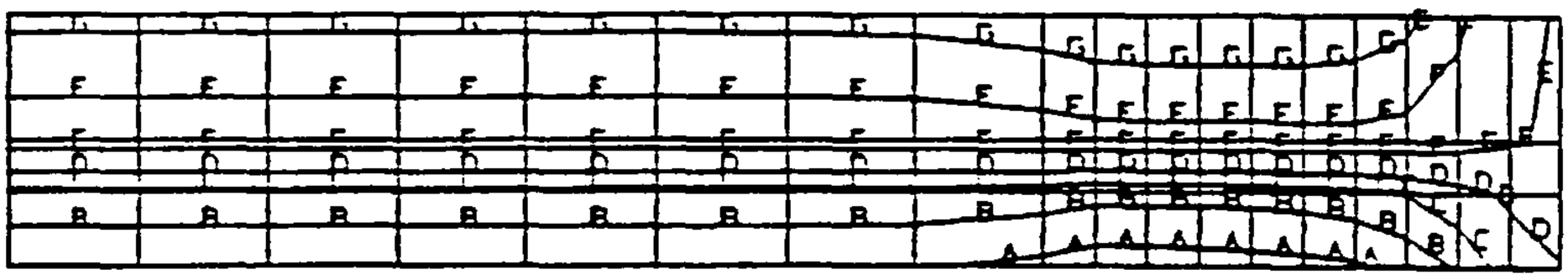

FIGURE (6.9) : LONGITUDINAL STRAIN DISTRIBUTION FOR THE BOLT SHANK AT 50% OF THE ULTIMATE LOAD.

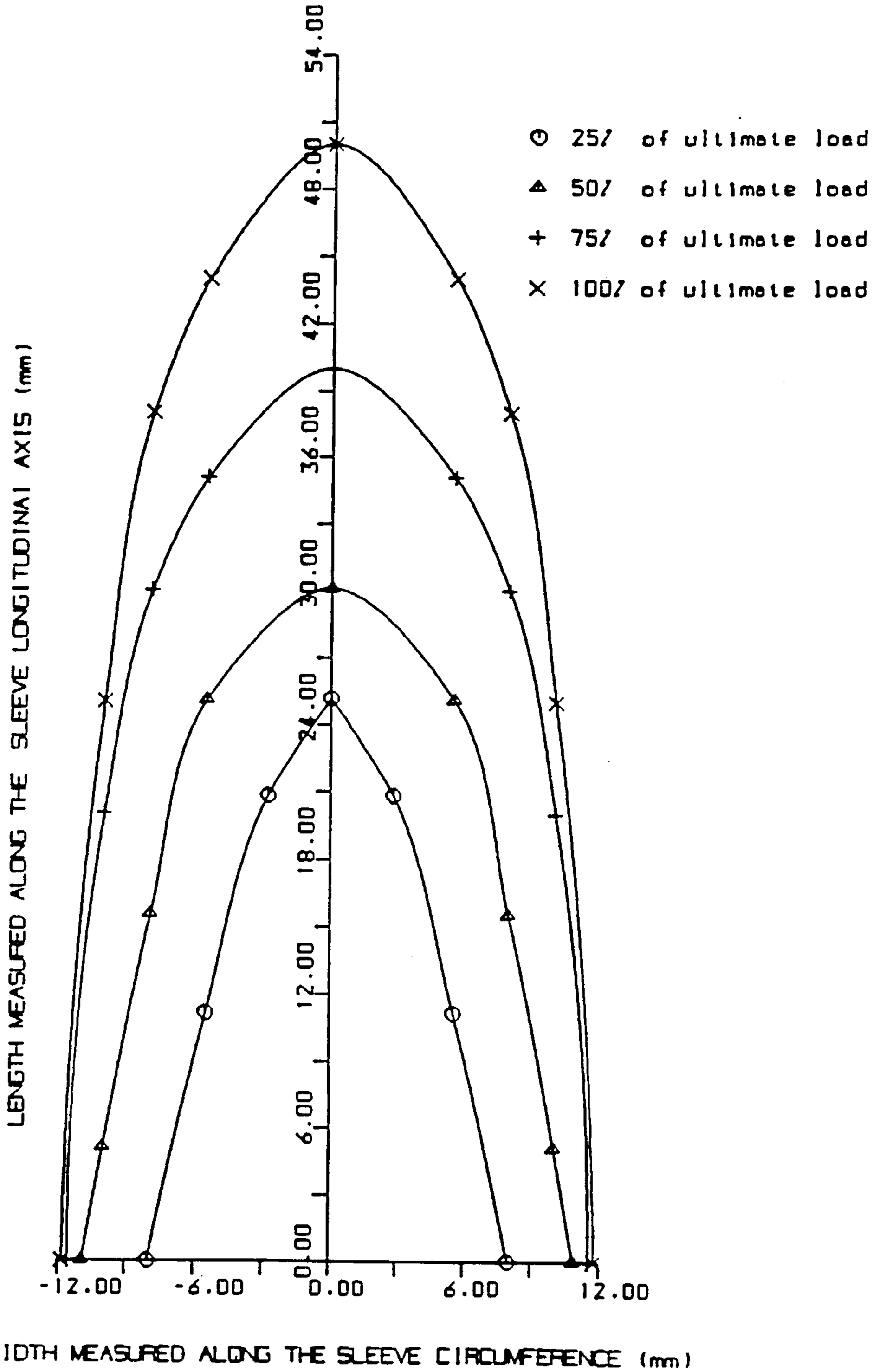


FIGURE (6.10) : PREDICTED CONTACT AREAS BETWEEN THE BOLT AND THE SLEEVE AT DIFFERENT LOAD VALUES.

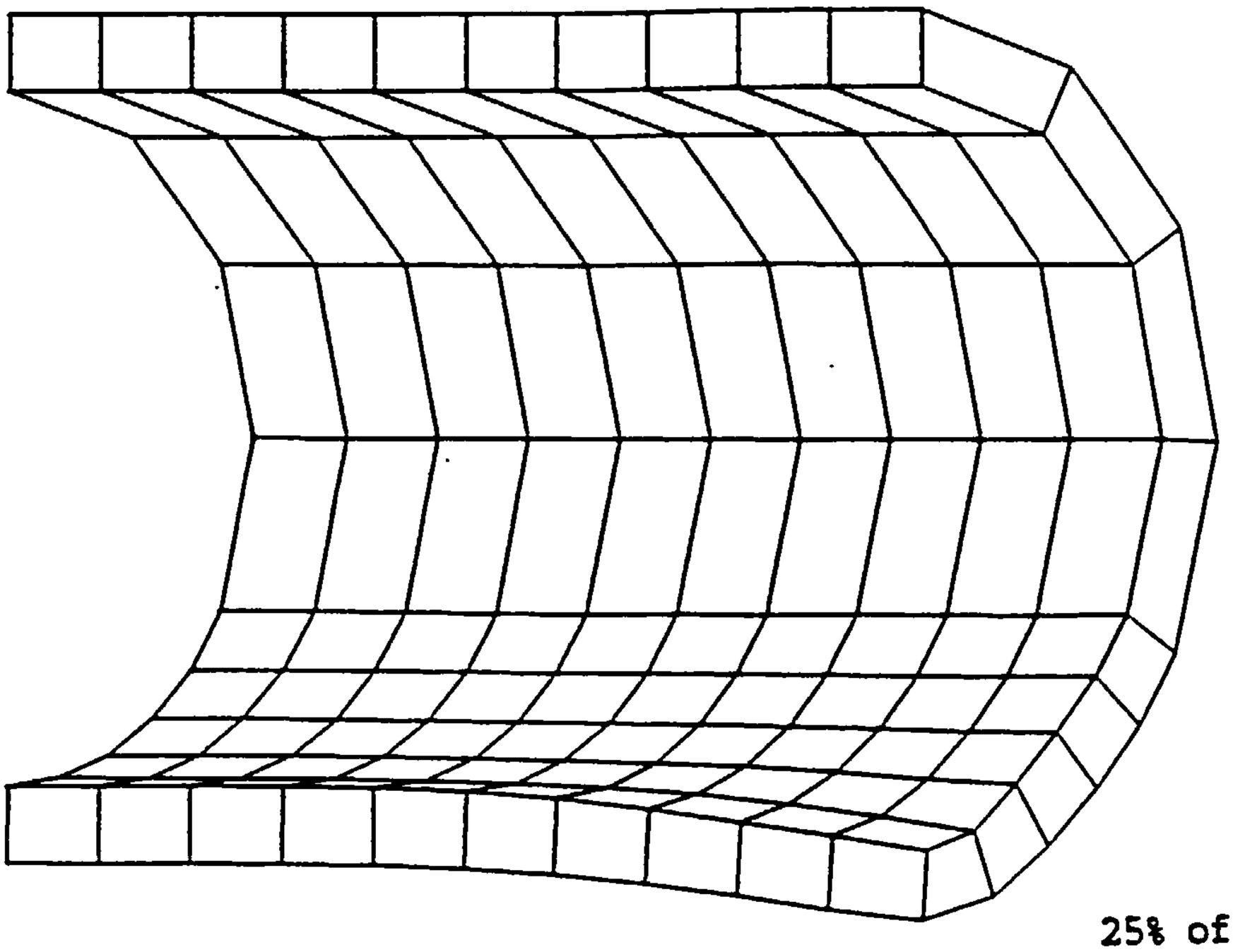

25% of the ultimate load

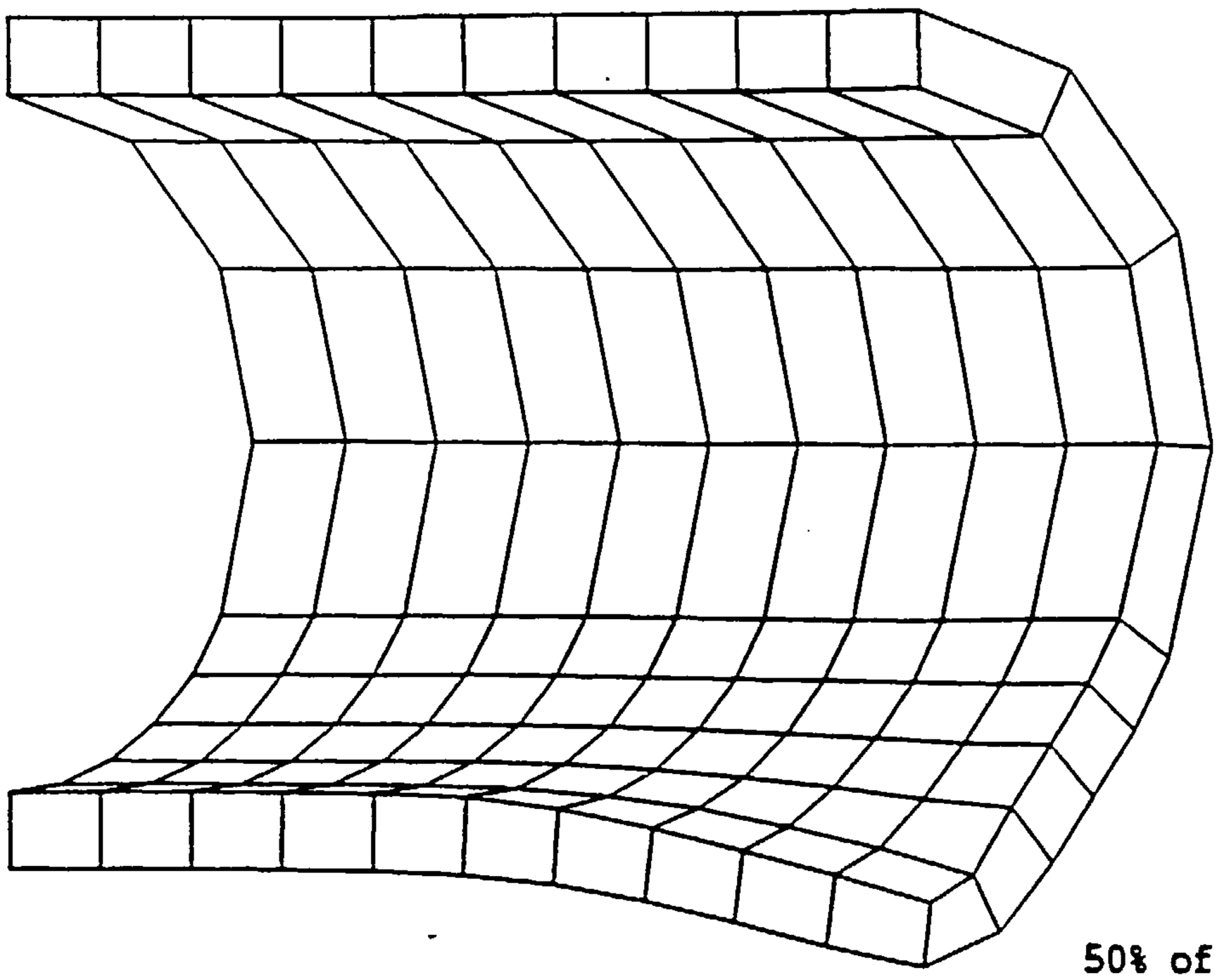

50% of the ultimate load

FIGURE (6.11) : DEFORMATION OF THE SLEEVE'S CROSS SECTION AT THE LOADED END FOR DIFFERENT LOAD VALUES.

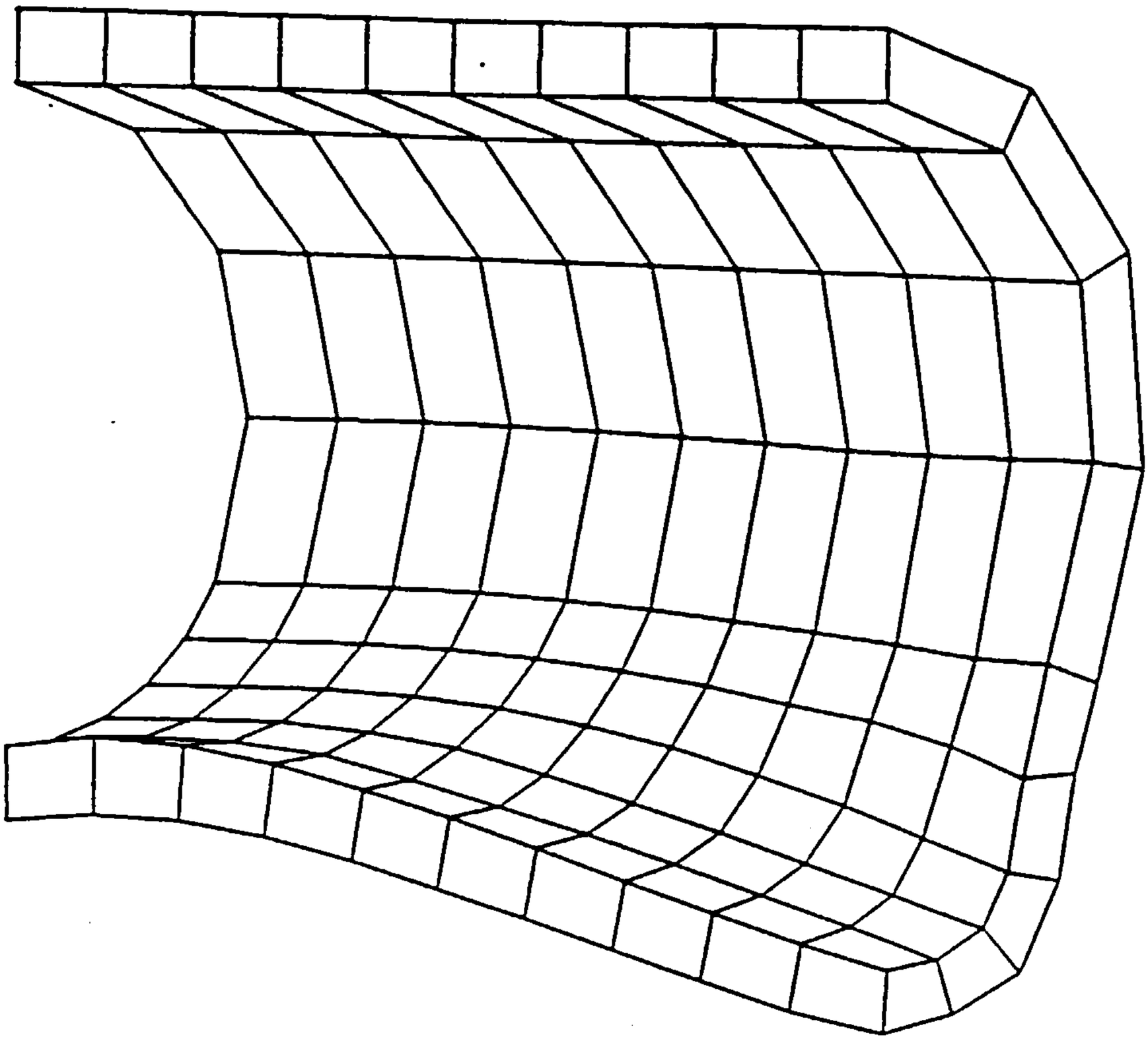

At the ultimate load

FIGURE (6.11) (CONTINUED)

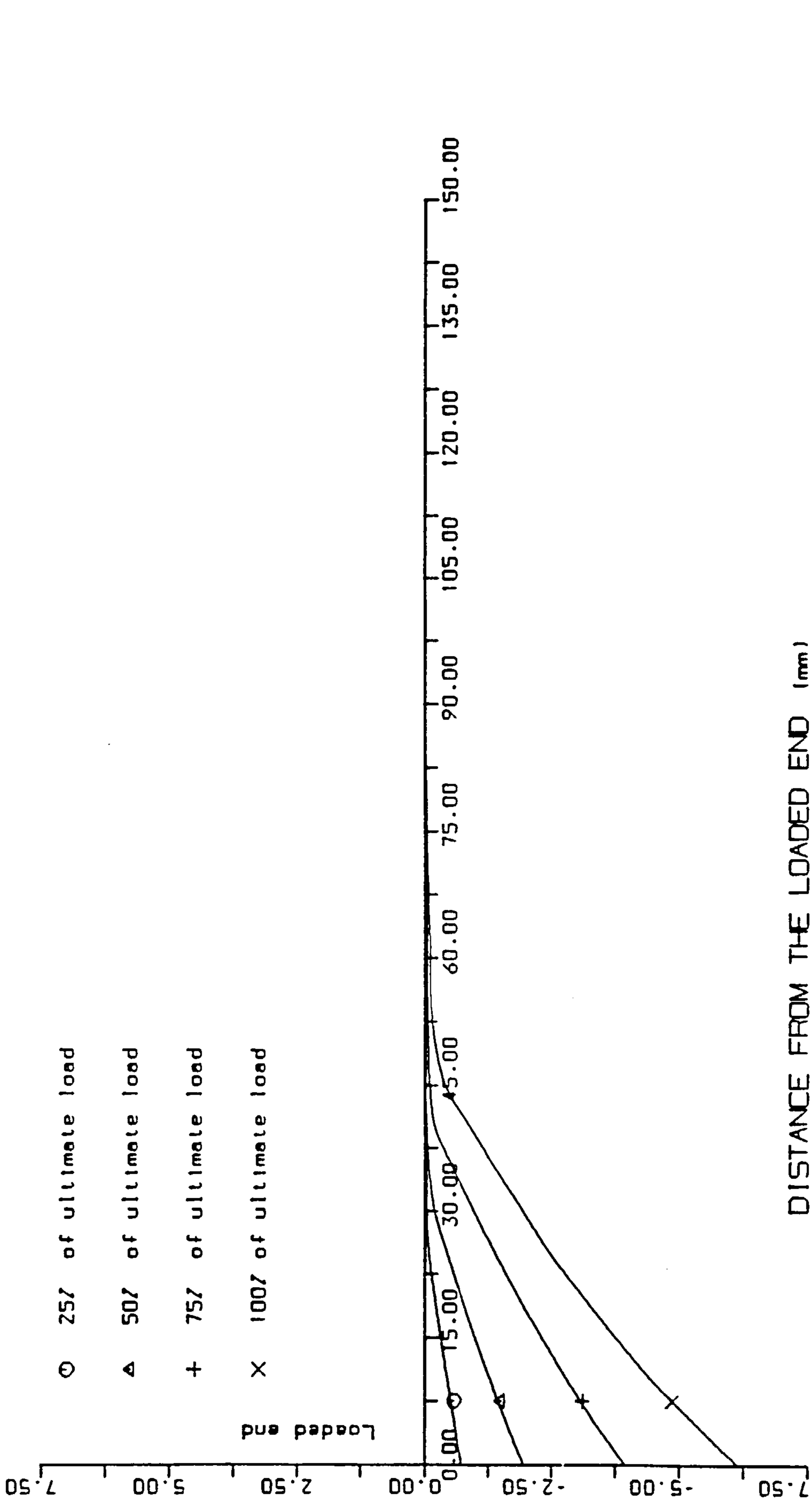


FIGURE (6.12) : VARIATION OF THE SLEEVE'S VERTICAL DEFLECTION ALONG THE LONGITUDINAL EDGE OF SYMMETRY.

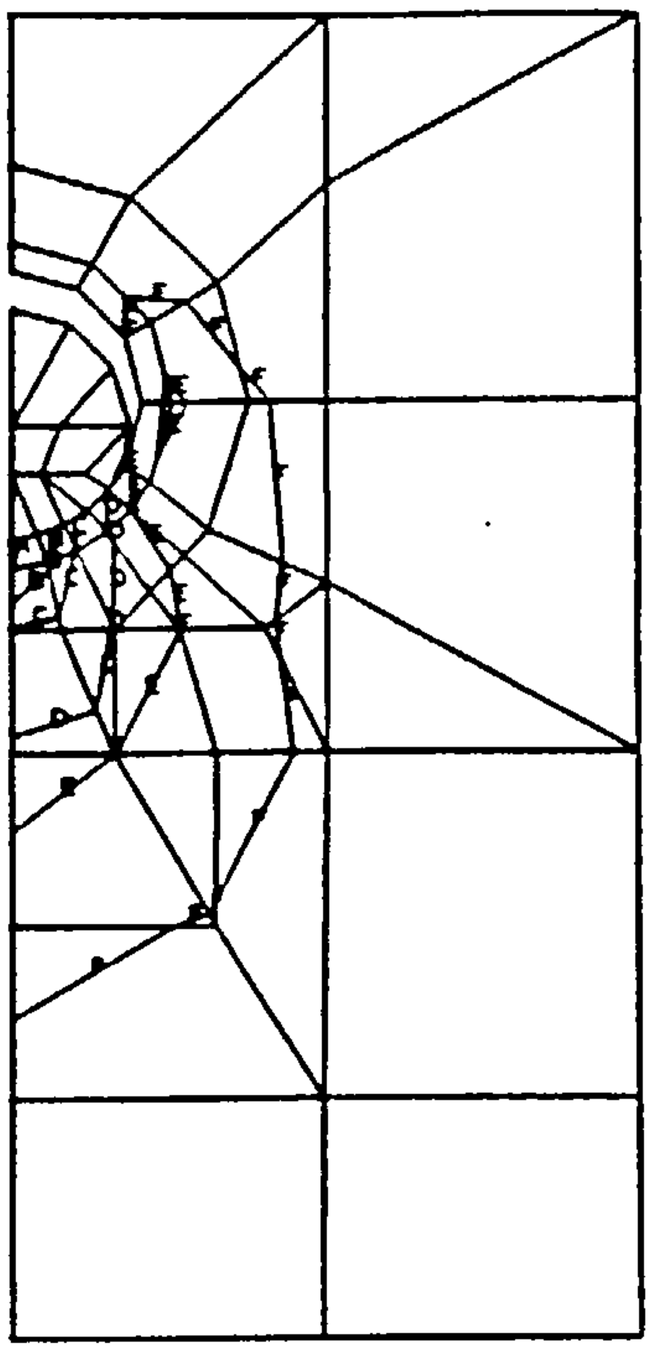

A = -2.00mm
B = -1.80mm
C = -1.60mm
D = -1.40mm
E = -1.00mm
F = -0.80mm

FIGURE (6.13) : VERTICAL DISPLACEMENT CONTOURS AT THE XY PLANE FOR MODEL 1 AT 50% OF THE ULTIMATE LOAD.

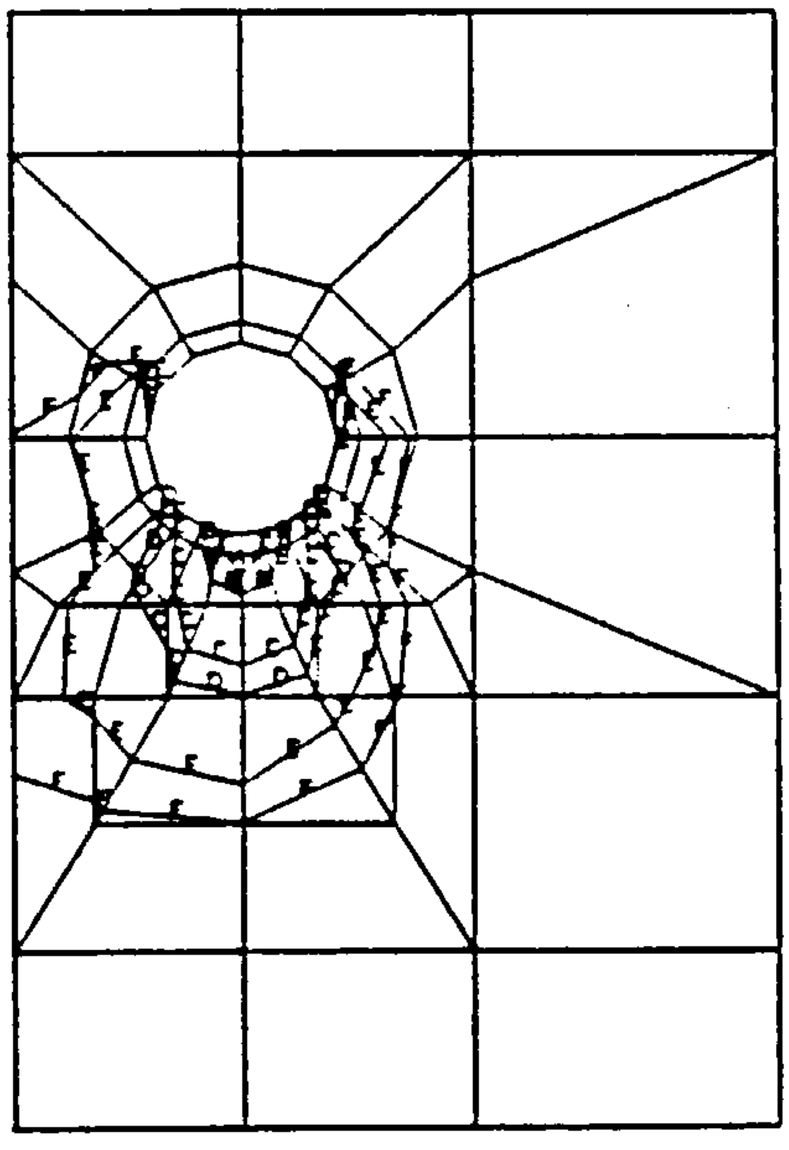

A = -1.90mm
B = -1.70mm
C = -1.40mm
D = -1.10mm
E = -0.80mm
F = -0.50mm

FIGURE (6.14) : VERTICAL DISPLACEMENT CONTOURS AT THE XY PLANE FOR MODEL 2 AT 50% OF THE ULTIMATE LOAD.

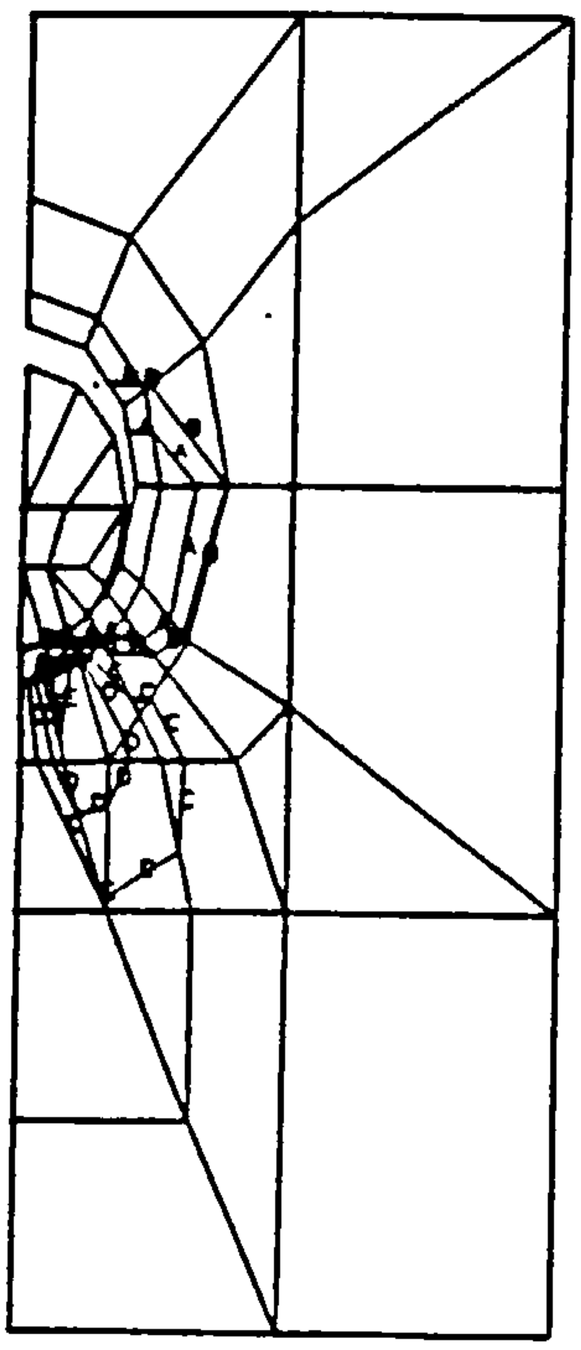

A = -0.075mm
B = -0.050mm
C = 0.150mm
D = 0.200mm
E = 0.250mm

FIGURE (6.15) : LATERAL DISPLACEMENT CONTOURS AT THE XY PLANE FOR MODEL 1 AT 50% OF THE ULTIMATE LOAD.

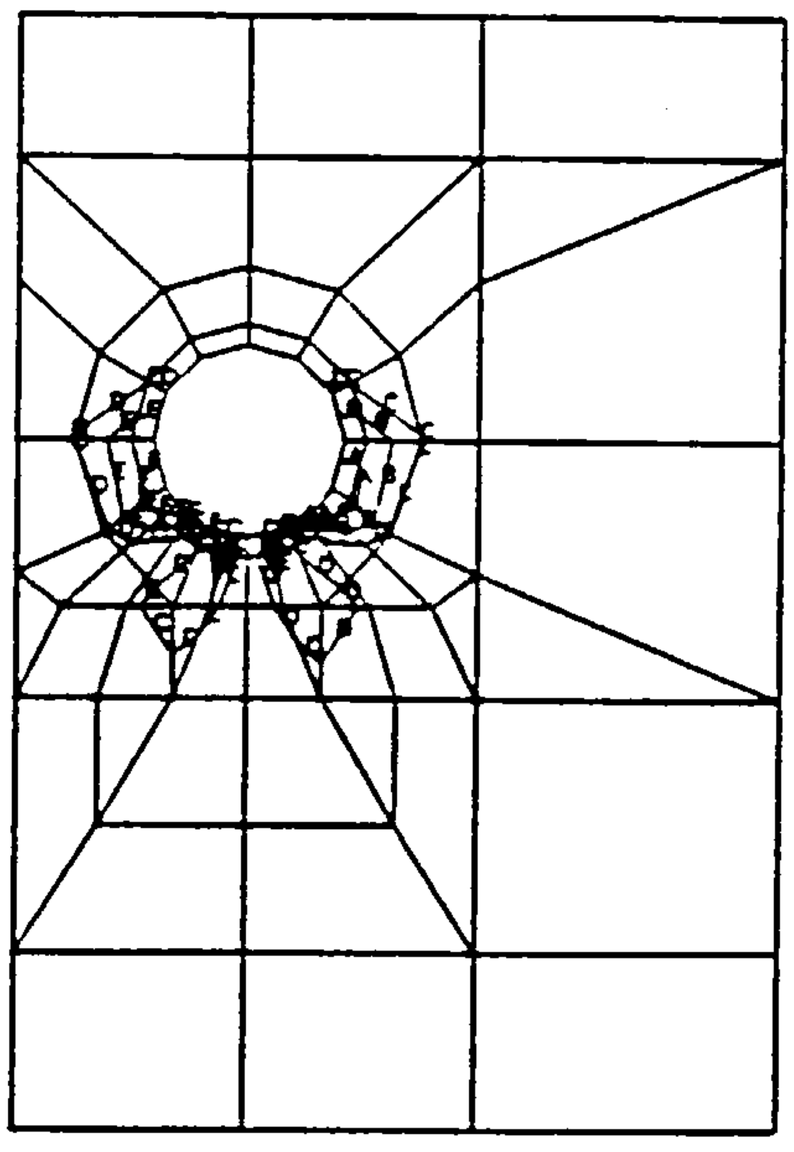

A = -0.30mm
B = -0.20mm
C = -0.10mm
D = 0.25mm
E = 0.35mm

FIGURE (6.16) : LATERAL DISPLACEMENT CONTOURS AT THE XY PLANE FOR MODEL 2 AT 50% OF THE ULTIMATE LOAD.

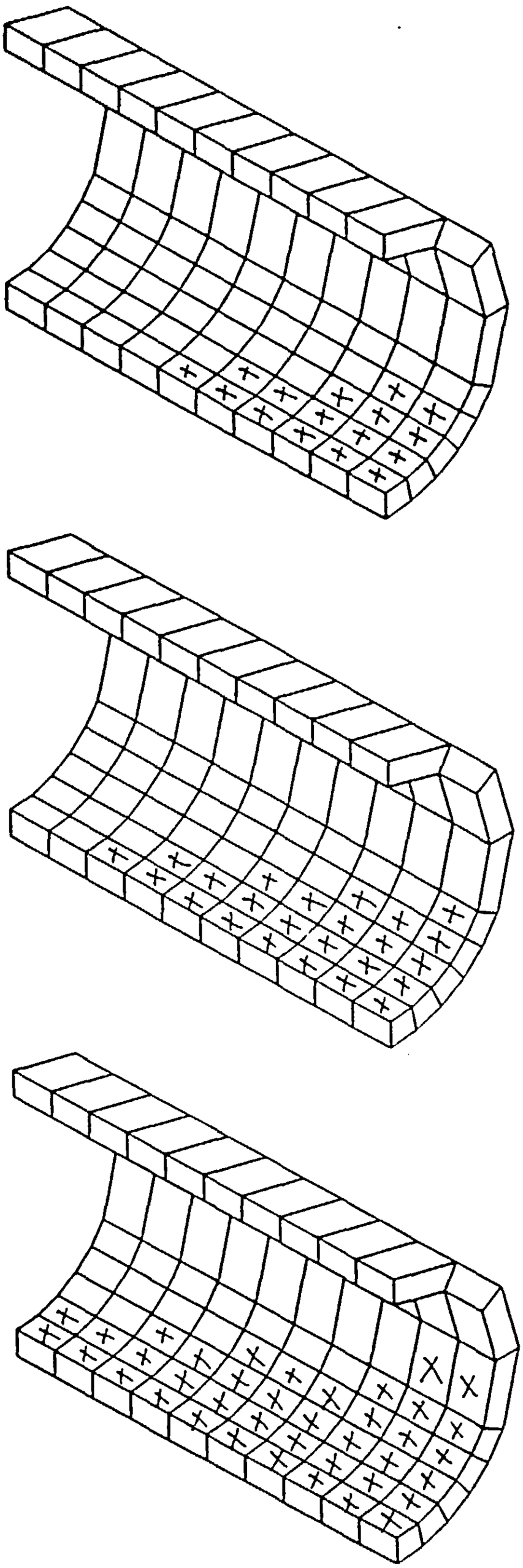


FIGURE (6.17) : DEVELOPMENT OF THE PREDICTED SLEEVE YIELD AREA.

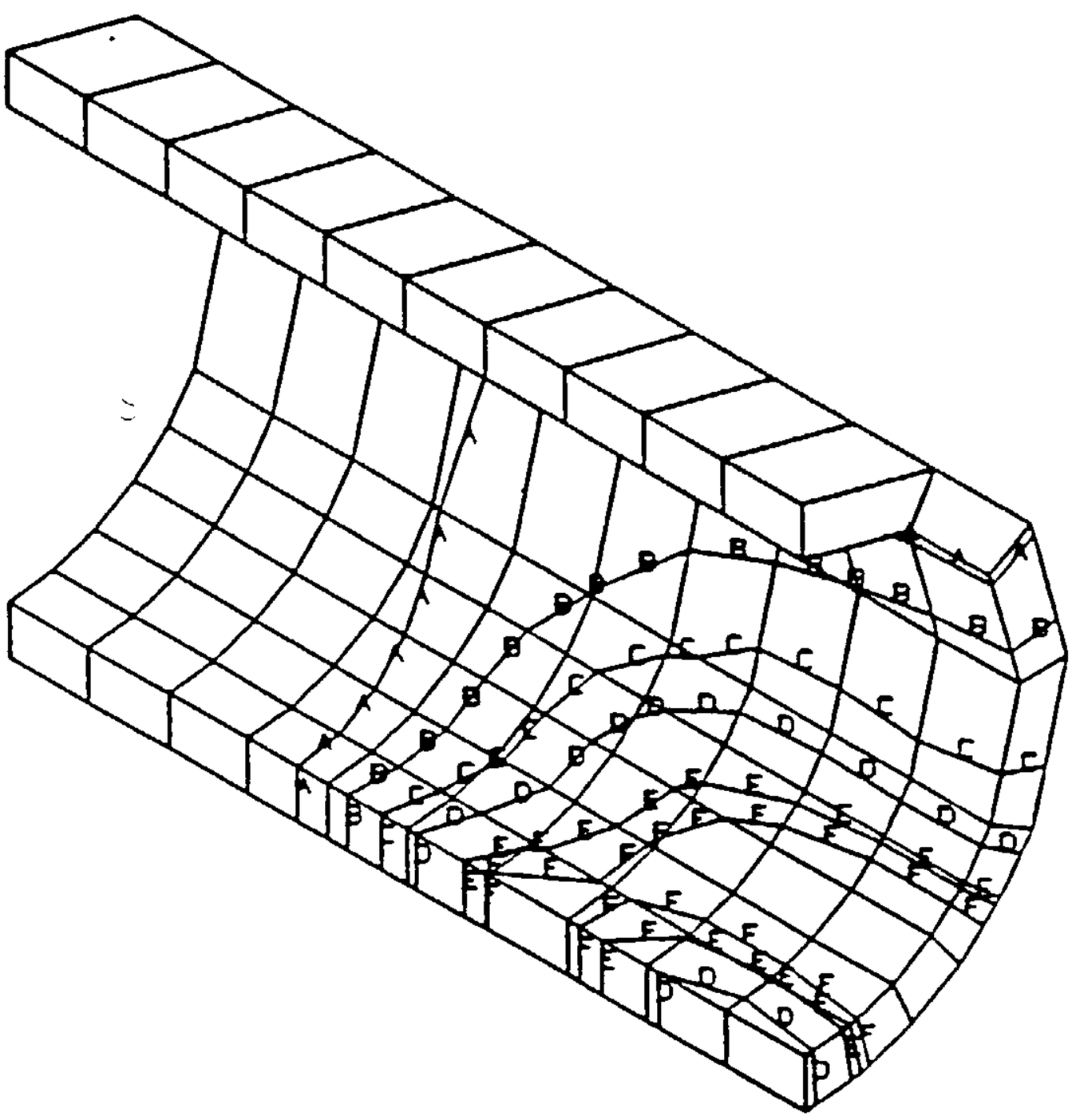


FIGURE (6.18) : SLEEVE COMPRESSIVE STRESS CONTOURS AT 50% OF THE ULTIMATE LOAD.

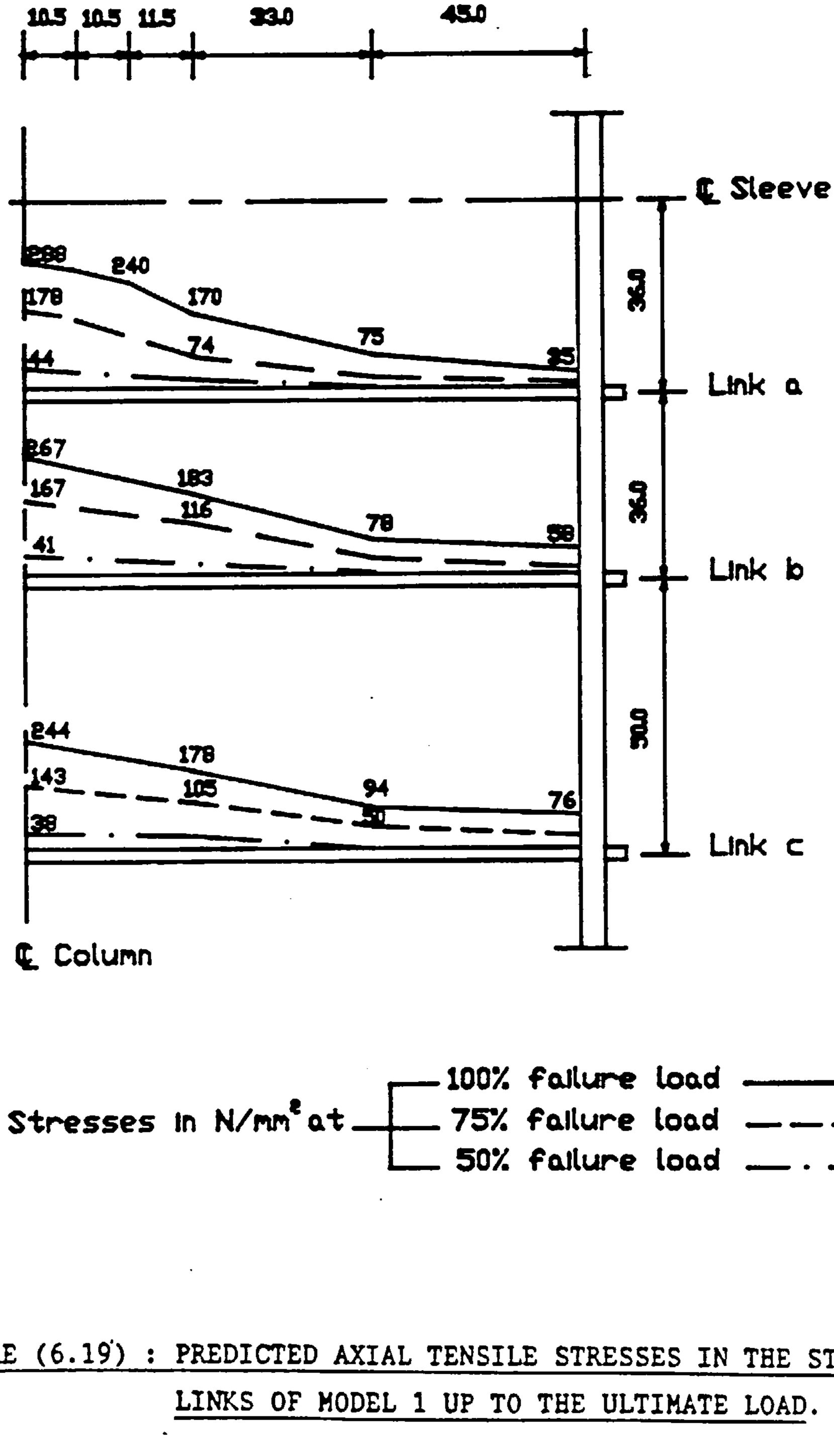


FIGURE (6.19) : PREDICTED AXIAL TENSILE STRESSES IN THE STEEL LINKS OF MODEL 1 UP TO THE ULTIMATE LOAD.

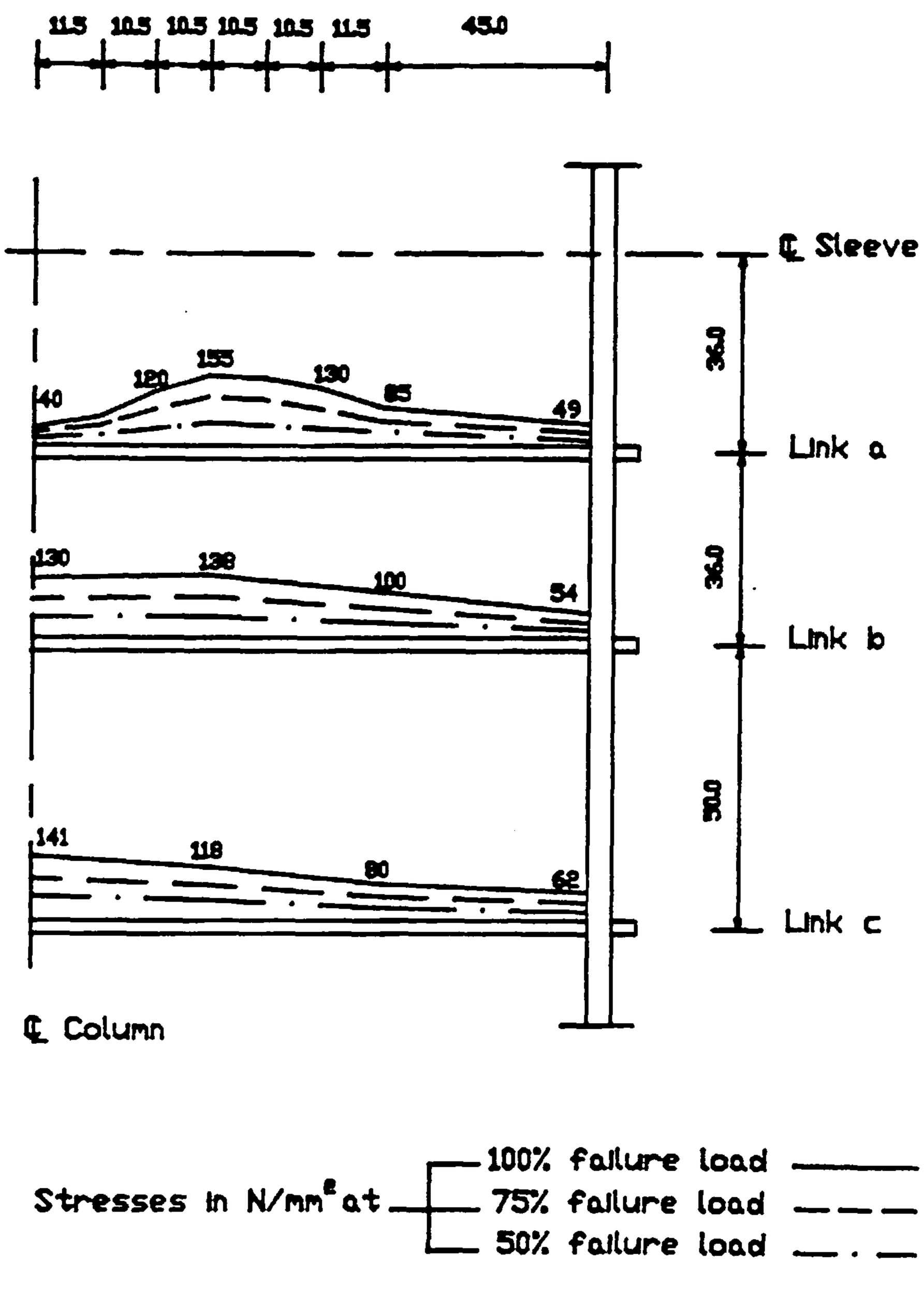


FIGURE (6.20) : PREDICTED AXIAL TENSILE STRESSES IN THE STEEL LINKS OF MODEL 2 UP TO THE ULTIMATE LOAD.

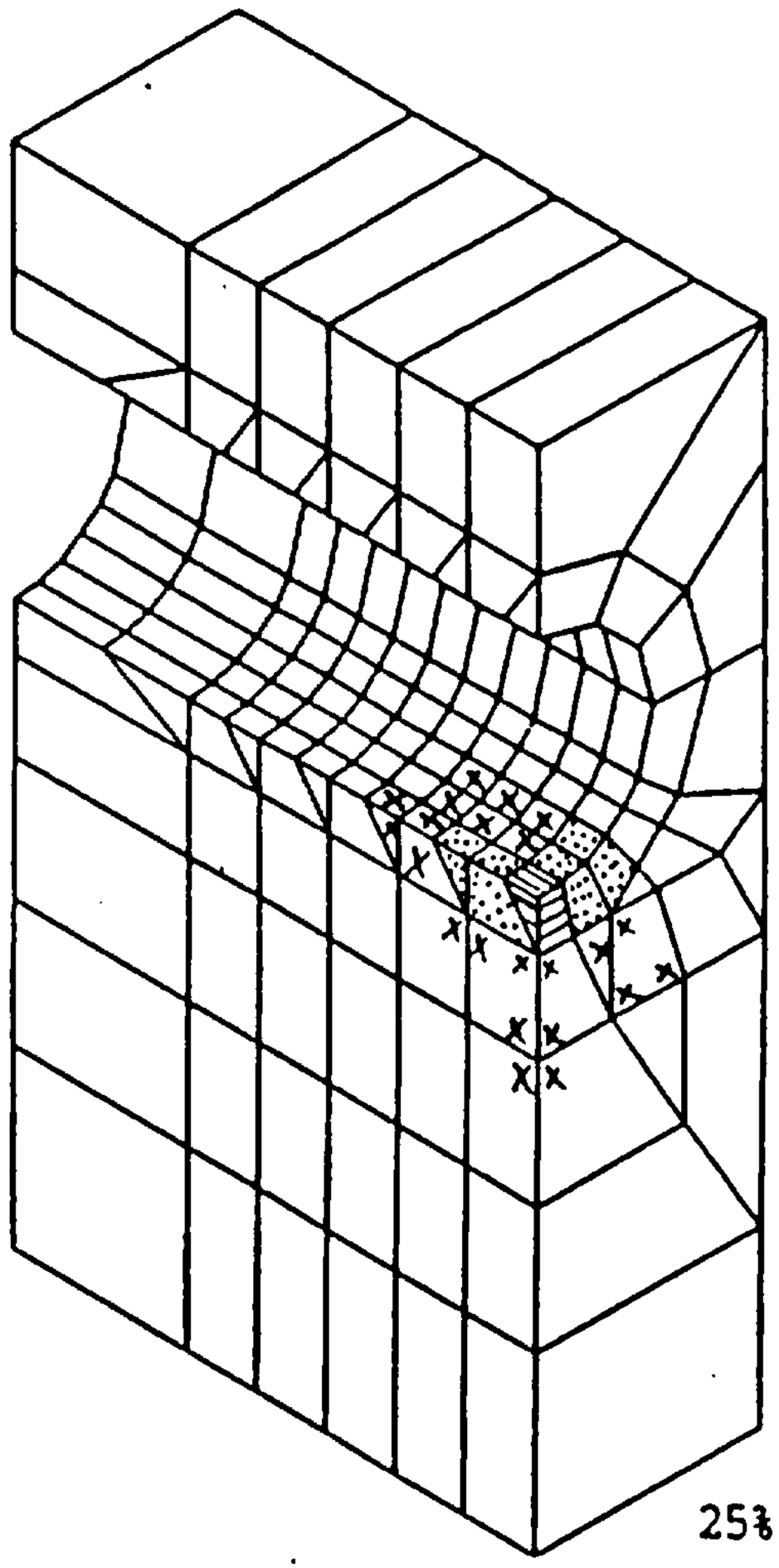

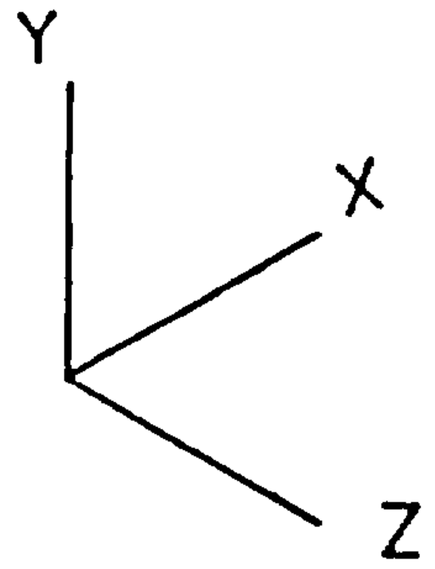


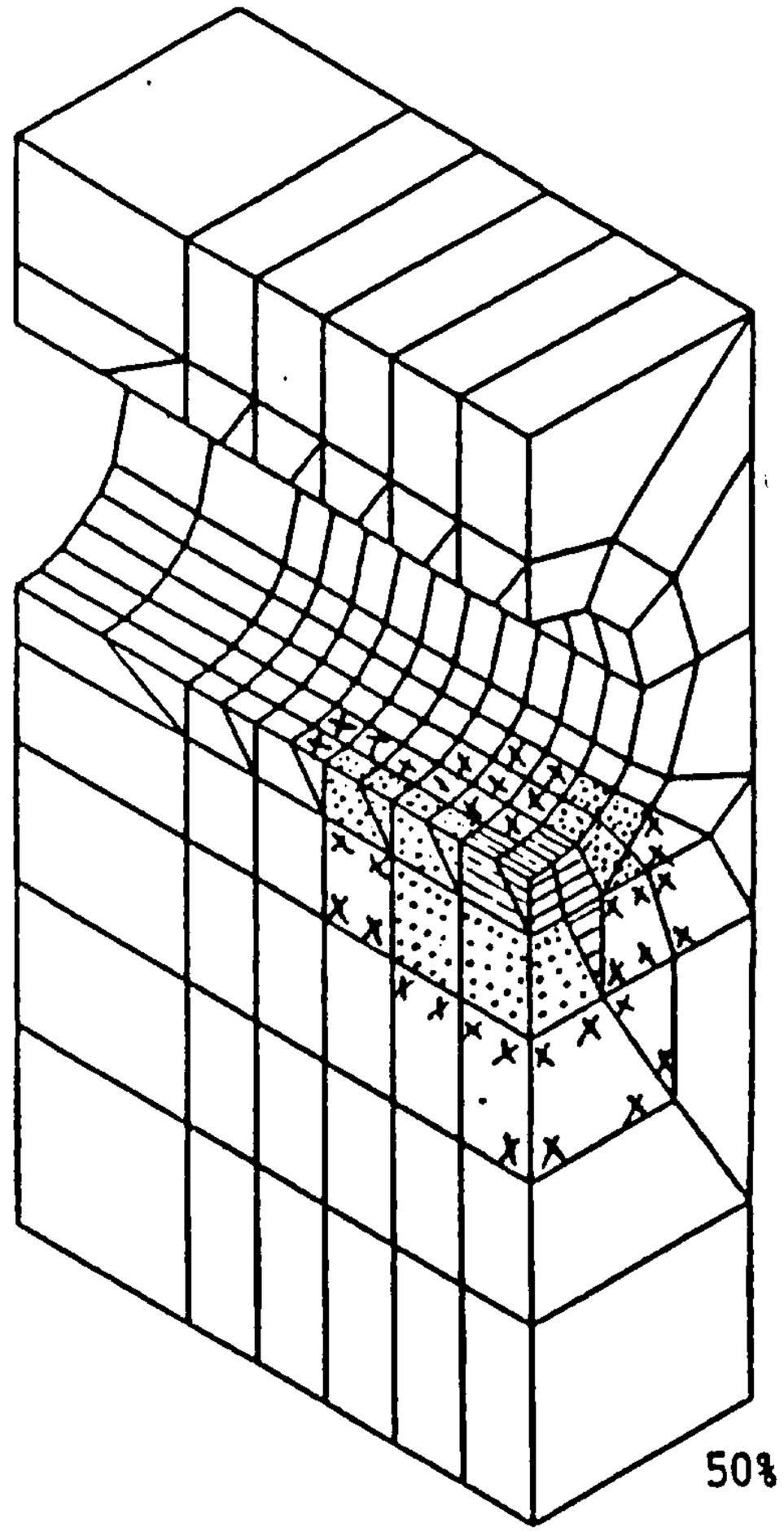

Elements with cracked integration points
Elements with 5 to 7 crushed integration points
Elements with 8 crushed integration points

25% of the ultimate load

50% of the ultimate load

**FIGURE (6.21) : DEVELOPMENT OF CRACKED AND CRUSHED ZONES IN THE CONCRETE SOLID OF MODEL 1.**

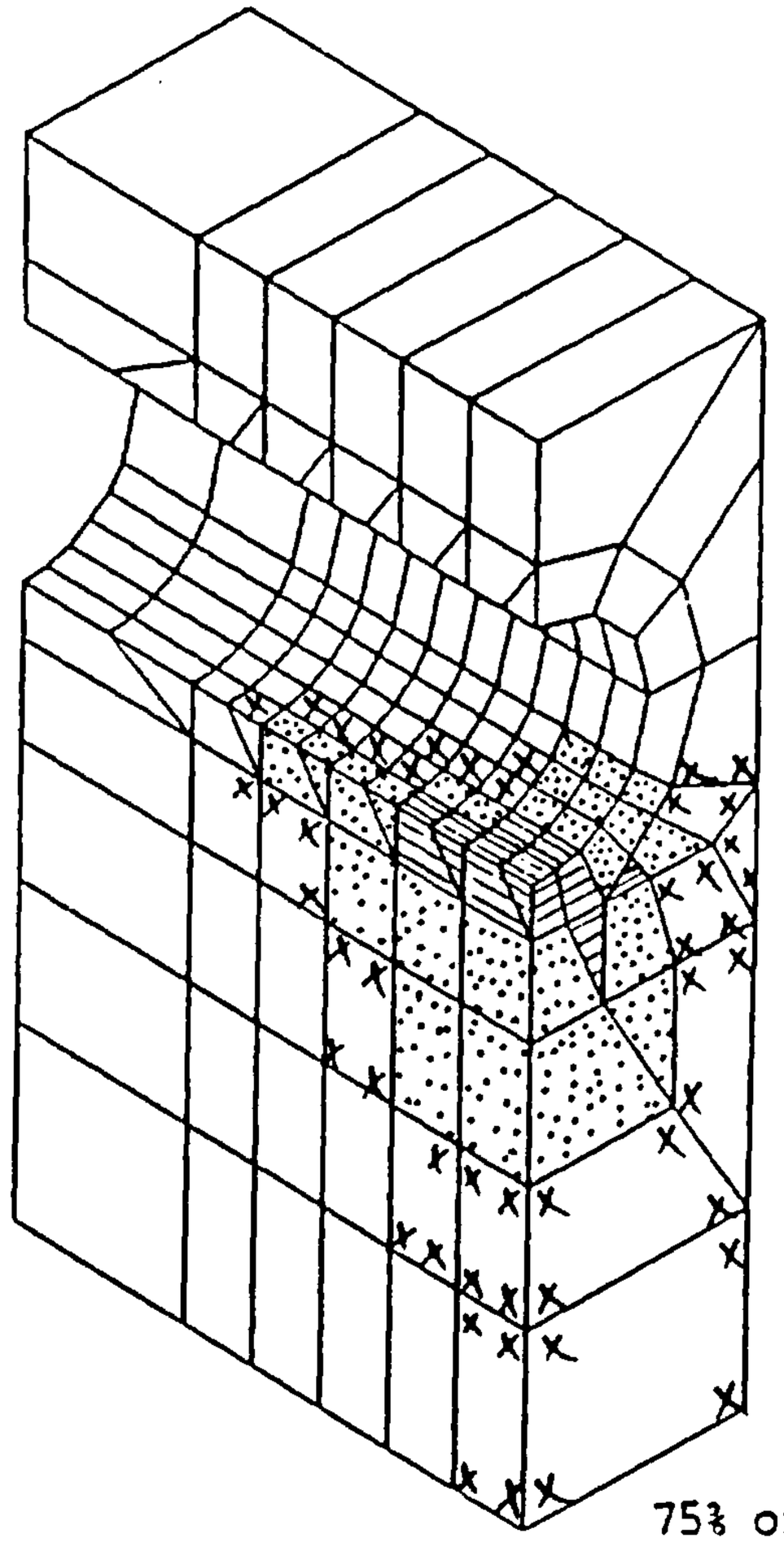

75% of the ultimate load

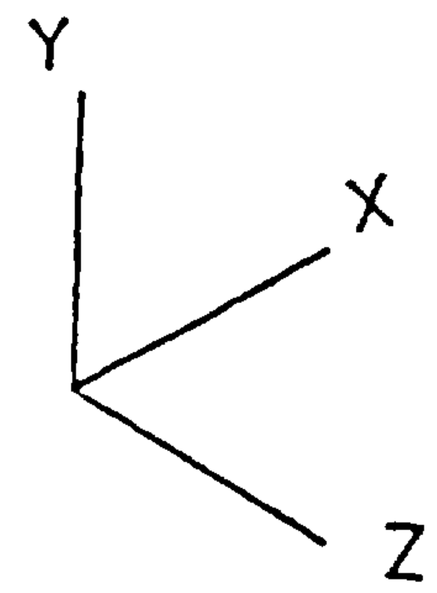


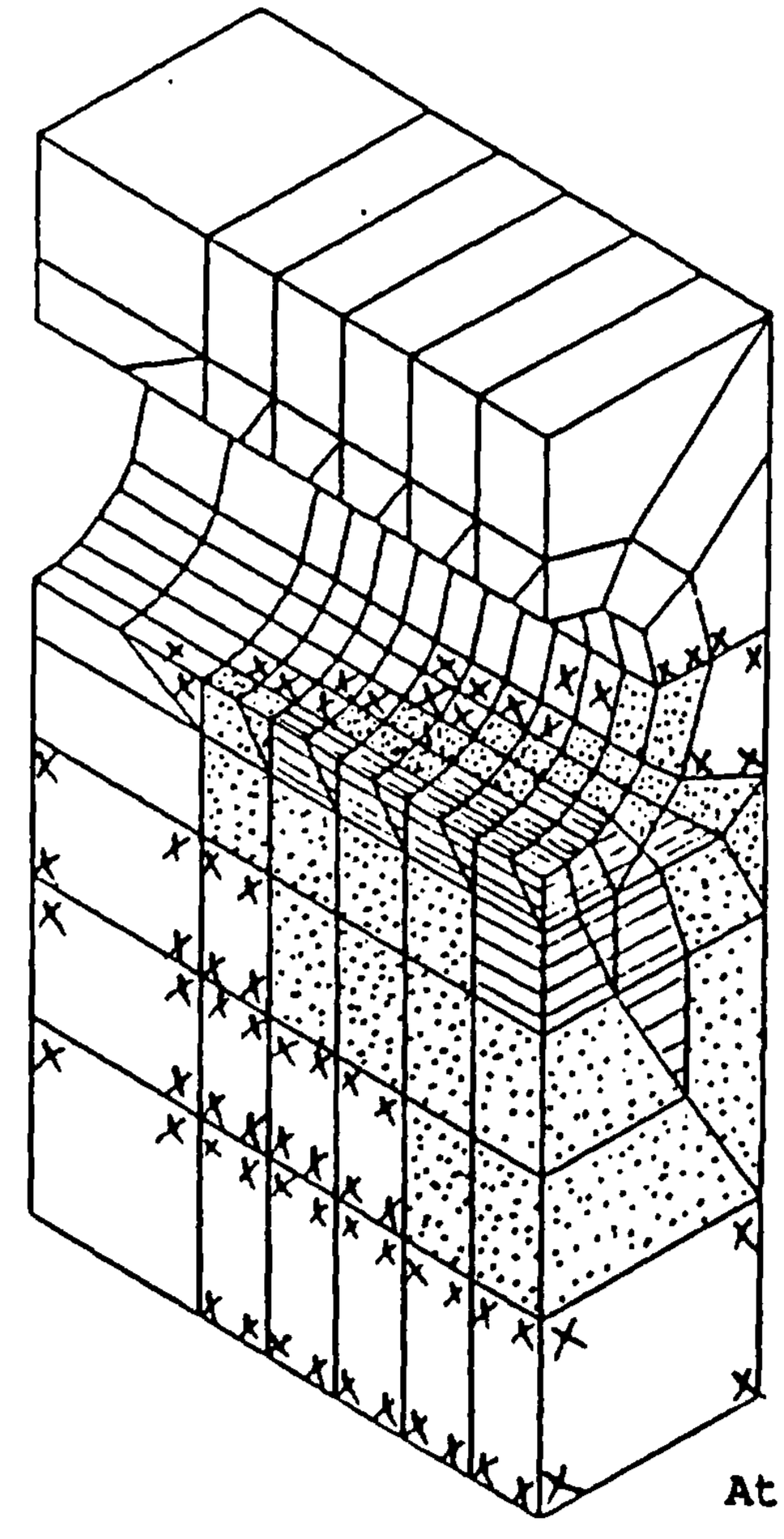

At the ultimate load

FIGURE (6.21) (CONTINUED)

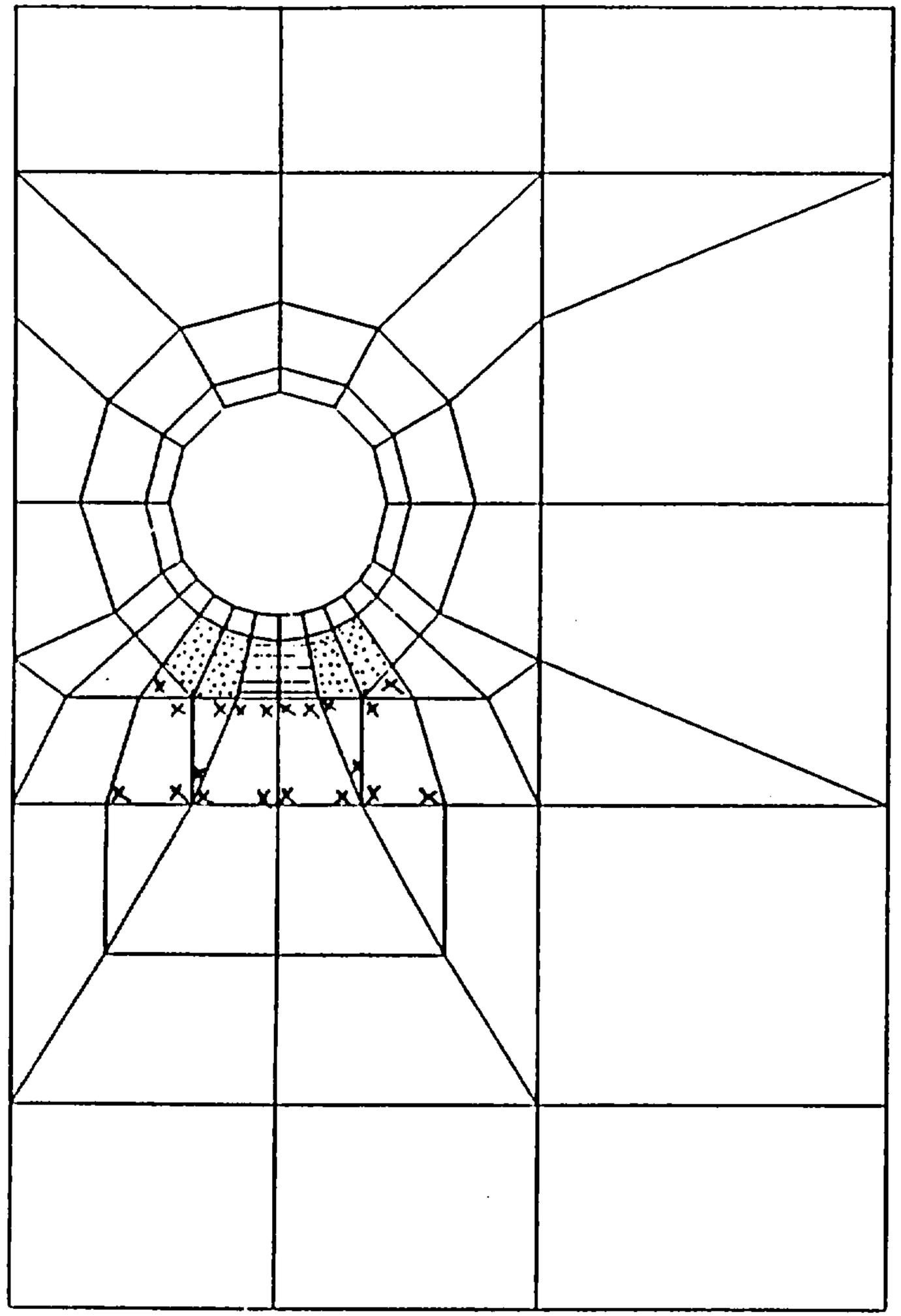

25% of the ultimate load

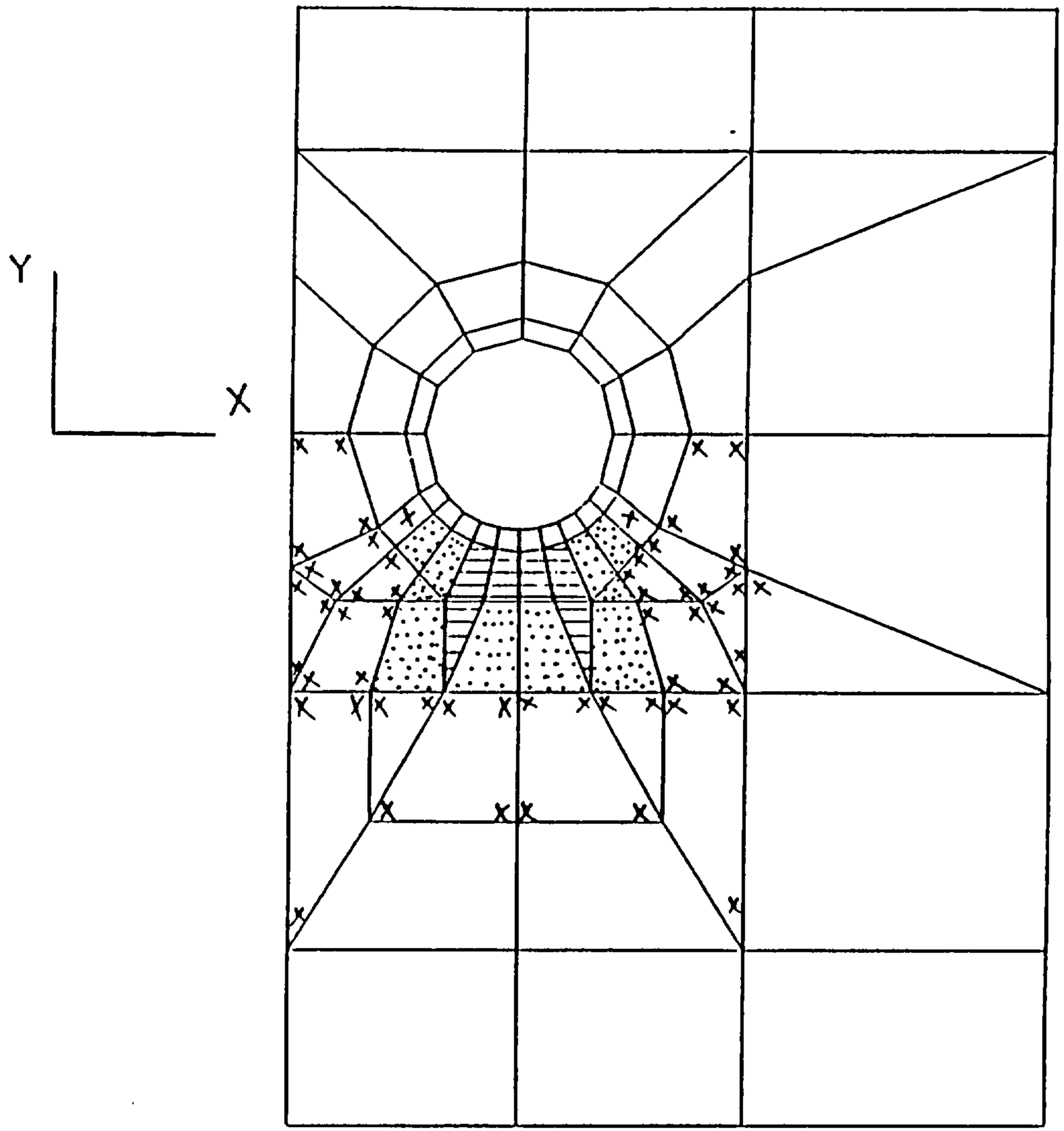


50% of the ultimate load

FIGURE (6.22) : DEVELOPMENT OF CRACKED AND CRUSHED ZONES IN THE CONCRETE SOLID OF MODEL 2.

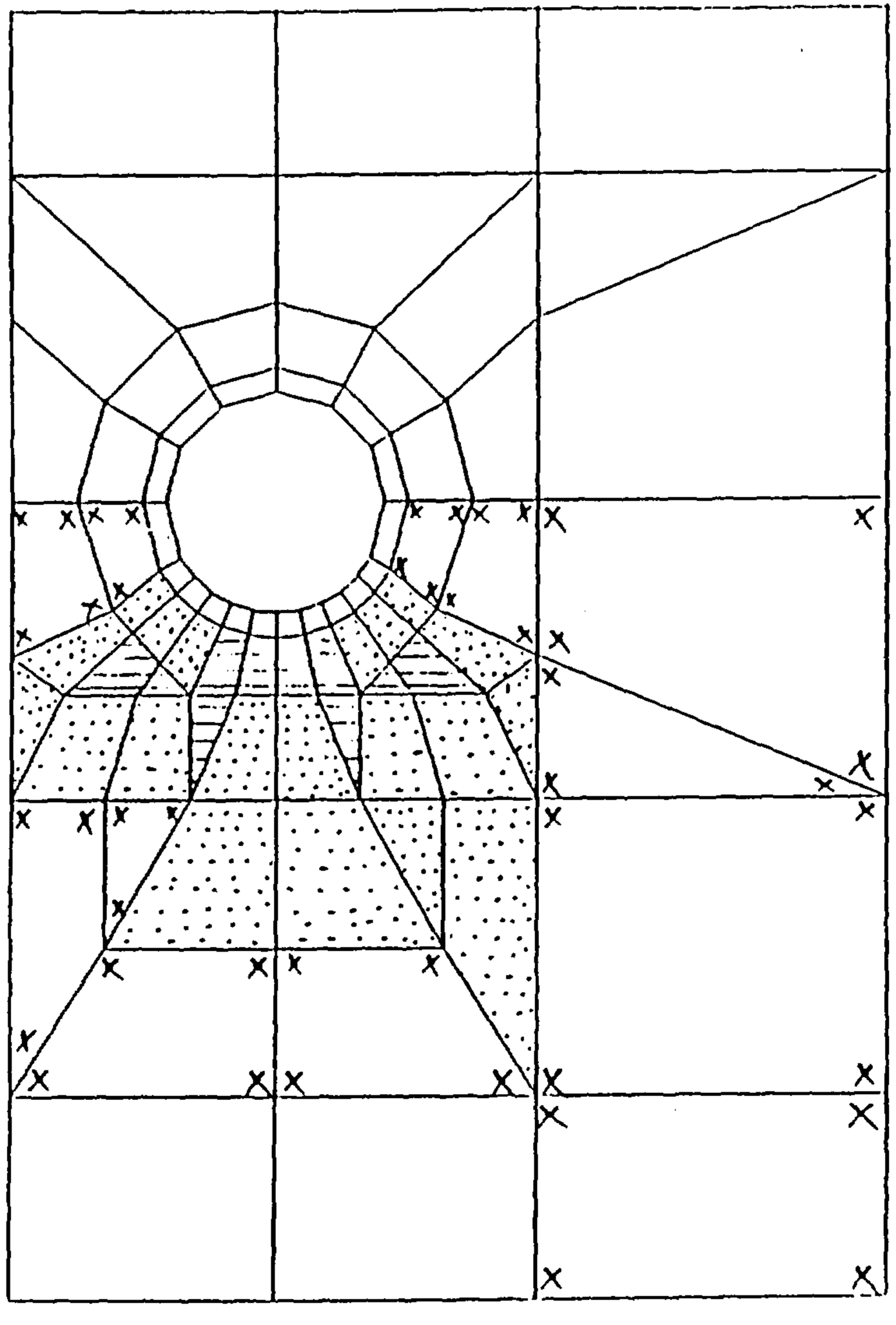

75% of the ultimate load

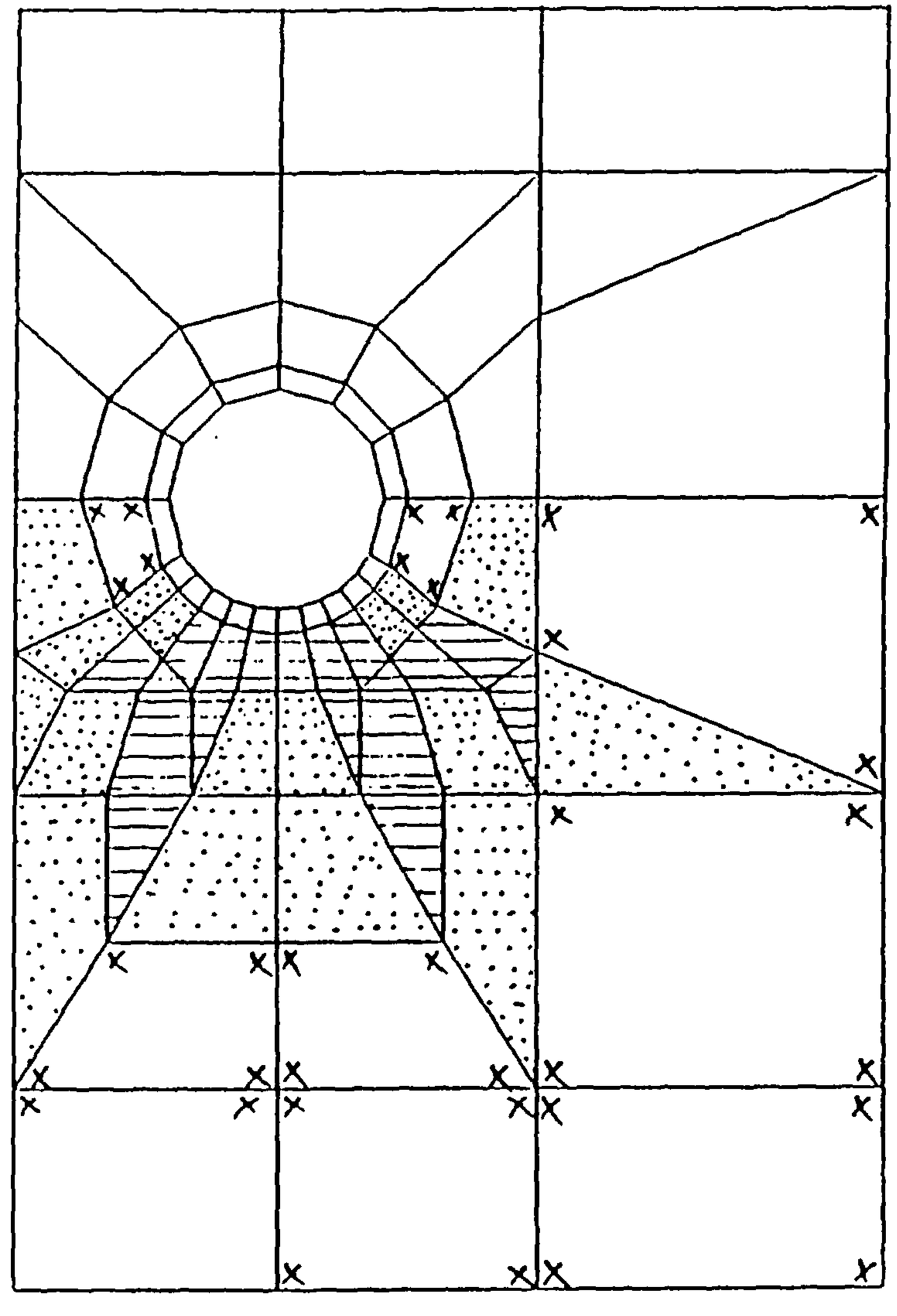

At the ultimate load

FIGURE (6.22) (CONTINUED)

A = 15.0 $N/mm^2$
B = 25.0 $N/mm^2$
C = 35.0 $N/mm^2$
D = 40.0 $N/mm^2$
E = 45.0 $N/mm^2$
F = 50.0 $N/mm^2$
G = 55.0 $N/mm^2$
H = 60.0 $N/mm^2$

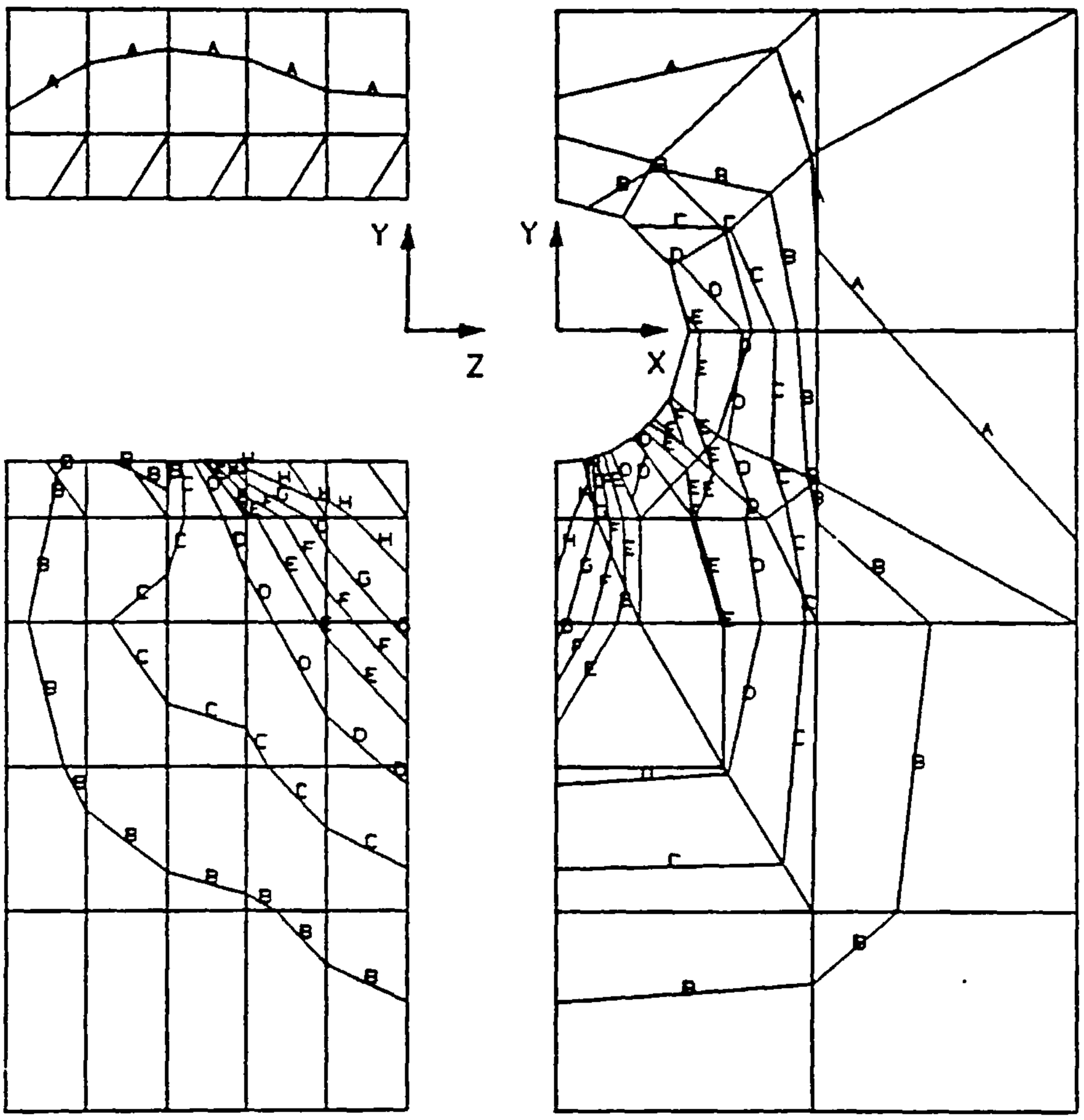


FIGURE (6.23) : SURFACE COMPRESSIVE STRESS CONTOURS OF THE CONCRETE SOLID OF MODEL 1 AT 25% OF THE ULTIMATE LOAD.

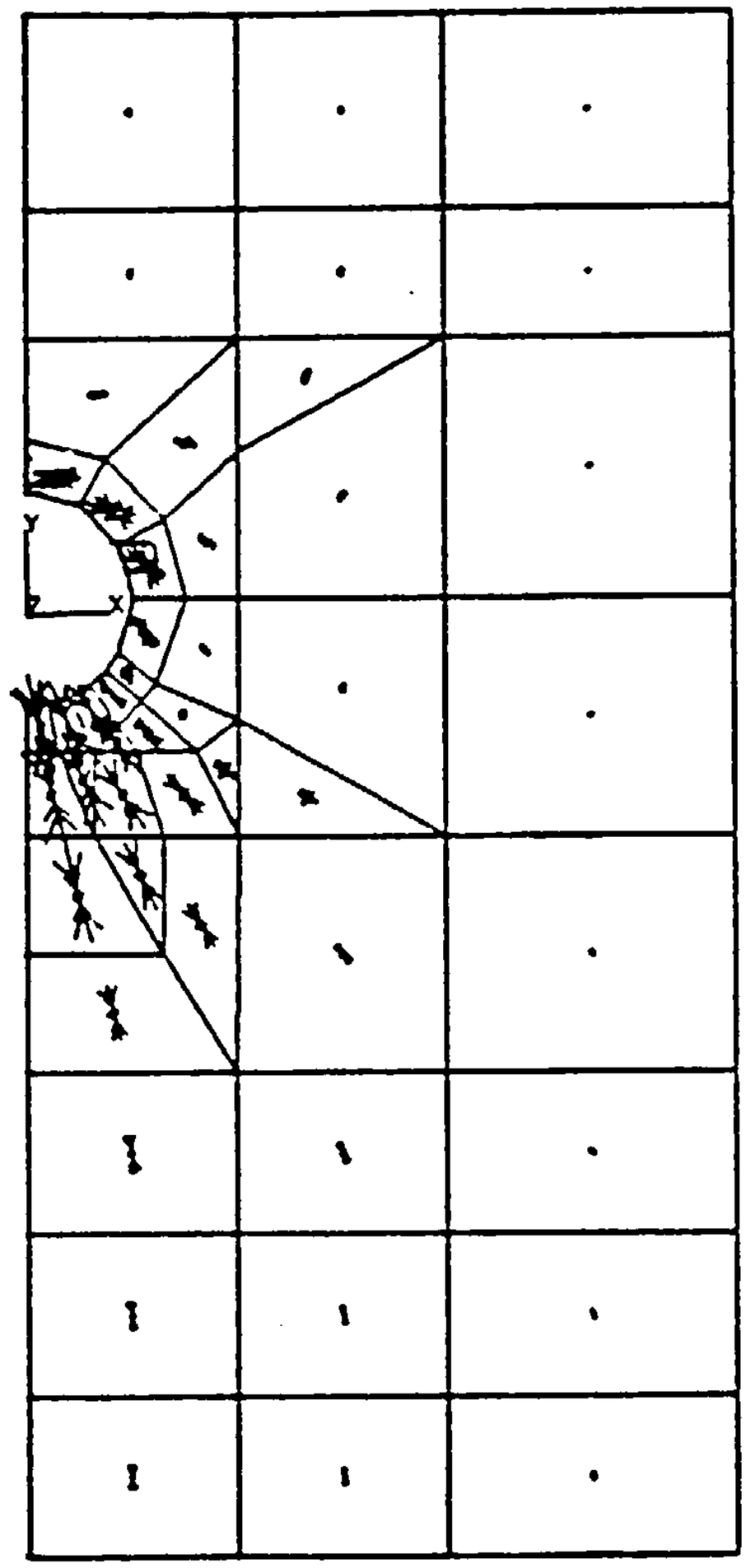

Arrow length represents stress magnitude.

FIGURE (6.24) : PRINCIPAL STRESS DISTRIBUTION AT THE COLUMN FACE OF MODEL 1.

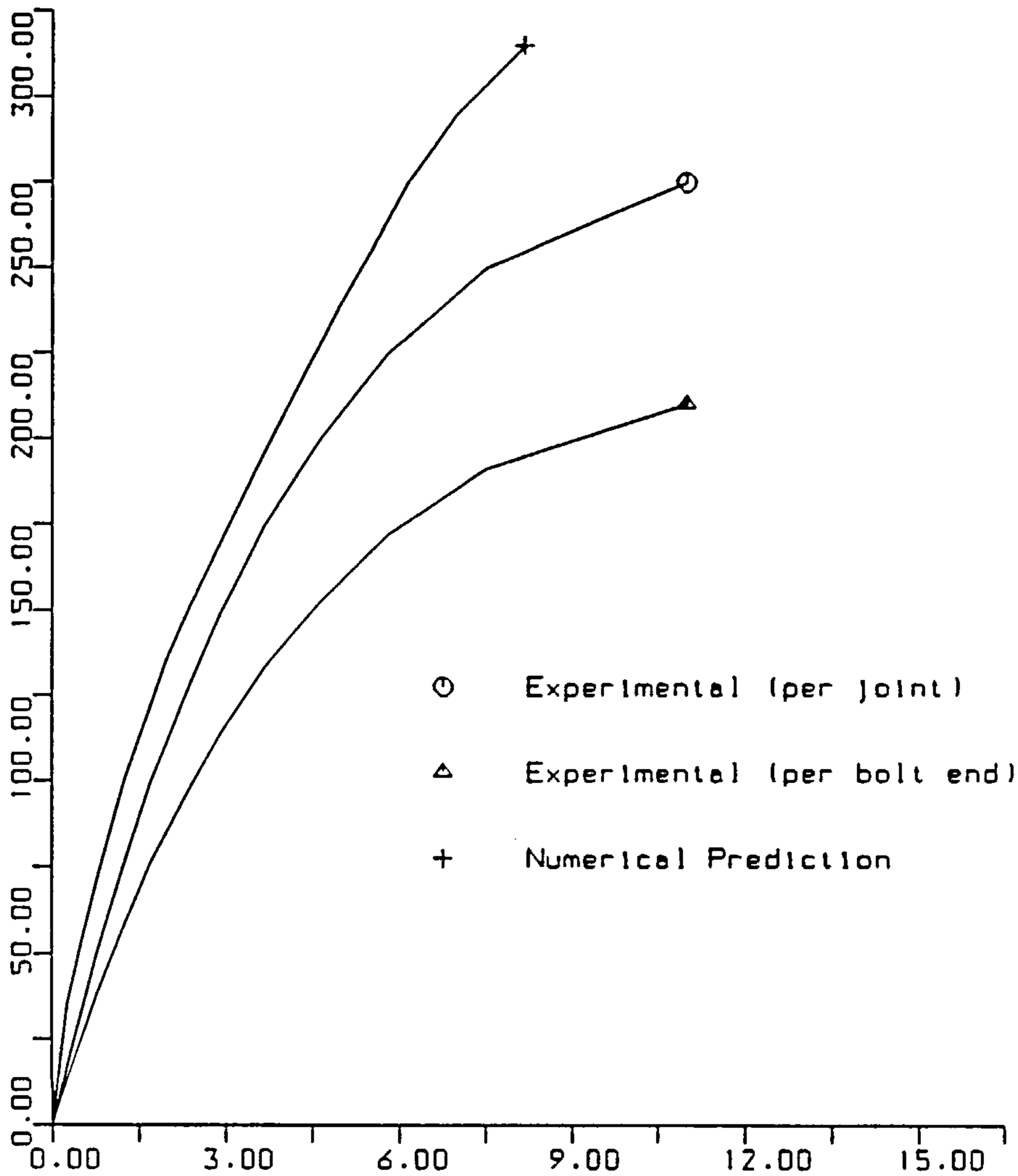


FIGURE (6.25) : COMPARISON OF EXPERIMENTAL AND NUMERICAL VERTICAL DEFLECTIONS AT THE LOADED END.

# CHAPTER SEVEN

# NUMERICAL AND EXPERIMENTAL STUDY OF CONCRETE STRENGTH EFFECT ON A SINGLE BOLTED JOINT

## 7.1 Introduction

In almost all the tests reported in Chapter 3, the failure of joints was governed by shear yielding of bolts. Although the tests showed no sign that concrete failure was imminent, if the concrete strength had been much lower such failure might have been possible. Also, the strong presence of the steel links below the joint level and the high confinement provided by the bracket's back plates prevented this type of failure. This argument is supported by the findings of the numerical analyses which showed the effectiveness of the steel links in sustaining the tensile stresses that could not be sustained by the concrete alone. In this chapter, an attempt to explore the effect of concrete strength and its confinement on the joint's load-carrying capacity and failure mode is reported.

A numerical model, Model 3, was developed to anticipate the behaviour of a single-bolted joint up to failure. In this model, a weaker concrete material with less steel links was employed. A comparison of the numerical results with those obtained earlier from Model 1 was made to clarify the role of concrete strength on the joint components' behaviour.

Following the numerical analysis, three tests were carried out on single-bolted joints to investigate the influence of concrete confinement upon the joint's failure mode. Details of tests and results are presented in this chapter. Finally, an assessment of Model 3 is given in view of the corresponding test results.

2. Values of 3.0 $N/mm^2$ and 250.0 $N/mm^2$ were assumed for the concrete tensile strength and yield stress for mild steel links, respectively.

Figure (7.2) shows the proposed stress-strain curve for the uniaxial concrete behaviour. As in Model 1, only 0.01% of the concrete elements' volume was used as smeared reinforcing material in the X, Y and Z directions. This material had the same stress-strain curve as that of concrete but with a much reduced slope after reaching the crushing stress. Material nonlinearity for all joint components was considered in the analysis.

The same convergence limits and boundary conditions, set for Model 1, were used in the present model. Also, perfect bond was assumed between steel and concrete.

## 7.3 Numerical Results

The basic results of the numerical analysis are discussed in this section. Load values used throughout the discussion are twice that obtained from the analysis due to symmetry in geometry and loading.

### 7.3.1 Ultimate Load

As for Model 1, the load was applied incrementally by forcing the bolt nodes at the XY face to have the same vertical displacement. The computed forces at these nodes were added together at the end of each load step to get the corresponding applied load. This load was completely transferred to the sleeve as the sum of the forces in the closed gap elements. From load value of 116.0 KN and onwards, computed load increments showed a marked decrease in value for the same applied displacement increment at the loaded end. As a result, the displacement increment was reduced in the following load steps. As the vertical displacement value exceeded

4.0mm, the model became unstable and a converged solution could not be achieved. At this stage, concrete damage was extending over a substantial area beneath the joint level. Thus joint failure was assumed and the job was terminated. Maximum load value was taken as 122.0 KN.

### 7.3.2 The Bolt

Figure (7.3) shows the load-deflection curve up to the ultimate load. Similar to Model 1, the joint had its maximum stiffness at the early stages of loading. The yield of sleeve elements, cracking and crushing of concrete elements in the loaded end region caused a gradual decrease in stiffness up to the joint failure. A marked change in the slope was obtained at a load value of 116.0 KN. This was a direct result of having a weak crushed concrete zone at the column face, i.e. the XY plane.

The bolt's remote end kept moving upward consistently until it came in touch with the sleeve soffit at a load value of 93% of the joint's ultimate load.

From the initial load, the bolt experienced an elastic bending. It continued to behave elastically until the load reached 65% of the joint's ultimate load. Then plastic strain initiated in the compressed bolt's elements at its bottom edge. On reaching the ultimate load, the existence of plasticity was limited only in the zone of the top and bottom edges.

The average vertical stress of the bolt at its loaded end was found to be 400.0 $N/mm^2$ at failure. This value is much less than the specified ultimate stress for the high tensile steel material even if it were applied on the threaded reduced section of the bolt. This finding suggests that the joint failure mode, in this particular case, could not be a direct bolt shear failure.

### 7.3.3 Steel Links

Three steel links were provided in the model, one located above the joint level while the remaining two were below it. Figure (7.4) shows the development of axial stresses in the steel links at different load steps. The plotted values are the average of computed stresses at adjacent elements. Tensile stresses were developed in their legs in the XY plane from the early stages of loading. Axial stresses in all links were in the elastic range up to 70% of the joint's ultimate load when the first link below the joint, i.e. link (b) started to yield. On reaching 86% of the joint's ultimate load, link (c) also reached its yield stress. As the load was increased, link (b) continued to behave plastically without much increase in stress values in the mid-span area. However, link (c) had a stress redistribution which resulted in an obvious stress increase in its rightmost member. This was accompanied with a reduction in the stress at its mid-span. This redistribution of stress was mainly due to the existence of a weak cracked concrete zone away from the link mid-span and its rapid progress towards the free column edge at the last stages of loading.

### 7.3.4 The Concrete Solid

As was expected, concrete behaviour was the governing factor in the overall joint behaviour. Figure (7.5) shows the crack and crushing propagation at different load values. Inclined cracks started at an early stages of loading beneath the sleeve. With increasing load, they extended simultaneously both downwards and towards the free column edge. This crack resulted in a continued stress redistribution in the region of cracks. The stage was reached, at 95% of the joint's ultimate load, when such redistribution could not maintain the stress level below the critical values and therefore crack extension continued to progress and propagated towards the column edge. At this stage, as many as 15 iterations had to be performed before solution

convergence was achieved. This led to the inevitable joint failure. Just before failure, some cracks appeared below the lower steel link.

At the last stages of loading, cracks appeared in the column side and extended to a depth of 30mm. Cracks also existed in the region above the joint level, however, they were not spread over a large region. They were mainly concentrated in the region attached to the plane of symmetry.

Concrete crushing started at a very early stage in the elements connected to the sleeve. As load was increased, crushing developed vertically in the XY face as well as in the Z direction.

## 7.4 Comparison with Model 1

Load-vertical deflection curves obtained from both models are shown in Figure (7.6). From this figure, it can be seen that both curves had almost the same initial stiffness at very low loads. Then Model 3 softens more rapidly, reflecting a pronounced nonlinear behaviour. This trend continued up to failure, giving rise to a steadily increasing gap between the two curves. At deflection value of 4.0mm, Model 3 predicted a load value of 60% of the corresponding value for Model 1.

The trend and values of outward displacements were in the same order of those obtained for Model 1. However, concrete spalling started at an earlier load and became more extensive towards the end of loading. Also the concrete had higher values of expansion below the joint level particularly close to the free column edge.

Although plastic strains in the bolt were small, they started to occur at much earlier load than that in Model 1. This is due to the higher deflection experienced by the bolt shank in Model 3 at the same load value.

The depth of the contact area was slightly less in Model 3 than in Model 1 at the same load value. This can be attributed to the concrete damage which occurred at early load stages at and close to the XY face. This damage accelerated the sleeve deflection at the loaded end, allowing the bolt to bend with a smaller radius of curvature and thus delaying the propagation of the contact area in the Z direction.

In the case of weak concrete, the developed tensile forces in the steel links below the joint level had higher values than in Model 1 for the same load value. The low concrete tensile strength contributed to the increased rate of this stress development. in addition to the low yield stress, the small diameter made both links in the present model reach plasticity at an early stage. In contrast to Model 1, the steel link above the joint level was found to be highly stressed at its mid-span. The axial stress in the link at this point was found to be 46% of its yield stress when the joint reached its ultimate load.

Concrete in the loaded end region was highly stressed in both models. However, concrete cracking and crushing were more extensive in Model 3. They also appeared in new areas, both above the joint level and at the column side.

## 7.5 Experimental Work

Under the application of a concentrated load, the concrete in the region below the joint level is confined against the developed bursting stresses by the column steel links. Another contribution to this confinement is provided by the bracket's back plate which becomes compressed against the column face at this region.

To examine the concrete confinement effect on the joint's ultimate load and failure mode, three tests were carried out on single-bolted joints. The tested joints were similar to the joint

modelled above, however, joints were provided with different degrees of confinement (low, medium and high) at the bracket-column interface. In this section, the description is given of the preparation and testing of the joints. This is followed by a discussion of the main experimental findings. For convenience, a letter used to define a test refers to one of the above degrees of confinement, e.g. Test L indicates that low degree of confinement is employed.

### 7.5.1 Test Specimens and Hardware

Each test specimen was a reinforced concrete column of 300mm square cross section and 1.00m height. The main vertical reinforcement consisted of four bright steel bars of 16mm nominal diameter while the links had a 6mm diameter.

Care was taken to ensure that links, above and below the joint level, were placed at the specified spacings to match those in Model 3. A 150mm vertical spacing was adopted for the remaining steel links. The sleeve location, 210mm from the specimen top, was also marked carefully. A solid timber dowel was screwed to the wooden mould at each end of the sleeve. This was to secure the sleeve position during casting. Dimensions of the test specimen with details of reinforcement are given in Figure (7.8).

As in the test setup described in Chapter 2, the same mounting frame was used in this test. For this reason, holes were drilled and tapped in the main column bars which were flush with the specimen top. A similar set of holes was made at the specimen bottom to secure the main bars in position during casting, thus maintaining a uniform concrete cover of 40mm.

In all three tests, the bolts and sleeves were identical in geometry and material to those used in the tests reported in Chapter 2. Two loading brackets were made by welding 15mm mild steel plates together. Brackets were designed to have an ultimate

capacity larger than that of the bolt. Horizontal and vertical welds were also designed to prevent any premature joint failure.

The transducers used in each test were as follows:

A 15mm transducer was positioned vertically above the bolt with its arm compressed against the top of the back plate. This was to measure the bolt's vertical deflection.

Five transducers with strokes of 15mm were mounted on each side of the column to measure the concrete sideway movement. They were vertically spaced in a such a way that the top three transducers correspond to the sleeve's centreline level and the steel links immediately above and below this level. Below these transducers, a vertical spacing of 60mm was adopted between the two remaining transducers.

All transducers were calibrated independently using a calibration micrometer. They were fixed with purpose-made aluminium channels which were later connected and fixed to the mounting frame. No remote fixing was used, to minimise any initial settlement of the transducers' holders.

### 7.5.2 Concrete Mix Design

Concrete mix was designed to give a target mean strength of 30.0 $N/mm^2$ after 7 days. It was white Portland cement, 5mm down fine aggregate, 10mm and 20mm coarse aggregate in the ratio 1 : 1.59 : 0.89 : 1.79, with a water/cement ratio of 0.485. Six 100mm cubes were cast with each specimen as control specimens. The concrete was cast in a wooden mould placed horizontally on a vibrating table. Its surface was trowelled to level after casting. After three days, each specimen was stripped from the mould and positioned vertically in the rig. The specimens and cubes were air-cured until testing.

### 7.5.3 Cube Testing

It was planned to test the first of the concrete cubes at an age of three days. This was to be followed by another cube in the following day and so on, until the target strength of 30.0 $N/mm^2$ was achieved. Once this value was obtained, the test was carried out in the same day. For Test L, the characteristic strength value was found to be 30.5 $N/mm^2$ while it was 33.0 $N/mm^2$ for Tests M and H.

### 7.5.4 Details of Confinement

In order to minimise the concrete confinement in test L and to allow the concrete to spall off under loading, two steel plates 3.0mm thick were introduced between the bracket's back plate and the column face at each side as shown in Figure (7.9). These plates worked as packing to create an almost uniform gap between the bracket and concrete. The plates had smooth surfaces so that the brackets could slide easily without affecting their vertical movement. In addition, adding these plates helped reducing the frictional force developed at the bracket-column interface. In this case, only a value of 0.2 was obtained experimentally for the static coefficient of friction. The brackets' back plates were machined to eliminate any curvature produced by the welding process.

At the time of test preparation, 6mm round steel bars with a 250.0 $N/mm^2$ yield stress, similar to that assumed in Model 3, were not commercially available. As a result, steel with higher yield stress had to be used. From simple tensile tests carried out on these 6mm bars, the value of yield stress was found to be in the range of 440-460 $N/mm^2$, i.e. 80% higher than the required value.

One way of overcoming this problem, was to reduce the cross section area of the bar until it yielded at a force similar to

that if the parent cross section had a 250.0 $N/mm^2$ yield stress. A segment of the link cross-section was removed along the legs which crossed beneath the sleeve in the stub column. A vertical distance of 2.25mm had to be cut off to provide a satisfactory cross-section area and the bars were subsequently tested in tension, see Figure (7.7).

This modification was only introduced in the first and second links below the joint level, i.e. where it was believed that they would have a noticeable effect on the joint's behaviour.

In Test M, the above modification of the steel links' cross section was adopted. However, no steel packing was used between the back plates and concrete, i.e. the machined back plates were initially in direct contact with the concrete. This gave rise to a value of 0.52 for the static coefficient of friction.

In Test H, the cross section area of steel links was not reduced. Also, the back plates were left unmachined and their thermally induced curvature provided the maximum confinement possible to the column face below the sleeve. The static coefficient of friction in this case was found to be 0.66.

### 7.5.5 Test Procedure

Once the test specimen was stripped from the mould, it was held vertically in position and centralized on the base of the testing machine. Insulation board was provided under the column to ensure even stress distribution under the column's squared base in the rig. The brackets were introduced to form a joint at both column faces. A hexagonal nut was finger-tightened at each end.

The transducers were positioned and mounted around the joint. Testing was carried out six days after casting. Loading procedure started as soon as the top of the 40mm-thick loading plates came in contact with the machine's top platten. Constant load

increments of 20KN were adopted until evidence of yielding was detected by relatively large deflections, then they were reduced to 10KN. At each stage of loading, the deflections were recorded, printed and cracks were monitored.

Load ,was stopped when the joints could not sustain the applied load. After testing, the bolt, sleeve, and cracked specimen were examined.

## 7.6 Test Results

### a) Failure Modes

In Test L, load was stopped when the joints could not sustain the applied load at the maximum load of 200KN per joint. Crack patterns obtained in the column are shown in Figure (7.10). In this figure, faces and one side of the column are shown (side by side) to show the extent of the crack development. During testing, no visible cracks could be observed until the joint load reached a value of 180KN when a horizontal crack appeared on both faces of the column. The cracks were at a vertical distance of about 245mm measured from the column top, i.e. just above the link located immediately below the joint level. At the following load increment, both cracks lengthened and propagated, at a shallow angle to their initial direction, and joined together at the column side.

At a joint load of 190KN, a splitting crack appeared along the vertical centreline at both ends of the sleeve. At the failure load, these vertical cracks extended almost to the base and top of the column on each face, see Plate (7.1). At this stage, it was clear that the joint behaviour is characterised by the development of these cracks.

Crushing and spalling of concrete beneath the sleeve initiated at an earlier stage of loading. At a joint load of 150KN, the 3.0mm

gap at both faces were closed by the spalled concrete. After the bracket's removal, it was found that the spalling zone extended to a depth of 90-100mm below the sleeve soffit at both faces.

Examining the bolt shank after testing revealed large plastic deformations at both ends. This was expected as the maximum load per bolt end was found to be 185 KN after allowing for the friction effect at the bracket-column interface. This load value represents 88% of the bolt's ultimate load reported earlier in Chapter 3.

In Test M, the joint failed by a bolt shear failure at a joint load value of 256 KN. The shear plane passed through the threads and the failure was accompanied with a loud noise. The failure load per bolt end, which was found to be 208 KN, is almost equal to that reported earlier in Chapter 3.

In Test H, another typical bolt shear failure was obtained at a joint load of 230 KN. This ultimate load gave rise to a failure load of 175 KN per bolt end. This slight reduction in the bolt's ultimate capacity may be attributed to the increase of the bolt's tensile force. This increase was due to the upward movement of the confining compressive force towards the bolt's centreline which resulted from the curvature of the bracket's back plate.

In Tests M and H, no visible cracks were found. Examining the column faces after brackets' removal revealed the existence of localised crushing areas, high friction and sleeve deformation. Also, the bolt ends were highly distorted in shear.

The above ultimate loads emphasise the fact that the concrete confinement effect plays a much larger role in the joint ultimate capacity than was originally anticipated. The constraint at the column face by the brackets, provided a significant enhancement to the concrete capacity, which delayed its cracking and crushing in the critical zone. This led to a different mode of failure. In

contrast, there seems to be no definite experimental evidence about the dependence of joint capacity on the concrete strength and ultimate loads obtained from Tests M and H were generally similar to that obtained in Test 1.

b) Deflections

For the three tested joints, the load-vertical deflection curves were characterised by an ascending branch up to failure. As the failure loads were approached, a considerable increase in deflections took place, with the same load increment. For the majority of the tests, an almost steady deflection rate was obtained for both brackets. The load-vertical deflection curves obtained for tested brackets are shown in Figure (7.11).

In Test L, sudden large deformations were recorded at the column sides as soon as cracking took place. A maximum value for concrete expansion of 1.76mm occurred below the joint level. Assuming that the deflection varies linearly along the column sides between measurement points, Figure (7.12) shows a general shape of the concrete expansion distribution for both sides at the last stages of loading. From this figure, it can be seen that higher deflections were recorded at the cracked side. These deflections decrease in value below the first link level. The vertical crack formed above the joint level caused some concrete expansion at this level.

In tests M and H, insignificant concrete expansion were recorded. This was expected as there were no visible cracks around the joint at any stage of loading.

## 7.7 Model Assessment

Despite the fact that the bolt in Test L reached a failure load in excess of the corresponding failure load predicted by Model 3, i.e. 52% higher, it is believed that this fact should not be used

solely to assess the model. The reason for this can be given as follows:

Once a joint load value of 150KN was reached, the deterioration of the column faces was obvious. As mentioned earlier, concrete spalling at this stage closed the 3.0mm initial gap between the back plate and column face. It should be noted that after allowing for the frictional force, the corresponding bolt load is 138KN which is only 13% higher than the predicted failure load. From the numerical analysis point of view, it is not possible to obtain a converged solution with such high outward deflection values taking the already concrete crushed state into account. Furthermore, confining the concrete from this load value onwards in the test, allowed each joint to carry an additional load of 50KN.

Load-vertical deflection curves obtained from Test L and from Model 3 are presented for comparison in Figure (7.13). From this figure, it seems that all curves have slight differences in the value of initial stiffness. From load value of 80KN onwards, the numerical prediction underestimates the joint stiffness and a more gradual decrease in its value can be seen. It should be noted that bolt yielding at its threaded ends had contributed much to the remarkably high deflection values experienced by the joint at the last stages of loading. As was explained earlier, the bolt thread was not taken into account in the numerical model due to the software limitation. Therefore, a comparison of deflection values at the last stages can not be performed.

Cracking above the joint level was successfully predicted by the model at a lower load value. The model showed a tensile region in the concrete elements close to the plane of symmetry. Side cracks predicted by the model at the free edge were also observed experimentally at one side of the column. However, the experimental cracks propagated to a greater depth. At the column face, two major cracks were obtained in the test, i.e. horizontal

and vertical cracks. In contrast, inclined cracks below the sleeve were predicted numerically. The predicted cracks extended downwards and took diagonal paths towards the column side. During the test, it was not possible to check the formation of such cracks in the modelled region as it was inaccessible due to the brackets presence. After bracket's removal, most of this region was found to be crushed.

It is worth mentioning at this stage, that a crack trend similar to that predicted by the model was obtained in an earlier test reported by the author elsewhere [21]. In this particular test, a concrete failure was obtained for a four-bolted joint loaded at one of its ends. Plate (7.2) shows the developed cracks and concrete spalling on the column face after bracket's removal.

The examination of the sleeve ends after testing gave an indication of obvious deformation. The measured vertical diameters, in Test L, were 31.86 and 32.7mm giving rise to a net deflection of 4.86 and 5.7mm which are still comparable with the predicted maximum deflection of 4.0mm.

## 7.8 Summary

It was evident from the tests, described in this chapter, that failure is prominently due to the bolt shear yielding. Concrete failure occurred only under certain conditions, i.e. minimum concrete confinement. As a result, this failure type can be conveniently prevented.

The effect of concrete strength on the joint ultimate strength was found to be less susceptible than anticipated. However, it should be ensured that a reasonable strength is used to obviate surface spalling at low loads.

The conservative ultimate strength predicted by the numerical model showed the importance of including all the connection

components in the analysis. For example, the modelling of the back plate would give more realistic confinement estimate which proved to be a critical factor for the joint's load-carrying capacity.

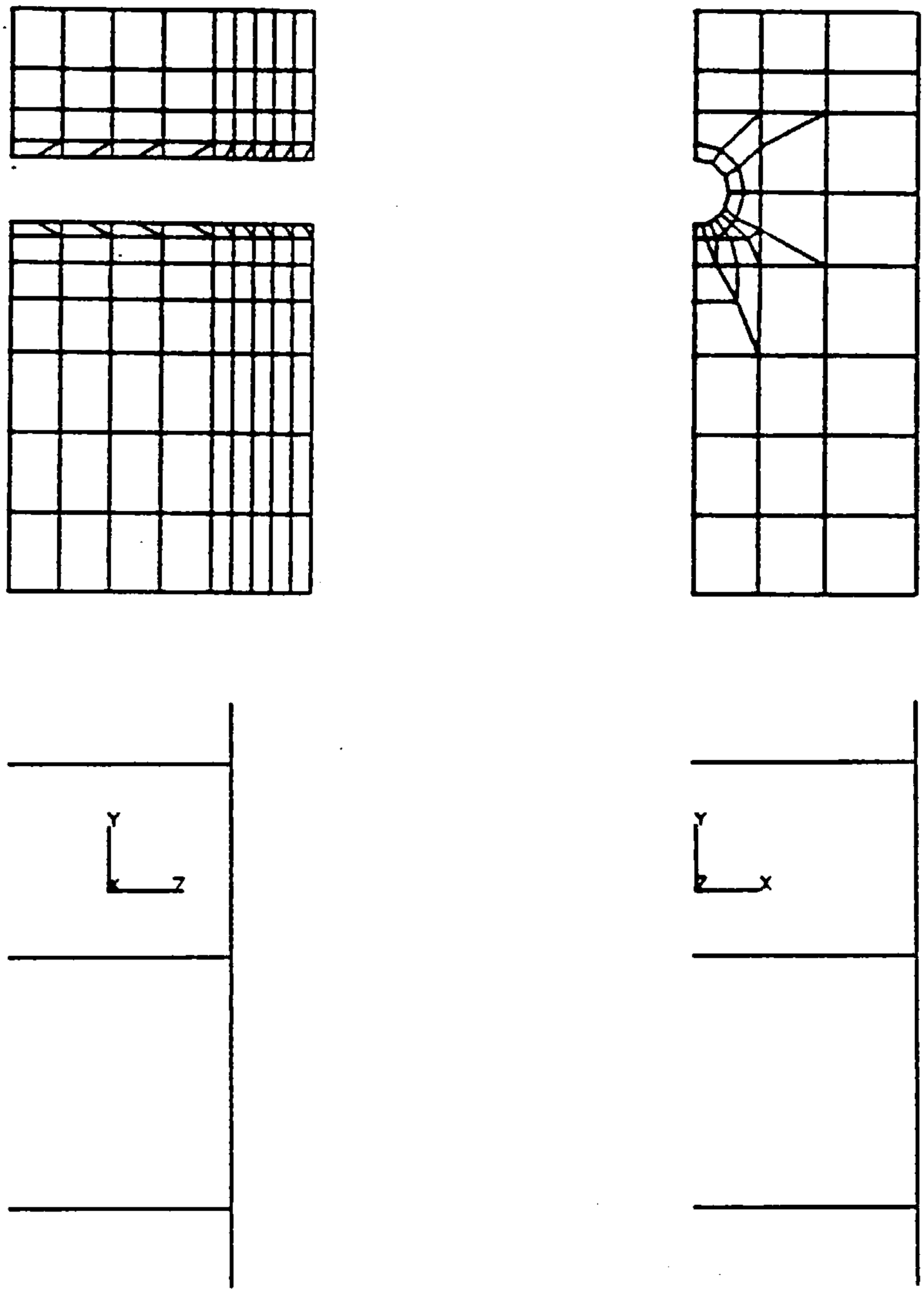


Left : Vertical section through plane containing sleeve axis.

Right : Face elevation.

Top : Concrete elements.

Bottom : Reinforcement elements.

A line of symmetry is located at the left of each view.

FIGURE (7.1) : FINITE ELEMENT DISCRETISATION OF THE CONCRETE SOLID WITH DETAILS OF REINFORCING BARS 'MODEL 3'.

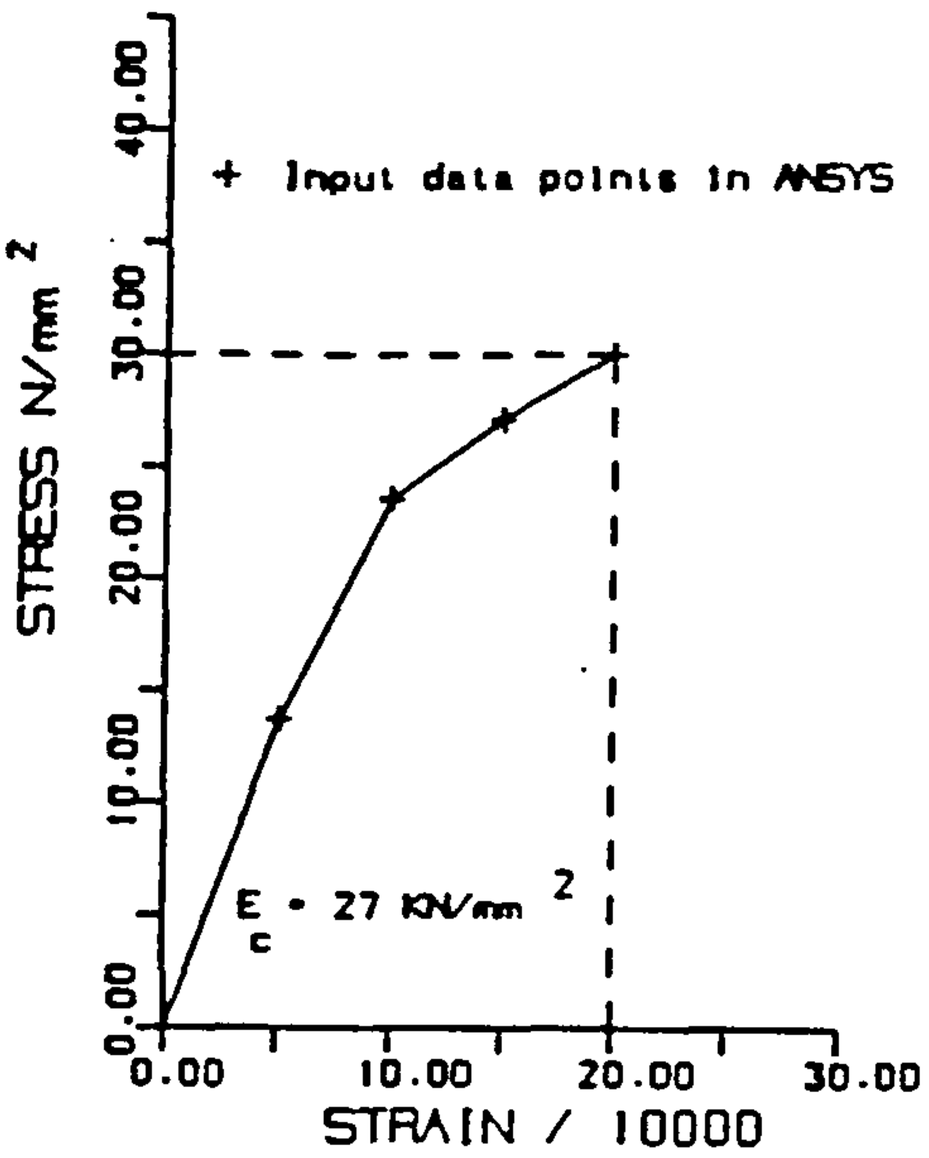


FIGURE (7.2) : MULTILINEAR IDEALISATION OF THE CONCRETE STRESS-STRAIN CURVE USED IN THE ANALYSIS.

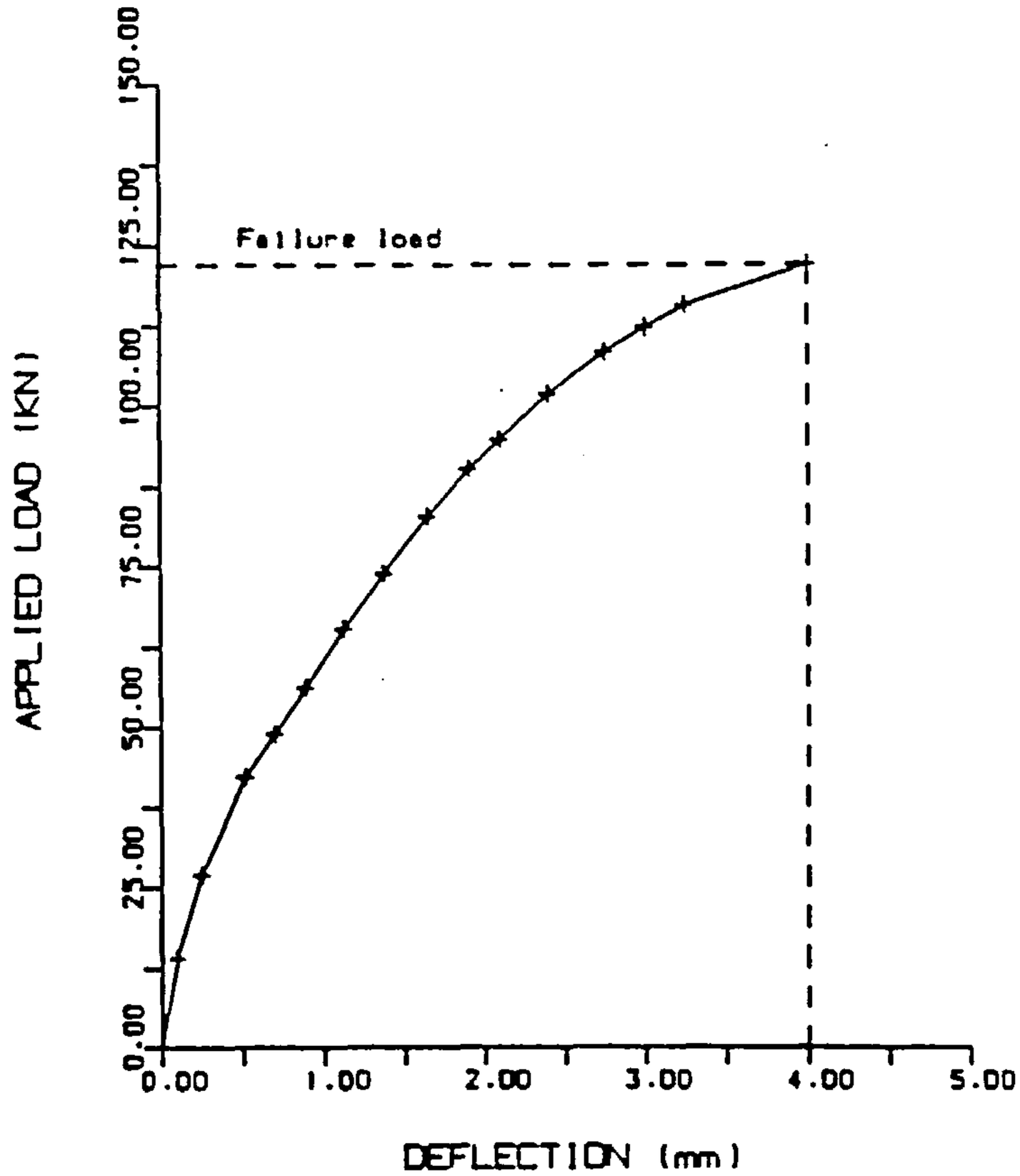


FIGURE (7.3) : PREDICTED LOAD-DEFLECTION RESPONSE AT THE LOADED END OF THE BOLT FOR MODEL 3.

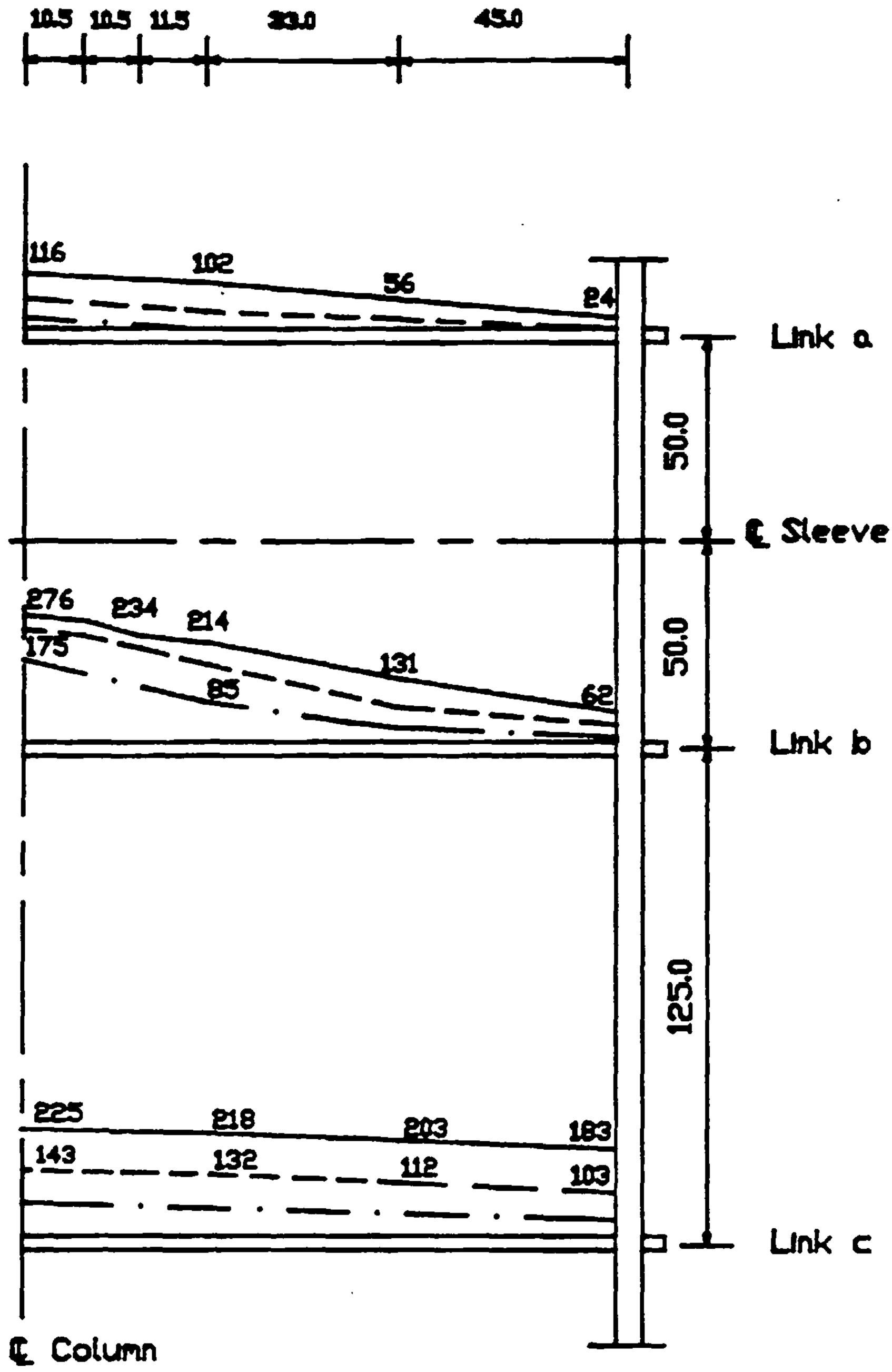


FIGURE (7.4) : PREDICTED AXIAL TENSILE STRESSES IN THE STEEL LINKS OF MODEL 3 UP TO THE ULTIMATE LOAD.

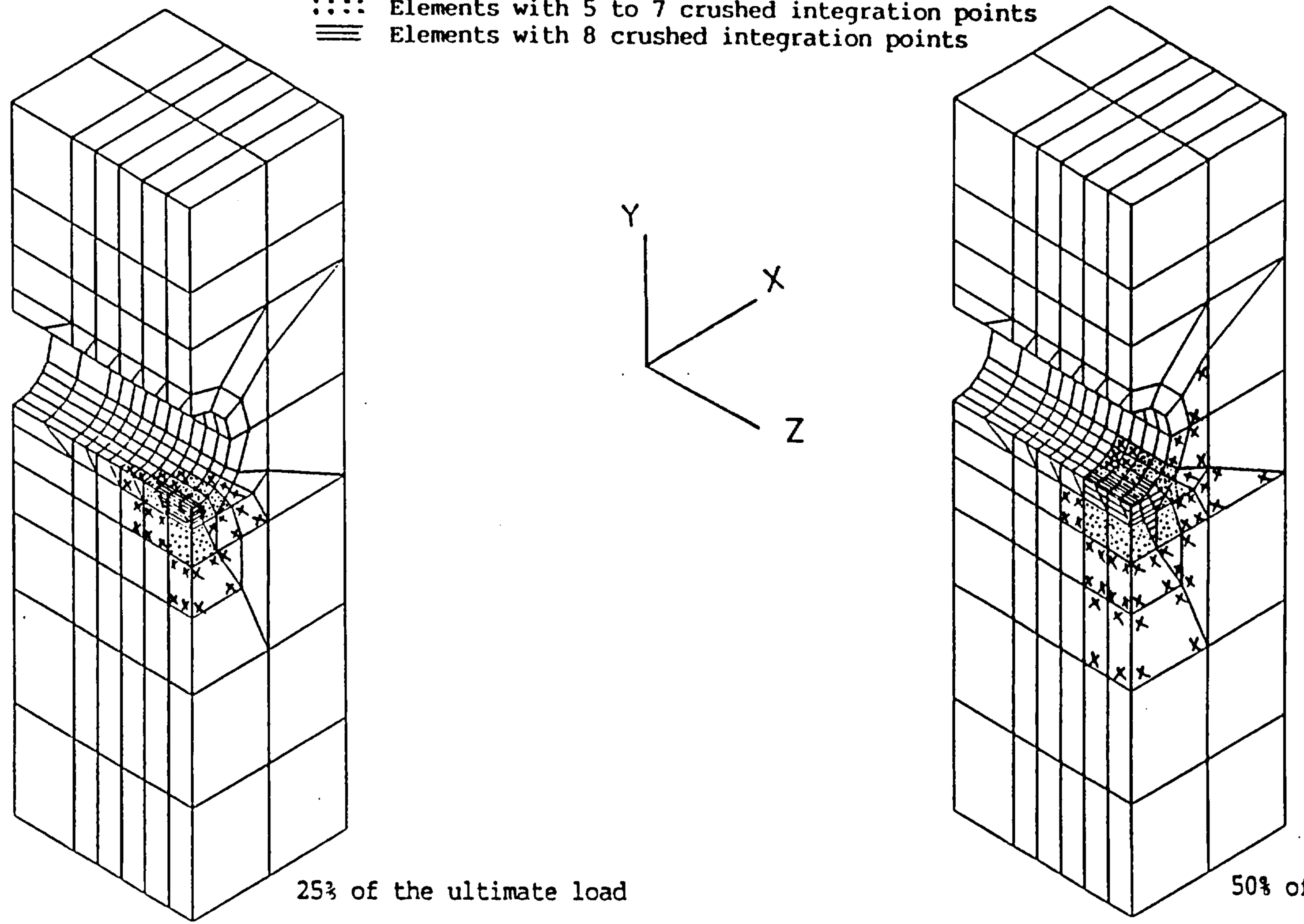


FIGURE (7.5) : DEVELOPMENT OF CRACKED AND CRUSHED ZONES IN THE CONCRETE SOLID OF MODEL 3.

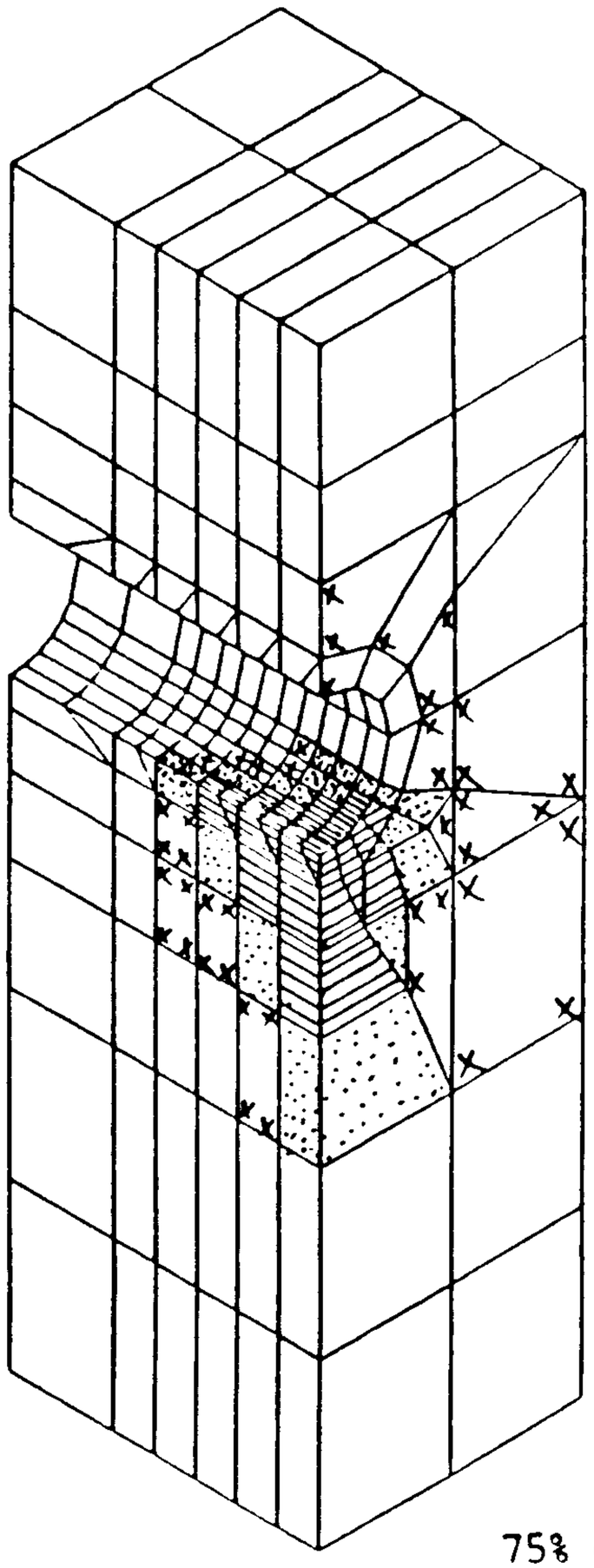

75% of the ultimate load

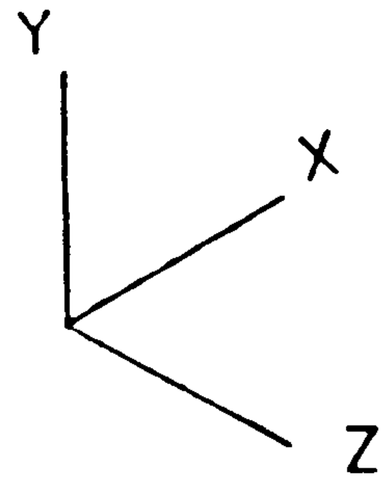


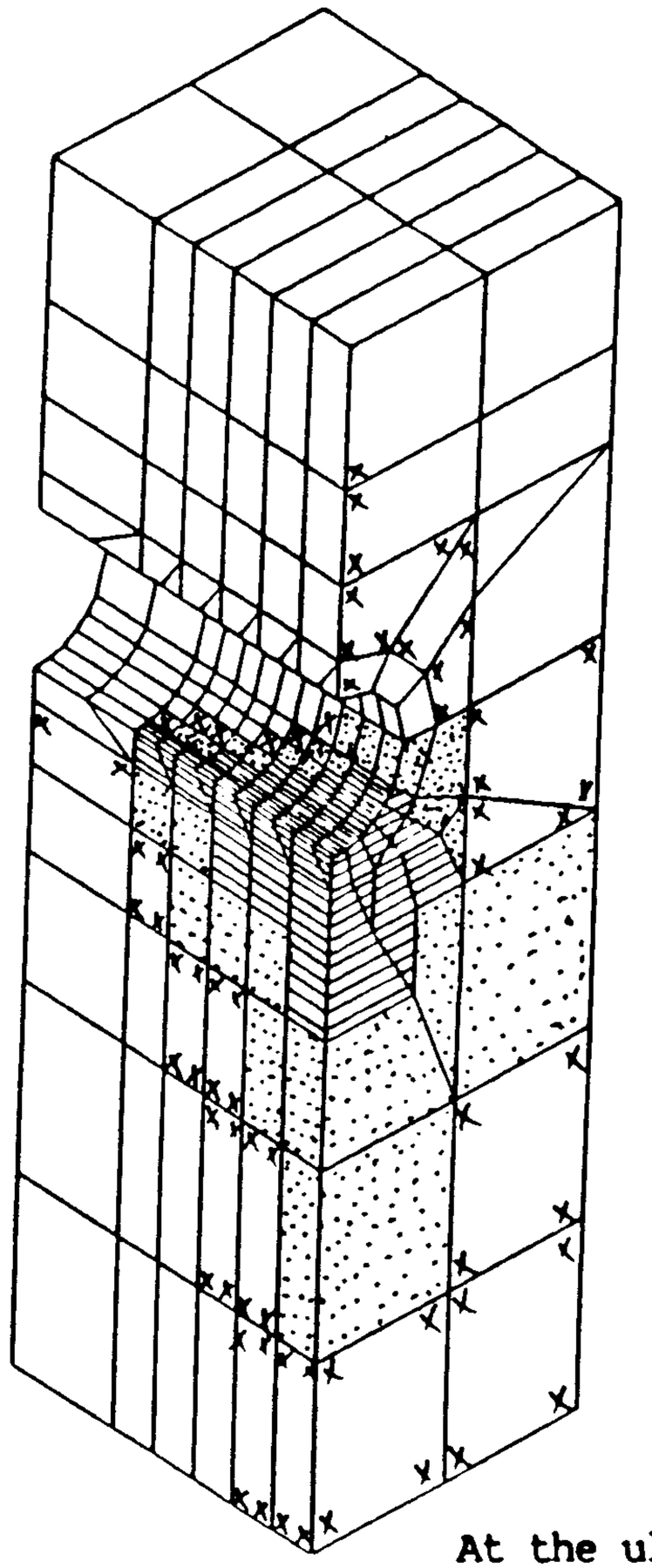

At the ultimate load

FIGURE (7.5) (CONTINUED)

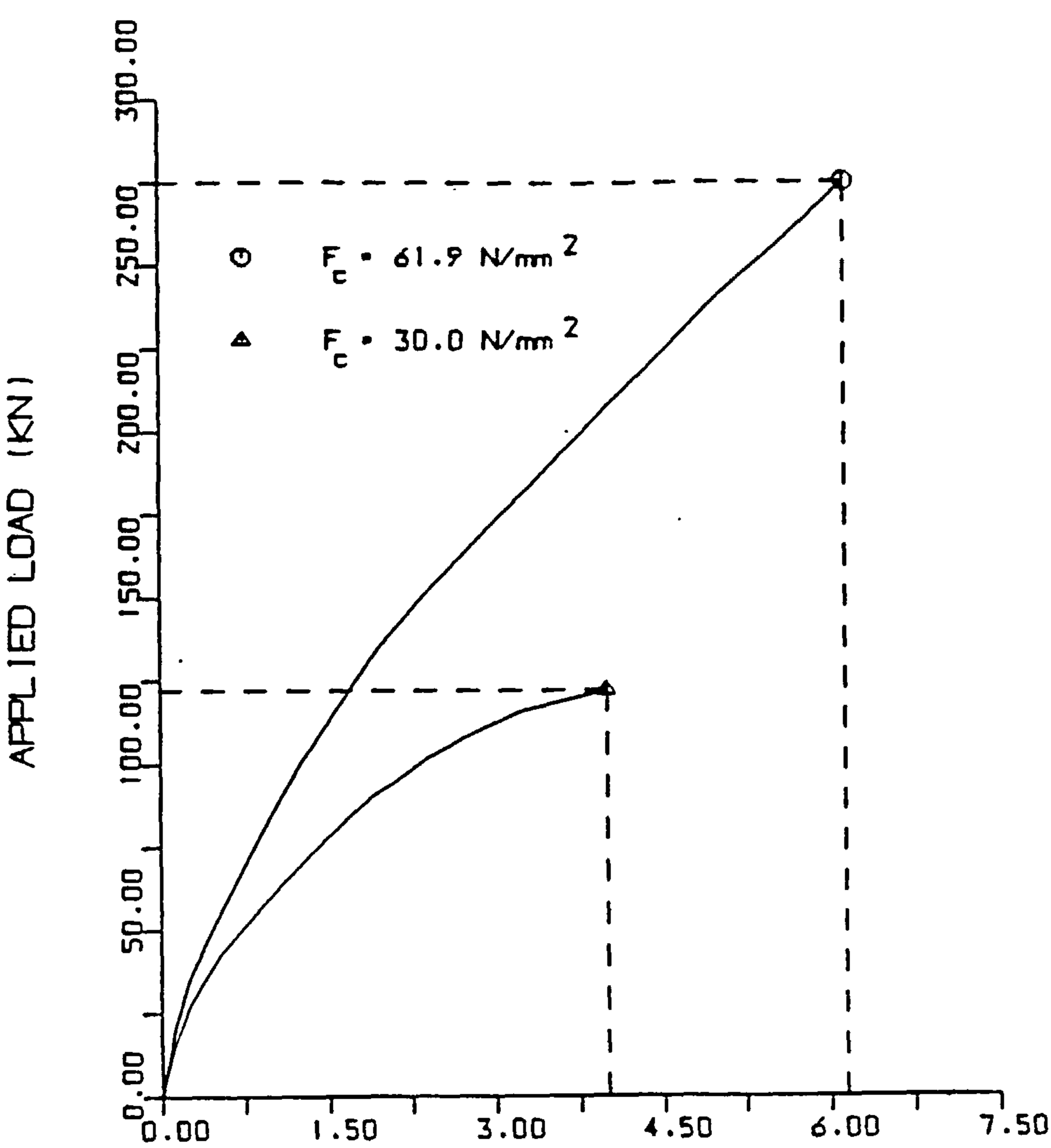


FIGURE (7.6) : PREDICTED LOAD-DEFLECTION CURVES FOR DIFFERENT CONCRETE STRENGTHS.

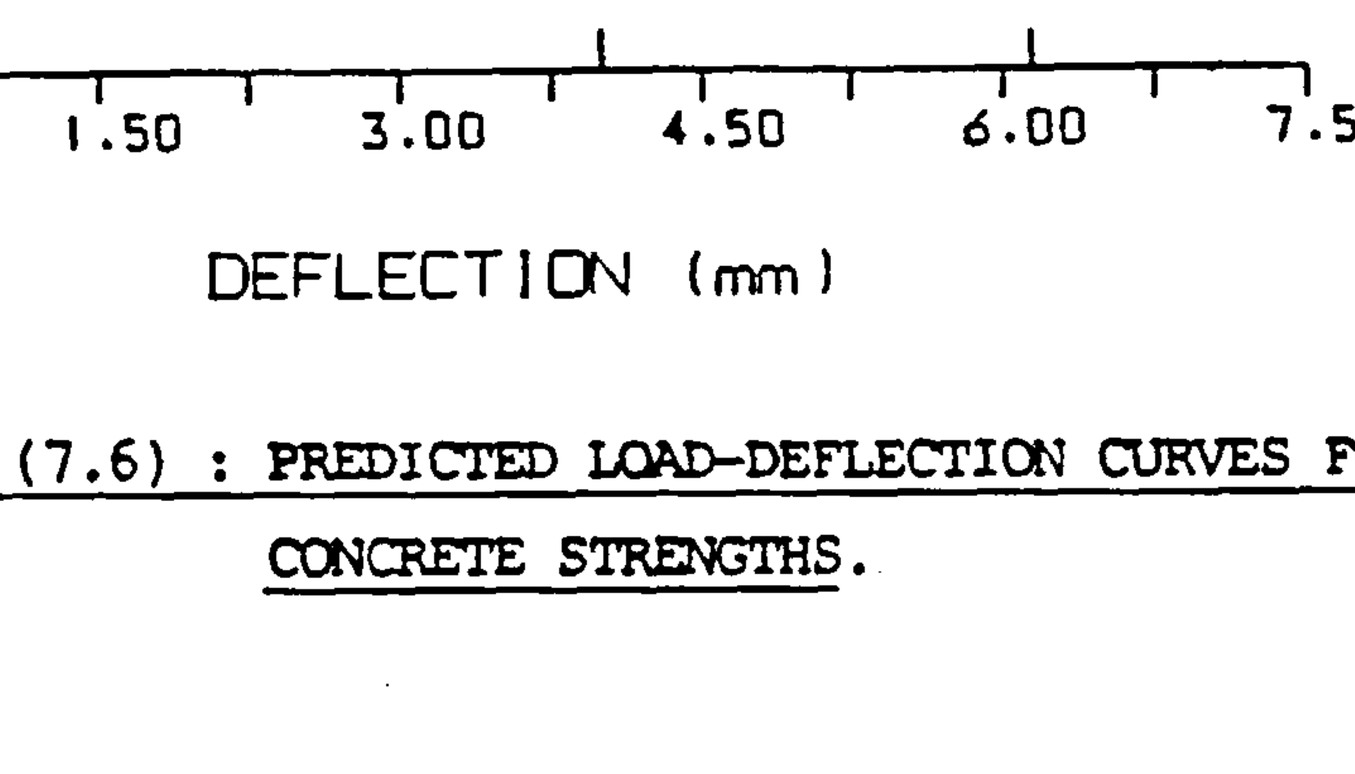


FIGURE (7.7) : CROSS SECTION AREA REDUCTION FOR THE STEEL LINKS.

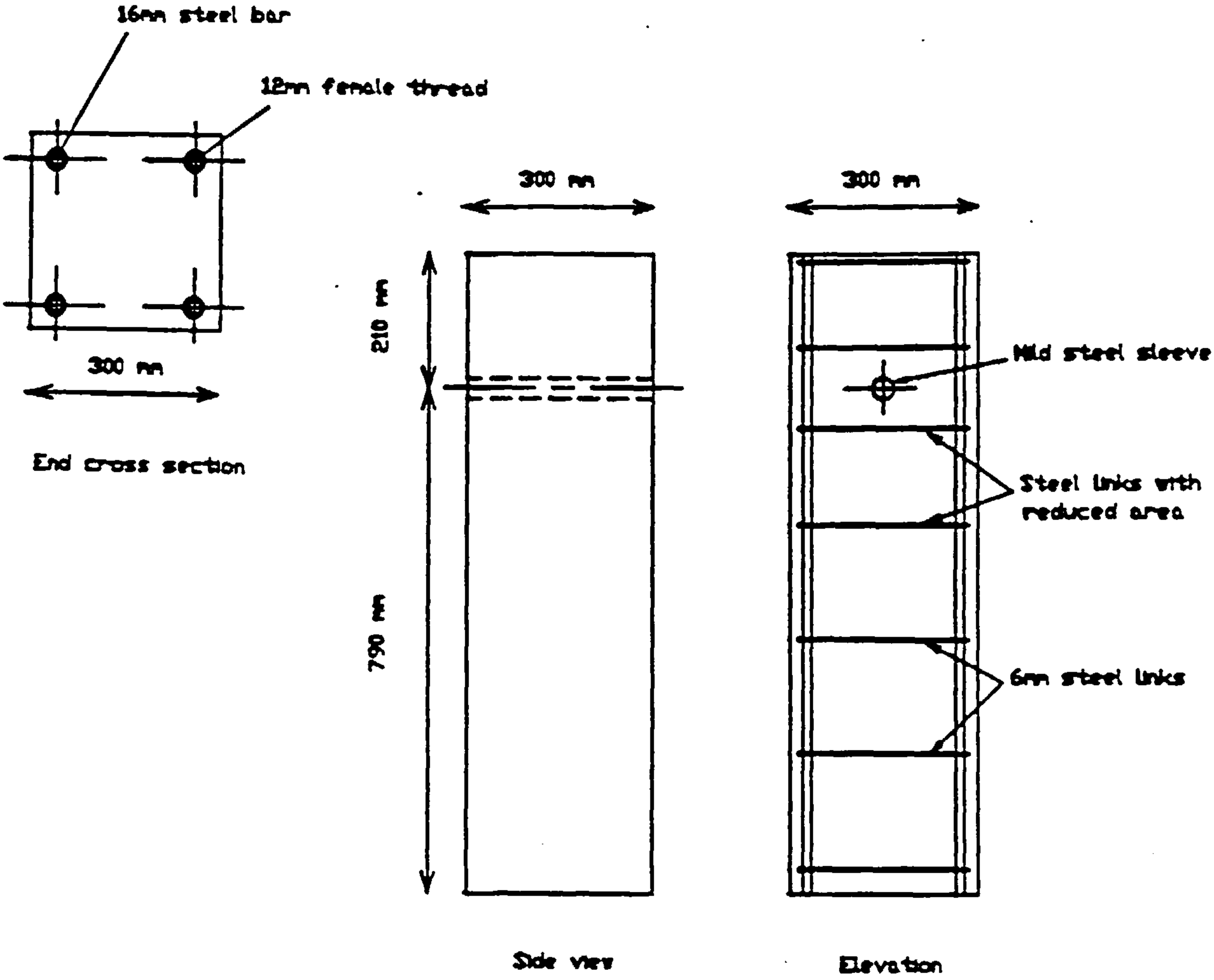


FIGURE (7.8) : DIMENSIONS OF THE TEST SPECIMEN WITH DETAILS OF REINFORCEMENT.

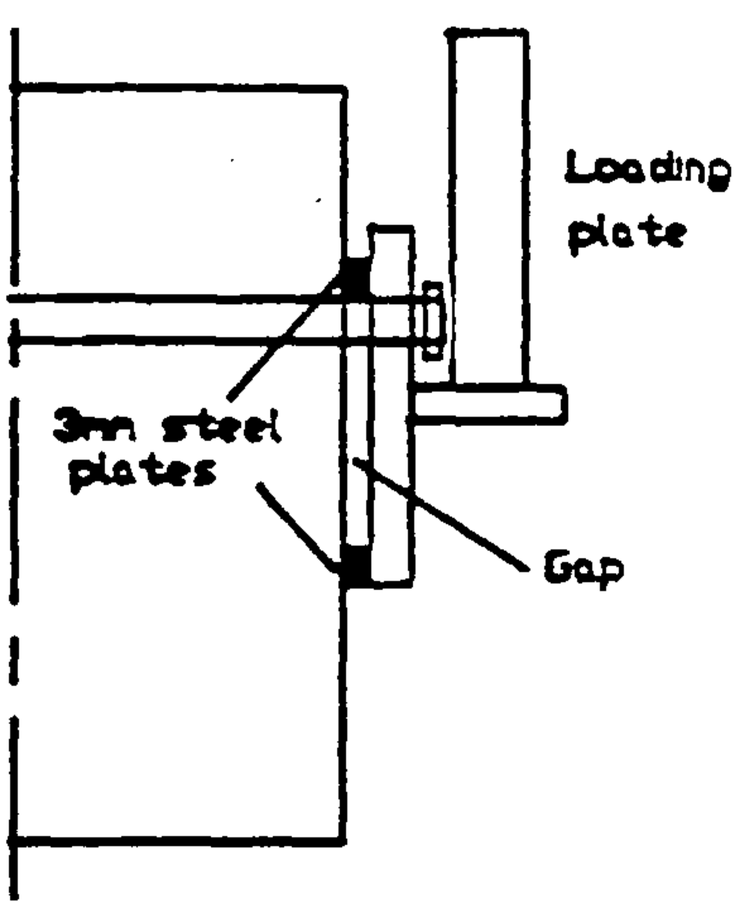


FIGURE (7.9) : A SIDE VIEW SHOWING THE INITIAL GAP BETWEEN THE BACK PLATE AND COLUMN FACE IN 'TEST L'.

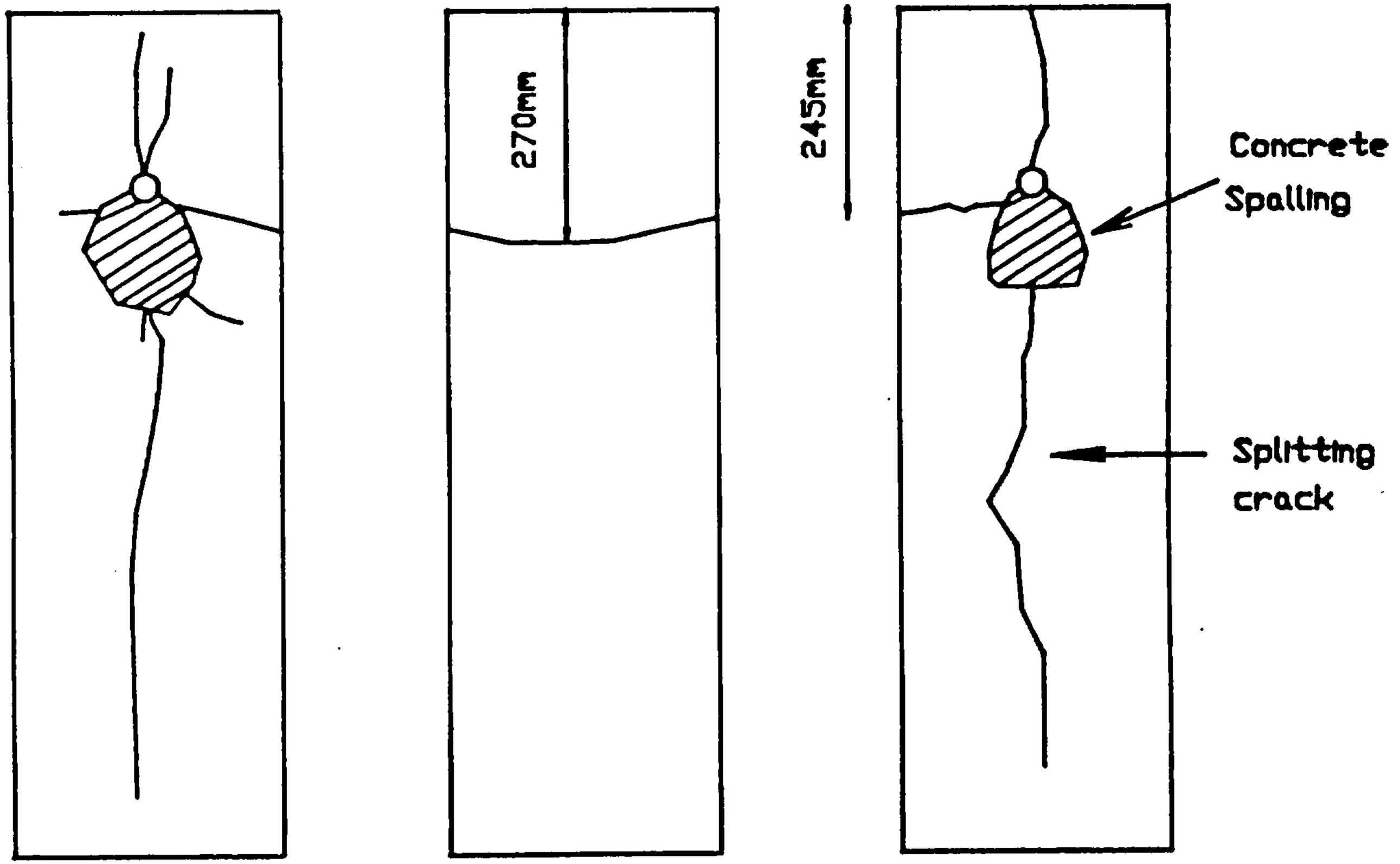


FIGURE (7.10) : CRACK PATTERNS IN THE COLUMN AT ULTIMATE LOAD 'TEST L'.

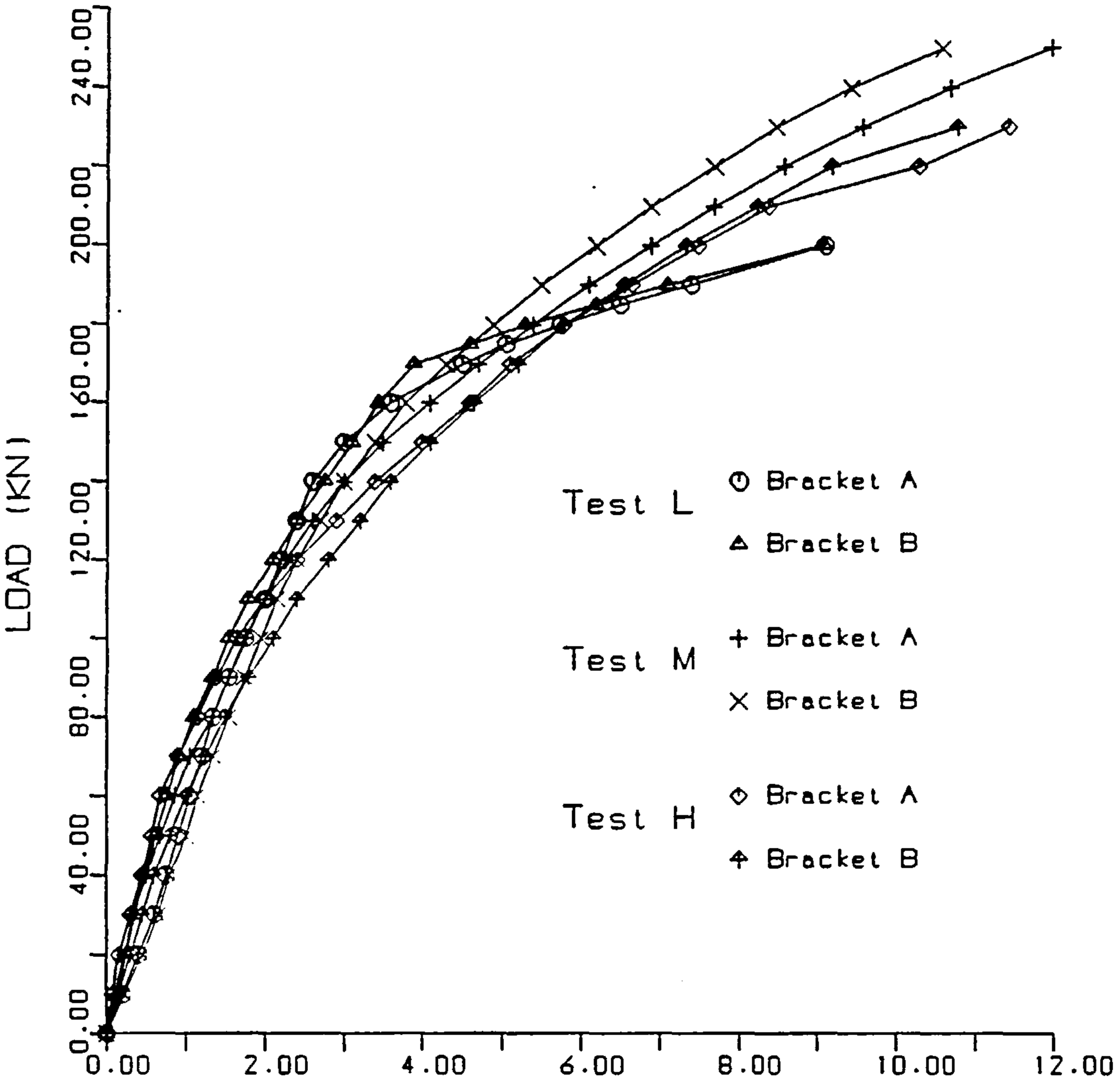


FIGURE (7.11) : EXPERIMENTAL VERTICAL DEFLECTIONS FOR ALL TESTED BRACKETS.

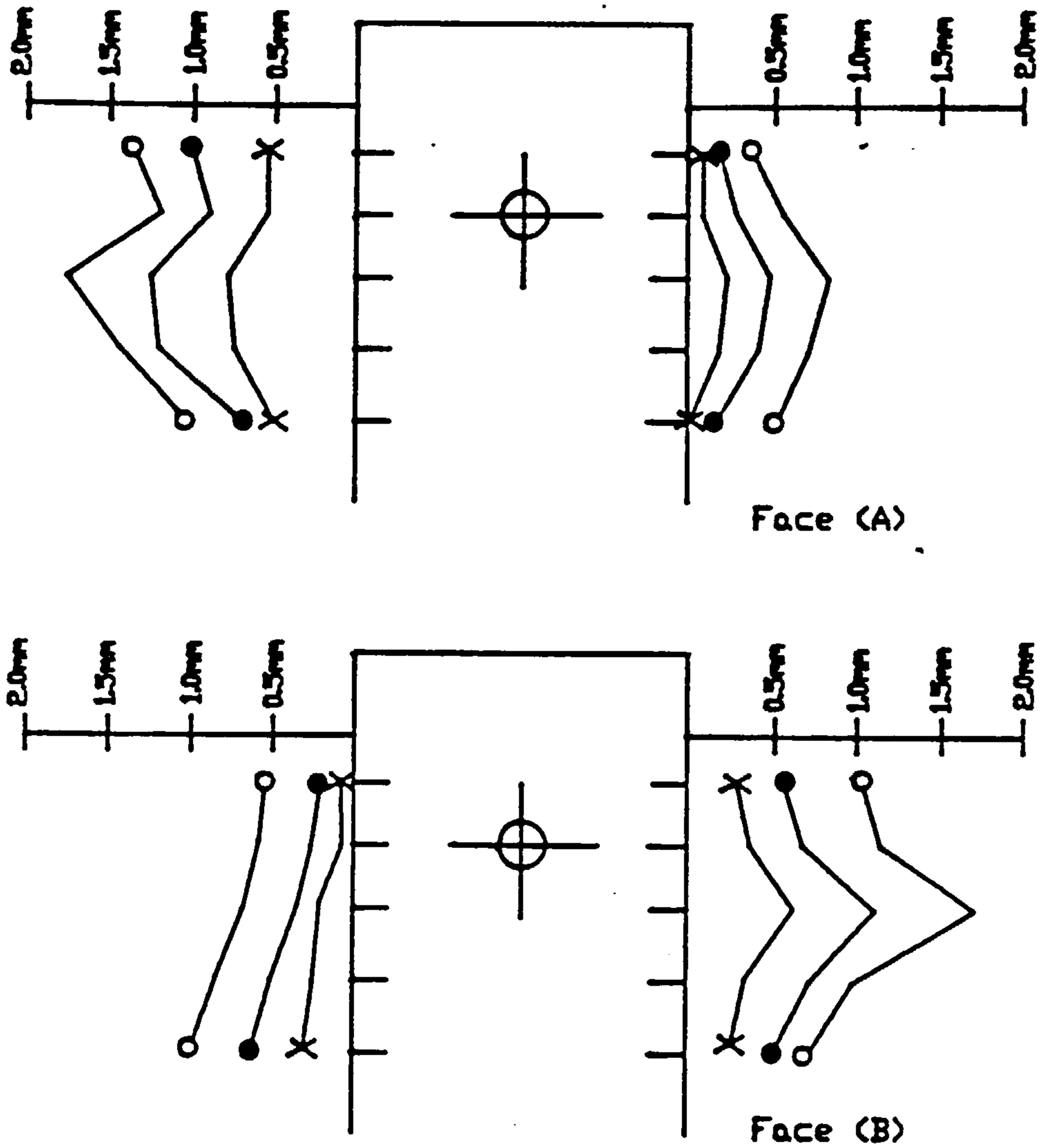


FIGURE (7.12) : CONCRETE TRANSVERSE EXPANSION DISTRIBUTION AT THE LAST STAGES OF LOADING 'TEST L'.

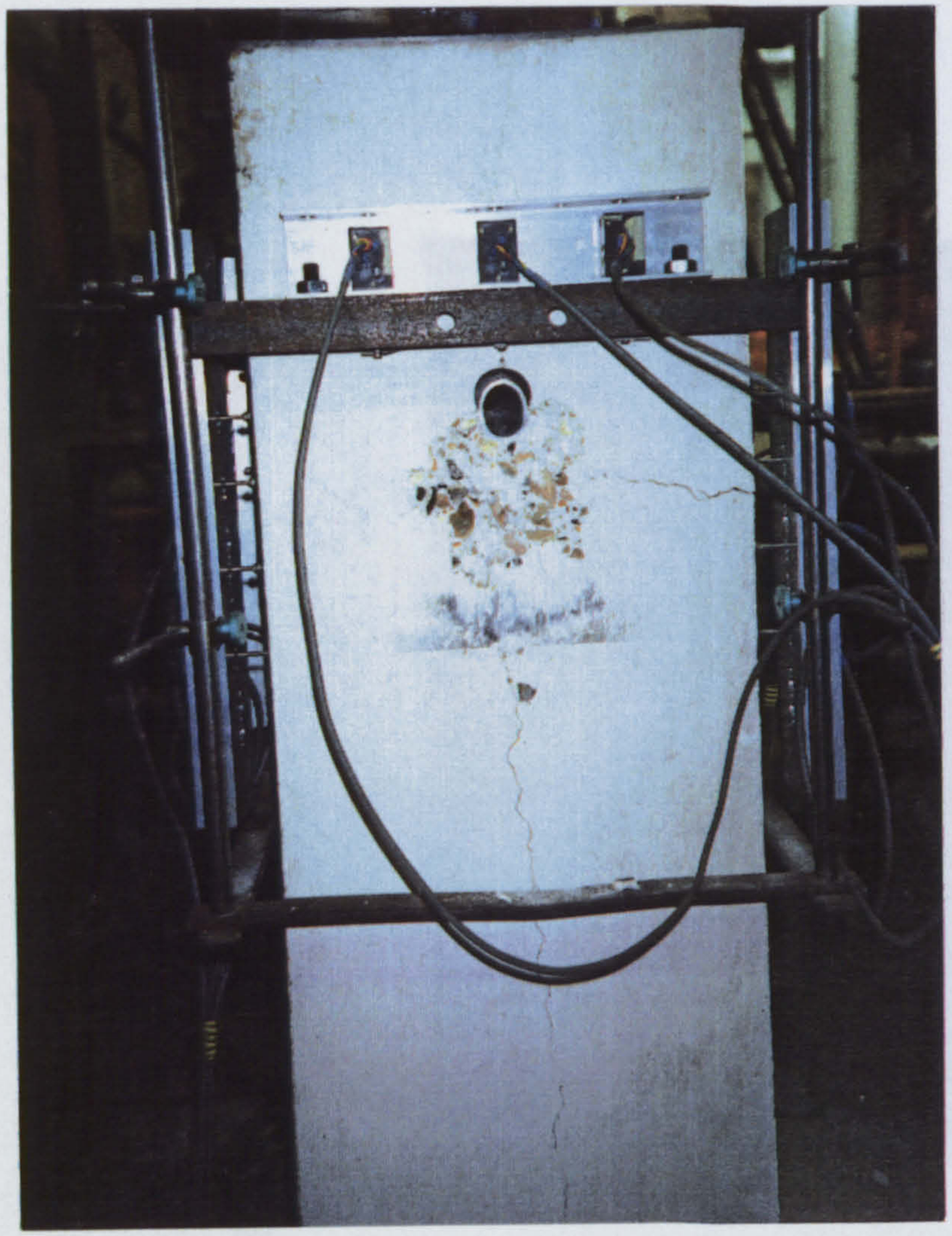

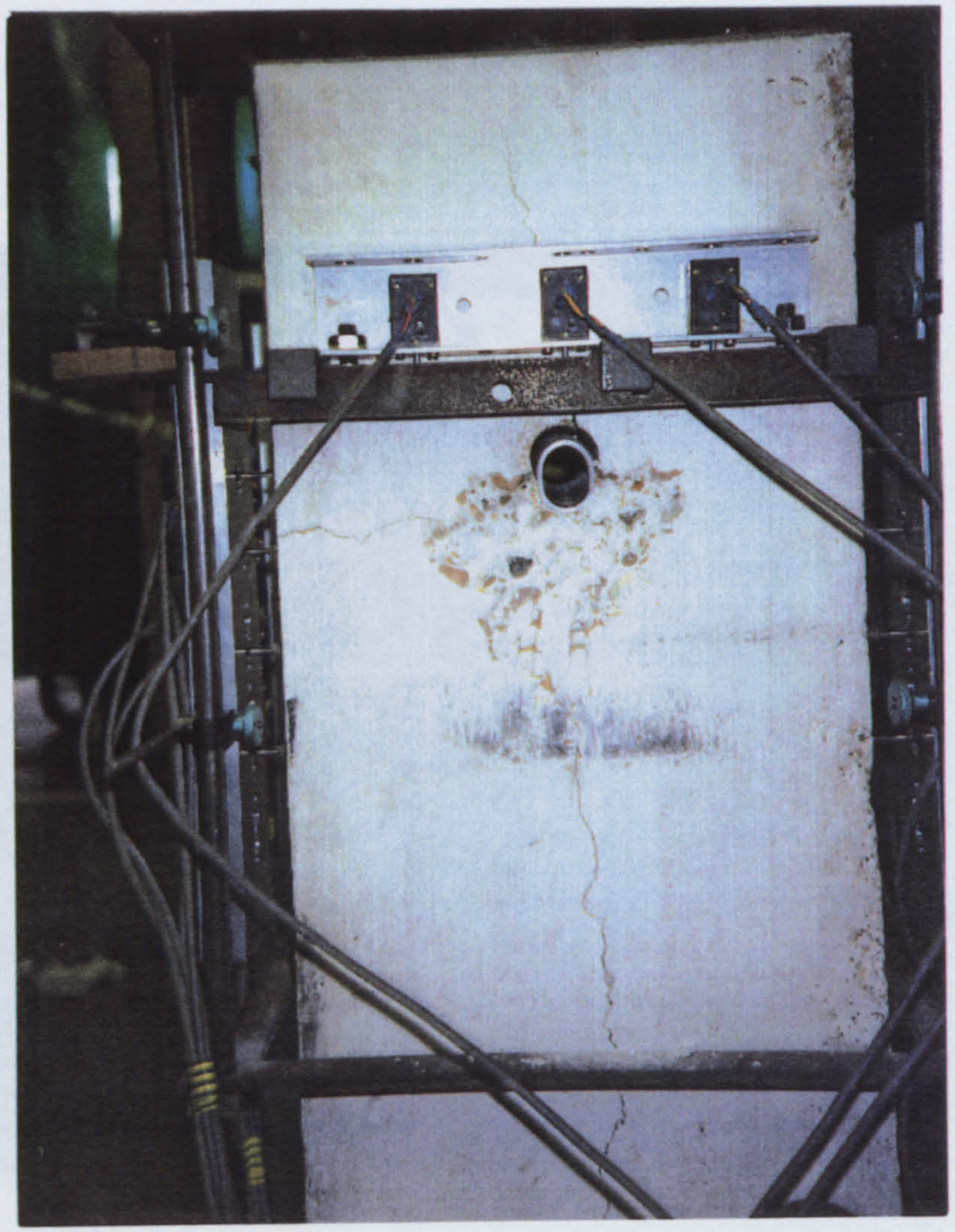

PLATE (7.1) : COLUMN FACES SHOWING CRACKS AND SPALLING OF CONCRETE WITH BOTH BRACKETS REMOVED.

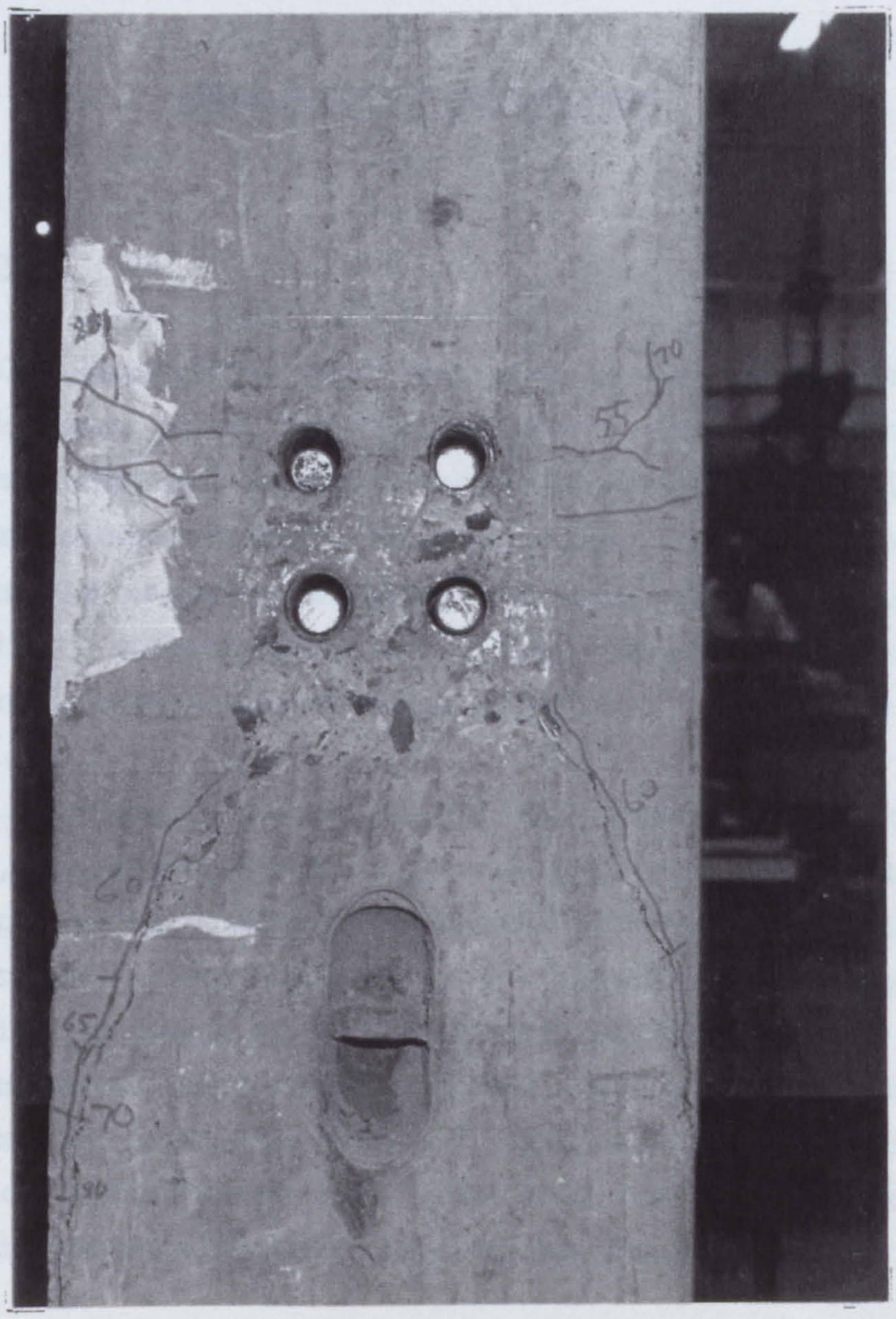


PLATE (7.2) : CONCRETE FAILURE CHARACTERISED BY THE DEVELOPMENT OF INCLINED CRACKS [21].

# CHAPTER EIGHT

# CONCLUSION AND FUTURE WORK

## 8.1 Summary

Sleeved bolts connections have been used in the precast concrete industry for many years, for their distinct advantages. However, present knowledge and research experience supply only limited information concerning their behaviour under loading. The study reported in the preceding chapters was undertaken, with the aim of a better understanding of their behaviour under the application of symmetrical vertical loading.

Through a systematic variation of the number of bolts per connection, an experimental study was conducted to investigate the influence of bolt density on the ultimate load and stiffness of connections. The bolts were loaded statically and monotonically in shear in the direction perpendicular to their longitudinal axis. Test results showed that bolt shear failure was the common governing mode of failure. The strength and stiffness of a connection were also found to be substantially increased by introducing more bolts to the connection.

The complex influences of the various parameters involved in connection formation and the difficulties associated with the experimental work, created the need to a numerical simulation using the Finite Element Method. This was achieved by using the numerical package ANSYS. Sample solutions were carried out in the process of verification of the elements implemented in ANSYS. The verification was needed to increase the degree of confidence in the elements before the execution of the numerical analysis.

Using the finite element modelling technique, three-dimensional models were developed to check the test observations and to provide complete information up to the ultimate load. The models were essentially nonlinear due to the nature of steel and concrete materials. Also, compression crushing and tensile cracking of concrete were considered to give a more realistic concrete representation. Geometrical and material parameters adopted in the test programme were used as input data for the numerical models.

The numerical models, simulating the single- and double-bolted connections, were verified by comparing their results with their experimental counterparts. The comparison indicated a good agreement between the results. Moreover, the numerical results presented an insight to the extent of concrete damage, the nature of developed stress in the steel links and the bending and yielding of the bolt shank at intermediate loading stages.

After carrying out the verification of the above models, further numerical analysis was performed on the single-bolted model, whilst the concrete crushing and tensile strengths, link tensile strength and confinement were reduced. The aim of this analysis was to determine the extent of effect on the connection's failure mode and ultimate load. As a result, a concrete failure was predicted at a lower load capacity. The model's numerical predictions were found to be conservative as they were later assessed experimentally.

Tests were carried out on single-bolted joints with different degrees of concrete confinement below the joint level. The experimental results showed that the confinement, provided by the steel brackets, had a significant effect on both the ultimate load and failure mode of the joint.

## 8.2 Conclusions

On the basis of the experimental and numerical investigations carried out and described in the previous chapters, the following conclusions can be made:

1. The increase in joint strength has been achieved by the increase of number of bolts per joint. For the two-bolts joint, the ultimate capacity was found to be about 1.7 times that of the single-bolt joint. Also, the three-bolts joint provided an ultimate strength which is almost 2.6 times that of the single-bolt joint.

2. By comparing the test data obtained for different joints, it was found that the load-deflection and moment-rotation characteristics of a joint can be improved by introducing more bolts to the joint.

3. In the case of having a high strength concrete, the joints failure mode was mostly governed by the bolts yielding in shear. The strong confinement provided by the steel links beneath the joint level eliminated the possibility of splitting crack formation. In these tests, most of the bolts showed a significant shear deformation, at their loaded ends, prior to failure. Sleeves had also yielded at their ends forming ovoid cross sections.

4. In the case of a weaker concrete, with minimum confinement, the cracks developed beneath the joint were responsible for its failure. Steel links found in this region were subjected to tensile stresses which were high enough to cause their yield. However, there was a strong evidence to suggest that increasing the confinement, for a similar concrete strength, can alter this failure mode, i.e. a bolt shear failure can be obtained.

5. The lower edge of the the bracket tends to embed itself in the concrete face as the bracket rotates. This edge then develops significant friction which transmits load into the column face in addition to that transferred through the bolt. Examination of the concrete face, after removal of the brackets, provided strong evidence of this friction. In attempt to obtain the net force carried by the bolt, the developed frictional forces were quantified.

6. Finite element models were able to predict the joints behaviour up to failure. They provide useful information which could not be obtained experimentally. In particular, the development of contact area between the bolt and sleeve, and distribution of stresses in the highly stressed zones.

7. The numerical results showed a parallel but lower vertical displacement, than was observed in the tests for a given load. More likely the presence of grout within the sleeve at the start of testing, into which bolt settlement have contributed to this difference. Furthermore, the shear deformation of the bolt threaded part, which was not modelled, provided large experimental deflection values at the last stages of loading.

8. Throughout the analysis, axial tensile stresses were computed in the steel links beneath the joint. The stresses increased as the concrete cracking and crushing progressed. At all levels beneath the joint level, maximum stress values occurred at the links' mid-span and decreased gradually towards the edges.

9. Bending of the bolt was numerically proved as tensile stresses were found at its top edge, with a transition to compressive stresses occurring at the bottom edge.

10. The predicted numerical results proved to be conservative. Predicted crack patterns and sleeve yield zone agreed reasonably well with the experimentally observed ones.

11. In the case of a double-bolted joint, there was a clear trend of stress accumulation in the region close to the plane of symmetry. A weak zone of crushed concrete developed in this area. This was accompanied with a stress increase in the steel links.

12. The confinement effect upon the joint ultimate strength proved to be critical. This fact highlighted the importance of including all the joint components in the numerical analysis if more realistic results are required.

13. The finite element method can be used to predict the performance of the zones with stress concentration in areas such as those beneath the sleeved bolts described in this research. However, the accuracy demanded of the solutions when there are such extensive non-linear material responses is even now limited by the computational power available.

## 8.2 Suggestions for Future Work

In the light of the concluding remarks listed above, it can be seen that the possible extensions of this study can take two directions. These are:

1. Experimental

Through a systematic variation of the principal joint parameters, their influence on the joint's ultimate load can be quantified. The following parameters are suggested to be varied in the tests:

a) Vertical and horizontal bolt spacings: This is to determine the optimum bolt pattern and the minimum allowed spacing to

avoid a joint premature failure.

b) Bolt diameter: Standard commercial bolt diameters should be employed in similar joints to investigate their direct effect on its capacity.

c) Type of applied load: In this work, only symmetrical vertical loading was considered. It would be appropriate to perform a series of tests to examine cases of unsymmetrical loading, existence of high tensile force and/or a bending moment applied by the beam to the joint.

2. Numerical Modelling

a) To reduce the number of full scale tests, the models already developed may be used to carry out a systematic survey on the parameters affecting the behaviour of the joints. This may be achieved by changing one or more of the associated material and geometrical properties.

b) Also it should be possible to use these models to simulate the behaviour of the three and four bolted joints. These should correspond with those tested in this work.

c) Further model verification can be made, i.e. consideration of the bolt thread and the steel bracket.

## REFERENCES


1. **The Institution of Structural Engineers:** Manual on Structural Joints in Precast Concrete. London, IStructE, August 1978. 56 pp.

2. **BLJUGER, F.:** "Design of Precast Concrete Structures", Ellis Horwood Limited, Chichester, 1988.

3. **Prestressed Concrete Institute:** PCI Design Handbook - Precast and Prestressed Concrete, Second Edition, Chicago, Illinois, 1978, 380 pp.

4. **HOLMES, M., and MARTIN, L.H.:** "Analysis and Design of Structural Connections: Reinforced Concrete and Steel", Ellis Horwood Limited, Chichester, 1983.

5. **BIRKELAND, P.W., and BIRKELAND, H.W.:** "Connections in Precast Concrete Construction", American Concrete Institute Journal, Vol. 63, No. 3, March 1966, pp. 345-368.

6. **CHUNG, M.H., FRASER, J.S., and REITH, R.D.:** "Precast Concrete Connection Details", Beton-Verlag GmbH, Dusseldorf, Germany, 1978.

7. **ACI Committee 117,** "Standard Tolerances for Concrete Construction and Materials (ACI 117- 81)", American Concrete Institute, Detroit, Michigan, 1984.

8. **Prestressed Concrete Institute Committee on Tolerances,** "Tolerances for Precast and Prestressed Concrete", Journal of The Prestressed Concrete Institute, Vol. 30, No. 1, January-February 1985, pp. 26-112.

9. **KRIZ, L.B., and RATHS, C.H.:** "Connections in Precast Concrete Structures - Strength of Corbels", Journal of the Prestressed Concrete Institute, Vol. 10, No. 1, February 1965, pp. 16-47.

10. **SOMERVILLE, G.:** "The Behaviour and Design of Reinforced Concrete Corbels", Cement and Concrete Association, Technical Report 42.472, London, August 1972, 12 pp.

11. **HERMANSEN, B., and COWAN, J.:** "Modified Shear-Friction Theory for Bracket Design", American Concrete Institute Journal, Vol. 71, No. 2, February 1974, pp. 55-60.

12. **CLARKE, J.L.:** "Behaviour and Design of Small Continous Corbels", Cement and Concrete Association, Technical Report No. 42-513, Wexham Springs, March 1976, 11 pp.

13. **MATTOCK, A.H.:** "Design Proposals for Reinforced Concrete Corbels", Journal of The Prestressed Concrete Institute, Vol. 21, No. 3, May-June 1976, pp. 18-24.

14. **JONES, G.:** "Design Charts for Reinforced Concrete Corbels", Journal of The Concrete Society, Vol. 10, No. 6, June 1976, pp. 28-30.

15. **JENSEN, B.C.:** "On the Ultimate Load of Reinforced Concrete Corbels", DIALOG 1-82, Miscellaneous Papers in Civil Engineering, Danish Engineering Academy, Lyngby, April 1982, pp. 119-137.

16. **HAGBERG, T.:** "Design of Concrete Brackets: On the Application of the Truss Analogy", American Concrete Institute Journal, Vol. 80, No. 1, January-February 1983, pp. 2-12.

17. **SOLANKI, H., and SABINS, G.:** "Reinforced Concrete Corbels-Simplified", American Concrete Institute Journal, Vol. 84, N0. 5, September-October 1987, pp. 428-432.

18. **BS 8110** The Structural Use of Concrete: Part 1: Code of Practice for Design, British Standards Institution, London, 1985, 121 pp.

19. **ACI Committee 318**, "Building Code Requirements for Reinforced Concrete (ACI 318-83)", American Concrete Institute, Detroit, Michigan, 1983, 111 pp.

20. **MAST, R.F.**:"Auxiliary Reinforcement in Concrete Connections", Journal of The Structural Division, ASCE, Vol. 94, No. ST6, June 1968, pp. 1485-1504.

21. **MOHAMED, S.A.M.**: "Beam-to-Column Connections in Precast Concrete Structures", MSc. Thesis, Department of Civil Engineering, University of Southampton, October 1988.

22. **FATTUHI, N.I.**: "Corbels with Shear Reinforcement in the Form of Stirrups or Fibres", Proceedings RILEM Symposium on Developments in Fibre Reinforced Cement and Concrete, University of Sheffield, Paper No. 8.8, July 1986, pp. 1-5.

23. **HUGHES, B.P., and FATTUHI, N.I.**: "Reinforced Steel and Polypropylene Fibre Concrete Corbel Tests", The Structural Engineer, Vol. 67, No. 4, February 1989, pp. 68-72.

24. **MARCAKIS, K., and MITCHELL, D.**: "Precast Concrete Connections with Embedded Steel Members", Journal of The Prestressed Concrete Institute, Vol. 25, No. 4, July-August 1980, pp. 88-116.

25. **MATTOCK, A.H., and GAAFAR, G.H.**: "Strength of Embedded Steel Sections as Brackets", American Concrete Institute Journal, Vol. 79, No. 2, March-April 1982, pp. 83-93.

26. **HOLMES, M., and BOND, D.:** "Tests on Beam-to-Column Connexion for Precast Concrete", The Structural Engineer, Vol. 41, No. 9, September 1963, pp. 293-297.

27. **HOLMES, M., and POSNER, C.D.:** "Factors Affecting The Strength of Steel Plate Connections between Precast Concrete Elements", The Structural Engineer, Vol. 48, No. 10, October 1970, pp. 399-406.

28. **MARTIN, L.D., and KOKOSZ, W.J.:** "Connections for Precast Prestressed Concrete Buildings-Including Earthquake Resistance", Technical Report No. 2, Consulting Engineers Group Inc., Prestressed Concrete Institute, Chicago, March 1982, 297 pp.

29. **KLINGER, R.E., and MENDONCA, J.A.:** "Tensile Capacity of Short Anchor Bolts and Welded Studs: A Literature Review", American Concrete Institute Journal, Vol. 79, No. 4, July-August 1982, pp. 270-279.

30. **KLINGER, R.E., and MENDONCA, J.A.:** "Shear Capacity of Short Anchor Bolts and Welded Studs: A Literature Review", American Concrete Institute Journal, Vol. 79, No. 5, September-October 1982, pp. 339-349.

31. **UEDA, T., KITIPORNCHAI, S., and LING, K.:** "Experimental Investigation of Anchor Bolts under Shear", Journal of The Structural Division, ASCE, Vol. 116, No. 4, April 1990, pp. 910-924.

32. **LYNCH, T.J. and BURDETTE, E.G.:** "Some Design Considerations for Anchors in Concrete", American Concrete Institute Journal, Vol. 88, January-February 1991, pp. 91-97.

33. **PEIER, W.H.:** "Model for Pull-Out Strength of Anchors in Concrete", Journal of The Structural Division, ASCE, Vol. 109, No. 5, May 1983, pp. 1155-1173.

34. **STANGENBERG, F., and JANKOWSKI, D.:** "Anchorages under Tensile Loading- A Nonlinear Numerical Analysis", International Journal of Pressure Vessels and Piping, Vol. 38, Part 5, 1989, pp. 341-353.

35. **SHAIKH, A.F., and YI, W.:** "In-Plane Strength of Welded Headed Studs", Journal of The Prestressed Concrete Institute, Vol. 30, No. 2, March-April 1985, pp. 56-81.

36. **EL-GHAZALY, H.A., and AL-ZAMEL, H.S.:** "An Innovative Detail for Precast Concrete Beam-Column Connections", Canadian Journal of Civil Engineering, Vol. 18, No. 4, August 1991, pp. 690-710.

37. **FRENCH, C.W., HAFNER, M., and JAYASHANKER, V.:** "Connections between Precast Elements - Failure within Connection Region", Journal of The Structural Division, ASCE, Vol. 115, No. 12, December 1989, pp. 3171-3192.

38. **SECKIN, M., and FU, H.C.:** "Beam-Column Connections in Precast Reinforced Concrete Construction", American Concrete Institute Journal, Vol. 87, No. 3, May-June 1990, pp. 252-261.

39. **CHEOK, G.S., and LEW, H.S.:** "Performance of Precast Concrete Beam-to-Column Connections Subject to Cyclic Loading", Journal of The Prestressed Concrete Institute, Vol. 36, No. 3, May-June 1991, pp. 56-67.

40. **ELLIOTT, K.S., DAVIES, G., and MAHDI, A.:** "The Effect of Moment Rotation on the Stability of Columns in Precast Concrete Structures", Current Research at the University of Nottingham.

41. **PARSA, A.:** "Finite Element Analysis of Shear in Reinforced Concrete Beams", MSc. Thesis, Department of Civil Engineering, University of Southampton, November 1987.

42. **MATTOCK, A.H., and THERYO, T.S.:** "Strength of Members with Dapped Ends", Final Report PCISFRAD Project No.6, Prestressed Concrete Institute, Chicago, Illionis, 1986.

43. **COOK, W.D., and MITCHELL, D.:** "Studies of Disturbed Regions near Discontinuities in Reinforced Concrete Members", American Concrete Institute Journal, Vol. 85, March-April 1988, pp. 206-216.

44. **BS 5400** Steel, Concrete and Composite Bridges: Part 4, Code of Practice for Design of Concrete Bridges, British Standards Institution, London, 1984.

45. **CLARK, L.A., and THOROGOOD, P.:** "Serviceability Behaviour of Reinforced Concrete Half Joints", Contractor Report 70, Transport and Road Research Laboratory, 1987.

46. **FISHER, W.F., and STRUIK, J.H.A.:** "Guide to Design Criteria for Bolted and Riveted Joints", John Wiley and Sons, U.S.A., 1974.

47. **BICKFORD, J.H.:** "An Introduction to the Design and Behaviour of Bolted Joints", Marcel Dekker Inc., New York, 1981.

48. **NARAYANAN, R.** [ed.]: "Structural Connections - Stability and Strength", Elsevier Applied Science, England, 1989.

49. **BJORHOVDE, R., BROZZETTI, J., and COLSON, A.:** "Connections in Steel Structures", A collection of Papers on the Behaviour, Strength and Design of Connections, Elsevier Applied Science, England, 1988.

50. **TEYCHENNE, D.C., FRANKLIN, R.E., and ERNTROY, H.C.:** "Design of Normal Concrete Mixes", Department of the Environment, HMSO, London, 1975.

51. **BS 5950** Structural Use of Steelwork in Building: Part 1, Code of Practice for Design in Simple and Continous Construction: hot rolled sections, British Institution Standards, London, 1985.

52. **ANSYS,** Engineering Analysis System User's Manual, Vols. 1 and 2, Version 4.4, Swanson Analysis System Inc., Houston, Pennsylvania, U.S.A., 1989.

53. **ANSYS,** Engineering Analysis System Theoretical Manual, Version 4.4, Swanson Analysis System Inc., Houston, Pennsylvania, U.S.A., 1989.

54. **SUIDAN, M., and SCHNOBRICH, W.C.:** "Finite Element Analysis of Reinforced Concrete", Journal of The Structural Division, ASCE, Vol. 99, No. ST10, October 1973, pp. 2109-2122.

55. **ZIENKIEWICZ, O.C., TAYLOR, R.L., and TOO, J.M.:** "Reduced Integration Technique in General Analysis of Plates and Shells", International Journal for Numerical Methods in Engineering, Vol. 3, January-March 1971, pp. 275-290.

56. **MAZURKIEWICZ, M., and OSTACHOWICZ, W.:** "Theory of Finite Element Method for Elastic Contact Problems of Solid Bodies", Computers and Structures Journal, Vol. 17, No. 1, 1983, pp. 51-59.

57. **BS 3692** Specification for ISO Metric Precision Hexagon Bolts, Screws and Nuts", British Standards Institution, London, 1967.

58. **ZIENKIEWICZ, O.C.:** "The Finite Element Method in Engineering Science", McGraw-Hill Book Company, London, 1977.

59. **IRONS, B.M.:** "A Frontal Solution Program for Finite Element Analysis", International Journal for Numerical Methods in Engineering, Vol. 2, No. 1, January 1970, pp. 5-32.

60. **American Society of Civil Engineers:** Finite Element Analysis of Reinforced Concrete, New York, U.S.A, 1982, 545 pp.

61. **CHEN, W.F.:** "Plasticity in Reinforced Concrete", McGraw-Hill Book Company, New York, U.S.A, 1982.

62. **BANGASH, M.Y.H.:** "Concrete and Concrete Structures: Numerical Modelling and Applications", Elsevier Applied Science Publishers Limited, England, 1989.

63. **BATHE, K.J., and RAMASWAMY, S.:** "On Three-Dimensional Nonlinear Analysis of Concrete Structures", Nuclear Engineering and Design, Vol. 52, Part 3, 1979, pp. 385-409.

64. **KOTSOVOS, M.D., and NEWMAN, J.B.:** "Behaviour of Concrete Under Multiaxial Stress", American Concrete Institute Journal, Vol. 74, No. 9, 1977, pp. 443- 446.

65. **CARRASQUILLO, R.L., NILSON, A.H., and SLATE, F.O.:** "Properties of High Strength Concrete Subject to Short Term Loads", American Concrete Institute Journal, Vol. 78, No. 3, May-June 1981, pp. 171- 178.

66. **WINTER, G. and NILSON, A.H.:** "Design of Concrete Structures", 9th Edition, McGraw-Hill Book Co., New York, U.S.A, 1979.

67. **HOGNESTAD, E.:** "A Study of Combined Bending and Axial Load in Reinforced Concrete Members", Bulletin No. 399, Engineering Experiment Station, University of Illinois, Urbana, Illinois, Vol. 49, No. 22, November 1951.

68. **DESAI, P. and KRISHNAN, S.:** "Equation for The Stress-Strain Curve of Concrete, American Concrete Institute Journal, Vol. 61, No. 3, March 1964, pp. 345-350.

69. **POPOVICS, S.:** "A Numerical Approach to The Complete Stress-Strain Curve of Concrete", Cement and Concrete Research, Vol. 3, September 1973, pp. 583-599.

70. **CARREINA, D.J., and CHU, K.H.:** "Stress-Strain Relationship for Plain Concrete in Compression", American Concrete Institute Journal, Vol. 82, November-December 1985, pp. 797-804.

71. **TSAI, W.T.:** "Uniaxial Compressional Stress-Strain Relation of Concrete", Journal of the Structural Division, ASCE, Vol. 114, 1988, pp. 2133-2136.

72. **KUPFER, H.B., HILSDORF, H.K. and RUSH, H.:** "Behaviour of Concrete Under Biaxial Stresses", American Concrete Institute Journal, Vol. 66, No. 8, August 1969, pp. 656-666.

73. **GREEN, S.J., and SWANSOM, S.R.:** "Static Constitutive Relations For Concrete", Technical Report AFWL-TR-72-244, U.S.Air Force Weapons Laboratory, Kirtland Air Force Base, New Mexico, 1973.

74. **BAZANT, Z.P.:** "Instability, Ductility and Size Effect in Strain-Softening Concrete", Journal of The Engineering Mechanics Division, ASCE, April 1976, Vol. 102, pp. 331-344.

75. **CHEN, W.F. and YAMAGUCHI, E.:** "On Constitutive Modelling of Concrete Materials", Proceedings U.S.-Japan Seminar on Finite Element Analysis of Reinforced Concrete Structures, ASCE, 1986, pp. 48-71.

76. **WISCHERS, G.:** "Application of Effects of Compressive Loads on Concrete", Betontech. Ber, Nos. 2 and 3, Dusseldorf, 1978.

77. **KONG, K.F., and EVANS, R.H.:** "Reinforced and Prestressed Concrete", Van Nostrand Reinhold Company Ltd.", England, 3rd Edition, 1987.

78. **CHEN, A.C.T., and CHEN, W.F.:** "Constitutive Relations for Concrete", Journal of The Engineering Mechanics Division, ASCE, Vol. 101, No. 4, August 1975, pp. 465-481.

79. **BUYUKOZTURK, O.:** "Nonlinear Analysis of Reinforced Concrete Structures", Computers and Structures Journal, Vol. 7, No. 1, 1977, pp. 149-156.

80. **BUYUKOZTURK, O., and SHAREEF, S.S.:** "Constitutive Modelling of Concrete in Finite Element Analysis", Computers and Structures Journal, Vol. 21, 1985, pp. 581-610.

81. **HU, H.T., and SCHNOBRICH, W.C.:** "Nonlinear Analysis of Cracked Reinforced Concrete", American Concrete Institute Journal, Vol. 87, No. 2, March-April 1990, pp. 199-207.

82. **CERVENKA, V., and GERSTLE, K.H.:** "Inelastic Analysis of Reinforced Concrete Panels: Experimental Verification and Application", International Association of Bridge and Structural Engineers, Vol. 32-II, 1972, pp. 25-39.

83. **CHEN, W.F., and SUZUKI, H.:** "Constitutive Models for Concrete", Computers and Structures Journal, Vol. 12, 1980, pp. 23-32.

84. **WILLAM, K.J., and WARNKE, E.P.:** "Constitutive Model for The Triaxial Behaviour of Concrete", International Association of Bridge and Structural Engineers, Seminar on Concrete Structures Subjected to Triaxial Stresses, Paper III-I, Bergamo, Italy, May 17-19 1974, pp. 1-30.

85. **RASHID, Y.R.:** "Ultimate Strength Analysis of Prestressed Concrete Pressure Vessels", Nuclear Engineering and Design (Lausanne), Vol. 7, No. 4, April 1968, pp. 334-344.

86. **PHILLIPS, D.V., and ZIENKIEWICZ, O.C.:** "Finite Element Nonlinear Analysis of Concrete Structures", Proceeding of The Institution of Civil Engineers, Part 2, Vol. 61, March 1976, pp. 59-88.

87. **BEDARD, C.:** "Nonlinear Finite Element Analysis of Concrete Structures", PhD. Thesis, University of London, 1983, 286 pp.

88. **GUPTA, A.K., and AKBAR, H.:** "Cracking in Reinforced Concrete Analysis", Journal of Structural Division, ASCE, Vol. 110, No. 8, August 1984, pp. 1735-1746.

89. **BAZANT, Z.P.:** "Crack Band Model for Fracture of Geomaterials" Proceedings, 4th International Conference on Numerical Methods in Geomaterials, University of Alberta, Edmonton, U.S.A., Vol. 3, 1982, pp. 1137-1152.

90. **BALAKRISHNAN, S., and MURRAY, D.W.:** "Concrete Constitutive Model for NLFE Analysis of Structures", Journal of Structural Divison, ASCE, Vol. 114, No. 7, July 1988, pp. 1449-1466.

91. **NGO, D., and SCORDELIS, A.S.:** "Finite Element Analysis of Reinforced Concrete Beams", American Concrete Institute Journal, Vol. 64, March 1967, pp. 152-163.

92. **AHMED, M.:** "Bond Strength History in Prestressed Concrete Reactor Vessels", PhD. Thesis, Thames Polytechnic, 1984.

93. **KOTSOVOS, M.D.:** "Behaviour of Beams with Shear Span-to-Depth Ratios Greater Than 2.5", American Concrete Institute Journal, Vol. 83, No. 6, November-December 1986, pp. 1026-1034.

94. **KOTSOVOS, M.D., and NEWMAN, J.B.:** "Effect of Boundary Conditions upon The Behaviour of Concrete under Concentrations of Load", Magazine of Concrete Research, Vol. 33, No. 116, September 1981, pp. 161-170.

95. **CHEN, A.C.T., and CHEN, W.F.:** "Nonlinear Analysis of Concrete Splitting Tests", Computers and Structures Journal, Vol. 6, 1976, pp. 451-457.

96. **ABOUSSALEH, M.:** "Application of Constitutive Models to Concrete Structures",PhD Thesis, School of Civil Engineering, Purdue University, West Lafayette, Indiana, U.S.A, 1989.

## APPENDIX I

### Calculation of Frictional Force

At any stage of loading, the set of vertical forces shown in Figure (3.1) should satisfy the statical equilibrium of the loaded bracket. This means that:

$$P = R_b + R_f \qquad (1)$$

Where P is the vertical applied load.

$R_b$ is the bolt reaction at the point of contact with the inside material of the bracket hole.

$R_f$ is the frictional force at the bracket bottom edge.

From moment equilibrium

$$P \times e = T \times z = C \times (d - 0.45x) \qquad (2)$$

Where C is the developed compressive force at the lower part of the bracket.

T is the tensile force in the top set of bolts.

e is the load eccentricity from the column face.

z is the internal lever arm.

d is the vertical spacing between the top set of bolts and bottom of the face of the bracket.

x is the neutral axis depth.

At the ultimate load, C can be expressed as $(0.67F_{cu} \times b \times 0.9x)$ where b is the width of the back plate; therefore

$$P \times e = 0.67 F_{cu} \times b \times 0.9 x \times (d - 0.45x)$$

x is the only unknown in the above equation. At the ultimate load of the single bolt joint, the following loading and geometrical data were used to find a value for x.

| | | | | | |
|---|---|---|---|---|---|
| P | = | 275.0 KN | e | = | 60.0 mm |
| $F_{cu}$ | = | 61.90 $N/mm^2$ | b | = | 160.0 mm |
| d | = | 175.0 mm | | | |

x was found to be 16.48 mm leading to a compressive force C of 98.42 KN.

From the fundamentals of friction, $R_f$ can be expressed as:

$$R_f = \mu \cdot C \qquad (3)$$

Where $\mu$ is the coefficient of friction between the concrete surface and the steel plate. For this particular test, a value of 0.66 was obtained experimentally for $\mu$.

$$R_f = 0.66 \times 98.42 = 65.0 \text{ KN}$$

From equation (1), $R_b$ is equal to 210.0 KN.

Using the above procedure, the depth of compression block x was found to be 29.18 mm, 46.50 mm, 32.4 mm, and 40.56 mm for joints 2, 3, 4A and 4B, respectively. These values are in compliance with the friction markings, found in the highly stressed regions and shown in Plate (3.4), which were measured after bracket's removal. The measured values were in the range of 30-60 mm. After deducting the calculated frictional force for each joint, the following shear forces $R_b$ were obtained as follows:

| | | | |
|---|---|---|---|
| $R_b$ for joint 2 | = 355.0 KN | $R_b$ for joint 3 | = 529.5 KN |
| $R_b$ for joint 4A | = 384.0 KN | $R_b$ for joint 4B | = 480.0 KN |

$\mu$ values were found to be dependent on the nature of both steel and concrete surfaces, e.g. $\mu$ had a value of 0.52 when the steel back plates were machined.

# APPENDIX II

## Calculation of Brackets' Load Difference

Assuming that there is a load difference between the tested joints, the total applied load will be divided into two vertical forces, i.e. $P_1$ and $P_2$ as shown in Figure (3.3). At any stage of loading, the resultant force R, acting at the column base, must be equal to the sum of these two vertical forces. The resultant force will act at a distance s from the base centreline.

From the principles of equilibrium:

$$P_1 \times L = R \times (0.5L - s)$$

Where L is the horizontal distance between the centres of the loading plates. From the test geometry, L = 420mm.

$$P_1 \times 420 = (P_1 + P_2) \times (210 - 10)$$

Assuming that the resultant eccentricity, s, is 10mm. This will lead to the following relationship.

$$P_1 = 0.475\ (P_1 + P_2)$$

Thus the applied load is divided into the ratio of 0.475 : 0.525 between both brackets. Smaller values for s, which should be expected in the tests, would lead to less load difference.

# APPENDIX III

## Calculation of Weld Loads

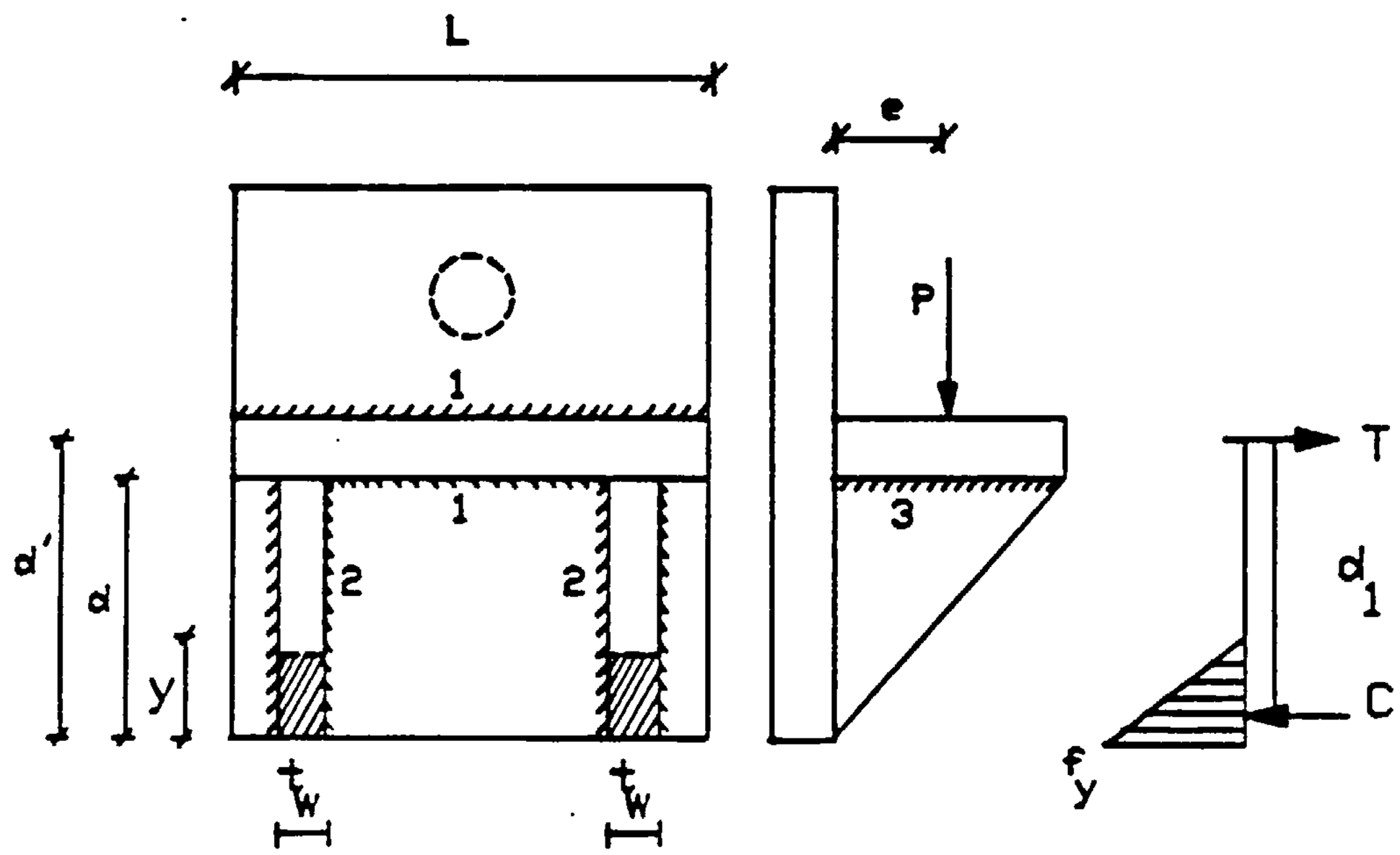


In this appendix, an estimate is made of the actual weld load capacity which caused fracture at bracket B in Test 4.

The bracket was made of grade 43 mild steel plates welded together with fillet welds marked 1, 2 and 3 as shown in the above sketch. The shape of welds were triangular and their sizes were specified by the leg length. Such sizes were designed to transfer safely the load between the connected parts under the anticipated maximum applied load.

Due to the eccentricity of the applied load, a value of moment M is created at the back plate. M, which has a value of the applied load P times the value of eccentricity e, is mainly resisted by two parts, namely

1. The welds marked 1 of the top plate.

2. The shaded areas of the webs.

In the meantime, the shear force at the back plate interface is resisted by the web welds marked 2.

From the above force diagram, satisfying the moment equilibrium at a certain value of load P leads to the following two equations:

$$M = P \times e = C \times d_1$$

$$C = 2 \times 0.5\, f_y \times y \times t_w$$

where C is the compressive force developed at the lower part of the bracket.

$d_1$ is the internal lever arm = d - (y/3).

y is the effective depth of the webs where compressive stress is developed.

$f_y$ is the yield stress for the steel material.

$t_w$ is the width of a single web.

From both equations, a quadratic equation in y can be obtained. Note that y is the only unknown variable in this equation. At bracket failure, the corresponding loading and geometrical data were as follows:

| | | | | | | | |
|---|---|---|---|---|---|---|---|
| P | = | 632.5 | KN | e | = | 40.0 | mm |
| L | = | 190.0 | mm | $t_w$ | = | 20.0 | mm |
| d | = | 115.0 | mm | $f_y$ | = | 265.0 | $N/mm^2$ |
| d' | = | 125.0 | mm | | | | |

$M = 632.5 \times 40 = 25300$ KN.mm

$= C [ 125 - 0.33y ]$ (1)

$$C = 2 \times 0.5 \times 265 \times y \times 20 = 5.3\,y \quad KN \qquad (2)$$

From (1) and (2)

$y = 43.1$ mm $\qquad C = T = 228.4$ KN

a) Check of the top plate weld

Both weld lengths marked 1 should be effective in resisting the value of the force T. The clear horizontal distance between both webs is 128.0mm. Therefore, the weld load f can be directly obtained as follows:

$$f = \frac{228.4}{190+128} = 0.72 \text{ KN/mm}$$

This value of strength is much less than 1.2 KN/mm which is the maximum allowable strength of the specified 8mm fillet weld [51]. However, from the measured values, given in Table 3, it was found that the average value of the actual top weld, along the length of the top plate weld, is 5.94mm. Assuming that the fracture occurred at the mid-thickness of the leg length, this value may be taken as a representative of the actual leg length of the weld used. It is of interest to note that f is also less than the strength of a 6mm fillet weld which is 0.92 KN/mm.

b) Check of the web welds

Having two webs, each of them had two side welds, made the total weld length equal to four times the web height. This length was designed to resist the total shear force transferred through the bracket. At failure, the weld length f can be calculated as:

$$f = \frac{632.5}{4 \times 115} = 1.375 \text{ KN/mm}$$

As before, this value is less than 1.5 KN/mm which is the strength for a 10mm fillet weld [51]. The actual value obtained as an average of the corresponding listed values in Table 3 is 5.00mm. This value gives a strength of 0.75 KN/mm which is much less than the above calculated load value.

If the strength of the top plate welds which is not required in tension is added to the vertical weld strength, then the design shear strength would be extended to

$$0.75 + (0.92-0.72) \times \frac{(190+128)}{4 \times 115} = 0.89 \text{ KN/mm}$$

This value is still less than 1.375 KN/mm and therefore the bracket would be expected to fail in shear.

# APPENDIX IV

## Effect of Geometrical Imperfection

In this appendix, an attempt is made to evaluate the effect of the slope of the top edge of the back plate on the measured vertical deflections at that edge. All notations used here are defined in accordance with Figure (3.13).

$t_e$ is the thickness of the back plate which is 20mm.

d is the vertical distance between the bolt's centreline and the bottom of the plate.

u is the recorded axial elongation of a bolt at a load step.

$\psi$ is the angle of rotation measured at the bottom of the plate.

$$\psi = \tan^{-1} (u/d)$$

y is the height difference between both top edges.

v is the vertical deflection component corresponding to the slope effect.

From the axial deflection diagram, it is assumed that the outward deflection has zero value at the extreme point of the bottom edge of the back plate where the plate presses hard against the concrete. This outward deflection varies linearly up the height of the plate until it reaches its maximum value at the top edge. Knowing the height of the bracket h, and using the recorded value of u at any stage of loading, an estimated value of u' can be calculated.

$$u' = u \times (h/d)$$

Using measured values of y and knowing the plate thickness $t_e$, the slope of the edge i, can be obtained.

$$i = (y/t_e) + \psi$$

Due to such a slope, u′ has a downward vertical component v, which equals i times u′. This component is included in the deflection which is measured by the transducers positioned at the top edge. As a result, values of v should have been added to obtain a better representation of the load-deflection curves.

To check the effect of v, the top of back plates of brackets used in joint 1 were measured. A number of readings were taken across the width of the plate by means of a metric vernier. It was also assumed that the transducer arm was positioned exactly at the mid-thickness of the top edge throughout the test. Calculated values of v were so small that they had an insignificant effect in those already recorded by the transducers.

# APPENDIX V

## Stresses in Steel Links of Models 1 and 2

In this appendix, the axial tensile stresses predicted by Model 1 and 2 are presented. In obtaining these values, the correct value for the links' cross section area was employed. The stresses are plotted at a load value equal to the maximum experimental load per bolt end(s).

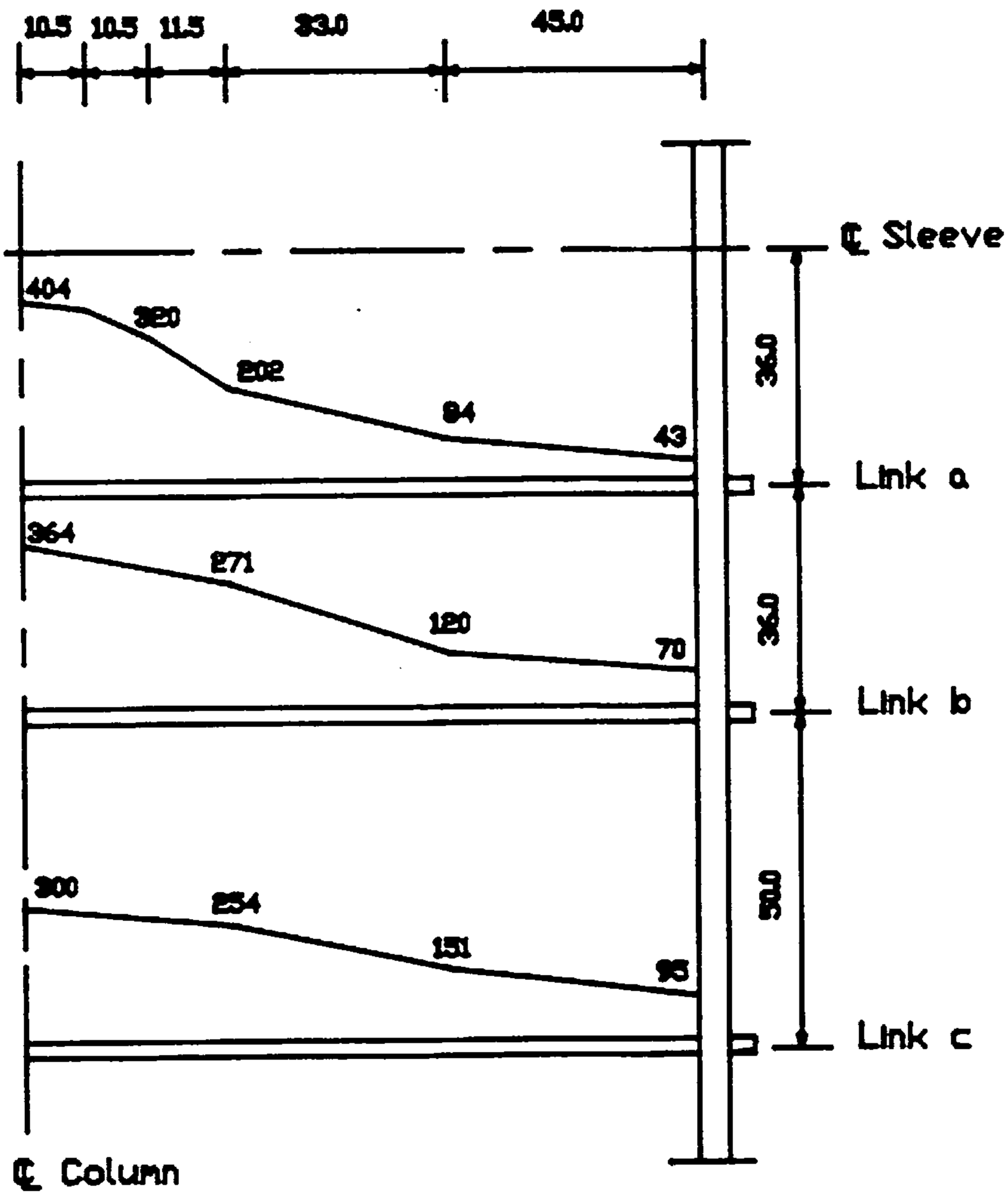


Model 1

Stresses are in N/mm²

Model 2

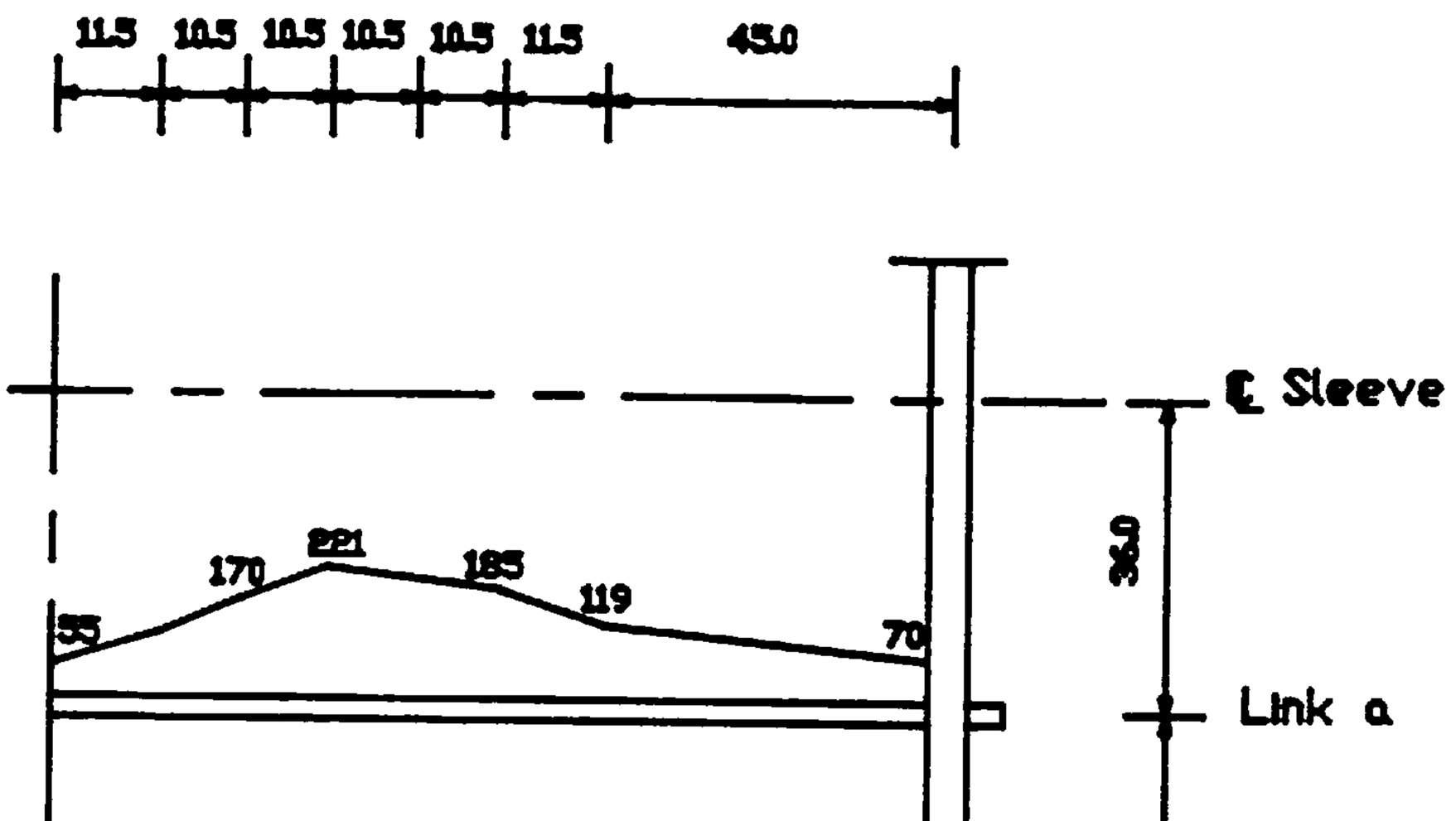


Stresses are in $N/mm^2$